EPA-R2-72-008
September 1972

ENVIRONMENTAL PROTECTION TECHNOLOGY SERIES

The Swirl Concentrator as a Combined Sewer Overflow Regulator Facility

Office of Research and Monitoring
U.S. Environmental Protection Agency
Washington, D.C. 20460

RESEARCH REPORTING SERIES

Research reports of the Office of Research and Monitoring, Environmental Protection Agency, have been grouped into five series. These five broad categories were established to facilitate further development and application of environmental technology. Elimination of traditional grouping was consciously planned to foster technology transfer and a maximum interface in related fields. The five series are:

1. Environmental Health Effects Research
2. Environmental Protection Technology
3. Ecological Research
4. Environmental Monitoring
5. Socioeconomic Environmental Studies

This report has been assigned to the ENVIRONMENTAL PROTECTION TECHNOLOGY series. This series describes research performed to develop and demonstrate instrumentation, equipment and methodology to repair or prevent environmental degradation from point and non-point sources of pollution. This work provides the new or improved technology required for the control and treatment of pollution sources to meet environmental quality standards.

EPA-R2-72-008
September 1972

THE SWIRL CONCENTRATOR

as a

COMBINED SEWER OVERFLOW REGULATOR FACILITY

Project 11023 GSC

Project Officer

Richard Field
Edison Water Quality Research Div.
National Environmental Research Center
Edison, New Jersey 08817

Prepared for

OFFICE OF RESEARCH AND MONITORING
U.S. ENVIRONMENTAL PROTECTION AGENCY
WASHINGTON, D.C. 20460

and the

CITY OF LANCASTER, PENNSYLVANIA

For sale by the Superintendent of Documents, U.S. Government Printing Office
Washington, D.C., 20402 - Price $2.25

EPA Review Notice

This report has been reviewed by the Environmental Protection Agency and approved for publication. Approval does not signify that the contents necessarily reflect the views and policies of the Environmental Protection Agency, nor does mention of trade names or commercial products constitute endorsement or recommendation for use.

ABSTRACT

A study was conducted by the American Public Works Association to determine the applicability of a combined sewer overflow regulator which by induced hydraulic conditions separates settleable and floatable solids from the overflow. The device, called a swirl concentrator, was originally developed in Bristol, England. The present study was conducted through the use of a hydraulic model test to determine swirl concentrator configurations, flow patterns and settleable solid removal efficiency. A mathematical model was also prepared to determine a basis for design.

Excellent correlation was found between the two studies. It was found that at flows which simulate American experience a vortex flow pattern was not effective. However, when flows were restricted, a swirl action occurred and settleable solids were concentrated in the outflow to the interceptor in a flow of two to three percent as compared to the quantity of overflow through a central weir and down shaft.

For a flow of 165 cfs, representing a five-year frequency storm it was determined that a 36-ft diameter tank, 9-ft deep with a 20-ft diameter weir would have an efficiency of 85 percent of maximum.

The swirl concentrator appears to offer a combined sewer overflow regulator that effectively regulates the flow and improves the quality of the overflow, with few moving parts.

The complete hydraulic laboratory and mathematical reports are included as appendices.

This report was submitted in fulfillment of the agreement between the City of Lancaster, Pennsylvania, and the American Public Works Association under the partial sponsorship of the Office of Research and Monitoring, Environmental Protection Agency, in conjunction with Research and Demonstration Project 11023GSC.

APWA RESEARCH FOUNDATION
Project 70-7

Richard H. Sullivan, Project Director

SPECIAL CONSULTANTS

Dr. Morris M. Cohn
J. Peter Coombes
Bernard S. Smisson
Alexander Potter Associates, Consulting Engineers
General Electric Company, Re-entry and Environmental Systems Division
LaSalle Hydraulic Laboratory, Ltd.

APWA Staff*

R.H. Ball
Mona Jordan
Shirley M. Olinger
Oleta Ward

*Personnel utilized on a part-time basis

CONTENTS

TABLES

FIGURES

FOREWORD

The report which follows presents the result of an intensive study conducted by the American Public Works Association Research Foundation concerning the development and basic design of a new type of combined sewer overflow regulator facility. The regulator, although basically a static facility due to the minimization of moving parts will, in addition to controlling the rate of flow to the interceptor, significantly reduce the amount of settleable solids in the overflow. With proper design it will also maximize insystem storage.

Although work was accomplished using a basic configuration developed in England, modified to meet American combined flow conditions, the study indicates that high solids removal efficiency can be obtained from relatively large flows in relatively small chambers. The significance to local officials of the ability to concentrate solids utilizing very short detention periods and almost no mechanical equipment is very great.

The American Public Works Association was fortunate to be able to utilize the services of three outstanding companies in the development of the study: Alexander Potter Associates, Consulting Engineers; LaSalle Hydraulic Laboratories, Ltd. and General Electric Company, Re-entry and Environmental Systems Division.

The Association believes that the swirl concentrator as a combined sewer overflow regulator may be very useful in many communities in alleviating much of the combined sewer overflow problem In addition, as a pretreatment device in a sanitary sewage or industrial wastes system it should allow treatment facilities to be constructed and operated more efficiently and at less cost.

As combined sewer systems are upgraded and improved regulators constructed to reduce the pollutional impact of overflows on receiving waters, we believe that the swirl concentrator should be considered wherever there is sufficient hydraulic head to allow its dry weather operation.

Samuel S. Baxter, Chairman
APWA Research Foundation

SECTION I
CONCLUSIONS, RECOMMENDATIONS AND OVERVIEW

CONCLUSIONS

1. A practical, simple facility has been developed which offers a high degree of performance in reducing the amount of settleable solids contained in combined sewer overflows as well as enabling the quantity of flow to the interceptor to be controlled, all with a minimum of moving equipment.
2. The design of the swirl concentrator has been developed for rapid calculation of the different elements enabling ready transferability to the regulation of various quantities of flow.
3. The swirl concentrator is very efficient in separating both grit and settleable solids in their middle (>0.2 mm) and larger grain size ranges. By weight, these fractions represent about two-thirds of the respective materials in the defined combined sewage. Separation of the smaller grain sizes was less efficient, although still appreciable.
4. The concentrator appeared to exhibit preferential limits of grain sizes separated according to the elements being tested.
5. The floatables trap and storage arrangements should capture most of the lighter than water pollutants. Its dimensions are such that oversize floating objects would jam it, and tend to go over the weir rather than stay in the chamber to clog the foul outlet.
6. Both the floatables trap and foul outlet are easy to inspect and clean out if necessary, during dry weather flows.
7. Sufficient head must be available either by depth to the interceptor sewer from the collector or by provision for insystem storage in the collector to allow operation of the facility.

RECOMMENDATIONS

1. A demonstration facility should be constructed of sufficient size to be totally effective for flows of 103 cfs. The facility should be monitored to verify the hydraulic and mathematical modeling which was accomplished in the study.
2. Research should be directed at narrower grain size bands; for example, a chamber which would separate only the fines might do so with a much higher efficiency.
3. Additional hydraulic and mathematical modeling should be accomplished to determine the effectiveness of the swirl concentrator concept in the various phases of primary sewage treatment. Such research should also have application in many industrial waste situations.
4. Further investigation should be made to determine if better efficiency could be obtained with two or more concentrators operated in parallel or in series.

OVERVIEW

A report by the American Public Works Association published in 1970 gave the results of a study of combined sewer overflow regulator facilities. Design, performance and operation and maintenance experiences from the United States and Canada, and in selected foreign countries were reported. It was evident that North American practice has emphasized the design of regulators simply as flow splitters, dividing the quantity of combined sewage to be directed to the treatment facilities, and the overflow to receiving waters. Little consideration was given to improving the quality of the overflow waste water.

In the current study, hydraulic laboratory tests and mathematical modeling strongly indicate that it is possible to remove significant portions of settleable and floatable solids from combined sewage overflows by using a swirl concentrator. The practical, simple structure has the advantages of low capital cost; absence of primary mechanical parts should reduce maintenance problems; and construction largely with inert material should minimize corrosion. Operation of the facility is automatically induced by the inflowing combined sewage so that operating problems normal to dynamic regulators such as clogging will be very infrequent.

The device, as developed, consists of a circular channel in which rotary motion of the sewage is induced by the kinetic energy of the sewage entering the chamber. Flow to the treatment plant is deflected and discharges through an orifice called the foul sewer outlet, located at the bottom and near the center of the chamber. Excess flow in storm periods discharges over a circular weir around the center of the tank and is conveyed to storage treatment devices as required or to receiving waters. The concept is that the rotary motion causes the sewage to follow a long spiral path through the circular chamber. A free surface vortex was eliminated by using a flow deflector, preventing flow completing its first revolution in the chamber from merging with inlet flow. Some rotational movement remains, but in the form of a gentle swirl, so that water entering the chamber from the inlet pipe is slowed down and diffused with very little turbulence. The particles entering the basin spread over the full cross section of the channel and settle rapidly Solids are entrained along the bottom, around the chamber, and are concentrated at the foul sewer outlet.

Figure 1, Swirl Concentrator Final Form, depicts the final hydraulic model layout showing details such as the floatables trap, foul outlet and floor gutters.

The swirl concentrator may have practical applications as a degritter, or grit removal device for sanitary sewage flows or separate storm water discharges of urban runoff waters. It may have capabilities for the clarification of sanitary sewage in treatment plants, in the form of primary settling or, possibly, final settling chambers. It might be used for concentrating, thickening, or elutriating sewage sludges. It may be serviceable in the separation, concentration and recycling of certain industrial waste waters, such as pulp and paper wastes or food processing wastes, with reuse of concentrated solids and recirculation of clarified overflow waters in industrial processing closed circuit systems.

In water purification practices, it may find feasible applications in chemical mixing, coagulation and clarification of raw water. Other uses may prove to be realistic and workable.

Complete reports describing the hydraulic laboratory study and the mathematical modeling are included as Appendices 1 and 2, respectively. The body of the report details the basis of the assumptions used to establish the character and amount of flow to be treated and the design of a swirl concentrator based upon the hydraulic and mathematical studies.

Although the study was performed for the City of Lancaster, Pennsylvania, with a specific point of application defined, all work was accomplished in a manner which allows ready translation application of the results to conditions which might be found at other installations and for other purposes.

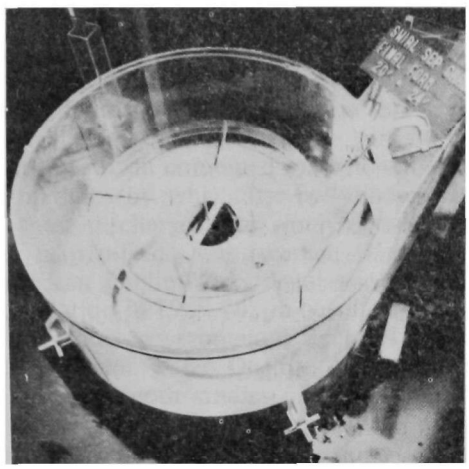

Floatables Trap

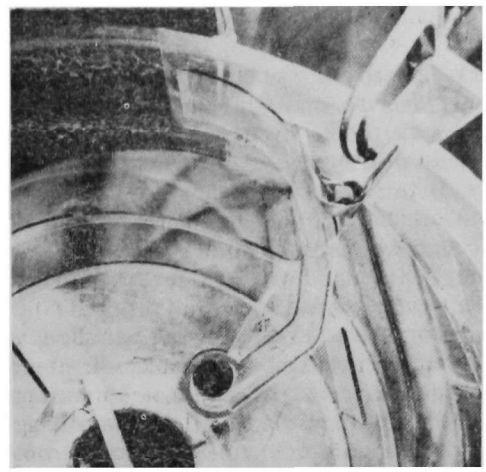

General Layout

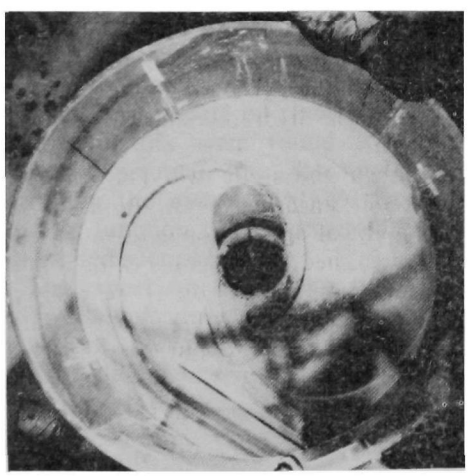

Floor Gutters, Foul Outlet
and Deflector

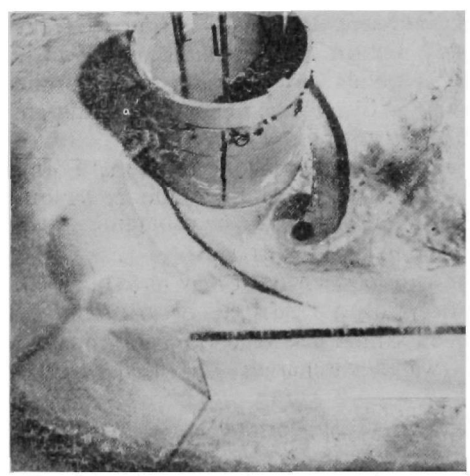

Detail of Foul Outlet
Note Deflector

FIGURE 1
SWIRL CONCENTRATOR FINAL FORM

SECTION II
THE STUDY

A national investigation of the means by which municipal jurisdictions in the United States and Canada regulate and control overflows from combined sewer systems, and of methods by which the pollutional effects of these discharges into receiving waters can be minimized, was carried out by the American Public Works Association Research Foundation in 1969-70, on behalf of 34 sponsoring local governmental agencies and the then Federal Water Quality Administration.

The in-depth studies of combined sewer system regulation practices produced data on the design, construction, operation, and maintenance of various types of overflow control devices and their abilities to cope with the large amounts and the frequency of combined sewer waste waters discharged into receiving streams. Of major significance was the finding that in American practice little or no effort was made to improve the *quality* of the overflow liquids and, thereby, to reduce the pollutional impact on receiving waters. In short, regulators were found to have, in American practice, the sole function of controlling the *quantity* of overflows; and even this function has been carried out with only limited success.

The report on the APWA studies[1,2] of this phase of sewer system management emphasized, perhaps for the first time, the possible "dual purpose" of combined sewer regulator facilities: (1) to control the frequency and duration of overflows to the greatest extent possible; and (2) to improve, by practical means, the quality of the overflow waters by diverting the greatest possible portion of the sewage and storm runoff solids to the interceptor sewer system and downstream treatment facilities. The report coined the phrase, the "two Q's" of overflow control to represent the two functions of quantity control and quality control.

The investigation disclosed that European practices laid greater stress, at least in some measures, on improvement of the quality of storm overflows from combined sewers by various mechanical-hydraulic means. These included types of screens or bar racks and scum baffling and retention devices. One of the promising methods of quality control in combined sewer regulator overflows was the so-called circular "vortex" device used in the City of Bristol, England. Two such devices were installed several years ago and have functioned satisfactorily.

This circular chamber concept was evolved in order to obtain adequate weir length for overflow discharge without the expense of constructing a long side-spill weir for this purpose. At Bristol, laboratory studies were carried out on this configuration to ascertain its hydraulic characteristics and performance, prior to construction of the facilities in 1964. As a bonus, it was found that this type of overflow control device was able to concentrate combined sewage solids by separation of the solids from the liquid phase in the flow pattern and to divert as much as 70 percent of these solids to the "foul sewer" tributary to the sewage treatment works. Thus, it was felt that this type of hydraulic regulator facility, without use of any moving parts, provided the "two Q" principle ennunciated by the APWA in its study and the report thereon.

In order to focus attention on the dual-purpose function of regulators and to emphasize the need for greater knowledge of the hydraulic means by which quality control can be enhanced, the APWA Report made the following recommendation:

> "Regulators and their appurtenent facilities should be recognized as devices which have the dual responsibility of controlling both quantity and quality of overflow to receiving waters, in the interest of more effective pollution control.
>
> "Further research should be sponsored by the FWQA to determine the ability of new devices to induce separation and interception of concentrated pollutional solids and liquors, and the decantation of dilute storm water–sanitary sewage admixtures to receiving waters; to determine

practical applications of such devices and systems; to demonstrate their potentiality by means of mathematical modeling; and to determine cost-benefit relationships."

Reference in the recommendation of the APWA study report was to "new devices;" the device which offered the most promising ability to separate solids from liquid and produce the "two Q's" results appeared to be the so-called "vortex" system researched and used in the Bristol installations. Staff members of the regulator research team visited the Bristol units, conferred with Bernard Smisson, Senior Engineering Assistant, City Engineer's Office, and reviewed his findings and reports on his research of the rotary motion principle involved in his units.

The British "Vortex": Solids Concentration by "Swirl" Action

Longitudinal flows of combined sanitary sewage and storm water tend to either hold solids admixed with the liquid phase, due to scouring velocities or agitation, or to allow solids to settle out or stratify in the liquid flows due to the influence of non-scouring velocities on suspended materials that are sufficiently heavier than water to react to gravity influence. The principle of sedimentation utilizes this phenomenon. The removal of heavier grit in grit separation units, and the eventual removal of lighter solid fractions in settling chambers utilize gravity solids-classification as the underlying means of removing unwanted materials from wastewater flows. Solid materials, or solidified liquid fractions that are lighter than water, become floating materials and are removed in standard treatment practice by means of intercepting baffle arrangements and/or by manual or mechanical skimming devices.

These removal processes are dependent on settling characteristics of solid particles and the time involved in producing the degree of removal desired. This time element is of great importance in the design of solids-removal facilities because they influence the size of chambers that will provide adequate volume for the lowering of velocities and the deposition of wastewater solids. The concept of removal of wastewater solids by means of other forces rather than vertical gravity phenomena, in relatively short periods of time, and therefore, in facilities of relatively small volumetric size and at greatly reduced cost, lies behind the proposal to utilize some form of concentric flow pattern to achieve this result. The so-called "vortex" principle utilized at Bristol, and discussed in the APWA study report on combined sewer overflow practices, utilizes this method of producing the separation and concentration of solids from such flows.

The "vortex" terminology used in Bristol, England, and referred to in the APWA studies was adequate to define and characterize the original concept. However, the investigatory work described in this report, working with much larger flows in minimum-sized chambers shows that a vortex flow pattern must be avoided. A different hydraulic condition can be developed which will still effectively remove solids. The device involved in this study for Lancaster, Pa., can be defined as a *swirl concentrator.*

The purpose of this flow configuration is to induce swirl action in the liquid and liquid-borne solids and, thereby, to induce the classification of the total flow into deposited solids, as a concentrated slurry, in the underflow; the discharge of clarified supernatant liquid in the overflow; and retention of floating solid fractions at the upper surface of the clarified effluent. This separation and concentration of the fractions would then provide for the discharge and transportation of the concentrated solids-liquid underflow to interceptor conduits and treatment works; the discharge and transportation of the clarified liquid to receiving waters, treatment devices, or to holding chambers which are designed for pump-back into the interceptor system during periods of non-peak flows; and the disposal of the entrapped floatables by whatever means best applying to such an installation.

This very simple description of the liquid-solids separation and concentration principle offers a restricted definition of the

application of such devices and configurations for the improvement of combined sewer overflow wastewaters discharged through regulator devices to receiving waters. If the principle is valid, the applicability of this flow configuration, and the geometrics of the structural chamber and its internal details to induce this type of flow pattern, should be applicable to many other processes and procedures in the handling and treatment of liquid-solids flows in the municipal and industrial fields.

The Lancaster, Pa., Installation

An opportunity to supplement the work carried out at Bristol, England, and to apply it under American combined sewer conditions, has been provided by the plan of the City of Lancaster, Pa., to construct a new combined sewer overflow storage-pump-back and partial-treatment facility downstream of a regulator installation. While specifically motivated by the Lancaster plan, such installations based on the swirl principle could have practical applications in other comparable combined sewer regulator-overflow problems.

A demonstration of the "two Q" dual function of combined sewer overflow regulators can be achieved at Lancaster by installing a swirl concentrator regulator to divert the greatest possible concentration of solids slurry to the interceptor and sewage treatment works. In Lancaster the regulator will act to minimize flow of solids to a flow equalization device (a deep silo). It will also be evaluated as to its suitability as a treatment device by itself. A flow sheet of the proposed Lancaster installation, showing the juxtaposition of the swirl concentrator, is presented in Figure 2, Lancaster Flow Diagram.

The Lancaster facility will provide a demonstration or prototype swirl concentrator which will receive the combined sewer flow; a silo-shaped storage chamber for the clarified overflow from the concentrator, and a wet well and pumping station to deliver the concentrate underflow slurry, via a "foul sewer" connection, into the interceptor sewer. The City of Lancaster plans to install a grit chamber on the foul sewer to protect the wet well and pumps. The silo will provide mixing-aeration of the stored liquid. The supernatant liquid may then be passed through a micro strainer and chlorinated before being discharged into Conestoga River. The contents of the silo, or any portion thereof, can be pumped back into the interceptor sewer during low-flow periods. Flexibility of design will enable any of the above storage and treatment devices except the swirl concentrator to be by-passed in order to demonstrate and evaluate their individual characteristics and performances, or the performances of any group of such units functioning together. Thus, the Lancaster installation will serve as a full-scale demonstration of various types of combined sewer handling methods, including the swirl concentrator. Adequate monitoring-sampling facilities and locations will be provided to determine the two factors of quantity and quality at various stages of combined sewer flow and treatment.

The Lancaster installation could provide a demonstration of the validity of the swirl principle if it is preceded by carefully planned and recorded hydraulic pilot studies and supported by mathematical modeling which would provide basic design criteria applicable to the Lancaster project and, coincidentally, to any other installation of comparable nature. At one and the same time, this procedure would confirm the original Bristol work; provide engineering data to rationalize modifications of the Bristol geometric configurations and flow patterns to American conditions; and develop design criteria correlations which could be used for the Lancaster swirl concentrator and be used by designers for other projects in the combined sewer field or any of the other applications described above.

Study Plan

To accomplish this purpose, the American Public Works Association, under contract with the City of Lancaster, Pa., has completed the research study. The scope of the study was to investigate the use of *vortex* storm sewage (combined sewer) separators,

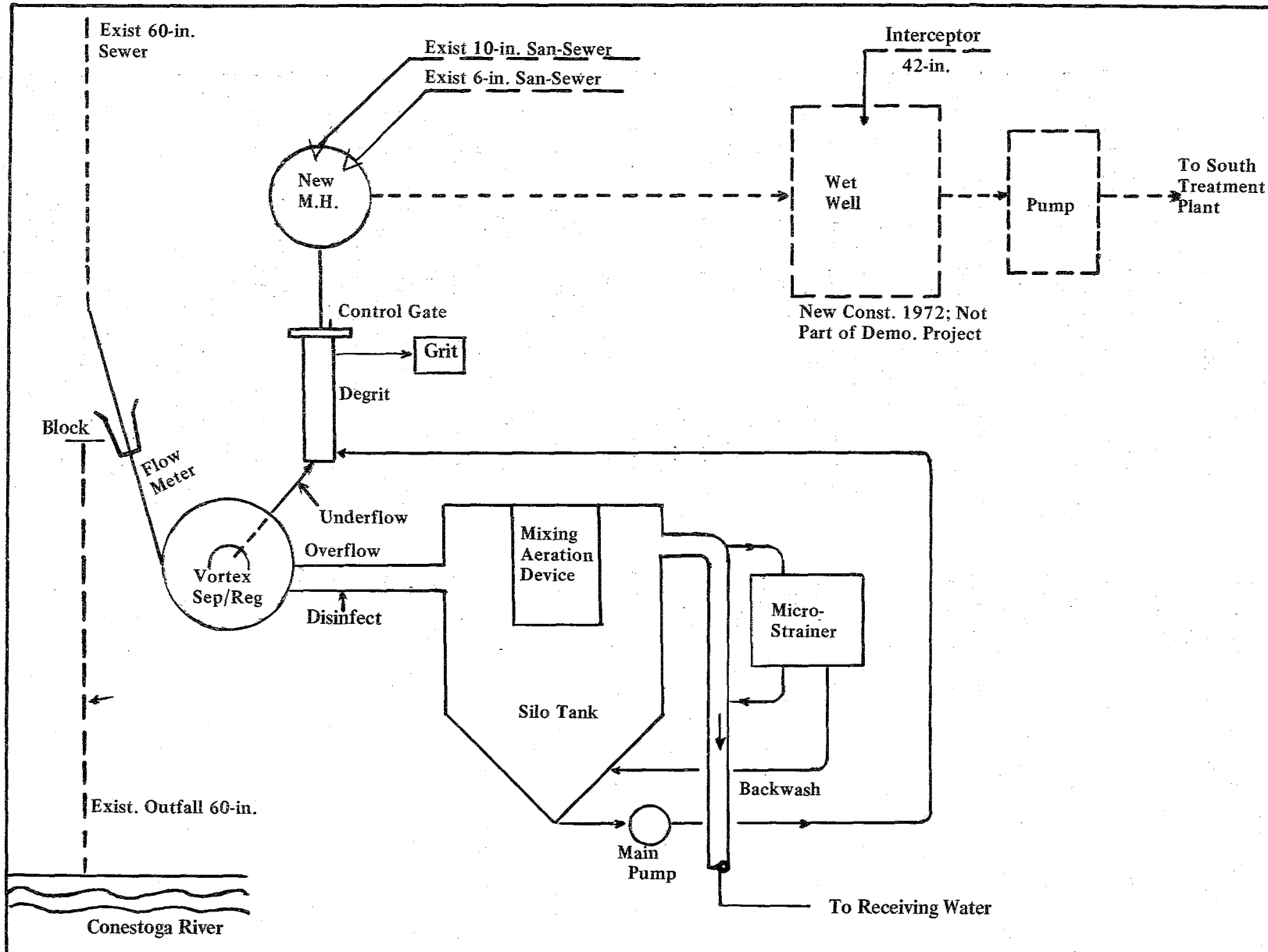

FIGURE 2
PRELIMINARY LANCASTER FLOW DIAGRAM

involving the development of studies by "mathematical modeling correlated with hydraulic laboratory modeling, to determine the degree of efficiency which might be associated with construction of such facilities and design relationships."

The La Salle Hydraulic Laboratory Ltd. (Laboratoire D'Hydraulique) La Salle, Quebec, Canada, was engaged to conduct the hydraulic modeling studies. The General Electric Company, Re-entry and Environmental Systems Division, Philadelphia, Pa., was retained to carry out the mathematical modeling phase of the study.

In order to utilize the basic knowledge and experience gained in the Bristol, England, investigations of the so-called "vortex" principles and the actual construction of two such regulator-separator units, the innovator and investigator of these developments, Bernard Smisson, was retained as consultant. Direct contacts with the American studies were maintained by Mr. Smisson by means of an on-site period of conferences and data reviews at the La Salle Hydraulic Laboratory, and by periodic exchange of data and other correspondence.

Consultative services were arranged with the firm of Alexander Potter Associates, New York City, a consulting engineering firm widely experienced in the hydraulics and design field, and with experienced individual engineers, to help guide modeling studies and to correlate the findings in the course of the hydraulic and mathematical modeling investigations. Section VII lists the many individuals whose efforts made this complex study possible.

Underlying Assumptions of the Modeling Studies

Before the hydraulic and mathematical modeling work could be undertaken, it was necessary to establish underlying assumptions that would assure the investigators that their work and their findings would be in consonance with recognized and expected liquid flow and solids characteristics in representative American combined sewer wastewaters, and therefore applicable to the Lancaster installation. These basic investigative assumptions had to be grounded in known principles of liquid flow and particle flow characteristics and phenomena under combined sewer conditions.

The following factors were accepted as the basic assumptions for the investigations by the technical consultative group and the two developers of the mathematical and hydraulic modeling data.

Configuration: The research work at Bristol and the actual details of the so-called "vortex" chamber installed at White Ladies Road were utilized as the basic starting point for the study of the swirl concentrator covered by this report. Modifications of dimensions, internal appurtenant structures and flow patterns for concentrated underflow solids, overflow liquid and floatables entrainment and removal were made to provide optimum performance of the "two Q" functions of the hydraulic model and of the mathematical confirmation of the hydraulic conditions.

The White Ladies Road device as shown in Figure 3, provided an 18-foot-diameter chamber; an overflow weir; a scum ring for retention of the floating material mounted on the central column; and a "foul sewer" outlet for the concentrated solids. Other essential features in the chamber were provided. Flow entered the circular chamber tangentially at the floor level. The foul sewer outlet was located on the floor of the chamber, near the central column, at a point where it would collect the solids deposited on the floor of the chamber. The supernatant clarified liquid overflowed the weir and was discharged to receiving waters.

Figure 4 contains general photographs of the model. Figure 5, Photograph of Initial Hydraulic Test Model, shows the model being operated at a simulated 165 cfs with and without a deflector. Without the deflector, a free vortex was formed which resulted in a low solids separation efficiency.

No Moving Parts: One of the fundamental advantages foreseen for the swirl concentrator principle is the absence of any moving or mechanical parts in the chamber, and its self-cleansing of deposited solids by

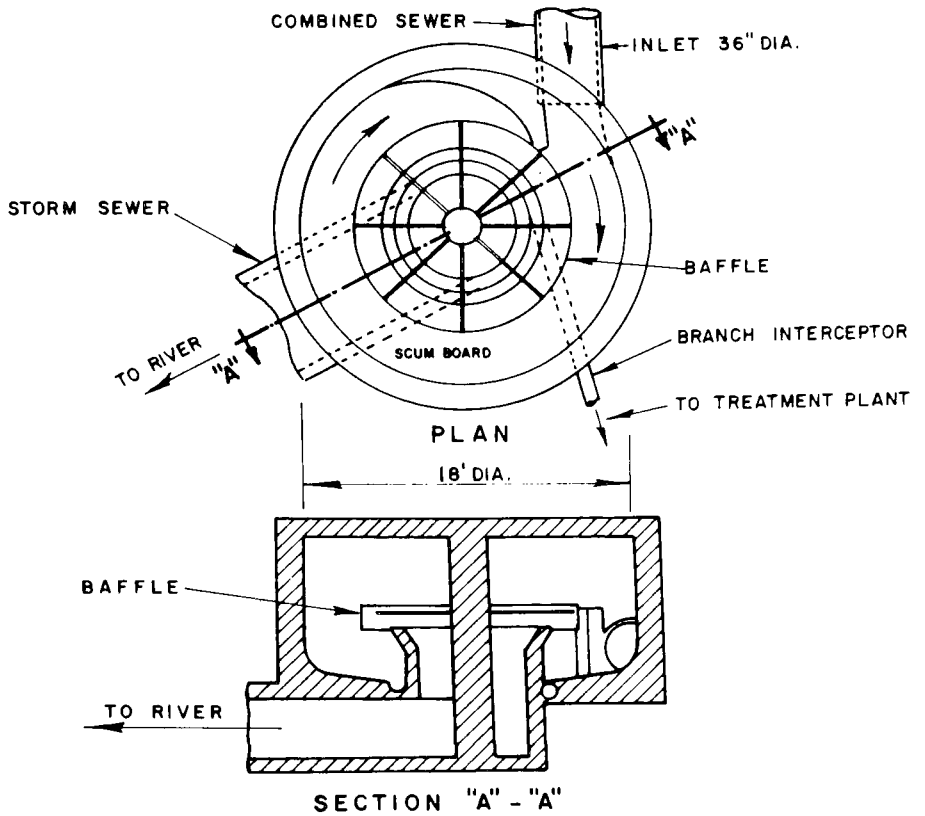

FIGURE 3
WHITE LADIES ROAD – VORTEX REGULATOR

utilization of the flow patterns created by the configurations of the device. This is in contrast with standard facilities for removing grit and lighter suspended settleable and floatable solids from sewage and other waste waters, which require some form of collection and removal mechanisms to perform this function.

The removal of such solids from the body of liquid and from the swirl chamber is induced by the liquid body itself as a result of the flow patterns set up by the geometric configuration of the unit. Absence of moving parts, which was one of the important assumptions established for the study of the swirl concentrator principle, overcomes hydraulic impedances caused by the intrusion of mechanical collection equipment and the sub-agitations caused by the movement of collectors even at slow rates. Mechanical breakdowns and the need for standby equipment for use during repair shut-downs are avoided in the swirl arrangement. Corrosion of metallic parts could be avoided by construction of a swirl chamber with inert materials.

Particle Sizes of Solids in Combined Sewer Flows: It was necessary to artificially simulate the solids components used in the hydraulic and mathematical model studies, for the purpose of making the laboratory investigations translatable into what might be assumed to be a representative combined sewer flow of admixed sanitary sewage and storm water runoff. Since it was not possible to use actual combined wastes in the scaled-down hydraulic model investigations, it was necessary to reproduce ranges of particle

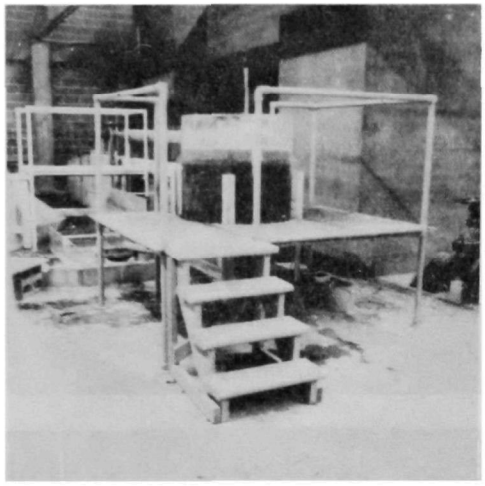

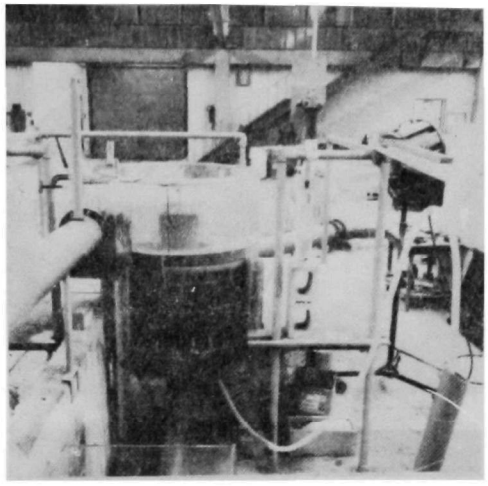

General Views of Model

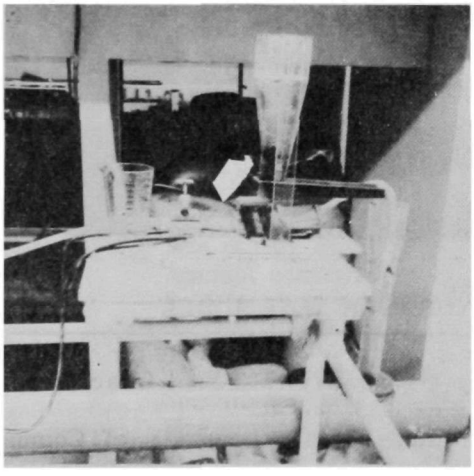

Vibrator Solids Injection System

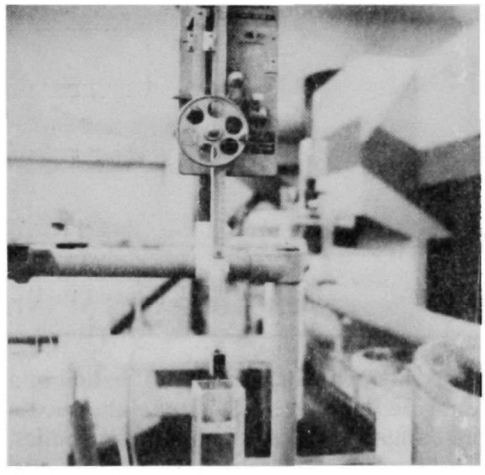

Precision Point Gauge to Measure Water Levels in Chamber

FIGURE 4
PHOTOGRAPH OF MODEL SETUP

sizes and specific gravity by simulation. It was not possible to reproduce all size and gravity ranges, nor was this essential to the accuracy of the model studies because combined sewer flows vary markedly in composition from day to day and from season to season in the same system, and even more markedly from community system to community system. As a result, no single truly representative combined sewage-storm water "analysis"

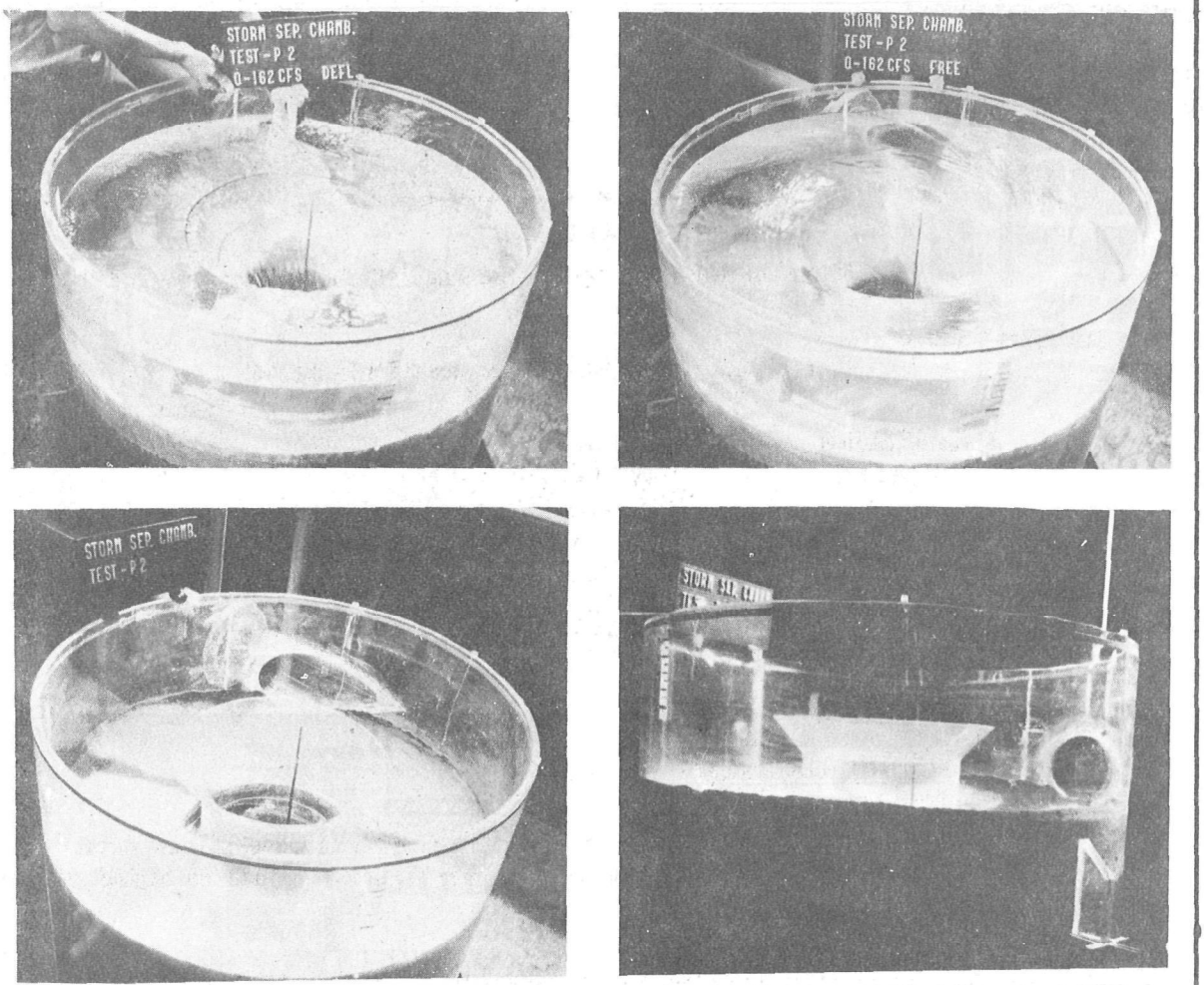

FIGURE 5
PHOTOGRAPHS OF INITIAL HYDRAULIC TEST MODEL

could be set forth for the studies. In lieu of a single agreed-upon solids size and specific gravity composition for the hydraulic studies, various ranges were investigated.

After intensive reviews of recorded analytical data for representative flows from various systems, and consideration of all of the factors outlined above, an acceptable "range" of particle sizes and specific gravities was chosen for the studies. Decisions were based on data provided by Alexander Potter Associates, the Environmental Protection Agency and the LaSalle Hydraulic Laboratory. Due consideration was given to information published on British practice and, in particular, the work of Smisson,[3] Ackers, Harrison, Brewer,[4] Prus-Chacinski and Wielgorski.[5]

Table 1, Determination of Combined Sewage Solids, presents the rationale used to develop the combined flow solids particle decisions on sizes, concentrations and specific gravity. The table is intended as symbolic of the distinctions made for the study between grit, suspended solids and floatable solids.

From the solids particle studies for the hydraulic-mathematical model studies it was necessary to make a basic assumption of the firm analytical data to be used. Table 2, Specific Gravity, Size and Concentration of Settleable Solids, indicates the settleable solids characterization simulated in the

hydraulic laboratory.

Simulation of these materials for use in the hydraulic model was based on settling velocities according to Stokes equation:

$$V = \frac{gd^2 (\rho_s - \rho_w)}{18\mu}$$

where: V is settling velocity
d is particle diameter
μ is water viscosity
ρ_w is density of water
ρ_s is density of solids

TABLE 1

Determination of Combined Sewage Solids

A. Sewage Composition

1. Average Composition of Domestic Sewage, mg/l[1] p 564

State of Solids (1)	Mineral (2)	Organic (3)	Total (4)	5-day, 20 C BOD (5)
1. Suspended	85	215	295	140
a. Settleable	50	130	180	65
b. Non-settleable	35	85	115	75
2. Dissolved	265	265	530	40
3. Total	350	480	825	180

2 Organic Matter:[1] p 563

40% nitrogenous matter
50% carbohydrates
10% fats

Settleable Solids: will settle to bottom of Imhoff cone in one hour.[2]
Non-settleable Solids: will not settle nor float to surface in period of one hour.[2]

3. Grit:[1] p 613

Specific gravity 2.65
Size usually captured in grit chambers up from 2×10^{-2} cm diameter
Amount collected: 1 to 12 (average 4) cu ft per million gallons
Daily maxima reported: 10-30 cu ft per million gallons and as high as 80 cu ft per million gallons

4. Sewage Solids except Grit[1] p 609

Specific gravity 1.0 to 1.2 on dry basis—1.001 on wet basis
Size up to several centimeters in diameter
Size of 10-1 cm will have settling velocity of 4.2×10^{-2} cm/sec

B. Suggested Synthetic Sewage – full size model

1. Grit

Specific gravity 2.65

	cuft/mg	lb/mg[a]	mg/l[b]
From Fair[1]	1	100	12
	4	400	48
	12	1200	144
	30	3000	

a) Assuming 100 lbs per cf
b) lb/mg ÷ 8.33

TABLE 1 (continued)

2. **Settleable Solids** (excluding grit)

	Fall Velocity mm/sec	sg	Size mm
Smisson	2.5 to 7.5	1.19	0.18 to 0.42
Ackers	61[3]	1.005	25
Prus-Chacinski	–	1.05	1.6 to 3.2
Fair	0.4	1.0 to 1.2	1 to 75
	for 1 mm size		
Use	0.4 to 2	1.1	1 to 5 mm

Velocity to settle in 10 foot tank in 2 hours
10 x 305 mm in 2 x 60 x 60 sec
= 3050 mm in 7200 sec
= 0.4 mm/sec

Quantity range from 200 to 800 mg/l

3. **Floatable Solids**

		Rise Velocity mm/sec	sg	Size
Smisson	perspex chips			
Prus-Chacinski	perspex chips			
Akers	actual sewage	61	0.995	25 mm
	polythene	21		2 mm

Quantity – assume 10% of settleable solids
Quantity 20 to 80 mg/l

4. **Settleable Solids – excluding grit**

Domestic

Suspended	295 mg/l
Settleable	180
Grit say	25 i.e., 50% of mineral
Settleable sg 1.05	155
Settleable (sg 1.05) =	$\frac{155}{295}$ x 100 = 52% of suspended, say 50% of suspended

For domestic sewage settleable (excl. grit) = 150 mg/l

From Journal WPCF Jan. 1968 p 122 Burm, Krawczk, Harlow, "Suspended solids consisted generally of between 70 and 90% settleable solids in both sewage systems." i.e., combined and separate storm.

TABLE 1 (continued)

Maximum suspended solids from reports

11024 FKN 11/69	p 156	1700 to 500 mg/l
Bucyrus, Ohio	p 157	1000 to 500 mg/l
	p 158	1000 to 300 mg/l
11023 FDD 03170	p 27	325 to 70 mg/l
Portland, Oregon		
111023 EVD 06170	p 26-27	498 to 21 mg/l

For combined sewage, settleable solids might range

from 70% x 300 = 210 mg/l
90% x 1700 = 1530 mg/l

Say, floatable = 10% of above

Use Floatable 20 to 150 mg/l
Use Settleable 200 to 1400 mg/l

Portland, Oregon Study[4]
Comparison of Combined Flow and Dry Weather Flow

	Mean	Min.	Max.	Mean	Min.	Max.
Settleable solids mg/l	3.1	1.5	5.0	4.8	2.5	7.0
Total suspended solids ml/l	146	70	325	129	50	244

Use of 165 mesh (105 micron opening) screen will remove 99% of floatable and settleable solids, and 34% of total suspended solids.

Note: 105 micron = 0.105 mm

---

[1] Fair, G.M. and Geyer, J.C., *Water Supply and Waste-Water Disposal,* (John Wiley and Sons, Inc., New York, 1954).
[2] Glossary—Water and Wastewater Control Engineering
[3] 0.2 ft/sec = 61 mm/sec
[4] 11023 FDD 03/70 *Rotary Vibratory Fine Screening of Combined Sewer Overflows*

TABLE 2
Specific Gravity, Size and Concentration of Settleable Solids

	Material	Specific Gravity	Concentration (mg/l)	Particle Size	Particle Size Distributed					
(1)	Settleable Solids excluding grit	1.05 → 1.2	200–1550	0.2 → 5 mm	Particle size (mm)	.2	.5	1.0	2.5	5.0
					% by weight	10	10	15	25	40
(2)	Grit	2.65	20–360	0.2 → 2 mm	Particle size (mm)	.2	.5	1.0	1.5	2.0
					% by weight	10	10	15	25	40
(3)	Floatable Solids	0.9 → .998	10–80	5 → 25 mm	Particle size (mm)	5	10	15	20	25
					% by weight	10	10	20	20	40

The material most used in the hydraulic testing program was gilsonite, a natural hydrocarbon with a specific gravity of 1.06 and a grain size between 1 and 3 millimeters. Following the Stokes relation at a scale of 1:12—laboratory test unit to full-sized prototype—this material reproduces grit between 0.36 and 1.06 mm and settleable suspended solids between 1 and 3 mm.

This grit range leaves a small part of the fines unrepresented, as well as a wide part of the coarser particles. The coarser end of the scale was assumed to be covered, since any larger particles would obviously settle out if those represented in the chosen material had settled. The fines at the lower end of the scale in turn were simulated with Petrothene®, a compounded plastic with grain sizes between 2 and 4 mm and a specific gravity of 1.01.

Similar reasoning was utilized in establishing particle characteristics to simulate settleable suspended solids. The large gilsonite covered a significant part of the middle size range and the larger particles were considered to have been removed if the gilsonite settled. On this basis, the large gilsonite represented 65 percent by volume of the settleable solids in the specified prototype combined sewage-storm water runoff. Two finer fractions of ground gilsonite were tested to cover the fines. The first, which passed 25-mesh and was retained on 30-mesh, had a mean particle size of 0.5 mm The second, retained on 50-mesh, had a mean particle diameter of 0.3 mm, thereby approximating the finer particles specified as 0.2 mm.

The rates of solids injection used in the hydraulic pilot unit correspond to the 50-300 mg/l range in the prototype flows. Confirmatory tests at a later time increased the settleable solids injection rate up to 1,550 mg/l established for the upper limit of combined wastewater in the Lancaster prototype.

Tests for the removal of floatables were carried out using uniformly sized polythene particles of 4 mm diameter, with a specific gravity of 0.92; and Alathon®, another plastic compound with particle size of 3 mm diameter and specific gravity of 0.96. Injection rates for this material varied from 30 to 150 mg/l, at prototype scale.

Liquid Flow Characteristics: The size of the proposed prototype swirl concentrator to be constructed at Lancaster would, of course, be dictated by the anticipated combined sewer flow conditions in that community's system. The flow information supplied by the city and its consulting engineers, Meridian Engineers, was as follows:

Peak sanitary dry-weather flow—2.9 cfs (say 3 cfs)

Storm flow: (a) intermediate frequency—100 cfs

Storm flow: (b) infrequent peaks—162 cfs

Storm flow: (c) gravity flow capacity of system—450 cfs

An attempt was made to evaluate the ratio of combined flow to sanitary sewage flow and to ascertain flow and velocity characteristics at Lancaster, by means of theoretical computations. Table 3, Flow and Velocity at Lancaster, estimates the flows at the site.

It was decided to evaluate model solids removal efficiencies in the ranges of grit, settleable suspended solids and floatables at not only the 165 cfs maximum range but also at 15 50 and 100 cfs flow levels. A swirl concentrator of the type proposed will have to function with suitable solids removal efficiencies under such widely varying flow conditions. To meet these conditions the chamber must function as a flow-through device, without any need for solids concentration, at dry-weather flow levels of 3 cfs—the same flow rate established as the capacity of the foul sewer outlet at the bottom of the chamber—and varying wet-weather flow conditions greater than 3 cfs.

Scaling—from Theory to Model, to Prototype: The study of the hydraulic model, and the mathematical model which simulated the scale size of the hydraulic laboratory unit, was intended to give confirmatory evidence of the flow patterns and solids behavior which will be produced in the prototype swirl concentrator at the Lancaster site, and other comparable installations. The studies were designed to develop specific design criteria for

the scaling of all component dimensions of swirl facilities by consulting engineers and municipal engineering officials, relating to inlet features, overflow features, foul sewer connection features, floatable solids entrapment and removal details, and incidental internal flow control features.

It is evident that the behavior of the liquid phase and solids phase of the separator-concentrator device will be

TABLE 3

Flow and Velocity at Lancaster

Preliminary Estimate (Rationale used prior to metering of flows)

Ratio of combined flow to sanitary flow

1. **Other Areas**

Camp – Sewage and Industrial Wastes April 1959

For storms of frequencies from 5 years to 25 years ratio of storm flow to average sanitary flow will be 50 to 200

Flow estimates for Staten Island by Alexander Potter Associates

Peak storm flow for 5-year frequency

Sanitary from residential area

Section	Area Acres	Storm cfs 5 yr	Av. San. cfs	Peak San. cfs	Ratio Storm Av. San.	Ratio Storm Pk. San.
1	393	827	3.2	10.7	258	77
8 (part)	100±	212	1.2	3.63	176	58
8 (part)	163	305	1.7	5.0	180	61
				Σ	614	196
				Av	205	68
	100	128	0.36	0.85	355	150

Assume density of 10 persons per acre and C = 0.3 instead of above

From the foregoing the ratio of the 5-year flow to the average sanitary flow may vary from 50 to 350.

2. **Study Area**

Study Area 130 acres

Assume 40 persons per acre

100 gpcd sanitary flow and infiltration

Av. sanitary flow = 130 x 40 x 100 = 520,000 gpd = 0.81 cfs

Peak sanitary flow = 0.81 x 36 = 3 cfs

Peak storm flow = 200 x 0.81 = 162 cfs

Present combined sewer is 60-inch diameter

For Q = 162 cfs D = 60 in. n = .013

s = 4 ft/100 ft

v = 8.6 fps

For Q = 2.9 cfs

$$\frac{q}{Q} = \frac{2.9}{162} = .18$$

From chart $\frac{d}{D} = 0.09$, $\frac{v}{V} = 0.37$

dependent on the following parameters: configuration and geometrical dimensions; the ratio of influent flows to foul sewer concentrated slurry flows; and particle sizes, concentrations and specific gravity in the influent flow. The proposal was to make qualitative analyses of the relationships between these basic factors in various combinations, in order to achieve maximum efficiency of solids removal and, thereby, to produce the highest possible overflow quality with the least adverse impact on receiving waters.

Normal scaling laws were used to establish the geometry of the hydraulic model and, in turn, of the mathematical model used in verifying the hydraulic findings. A ratio of 1:12 was used for converting the laboratory model to actual prototype size.

The liquid mass, being water, remained constant in both the model and the translated prototype unit. Consequently, the solids particles were scaled down in the model studies to represent full-scale size and specific gravity conditions that will be experienced in the prototype unit. The expected solids characteristics in the combined sewer flows would thus be simulated in the hydraulic laboratory work. Limitations in such solids scale-downs were recognized, as outlined previously. If the sizes of particles were scaled down to simulate laboratory conditions, the coefficient of drag of the particles imposed by the liquid would cause the particles to behave under different settling velocities than those which will be passing through the full-scale prototype installation. To reproduce prototype conditions, settlement velocity curves were developed and confirmed by both hydraulic and mathematical modeling. This involved relating particle size to specific gravity, making it possible to follow the Stokes equation in reducing the scale size to one-twelfth of the proposed prototype size and in altering the particle sizes and specific gravities to reproduce the same velocity settlement characteristics for any combination of solids characteristics.

For example, gilsonite having a size of 1 to 3 mm and a specific gravity of 1.06 reproduced grit particles at the prototype scale between 0.36 and 1.6 mm and a specific gravity of 2.65. The greater laboratory-scale size and the lower specific gravity reproduced the expected combined sewage characteristics having a smaller size and higher specific gravity. This same settling efficiency was duplicated in the hydraulic tests with lighter settling solids having a size range from 1 to 3 mm and a specific gravity of 1.01 to 1.2.

Hydraulic scaling was applied to a limited number of cases. Actual modeling was based upon similitude of settling velocities, i.e., a 1-3 mm gilsonite particle will settle at the same rate as suspended solid particles of specific gravity 1.2 with a size range of 0.34-1.00 mm, as well as grit.

Translating Model Studies to the Bristol Investigations

Reference has been made to the original investigations of the swirl concentrator principle (there referred to as the "vortex") at Bristol, England, and to the actual performance of this system at two locations in that city. In essence, the Bristol development was based on cut-and-try procedures, with configuration modifications made in model units to produce the desired solids removal efficiencies. What was lacking in the British experience was a mathematical evaluation of the liquid and solids flow patterns achieved in the chamber and the conversion of this evaluation into specific design criteria. The studies involved in the current project were designed to provide these missing facts.

The Bristol pioneering work, in that sense, served as the preliminary phase of the swirl chamber investigation. It provided the guidelines for shaping and dimensioning the American hydraulic model, subject to mathematical confirmation of the geometric patterns utilized and the subsequent changes of configurations built into the model to improve liquid-solids control, separation and concentration.

As stated by the LaSalle Hydraulics Laboratory in its final report, Appendix 1, on its modeling investigations: "The general principle which Mr. Smisson had developed and utilized did not fit the definition of

known laws of either vortex or simple gravity settlement, but rather appeared to be a controlled combination of the two . . . . . Mr. Smisson's publications covered his work up to 1967, and the first hydraulic tests served as a verification of these principles. Since 1967, his research has led him to modify the geometry of the chamber in some degree.

"The main difference in the European and North American conditions was in the discharge/chamber volume ratio. The aim was to use a similarly sized chamber as Mr. Smisson utilized but to treat from four to six times as much flow.

"The first model geometry selected for the hydraulic studies was based on the latest data from Bristol. It took the form of a flat-floored chamber, with a central column one-sixth of the chamber diameter, supporting a flat weir plate about five-sixths of the chamber diameter. A weir and weir skirt were attached to the outer circumference of the weir plate. The research program investigated the importance of chamber depth, the shape of the entrance to the chamber, and different weir diameters to obtain the optimum removal of settleable solids through the foul sewer outlet.

"The latest Bristol work included the use of an oblique entry to the chamber. With the flow from the chamber wall toward the central shaft, it had been proven possible to trap floatables under the weir. It was found that a skirt hanging below the weir would retain the floatables under the weir plate. When the water level dropped in the chamber, these trapped, lighter-than-water solids descended on the water surface and could be evacuated through the foul sewer outlet.

"The skirt served the purpose of creating a shear zone which effectively divided the chamber into two water mass parts: an exterior liquid mass in which the flow moved relatively rapidly; and an interior liquid mass which rotated more slowly. Proper exploitation of these two zones could enhance the ability of the chamber to produce solids separation and concentration. The longer trajectory of the outer mass would allow sufficient time for heavier solids to settle to the floor while the slower movement in the inner mass would allow finer settleable solids to settle out. Manipulation of these research parameters was directed toward organizing the flow in the chamber to pass continuously through the two zones so as to take maximum advantage of their respective hydraulic characteristics."

The Hydraulic Model and Testing Procedures

The LaSalle Hydraulics Laboratory report on various changes in its model and the testing procedures used to determine the flow patterns and solids removal characteristics of all modifications is contained as Appendix 1 to this report.

The Mathematical Model

The methods utilized by the General Electric Company in carrying out the mathematical modeling work on the swirl concentrator are described in its final report, which is included as Appendix 2 to this report.

The general objective of the mathematical model study was to develop a representative model and computer simulation of a swirl chamber device to separate floatable solids, grit and suspended solids from storm water overflows and to produce, thereby, a higher quality of supernatant wastewater for discharge into receiving waters or into storage and/or storm water overflow treatment facilities. In conjunction with the hydraulic laboratory studies carried out at the LaSalle Laboratory, the analytical model was devised and used to predict variations in performance of the swirl concentrator under conditions of variable design criteria and, thereby, to arrive at an optimum configuration for the unit.

A prototype chamber was modeled in hydraulic and mathematical studies and specific calculations were performed for both the laboratory model and the proposed prototype unit to be installed at Lancaster, Pa. Over and above the specificity of the mathematical investigations of Lancaster conditions, the results are applicable to a broad range of chamber sizes, flow rates and particle characteristics. This broad applicability was achieved by developing a set of scaling laws based on the necessary

governing equations. With the scaling laws, the results of the hydraulic studies and the computer calculations can be extended to chambers of other sizes and flow rates, provided only that geometric similarity is maintained.

The following information on liquid flow calculations and particle flow calculations in the mathematical modeling procedures has been excerpted from the General Electric Company report, to serve as an introduction to this work.

"The general approach of this study has been to calculate the liquid flow field within the swirl concentrator, neglecting the presence of the particles (i.e., assuming a dilute mixture). This was accomplished by using a relaxation procedure to numerically solve the equations for turbulent axisymmetric flow. A three-dimensional eddy viscosity model was used to relate the local turbulent Reynolds' stresses to the gradients of the mean flow properties. Once the liquid flow had been calculated, the particle flow through the liquid was computed. At each mesh point at which the liquid flow was computed the three particle momentum equations, and the equation of continuity were solved to determine the particle velocities and concentration. The equations included turbulent diffusion terms, virtual mass effects, gravity forces, and drag. The equations were solved with a time-dependent scheme, integrating forward in time until a steady-state was achieved.

"The liquid flow calculation was calibrated by adjusting the mixing length and friction coefficient to provide the best match with the experimental data. The agreement was generally good, but limited by non-axisymmetric flow effects in the physical model due to the inlet and baffle plate arrangements. Using the calibrated liquid flow, particle flows were calculated for several flow rates, particle sizes, and chamber sizes. The results generally showed favorable agreement with the laboratory data although the model tended to over-predict the separation efficiency.

Liquid Flow Calculation

"The calculation of the liquid flow field within the swirl concentrator required making several simplifying assumptions. The two chief assumptions were that the flow was axisymmetric, and that its turbulent character could be modeled. The axisymmetric assumption meant that the flow could be described with only two independent variables (r and z), and was independent of the angular position. This assumption required that the inlet flow which in the actual device entered tangentially through a square duct, be represented by a circumferential region of the wall through which the inflow occurred. The inlet flow through the wall was assumed to have a cubic velocity profile as illustrated in Figure 6, Cross Section of Swirl Concentrator as Represented in Axisymmetric Mathematical Model, with the magnitude adjusted to give the proper mass flow rate. The tangential velocity of the incoming flow was assumed to be constant, and equal to the mean velocity in the entrance channel. These assumptions gave the correct tangential velocity near the outer wall. Also, since the inflow was spread over a large area, the inflow velocity was small, and did not differ appreciably from the actual case in which the radial velocity vanished at the wall.

"The axisymmetric model thus approximated the average behavior of the flow at most radial locations. The differences were largest in the vicinity of the inlet, and, of course, the model could not reproduce non-axisymmetric behavior such as local vortices observed in testing. Similarly, the effect of the baffle plate at the inlet could not be reproduced exactly. However, the chief effect of the deflector baffle was to raise the tangential velocity of the liquid under the weir. This effect could be simulated in the model by proper adjustment of the free constants associated with the eddy viscosity and the wall shear. This procedure gave good agreement with the mean tangential velocity profiles observed in the test program.

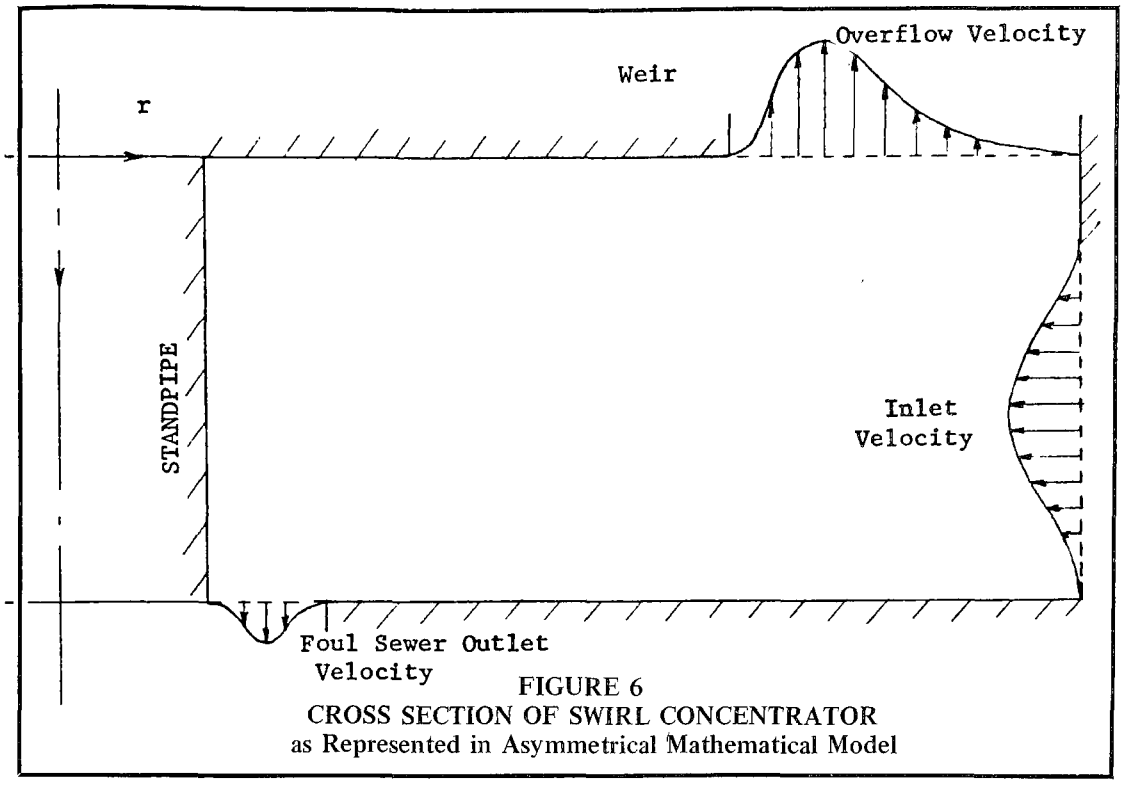

FIGURE 6
CROSS SECTION OF SWIRL CONCENTRATOR
as Represented in Asymmetrical Mathematical Model

The actual turbulent flow was very complicated, and many models could be used to represent the effect of turbulence on the mean motion. The art of turbulent flow calculation is not far advanced, and even for the simpler case of a boundary layer flow, two different computational schemes can give results which differ by as much as 50 percent in some respects. The present model used an elementary eddy viscosity approach which related the turbulence to the gradients of the mean velocities through the use of a mixing length concept. Such a crude approximation could not hope to duplicate the details of the turbulent, time varying flow structure. However, the main features of the internal flow were reproduced reasonably well, and the results gave considerable insight into the behavior of the streamlines within the swirl chamber.

"In keeping with the axismmetric nature of the model, the overflow velocities need to be specified as uniform around the circumference of the weir. This was accomplished by using smooth power series profiles. This procedure represented the overflow velocity fairly well except near the inlet where disturbances due to the baffle plate occurred. The underflow, however, was in reality withdrawn through a single port in the floor rather than uniformly through an annulus as assumed in the mathematical model. For small values of the underflow fraction, the differences were not large. For sizeable underflows, significant non-axisymmetric effects could have been anticipated.

"An additional detail of the actual swirl chamber which could not be modeled, was the skirt which hung below the weir to trap floatables. The computational mesh used for the present calculation was too coarse to permit this detail to be modeled without causing numerical instabilities.

Particle Flow Calculations

"The particle flow within the swirl chamber was calculated, assuming that with sufficiently low concentrations, particle collisions and coalescence could be neglected. The effect of the particles on the structure of the liquid flow field was also neglected. For

sewage concentration less than 1000 mg/l, these were both reasonable approximations. Additional approximations were required to calculate the particle flow. The most significant approximation concerned the effect of turbulence. The turbulent fluctuating liquid velocity induced fluctuations in the particle velocities. In addition, and more importantly, it also causes a diffusion of particles away from the paths they would follow for a laminar motion. The modeling of this effect was crucial because in the absence of turbulence, the particles in many cases would sink directly to the bottom. The turbulence, however, scattered the particles into the vicinity of the weir where they were entrained with the overflow. For this study, the effect of the turbulence was accounted for by adding the approximate diffusion terms to the equations of motion and continuity. The eddy diffusion coefficient was modeled in the same way as the eddy viscosity for the liquid flow."
liquid flow."

Based on the comparisons discussed in the full report, the model appeared to be quite satisfactory in its mathematical form.

SECTION III
GENERAL FEATURES

The swirl concentrator must be sized to function efficiently at a design flow based upon the capacity requirements of the collector system. It will be subjected to widely varying flow and solids content conditions characteristic of combined sewer networks. For an essentially static device to perform efficiently under such conditions, special attention must be given to the various pertinent elements within the chamber as learned from the modeling study.

Figure 7, Isometric View of Swirl Concentrator, identifies the various special features hereinafter discussed.

(a) Inlet Ramp—The inlet ramp was designed to introduce the incoming flow at the bottom of the chamber while preventing a surcharge on the collector sewer immediately upstream. The principal purpose of introducing the inflow at the chamber floor is to introduce the solids at as low a position as possible. The slope of the ramp chosen in the hydraulic model was 1:2. Greater efficiency of separation can be expected as this slope is decreased, making the inflow less turbulent. Local conditions will govern as modifications to the collector sewer upstream of the chamber may be necessary to reduce the slope, and the affected section of the collector sewer would be surcharged during overflow periods.

The floor of the inlet ramp should be V-shaped to the center providing self-cleansing capability during small storm flow events or delay of the hydrograph and a channel for the peak dry-weather flow. It is recommended that the minimum crossflow be one inch per foot.

It is essential that this ramp and its entry port introduce the flow tangentially so that the "long path" maximizing solid separation in the chamber may be developed.

(b) Flow Deflector—The flow deflector is a vertical free-standing wall which is the straight line extension of the interior wall of the entrance ramp extending to its point of tangent. Its location is important, as flow which is completing its first revolution in the chamber strikes, and is deflected inwards, forming an interior water mass which makes a second revolution in the chamber, thus creating the "long path."

Under the energy conditions normal to combined sewer flows, rotational forces in the chamber would quickly form a vortex of negligible separating efficiency if the flow deflector were not used.

The height of the deflector is the height of the inlet port, thus ensuring a head above the wall slightly greater than the weir height during overflow events. This head passes over the flow deflector after one revolution in the chamber and acts as a damper on inflow thus tending to keep incoming solids nearer to the floor and clear liquid at overflow elevations.

(c) Scum Ring—The purpose of the scum ring is to prevent floating solids from overflowing. It, therefore, should extend a minimum of six inches below the level of the overflow weir crest and extend vertically above the crest of the emergency weir. Its diameter is such that its edge is located vertically above the flow deflector, thus further establishing a boundary between the outer and inner flow masses. During overflow events and because of the great difference in volume of water overflowing and discharging to the interceptor, the velocities of the outer flow mass are much greater than those of the inner flow mass, allowing solids in the inner zone a greater opportunity to settle.

For large diameter scum rings—weir configurations, the upward overflow velocity component will be large. Any particles entrained in this flow will be readily swept out with the overflow. As the scum ring diameter is decreased with constant weir diameter the cross section area between the scum ring and weir is decreased and the upward velocity is increased.

(d) Overflow Weir and Weir Plate—The optimum diameter of the overflow weir is not totally dependent on the total design overflow. The diameter must be such that an underflow beneath the scum ring will not be created that would allow floating solids to be

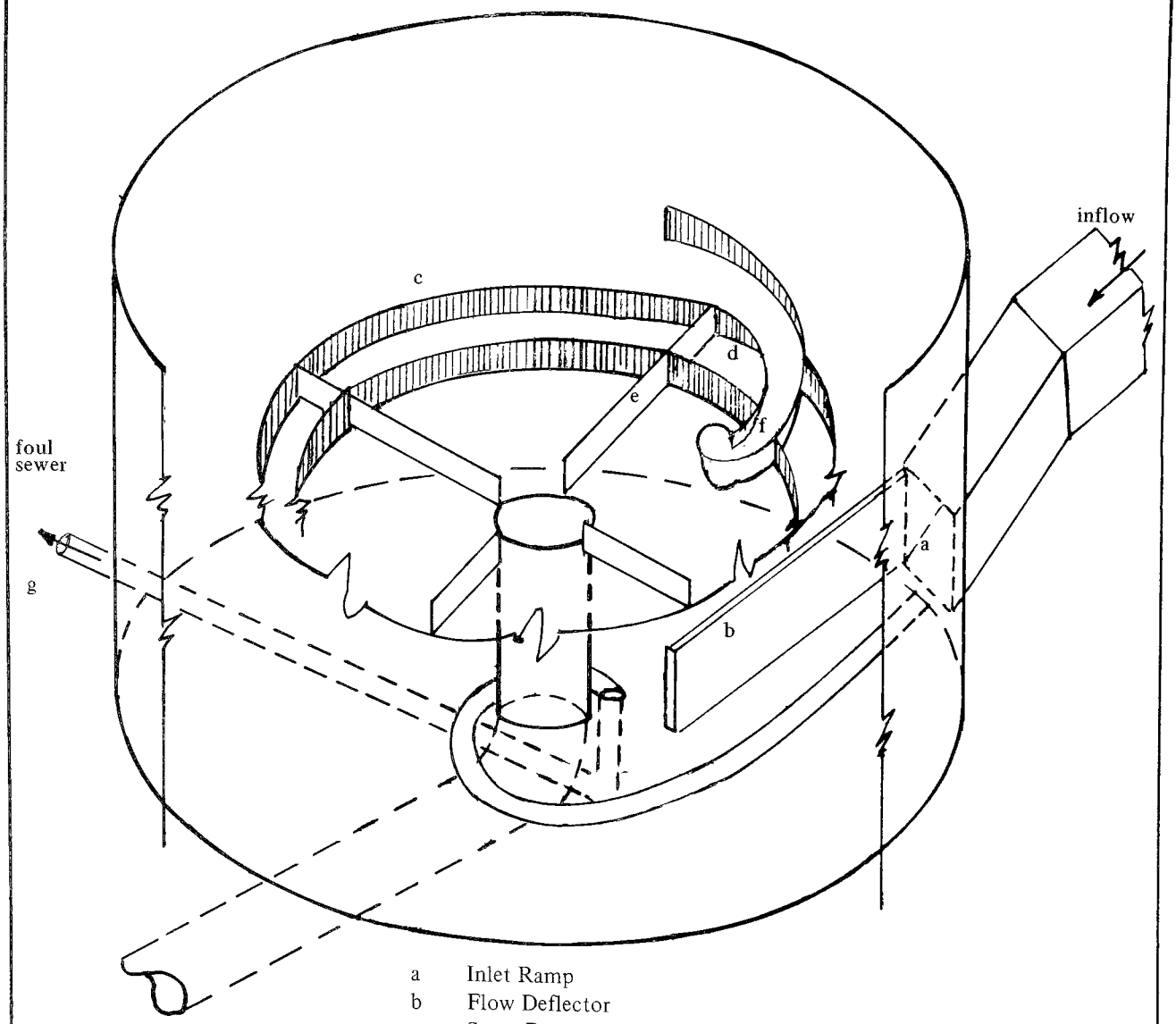

a Inlet Ramp
b Flow Deflector
c Scum Ring
d Overflow Weir and Weir Plate
e Spoilers
f Floatables Trap
g Foul Sewer Outlet
h Floor Gutters

FIGURE 7
ISOMETRIC VIEW OF SWIRL CONCENTRATOR

lost to overflow. Experiments in the hydraulic laboratory indicated that the relation between the weir diameter and the scum ring diameter should be 5:6.

The weir plate connects the overflow weir to a central column, carrying the overflow liquid to discharge. Its underside acts as a storage cap for floating solids directed beneath the weir plate through the floatables trap. The vertical element of the weir is extended below the weir plate to prevent floating material escaping to overflow. The weir should be extended a minimum of eighteen inches below the weir plate, but not lower than the top of the flow deflector.

The mathematical model studies evaluated the efficiency of two weir sizes on a 36-ft diameter swirl concentrator. The results are recorded in Table 4. This information is valid when considering a device not equipped with a scum ring. If floatables are to be collected, the diameters mentioned in the table are for the scum ring, and the ratio of weir to scum ring is 5:6.

TABLE 4

Effect of Weir Size on Concentrator Performance

Particle Settling Velocity (prototype scale–ft/sec)	% Captured 24-ft Weir	32-ft Weir
0.0275	31.2	27.6
0.717	63.1	51.6
0.212	93.2	79.4
0.432	100.0	90.3

The efficiency does not take into consideration self-cleansing.

(e) Spoilers—Spoilers are radial flow guides, vertically mounted on the weir plate extending from the center shaft to the scum ring. They are required to break up rotational flow of the liquid above the weir plate, thus increasing the capacity of the overflow downshaft. These spoilers should extend in height from the weir plate to a position approximately six inches above the crest of the emergency weir, thus ensuring efficient and controlled operation of the swirl concentrator well beyond the design flow and preventing formation of a free surface vortex under all loading conditions.

Figure 8, Photograph of Final Form Surface Flow Condition, indicates the effect of the spoiler in elementary vortex conditions at low flows and the extreme turbulence developed when vortex conditions are reached.

(f) Floatables Trap—A surface flow deflector extends across the outer rotating flow mass and directs floating material into a channel crossing the weir plate to a vertical vortex cylinder located at the wall of the overflow down shaft. Floating material is drawn down beneath the weir plate by the vortex and dispersed under the plate around the down shaft. The trap and its deflector are located at the point of least surface velocity in the liquid mass outside the scum ring. Location of the device in other positions resulted in floating materials which were collecting at the mouth of the channel being swept under the deflector and scum ring, and then over the weir to overflow. The depth of the deflector should coincide with that of the scum ring. If lower, eddy currents under the deflector will increase the loss of floating material into the overflow.

Figure 9, Photograph of Final Form Floatables Handling, shows the handling of floatables by the hydraulic model.

(g) Foul Sewer Outlet—The foul outlet is the exit designed to direct peak dry-weather flow and settled solids in the form of a concentrated slurry, to the interceptor. It has been positioned at the point of maximum settlement of solids and is vortex shaped to draw down the surface in dry-weather flow thus improving the efficiency and reducing the clogging problems of a horizontal orifice. Its down draft velocities minimize deposited solids in the vicinity and floatable materials on the surface of the water at a depth of one foot.

During the course of hydraulic laboratory investigation, it was determined that the optimum location of the floatables trap and the foul sewer outlet were similar in plan view. Consequently, they have been located in vertical alignment so that these important elements of the swirl concentrator can be readily inspected from above the device.

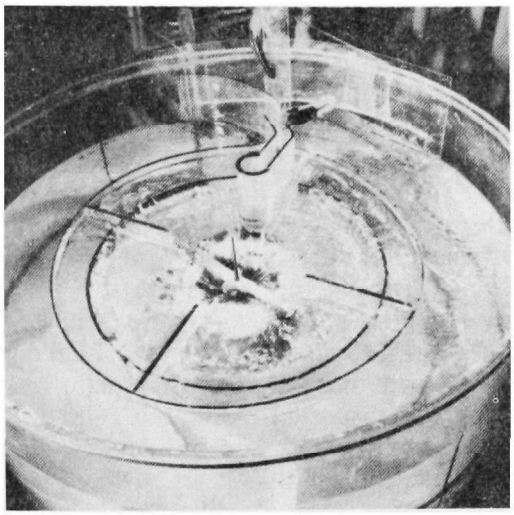

100 cfs Storm Overflow
3 cfs to Foul Sewer

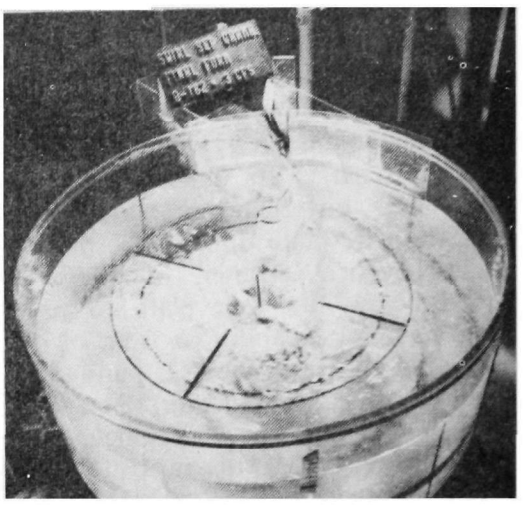

162 cfs Storm Overflow
3 cfs to Foul Sewer

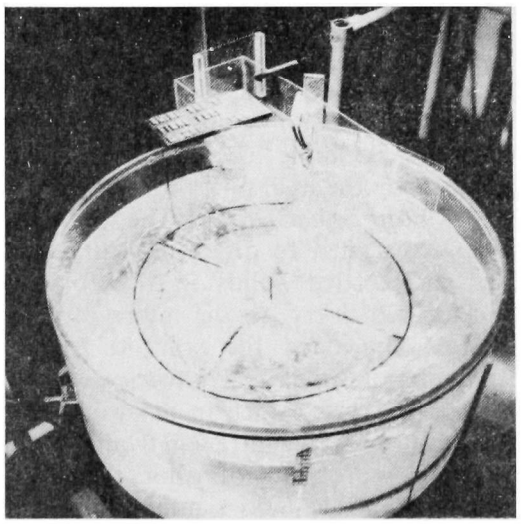

250 cfs Storm Overflow
3 cfs to Foul Sewer

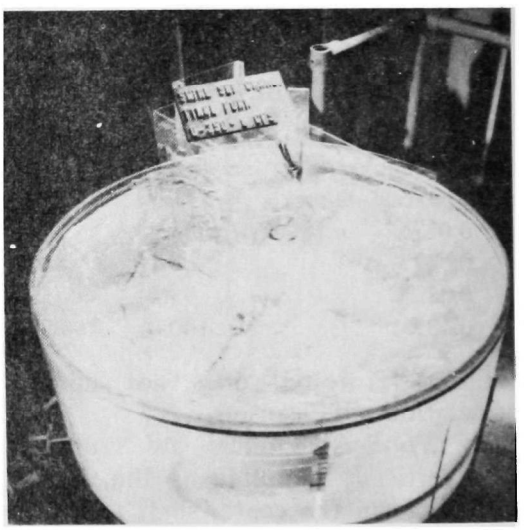

350 cfs Storm Overflow
6 cfs to Foul Sewer

FIGURE 8
PHOTOGRAPH OF FINAL FORM SURFACE FLOW CONDITIONS

Floatables Trap

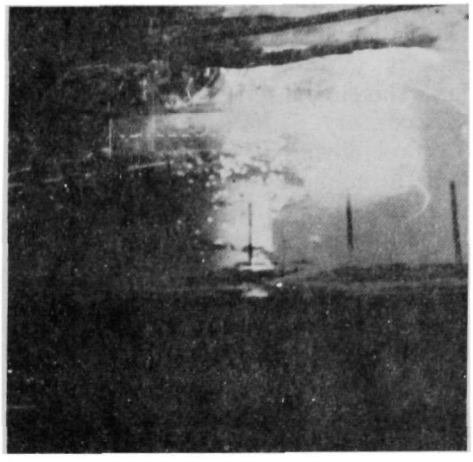

Floatables Emerging Under
Weir Through Trap Cylinder

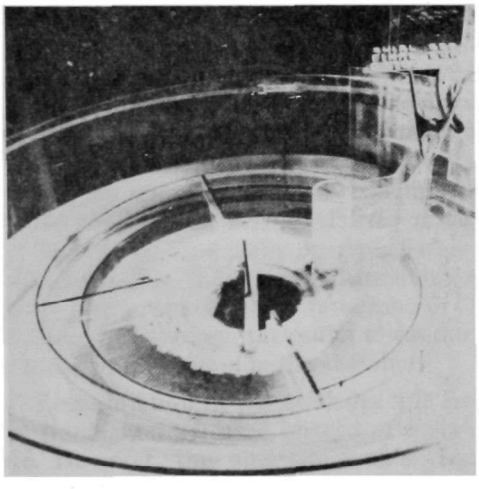

Polythene and Alathon Trapped
Under Weir After 100 cfs Test

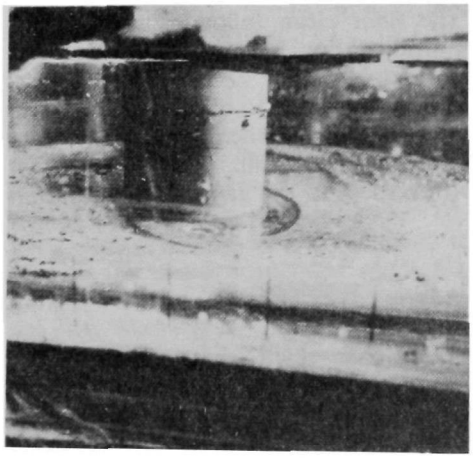

Random Settlement of Floatables on
Floor After Storm
Note Vortex at Foul Outlet

FIGURE 9
PHOTOGRAPHS OF FINAL FORM FLOATABLES HANDLING

(h) Floor Gutters—The primary floor gutter is the peak dry-weather flow channel connecting the inlet ramp to the foul sewer outlet. Its location has been chosen to eliminate shoaling of settled solids.

A secondary gutter follows the wall of the overflow downshaft and aids the primary gutter in the minimization of deposits.

Although rectangular shaped gutters were used in the laboratory model, a semi-circle of pipe section should prove more efficient in minimizing shoaling of solids.

(i) Floor Shape—Under design flow conditions, flat floors performed very well; however, at low flow conditions and reduced chamber velocities, settlement to the floor and local shoaling becomes a problem. Therefore, the floor should be sloped toward the center. A minimum slope of one-quarter inch per foot is desirable to permit the chamber to be flushed out.

To facilitate flushing out the chamber a ring water main should be installed around the outer perimeter wall with radial jets to flush the floor clean following storm water runoff events. For greatest efficiency, this flushing action should be activated by level control sensors, timed to operate as the water level, on draining, reaches the floor level at the exterior chamber wall.

With respect to the general configuration of the swirl concentrator, increasing the depth or the width of the chamber will have the effect of reducing the available energy for transporting settled solids to the foul sewer outlet which may result in shoaling problems with coarse, or heavier solids. Reducing the depth or the width of the chamber will have the converse effect, heavier material will be directed to the foul sewer, shoaling will not be a problem, but fine materials will not settle and will be lost to overflow.

Small changes in the design of the concentrator and its appurtenant elements may produce wide variations in its operation efficiency. In this regard, particular care must be taken during design and construction to avoid irregularities or intrusions in the walls, floors, and elements of the device.

Efficiencies of solids separation noted in this report relate to specific gravities, sizes, and concentration mentioned in Section II. Such conditions of size and specific gravity may not reflect local conditions. If, for example, grit is a problem in a particular design area, scaling down of concentrator dimensions established by the hydraulic design should be considered. An examination of the mathematical modeling design methods in Appendix 2 will indicate necessary adjustments for greater removal efficiency of specific particle types.

SECTION IV
DESIGN OF SWIRL CONCENTRATOR FACILITIES

Hydraulics

Three flow quantities must be considered in the design: (1) the peak dry-weather flow; (2) the design flow, i.e., the flow for which the optimum treatment is desired and (3) the maximum flow likely to occur through the chamber.

The peak dry-weather flow should pass through the chamber without delay while being retained in the gutter. The diameter of the foul outlet for the dry-weather flow should be a minimum of 8 inches and preferably be 10 or 12 inches. At low flow rates, discharge through the outlet pipe may occur as gravity flow while at higher flows discharge will occur as in a pressure pipe. It is difficult to size the pipe to act as a "throttle" pipe to pass a specific peak dry-weather flow. Therefore, it is recommended that a sluice gate or other flow control device be installed on the pipe in a manhole located outside the chamber. The use of a gate will permit adjustment of the opening and the discharge rate; further, it will allow the use of larger size pipe with less chance of clogging and, if clogging occurs at the gate, the gate can be opened to clear out the debris.

The use of a manually operated gate with a fixed opening (between adjustments) will result in considerable variation in the discharge rate through the outlet sewer due tc variation in water level in the chamber.

Less variation in the discharge will occur if a tipping gate is used instead of a manual gate. However, this alternate would require the installation of two manholes to provide access to the upstream side as well as downstream side of the gate for maintenance purposes.

If it is necessary to limit the variation in flow of the foul sewage to a minimum, then a motor or cylinder-operated gate should be used. Such gates could be controlled by either the downstream water level or the water level in the chamber. Electrical power would be required to operate the gate.

Tipping, motor-operated and cylinder-operated gates are described in the EPA Publication, Combined Sewer Regulation and Management, A Manual of Practice, and are not further considered in this report.

The size of the facility will depend upon the flow for which optimum treatment is to be provided. For the purposes of this study it was decided that a flow representing an infrequent peak flow (165 cfs) should have settleable solids in its flow reduced by about 85 percent of maximum removal by the device. On this basis it was found that for an intermediate frequency flow (100 cfs), optimum settleable solids removal would be provided. As the cost of the facility and the hydraulic head loss for dry-weather flows increase with the flowrate to provide optimum solids removal, choice of the design flow and degree of settleable solids removal is very important.

The amount and rate of flow of settleable solids is not directly related to the total flow. The University of Florida, as a subcontractor to the City of Lancaster, developed through computer modeling both outflow hydrographs and pollutographs, i.e., a representation of the amount of specific pollutants. Information concerning six storms was provided as shown in Figures 10a and 10b, Flow and Suspended Solid Load for Six Storms. The peak suspended solids load for these storms did not occur at the same time as the peak discharges.

An analysis was made of storms 4-6 to determine an estimate of the pounds of solids which might be lost due to the chamber size criteria used. Table 5, Analysis of Pounds of Suspended Solids Lost, Storm 5, is a sample of the calculation technique utilized. From the Table, it can be seen that perhaps 344 pounds of settleable solids, or 17 percent of the total settleable solids, may be lost during the ninety minutes that the flow rate exceeded 100 cfs. Table 6, Analysis of Six Storms, indicates that due to size limitations, if the flow exceeds 250 cfs, perhaps 15-20 percent of the total suspended solids may be lost. It should be remembered, however, that self cleansing efficiency is improved at smaller diameters because of the tendency of the

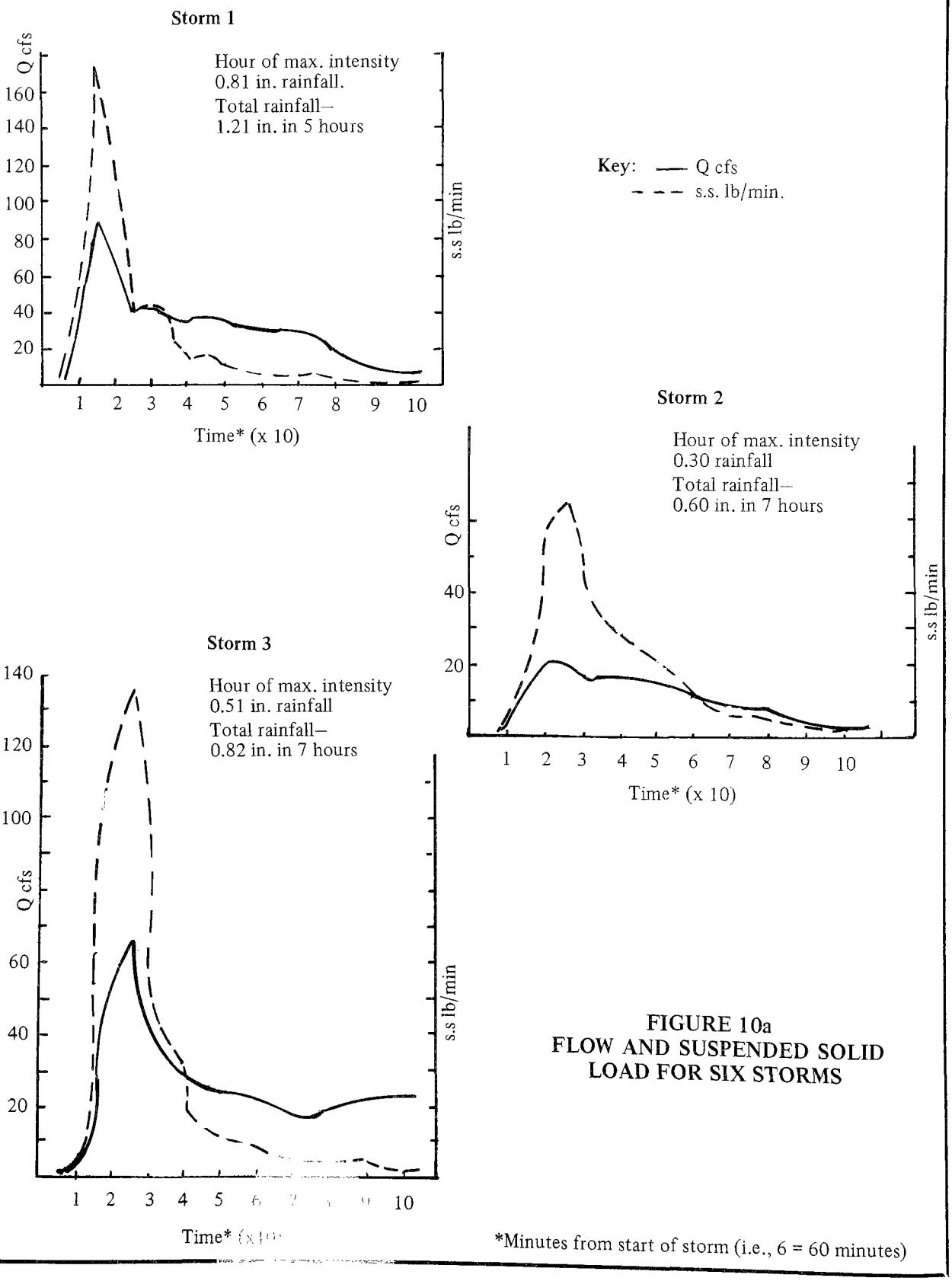

FIGURE 10a
FLOW AND SUSPENDED SOLID LOAD FOR SIX STORMS

*Minutes from start of storm (i.e., 6 = 60 minutes)

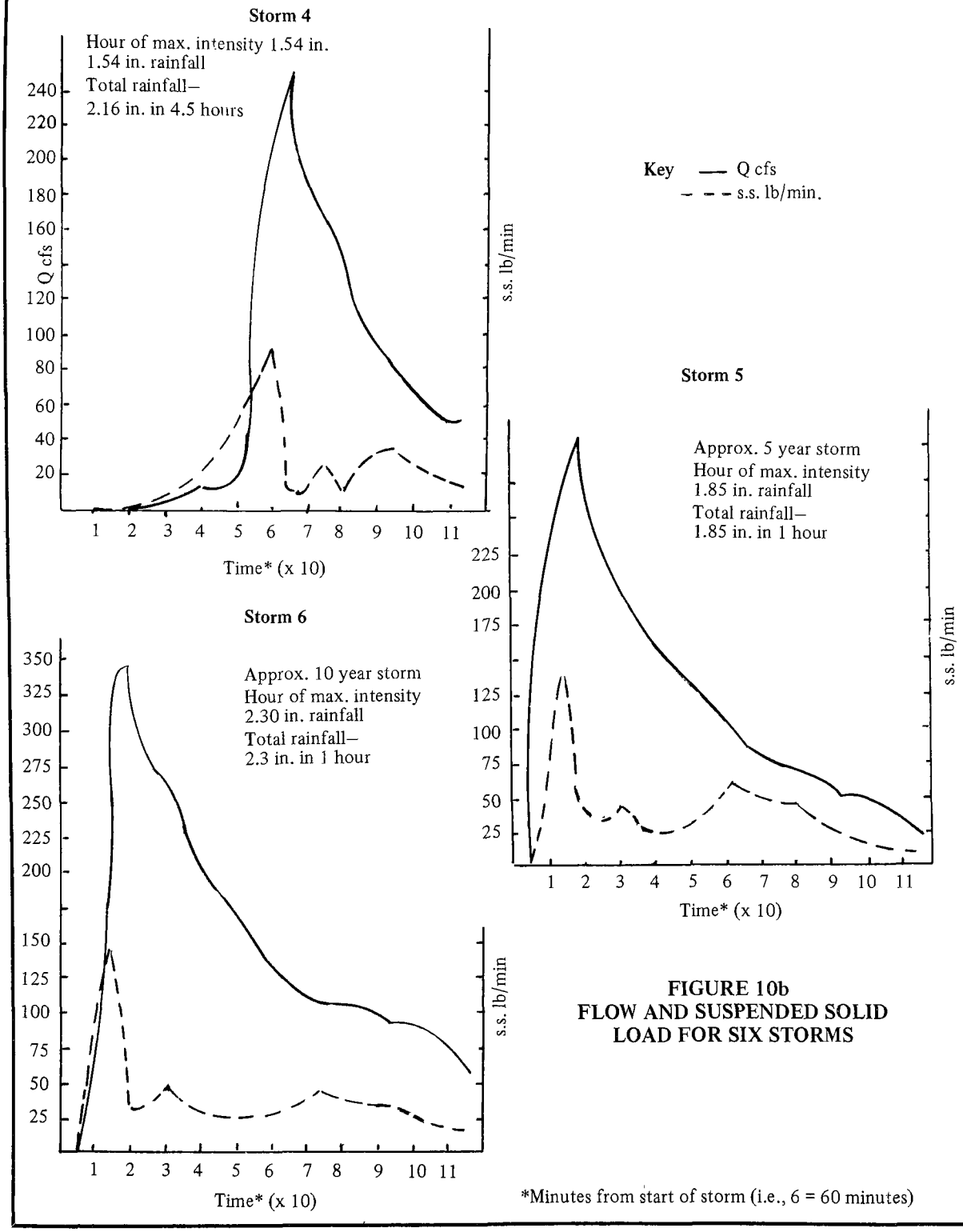

FIGURE 10b
FLOW AND SUSPENDED SOLID LOAD FOR SIX STORMS

*Minutes from start of storm (i.e., 6 = 60 minutes)

TABLE 5

Sample Calculation

Analysis of Pounds of Suspended Solids Lost Due to Undersize Chamber

Storm 5

Time	Av. Q[1] cfs	Min.	Av. SS[1] lb/min.	Eff. of[2] Recovery	Suspended[3] Solids Not Recovered
15-20	295.3	5	94.0	47.5	246.7
20-25	271.7	5	38.7	58	81.2
25-30	219.1	5	39.1	71	56.7
30-35	192.1	5	39.8	76	48.0
35-40	167.0	5	31.7	84	25.3
40-45	148.0	5	31.9	90	15.9
45-50	135.8	5	32.1	94	9.6
50-55	124.5	5	35.8	97	5.4
55-60 or 1:00	111.2	5	43.9	99	2.2
1:00-1:05	98.2	5	52.6	100	-0-
				Total	491 lb
			Total lb suspended solids for storm		2,869.7

lb settleable solids lost = 491 x 70% = 343.7 lb

% not received = $\frac{491}{2,869.7}$ x 100 = 17%

[1] From University of Florida

[2] From LaSalle Hydraulic Laboratory

[3] Assume suspended solids and settleable solids overflow in equal proportions

TABLE 6

Analysis of Six Storms--Lancaster, Pa.
(data from University of Florida)

Storm No.	Q Max. (cfs)	SS Max. (lb/min.)	Tot SS (lb)	Settleable Solids - lb lost due to size of regulator (70% of ss)	% Lost
1	42.3	172.4	3036.8	-0-	-0-
2	20.6	63.8	2285.6	-0-	-0-
3	65.5	134.8	3264.3	-0-	-0-
4	250.4	94.8	3098.1	114	5
5	310.4	14.6	2869.7	491	17
6	346.7	148.9	2858.9	433	15.2

solids to shoal at low rotational velocities.

The maximum flow will determine the elevation of the chamber with respect to the inlet sewer. An important consideration is whether the inlet sewer can be surcharged and, if so, to what extent. Having determined the permissible water level at the inlet sewer, the circular weir must be set below this level so the weir discharge will equal the maximum flow. Equations are not available for determining the required head over the chamber weir; therefore, data obtained from the hydraulic model runs must be used. Stage discharge curves based on laboratory data are given in Figure 18 of the LaSalle Report, Appendix 1, for a 20-foot diameter weir. Data derived from Figure 18 are plotted on Figure 11, Head Discharge Curve for Circular Weir, to indicate the discharge per linear foot of weir.

The discharge over the circular weir is compared to the discharge of a straight sharp-crested weir with no velocity of approach in Table 7, Head Discharge Data. Between heads of 0.5 feet and 3.0 feet the discharge of the circular weir ranges from 74 percent to 28 percent of that for a straight weir. At the higher heads the flow over the circular weir was affected by submergence of the weir.

Assuming the maximum flow is 300 cfs and the circular weir length is 62.8 feet, the discharge per foot of the weir would be 4.8 cfs. From Figure 8 this would indicate a head of 3.0 feet. Neglecting entrance losses this would require that the weir crest be set 3.0 feet below the allowable hydraulic gradient of the inlet sewer.

In some cases it may be permissible to provide a side overflow weir on the periphery of the chamber to take part of the flow when the flow exceeds the design flow based on the minimum size necessary to acheive the desired removal of suspended solids. For instance, assume the design flow is 165 cfs, the maximum flow 300 cfs, the circular weir 62.8 feet long and a side weir 28 feet long which is set 1.2 feet above the circular weir. Then the conditions shown in Table 8, Combined Discharge Over Circular and Side Weir, would result.

Thus with the use of a side weir on the periphery of the chamber, the circular weir could be set 2.0 feet below the maximum hydraulic gradient for a flow of 300 cfs instead of 3.0 feet as required if the circular weir were to take the entire flow

In the foregoing example, it has been assumed that the discharge-head relations shown in Figure 11 are applicable to a side overflow weir. While this may not be correct, no better basis for estimating the flow is available.

Sizing

The results of laboratory model studies on open hydraulic structures can be used to determine the size of the prototype if the geometry is made similar and the Froudes number for the circular weir discharge are the same. On this basis the discharge ratio of the prototype to the model will equal the five-halves power of the scale ratio.

For any given design discharge the diameter of the chamber may be determined from Figure 20, Appendix 1, Storm Discharge vs Chamber Diameter Design Curve. From Figure 20, the chamber diameters are 29.5 feet for 100 cfs and 22.5 feet for 50 cfs.

The other dimensions of the chamber should have the same ratio to the diameter as those in the model. These ratios are shown in Figure 21, General Design Detail, Appendix 1. The location of the various dimensions are shown in Figures 12, 13 and 14, Plan and Elevation. On the basis of the foregoing the dimensions for design discharges of 50, 100 and 165 cfs are shown in Table 9, Chamber Dimensions.

The percent of solids diverted to the foul sewer can be obtained from Figure 22, Appendix 1, for any given discharge. Thus, at design discharge the flow through the foul outlet will contain 90 percent of grit larger than 0.35 mm and of settleable solids larger than 1.0 mm. Smaller percentages of finer materials would also pass through the foul outlet.

It should be noted that the dimension d_2 is the vertical distance from the invert of the inlet sewer to the bottom of the chamber. This drop was used in the model to prevent

TABLE 7

Head Discharge Data

H Feet	Discharge in cfs/ft: Circular Weir	Discharge in cfs/ft: Straight Weir[1]	Ratio of Circular Weir Discharge to Straight Weir Discharge
0.5	0.86	1.17	0.74
1.0	2.04	3.33	0.61
1.5	3.15	6.12	0.52
2.0	3.98	9.42	0.42
2.5	4.52	13.16	0.34
3.0	4.85	17.30	0.28

[1] $Q = 3.33\ H^{3/2}$

TABLE 8

Combined Discharge Over Circular and Side Weir

Head–Feet: Circular Weir	Head–Feet: Side Weir	Discharge–cfs: Foul Outlet	Discharge–cfs: Circular Weir	Discharge–cfs: Side Weir	Total
1.2	0.0	3	162	0	165
2.0	0.8	3	248	45	296
3.0	1.8	3	304	102	409

the inlet sewer from being surcharged. This arrangement is not critical. If there is no objection to surcharging the inlet sewer then the dimension d_2 may be decreased.

Design Elements

The primary element is the circular chamber which normally would be constructed of reinforced concrete. However, it is not necessary to make the interior wall surface a perfect circle and the use of two-foot-wide prefabricated steel forms is considered permissible.

The use of a flat floor in the chamber is permissible. However, for drainage purposes, it is suggested the floor have a minimum slope of 1/4 inch per foot from the wall toward the center.

The layout of the gutter is extremely critical in elimination of deposits on the floor. The foul outlet should be located at the 320° position. The floor should have a circular depression around the outlet sewer with a diameter of about 3 times the diameter of the outlet sewer. While the gutter in the model was rectangular in shape the use of a semi-circular shape is permissible and considered preferable for moving solids in low flow periods. The gutter should have sufficient capacity for the peak dry-weather flow.

The size of the outlet sewer will be governed to a large extent by the required size of sluice gate on the outlet pipe.

The inlet to the chamber must be aligned so as to introduce the flow tangentially to the outer periphery of the chamber. An important element is the "flow deflector," a free standing wall extending from the entrance of the inlet sewer to the 0° position of the chamber. The top of this wall is the same level as the bottom of the weir skirt and is not connected thereto. Storm water entering the chamber is directed toward the outside of the chamber by this deflector. Storm water rotating in the chamber passes

FIGURE 11
HEAD DISCHARGE CURVE FOR CIRCULAR WEIR

over the deflector wall and tends to cause the entering solids to be directed downward in the chamber.

It is important that the inlet sewer enter the chamber with its invert at the same elevation as the chamber bottom. Meeting this criteria results in more rapid settling of solids to the bottom. In the model studies a ramp with a slope of 1 on 2 was used in the approach to the chamber. If it is possible to surcharge the inlet sewer then the chamber can be raised the amount of the surcharge and the drop in the ramp decreased accordingly.

It is suggested that the "clear water" downshaft and the weir be constructed of steel. The use of steel rather than concrete: (1) makes the structure thickness similar to those used in the model, (2) may be more economical, and (3) will make it possible to make revisions if further model studies or operation results indicate revisions are needed. The downshaft supports a horizontal circular plate. The outer edge of the plate has a vertical plate welded to it which forms a weir above and a skirt below the plate. So-called "spoilers" are vertical plates located on the circular plate to prevent vortex action in the downshaft. At least four to eight spoilers should be used extending from the edge of the downshaft to the weir. To prevent floatables from flowing over the weir, a scum plate is set away from the weir with the lower edge of the scum plate 6 inches below the weir crest. This scum plate can be supported by the spoilers or by separate brackets extending from the weir to the scum plate.

Other studies in combined sewer regulators have indicated there is less collection of debris on broad-crested weirs than on sharp-crested weirs. Therefore it is suggested the weir be semi-circular in shape with radius of two to four inches.

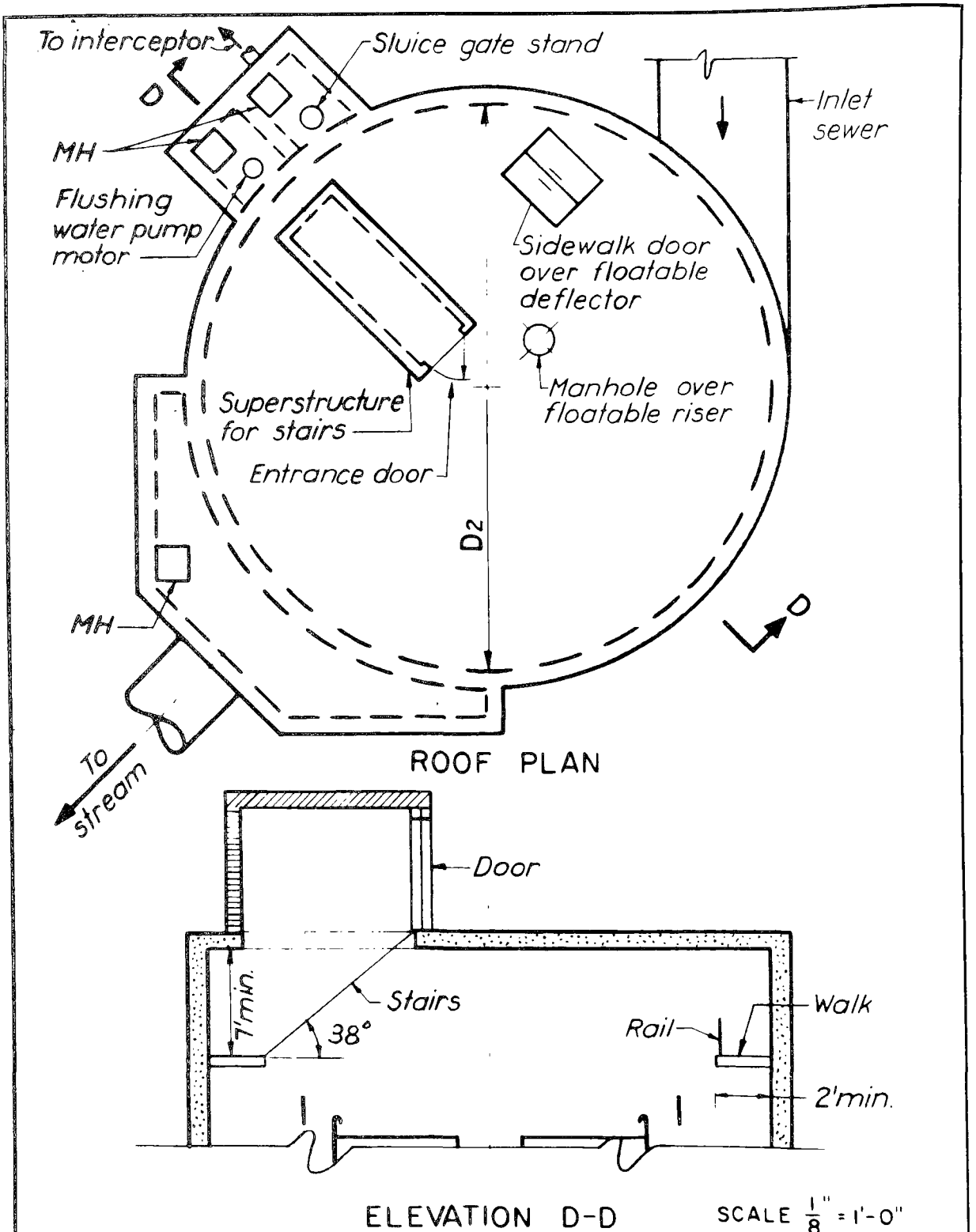

FIGURE 12
PLAN AND ELEVATION – ROOF AREA

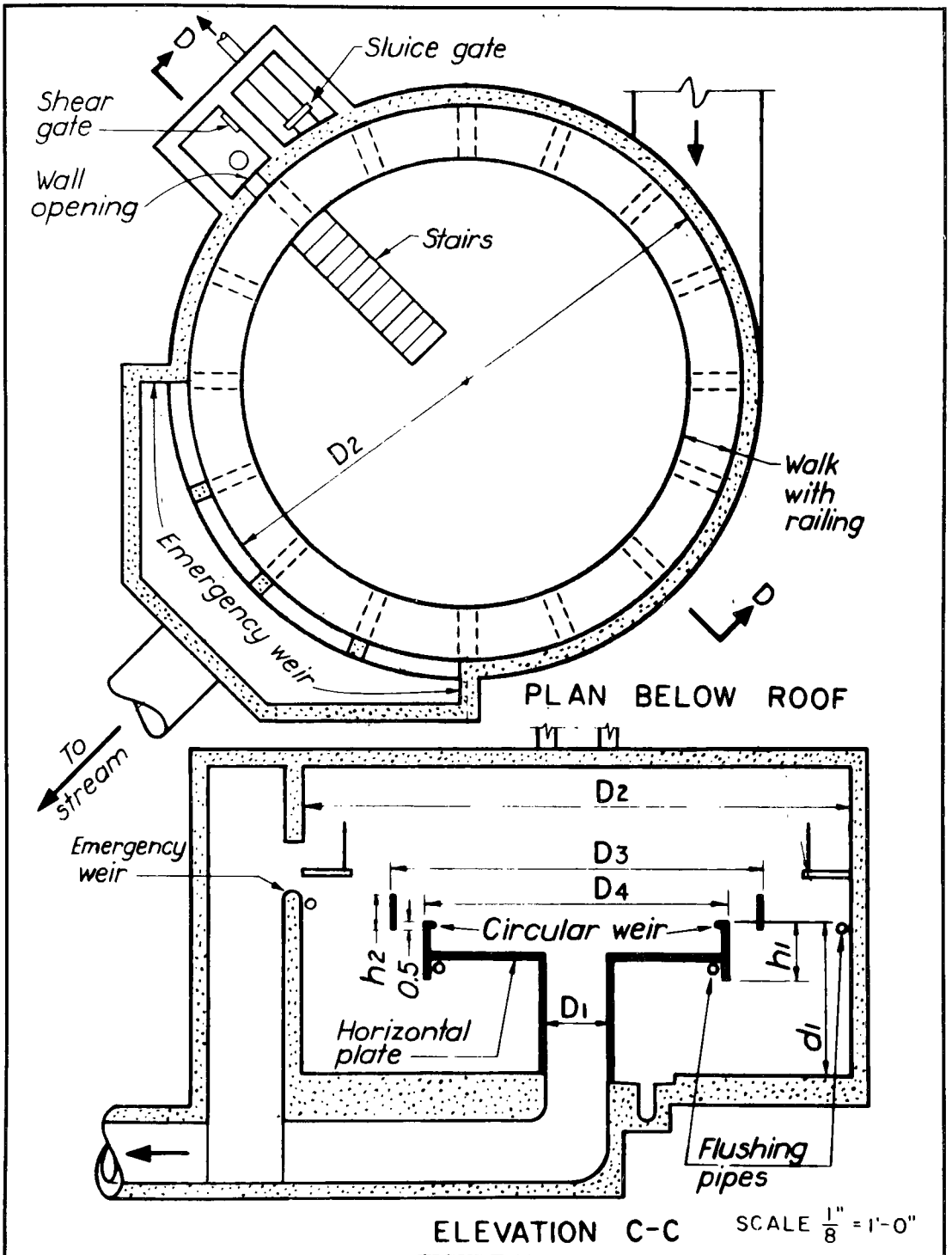

FIGURE 13
PLAN AND ELEVATION – BELOW ROOF

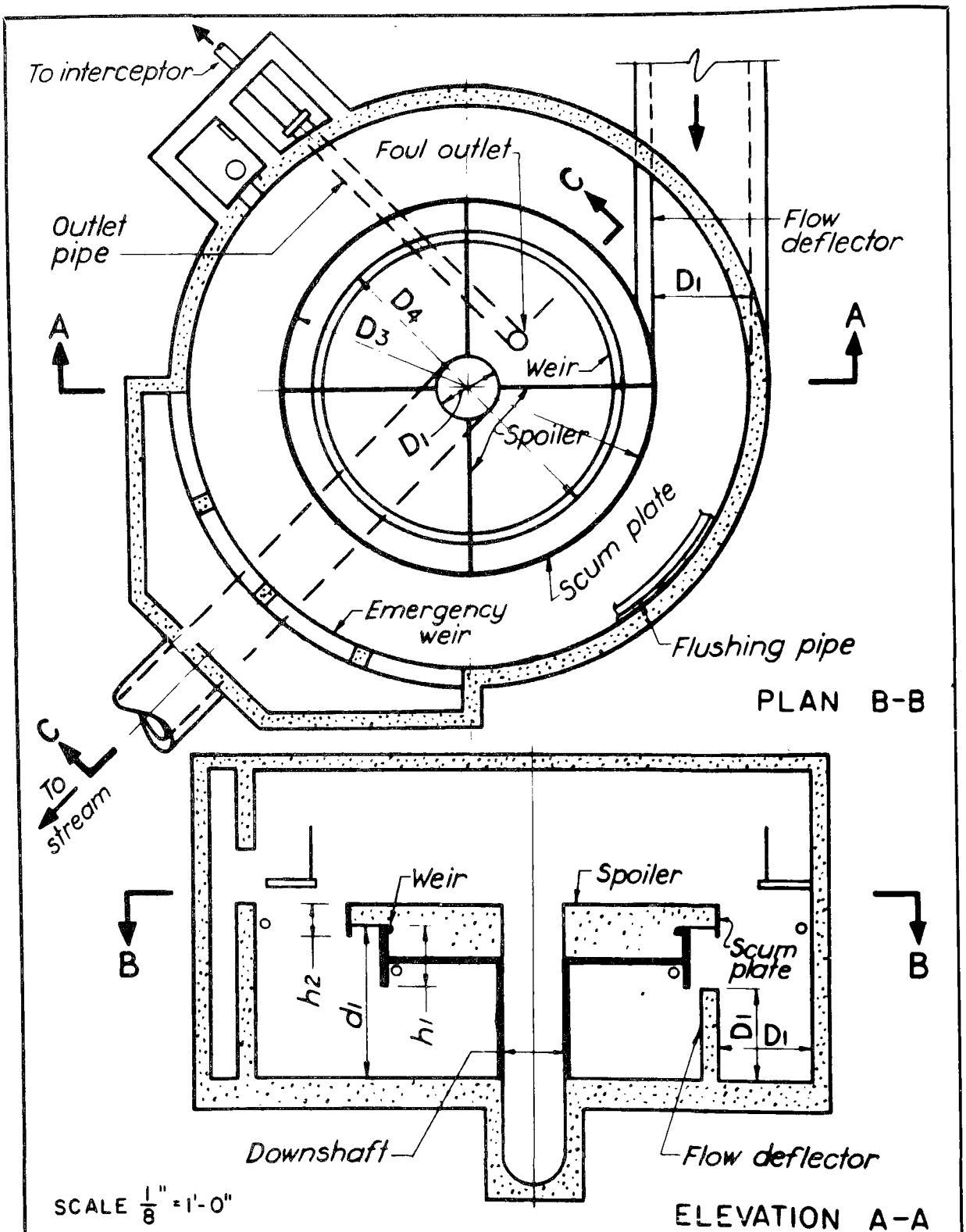

FIGURE 14
PLAN ELEVATION – FLOOR AREA

TABLE 9

Chamber Dimensions

(all dimensions in feet)

Design Storm Discharge – cfs					50	100	165
Diameter of Chamber	=	D_2	(Fig. 20, Apdx. 1)		22.5	29.5	36.0
Diameter of Overflow and Diameter of Inlet	=	D_1		1/6 D_2	3.75	4.92	6.00
Diameter of Circular Scum Ring	=	D_3	=	4 D_1	15.00	19.68	24.00
Diameter of Circular Weir	=	D_4	–	3 1/3 D_1	12.50	16.40	20.00
Radius of Inlet Gutter (0-90°)	=	R_1	=	2 1/3 D_1	8.75	11.48	14.00
Radius of Inlet Gutter (90-180°)	=	R_2	=	1 1/2 D_1	5.62	7.38	9.00
Radius of Secondary Gutter (90-270°)		R_3	=	5/8 D_1	2.34	3.08	3.75
Radius of Secondary Gutter (0-90°)	=	R_4	=	1 1/8 D_1	4.22	5.54	6.75
Radius of Secondary Gutter (270-360°)	=	R_5	=	3 2/3 D_1	13.75	18.04	22.00
Difference in Radius Between Secondary and Circular Weir	=	b_1	=	1/3 D_1	1.25	1.64	2.00
Offset Distance for Determining Gutter Radii	=	b_2	–	1/6 D_1	0.62	0.82	1.00
Distance Between Floor and Top of Circular Weir	=	d_1	=	1 1/2 D_1	5.62	7.38	9.00
Depth Invert to Bottom of Chamber	=	d_2	=	5/6 D_1	3.12	4.10	5.00
Height of Circular Weir	=	h_1	=	1/2 D_1	1.87	2.46	3.00
Height of Scum Ring	=	h_2	–	1/3 D_1	1.25	1.64	2.00

The floatable deflector consists of a steel plate extending from the outer wall of the chamber to the scum ring and having the same dimensions as the scum ring. From the scum ring two plates form a passage one foot wide to the weir. From the weir two plates resting on the horizontal plate form a passage to a point near the center. At this point a cylinder is provided through the horizontal plate. Vortex action at this point carries the floatables to the underside of the circular plate. The floatable deflector should be constructed as shown in Figures 16 and 17c of Appendix 1. The vortex cylinder through the circular plate should be located directly above the foul sewer outlet.

Design Features

Plans and sections through a typical chamber are shown on Figure 14.

The provision of a roof for the chamber is not necessary for functional reasons but is considered desirable for safety and esthetic considerations. Several openings are required in the roof. A manhole 24 to 30 inches in diameter should be placed directly over the vortex cylinder for the floatables. This will permit rodding of the cylinder in case of clogging. Since the cylinder is located directly over the foul sewage outlet this manhole will also permit rodding of the outlet pipe. A large sidewalk door should be provided to permit removal of large floating objects. The size of the door should be related to some extent by the size of the inlet sewer and the possible size of floating objects.

Three types of entrance stairs are shown in Figure 6.1.3 of the Combined Sewer Overflow Regulator Manual of Practice. The preferred access is the use of a 38-degree stairway with 7 3/4-inch risers, and 10-inch treads surmounted with a superstructure with exterior dimensions of 13 feet by 5 feet by 8 feet high. Minimum openings of 2 feet square should also be provided in the sluice gate manhole and the overflow manhole.

An inspection walk should be provided

around the periphery of the chamber with a minimum width of two feet. The walk should be located so that the weir and scum plate can be cleared of debris if required. A pipe handrail 42 inches high should be provided on the walk and stairs.

After each storm the chamber should be inspected. It may be necessary following storms to flush down the bottom of the chamber to prevent subsequent nuisance odors. During the model runs in the laboratory the material used to simulate the floatables collected under the horizontal plate. When the water level receded some material had a tendency to remain attached to the plate. Floatables in an actual structure will be subjected to heads of up to five feet and this may cause the floatables to adhere to the horizontal plate as occurred in the model. Therefore, it may be necessary to remove the materials by flushing after each storm. In cities with many regulators, several days may elapse after a storm before each regulator can be inspected. Hence it is suggested that automatic cleansing of the chamber bottom and horizontal plate be provided.

If water used for this purpose comes from a potable supply there should be no physical connection between the supply and the flushing system. A more feasible source of flushing water may be either the nearby receiving waters to which the chamber discharges or the storm water that passes through the chamber. The use of receiving water requires the construction of a sump and pumps. The use of storm water requires the construction of a reservoir adjacent to the chamber to store the storm water during the storm so that it can be used after the storm is ended.

One suggested method of using storm water for flushing the chamber is shown in Figure 12. This comprises a 4-foot-square manhole 9 feet deep adjacent to the sluice gate manhole. The capacity is about 1,000 gallons. Storm water enters the manhole through a 12-inch-square opening in the chamber wall set with top of opening level with the circular weir crest. The opening is covered with 1/2-inch mesh to prevent solids from entering. The velocity parallel to the chamber wall should keep the screen from clogging. A shear gate is installed in the common wall between the two manholes so that the storm water manhole can be emptied into the sluice gate manhole after each storm. A vertical wet pit non-clog pump is used to pump the storm water into the flushing lines. A 4-inch-diameter pipe is installed on the underside of the horizontal plate adjacent to the skirt. This pipe has eight 3/4-inch nozzles aimed upward at the bottom of the plate. When the water level in the chamber has fallen to some point below the plate the pump will operate for 5 minutes, discharging 80 gallons per minute at 40 psi.

For flushing the bottom of the chamber another 4-inch-diameter pipe is attached to the chamber wall at about weir level with sixteen 3/4-inch nozzles pointed straight downward. When the water level in the chamber has fallen to below the chamber bottom the pump will again operate for about 5 minutes. The foregoing flushing procedure is suggested for use on a trial basis.

Hydraulic Design

Most combined sewer overflow regulators are designed for use in connection with existing combined sewers and either existing or proposed intercepting sewers. The vertical distance between the hydraulic grade lines in the combined sewer and interceptor must be great enough to permit installation of the regulator. It may be necessary to run through the hydraulic computations at any specific location in order to determine if the swirl concentrator can be used. Table 10, Design Example, indicates the nature of the computations required to illustrate the factors that should be considered.

In the following computation the "foul sewer" is the outlet pipe from the chamber to the sluice gate manhole and the "branch interceptor" is the sewer from the sluice gate manhole to the interceptor.

As stated previously, some type of control device should be provided on the foul sewer where it leaves the chamber. In the following computations the control is assumed to be a manually operated sluice gate. This type of control will result in the

TABLE 10

Design Example (from hydraulic model data)

Sample Computations

L	=	Length in feet
A	=	Cross sectional area in square feet
D	=	Diameter in feet
V	=	Velocity in feet per second (fps)
d	=	Depth of flow in feet
Q	=	Discharge in cubic feet per second (cfs)
b	=	Width of opening in feet
g	=	Acceleration of gravity (32.2)
C	=	Coefficient
W.S.	=	Water Surface
H.G.L.	=	Hydraulic Grade Line
E.L.	=	Energy Line
n	=	0.013 (Manning)
S	=	Slope (ft/ft)
d_1	=	Depth of swirl concentrator

Interceptor

D = 3.0; invert el. = 10.0; W.S. = 12.4

Combined Sewer

D = 6.0; invert el. = 19.14; S = 0.005
Peak Dry Weather Flow = 3 cfs
Design Flow = 165 cfs
Maximum Flow = 300 cfs

		Invert	H.G.L.	E.L.
Interceptor				
Assume		10.00	12.40	
Branch Interceptor				
L	= 100 ft., Q = 3 cfs			
D	= 1.0 ft., S = 0.007			
V (full)	= 3.8 fps			
d/D	= 0.8			
V (0.8 full)	= (1.14) (3.8) = 4.3			
$V^2/2g$	= 0.28 ft.			
Set downstream end so flow line is same as interceptor			12.40	
Invert 12.40 - 0.8		11.60		
Exit loss	= 0.28; 12.4 + 0.28			12.68
Upstream end				
Rise	= (100) (0.007) = 0.70			
	11.60 + 0.70	12.30		
	12.40 + 0.70		13.10	
	12.68 + 0.70			13.38

TABLE 10 (continued)

	Invert	H.G.L.	E.L.
Sluice Gate Manhole	12.30		
Entrance loss $(0.5)\frac{V^2}{2g} = 0.14$			
13.38 + 0.14			13.52
Assume loss of velocity head in manhole		13.52	
Sluice gate			
Use 12 inch by 12.inch gate			
Assume opening 0.67 ft high			
V = 3/0.67 = 4.5 fps			
$V^2/2g$ = 0.31 ft			
Exit loss = 0.31			
13.52 + 0.31			13.83
Contraction loss at gate			
$0.3V^2/2g$ = 0.09			
13.83 + 0.09			13.92
Set gate invert at manhole invert	12.30		
Use 1.0 ft square conduit			
Top conduit 13.30			
V = 3/1 = 3 fps			
$V^2/2g$ = 0.14 ft			
13.92 - 0.14		13.78	
Outlet Pipe			
D = 1.0 L = 20 A = 0.785			
Start pipe 1 ft upstream of gate	12.30		
V = 3/0.785 = 3.8 fps			
$V^2/2g$ = 0.22 ft			
Enlargement loss = (0.25) (0.22) = 0.06			
E.L. = 13.92 +0.06			13.98
H.G.L. = 13.98 - 0.28		13.70	
L = 20 ft S = 0.007			
Rise = (20) (0.007) = 0.14			
Upper end 12.30 + 0.14	12.44		
13.70 + 0.14		13.84	
13.98 + 0.14			14.12
Use 90° C.I. bend			
Length invert to bell 1.85 ft			
Top of bell 12.44 + 1.85 = 14.29			
Bend loss $0.25V^2/2g$ = 0.06			
E.L. = 14.12 + 0.06			14.18
H.G.L. = E.L.		14.18	
H.G.L. is below top of bell at 14.29			

TABLE 10 (continued)

	Invert	H.G.L.	E.L
Chamber Bottom			
Gutter invert	14.29		
Make gutter 0.75 ft deep			
Chamber invert at center			
14.29 + 0.75	15.04		
Use transverse slope of 1/4 in. per ft			
Rise = (15) (1/4) = 3 3/4 in. = 0.31 ft			
Chamber invert at wall			
15.04 + 0.31	15.35		

Gutter

Try one-half 18-in. pipe
Length from end of ramp to foul outlet = 64 ft scaled from Figure 16 (Appendix 1)
Total fall = (12) (1/4) = 3 in. = 0.25 ft
S = 0.25/64 = 0.004
Q = 6.5 cfs (full pipe)
V = 3.7 fps (full pipe)

One-half pipe
Q = (0.5) (6.5) = 3.2 cfs > 3.0 OK
V = (1.0) (3.7) = 3.7 fps OK

Chamber	**Weir**	
For design flow of 165 cfs		
d_1 = 9.0 (Table 9)		
Weir crest 15.35 + 9.00	24.35	
Weir diameter = 20 ft		
Weir length = 62.8 ft		
Weir discharge per ft $\frac{165}{62.8} = 2.6$		
Weir head = 1.2 (Figure 11)		
H.G.L. for 165 cfs		
24.35 + 1.2		25.55

Set emergency weir 28 ft long at elevation 25.55
Determine W.S. for maximum flow of 300 cfs

TABLE 10 (continued)

			Weir	H.G.L.	E.L.
By trial and error					
	H	Q			
Circular weir	2.0	248			
Emergency weir	0.8	45			
Foul outlet		3±			
		296			
Water surface 24.35 + 2.0				26.35	
This is at 180° position					
Assume same at 0° position					
At 0° position area between deflector and wall equals					
(6) (9 + 2.0) = 66 sq ft					
$V = \frac{300}{66} = 4.6$ fps					
$V^2/2g = 0.33$ ft					
At 0° position			24.35	26.35	26.68
Inlet Pipe					
D = 6 ft A = 28.3 sq ft					
V = 10.6					
$V^2/2g = 1.74$					
			Invert		
Enlargement loss					
(0.25) (1.74 - 0.33) = 0.35					
Required E.L					27.03
Required H.G.L.				25.29	
Required invert so pipe is not surcharged 25.29 - 6.0			19.29		
Required vertical distance from W.S. in interceptor to invert of inlet sewer 19.29 - 12.40 = 6.89 ft					
Determine flow to interceptor when maximum flow is 300 cfs and W.S. in chamber is 26.35					
Assume 8.6 cfs					
Interceptor					
Assume W.S. as before				12.40	

TABLE 10 (continued)

	Invert	H.G.L.	E.L.
Branch Interceptor			
D = 1.0; V = 11.0; $V^2/2g$ = 1.88 S = 0.06			
Exit loss	1.88		14.28
Rise = (100) (0.06) = 6.00			20.28
Manhole			
Entrance loss $0.5\,V^2/2g$ = 0.94			21.22
Sluice gate (from before) A = 0.67; V = 12.9; $V^2/2g$ = 2.58			
Exit loss	2.58		23.80
Contraction loss (0.3) (2.53) = 0.77			24.57
Outlet Pipe			
L = 20 S = 0.06 Rise = (20) (0.06) = 1.20			25.77
Bend loss (0.25) (1.88) = 0.47			26.24
H.G.L. for 8.6 cfs		26.24	
Actual H.G.L.		26.35	
Therefore discharge thru foul outlet will be about 8.6 cfs when maximum flow of 300 cfs occurs.			

greatest variation in flow to the interceptor between dry and wet-weather periods. One way to decrease the amount of the variation is to design the branch interceptor to flow full under peak dry-weather conditions. Increasing the length of the branch interceptor will also help to decrease the variation. Under these conditions when wet-weather flows occur, the flows will surcharge the sewer and the hydraulic grade line will rise and limit the discharge capacity.

If the variation in flow is too great, then a tipping gate or motor or cylinder-operated gate should be used instead of the manually operated gate.

The hydraulic gradient and energy lines for peak dry-weather flow should be computed starting at the interceptor and proceeding upstream through the sluice gate manhole to the chamber. The quantity diverted to the interceptor during storm periods is determined in a similar manner by trial and error method assuming various discharges.

In the initial computation, the hydraulic computations should start at the water surface in the interceptor at peak dry-weather flow. In subsequent trials it may be necessary to raise the branch interceptor at its junction with the main interceptor which will result in flow at critical depth at the end of the branch interceptor. In this case it may be necessary to compute the backwater curve for the flow in the branch interceptor to determine the depth of flow at the upstream end. Figures 15 and 16, Hydraulic Profile for 3 cfs and 8.6 cfs, present the results of the design computations for flow in the foul outlet.

Sizing from Mathematical Model

The sizing of the chamber in the foregoing discussion is based on the results of the hydraulic laboratory study as reported in Appendix 1.

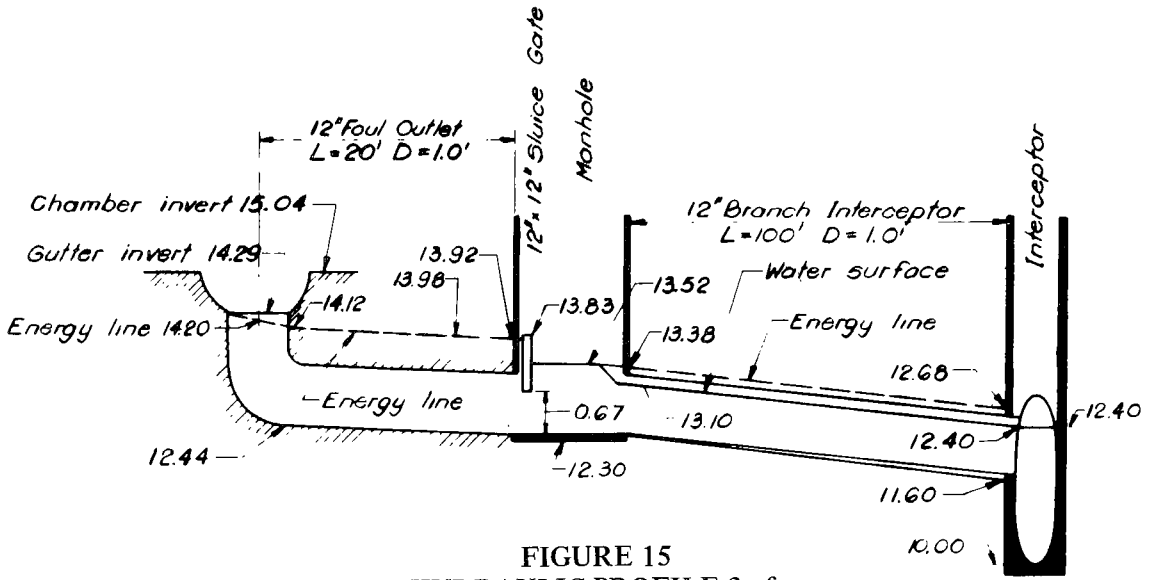

FIGURE 15
HYDRAULIC PROFILE 3 cfs

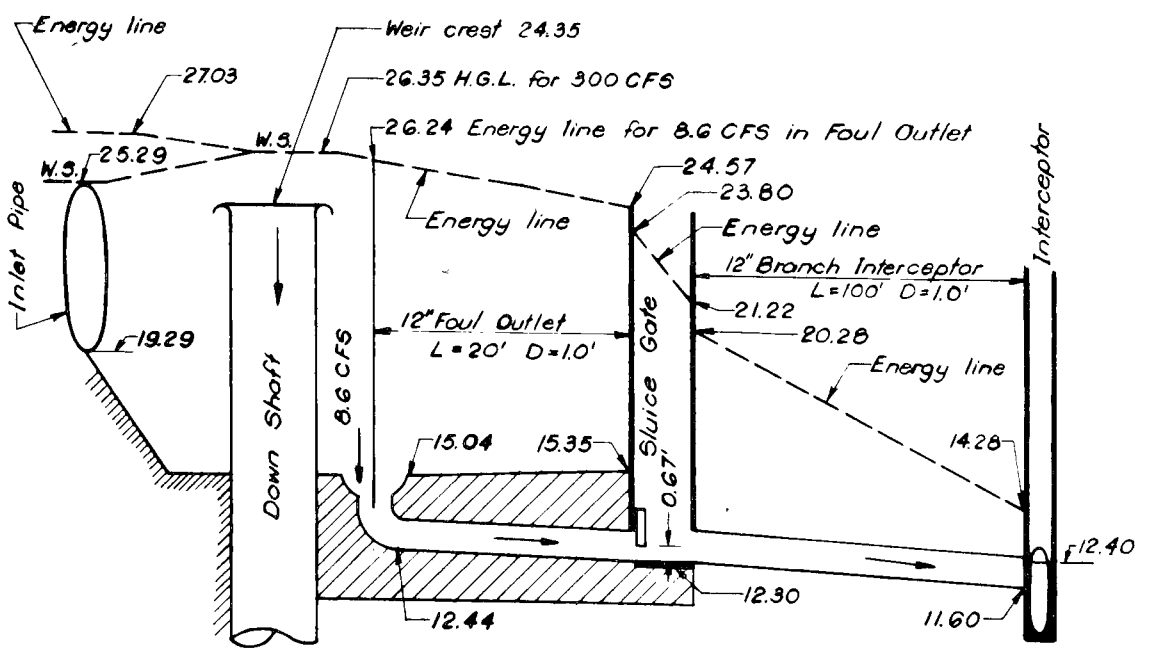

FIGURE 16
HYDRAULIC PROFILE 8.6 cfs

TABLE 11

Design Examples

(from mathematical model data)

Example No. 1

Design Q = 165 cfs

Remove 90% of settleable solids greater than 1.0 mm (0.0394 inches) with specific gravity of 1.2. (To conform with Fig. 20, Storm Discharge vs Chamber Diameter Design Curve, Appendix 1).

From Figure 30, Particle Settling Rates, Appendix 2:

Enter with particle diameter of 0.039 inches and specific gravity of 1.2.

Then Vs = 0.145 fps

$$\text{Then } \Psi = \frac{Q}{V_s^5} = \frac{165}{(0.145)^5} = 2.57 \times 10^6$$

From Figure 31, Scale Factor Diagram, Appendix 2:

Enter with Ψ of 2.57×10^6 and

E of 90%

Then $\theta = 0.16$ and $\Phi = 0.036$

$$S = \left(\frac{Q}{\theta}\right)^{0.4} = \left(\frac{165}{0.16}\right)^{0.4} = 16.0$$

$$S = \left(\frac{V_s}{\theta}\right)^2 = \left(\frac{0.145}{0.036}\right)^2 = 16.2$$

Use S = 16

Then D = (16) (3) = 48 feet

This compares with 36 feet as determined from Figure 20, Storm Discharge, Appendix 1.

Determine other dimensions of chamber from Figure 21, Appendix 1, General Design Details.

Example No. 2

Increase size of settleable solids from 1.0 mm to 2.0 mm

Design Q = 165 cfs

Remove 90% of settleable solids greater than 2.00 mm (0.078 inches) with specific gravity of 1.2

From Figure 30, Appendix 2:

V_s = 0.28 fps

$$\text{Then } \Psi = \frac{Q}{V_s^5} = \frac{165}{(0.28)^5} = 9.59 \times 10^4$$

From Figure 31, Appendix 2:

$\theta = 0.28$ $\Phi = 0.078$

$$\left(S = \frac{Q}{\theta}\right)^{0.4} = \left(\frac{165}{0.28}\right)^{0.4} = 12.8$$

$$\left(S = \frac{V_s}{\Phi}\right)^2 = \left(\frac{0.28}{0.078}\right)^2 = 12.9$$

Say S = 13

Then D = (13) (3) = 39 feet

Concurrent with the hydraulic laboratory work a mathematical model of the swirl chamber was developed. This was the first attempt to rationalize the design of such devices to determine operating principles. A method was developed for sizing the chamber based on a given design flow and the desired percentage removal of solids with a given size and specific gravity. Hence, the applicaton of this method is more universal than the hydraulic laboratory model, which is based on the removal of solids in a synthetic sewage.

The sizing of the chamber by the two methods does not give exactly the same results. This is primarily due to the difference in interpreting the characteristics of the solids used in the hydraulic laboratory model. Hopefully the construction of the full size chamber and the resultant testing thereof will yield data which will confirm the design methods.

For illustrative purposes the design method developed in the mathematical model is given in Table 11, Design Examples (from mathematical model data)

From the Design Example based upon the mathematical model for a solids size of 2.0 mm a chamber only slightly larger (39 vs 36 feet) will be required as compared to the hydraulic model curve for a solids size of 1.0 mm. This is due, in part, to the different interpretation of the relation of the gilsonite size to the solid size in the prototype – mathematical model deriving larger solids sizes in the prototype for the gilsonite than from the hydraulic model.

SECTION V
IMPLEMENTATION

Consideration of the use of a swirl concentrator as a combined sewer overflow regulator facility requires an evaluation of many factors which include:

1. hydraulic head differential between the collector and interceptor sewers and head available in collector sewer to allow insystem storage;
2. hydraulic capacity of collector sewer;
3. design flow;
4. dry-weather flow and capacity of interceptor sewer; and
5. amount and character of settleable solids.

Although many of these items have been mentioned in the preceeding sections of the report, the importance of each will be highlighted in order to emphasize the importance of each point in a preliminary evaluation of the use of the swirl concentrator.

Hydraulic Head Differential. There must be sufficient hydraulic head available to allow dry-weather flows to pass through the facility and remain in the channel. The total head required for operation is shown in Figure 17, Hydraulic Head Requirements. Determination of the maximum elevation in the collector sewer that can be utilized for insystem storage and the differential elevation between the collector and interceptor sewers is the total available head.

The head required will vary directly with flow and the outlet losses in the foul sewer.

If sufficient head is not available to operate the foul sewer discharge by gravity, an economic evaluation would be necessary to determine the value of either pumping the foul sewer outflow continuously, or pumping the foul flow during storm conditions and bypassing the swirl concentrator during dry-weather conditions, perhaps with a fluidic regulator.

Hydraulic Capacity of Collector Sewer System. The facility must be designed to handle the total flow which might be delivered by the collector system. Thus a study of the drainage area must be made to determine the limiting grade and pipe sizes which control the quantity of flow. Solids removal from a peak flowrate may not be required. If the chamber is not designed for such maximum flows, however, velocity energies which could be developed at such full flow conditions should be avoided by providing a bypass in the form of a side overflow weir.

Design Flow. Selection of the design flow for sizing the chamber should be accomplished on the basis of a complete hydrological study to determine frequency and amount of precipitation which can be anticipated as well as runoff hydrographs. Computer models such as developed by the University of Florida for USEPA can be of assistance in determining the solids load which may be associated with various amounts and intensity of precipitation. Provision of maximum solids removal for a two-year frequency storm for the Lancaster, Pennsylvania, Project was made on the basis of engineering judgment and an evaluation of local receiving water conditions. As the cost of construction will increase in direct proportion to design flow, an economic evaluation should generally be used to select the flow capacity. The efficiency curve for the facility is rather flat over a wide range of flows, resulting in perhaps large increases in cost for marginal improvements in efficiency.

A major constraint in selecting large design flows is the anticipated shoaling problems of solids at low flow rates in large facilities. Self cleaning is enhanced by reduced diameters. This consideration may make it desirable to design for lower flows, particularly where some form of overflow treatment is to be provided. Again the computer model can be used to determine the magnitude of the solids carry-over problem to the secondary device.

A third consideration is the maintenance of low-inflow velocities, with turbulence minimized. At the design flow the inflow velocity should be in the range of three to five fps. The inflow velocity may require

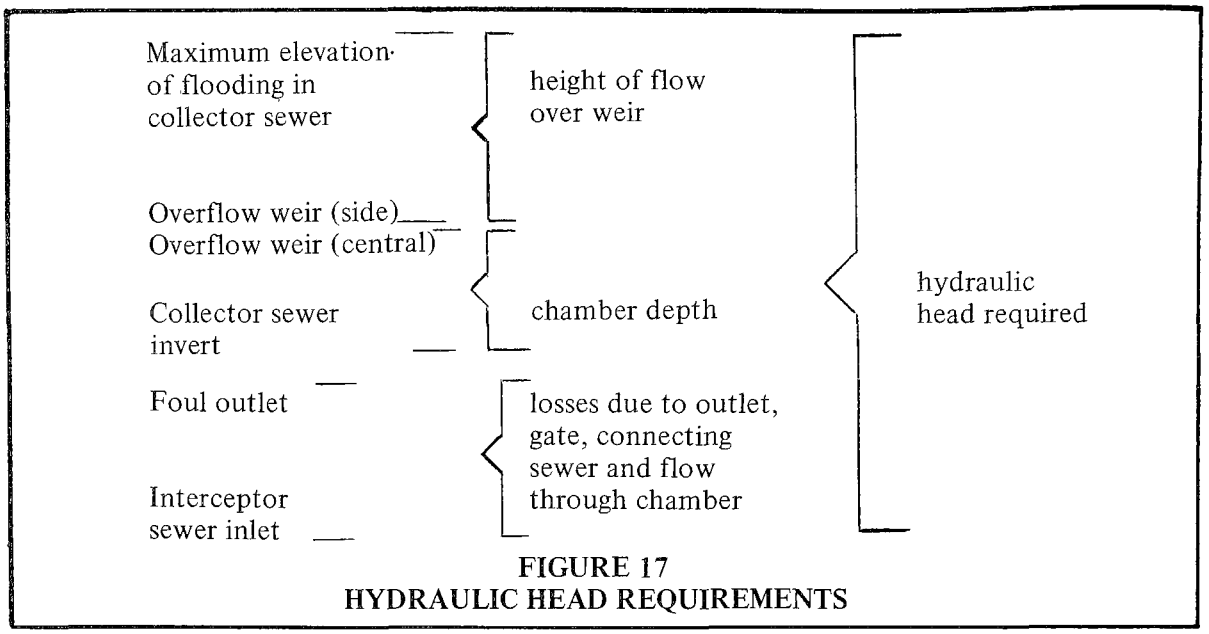

FIGURE 17
HYDRAULIC HEAD REQUIREMENTS

reduction by enlarged pipe sections or other means to achieve this rate.

Dry Weather Flow and Capacity of Interceptor Sewer. Sizing of the foul sewer, the foul outlet and the gutter depend upon a determination of the dry-weather flow In addition, the capacity of the interceptor sewer to handle the foul flow must be known. The foul sewer must be large enough to maintain and not be subject to blockage—usually a minimum 12-in. diameter. However, the head on the outlet during overflow conditions will allow considerable variations in the foul discharge if it is not controlled.

The efficiency of the chamber is affected by the ratio of foul flow to overflow—although there appears to be a broad operating range over which reasonable removal efficiencies can be maintained.

Maximum advantage should be taken of capacity in the interceptor system, particularly during the period when the chamber is being drawn down. Thus, sensing of the flow in the interceptor and the use of a control gate on the foul sewer appear desirable to obtain maximum results from the use of the chamber.

Amount and Character of Settleable Solids. The sewer system must provide capacity to handle the increase in settleable solids which will be captured from the combined sewer overflow and discharged to the treatment plant. In the case of Lancaster, Pennsylvania, this could amount to more than a ton of solids from one device in a very short period of time. Additional grit removal and sludge processing equipment may be necessary. Should the foul flow be pumped, sumps and pumps should be designed to handle the anticipated high solids content.

If the settleable solids which can be anticipated in the combined sewer overflow can be defined by the amount, specific gravity, and particle size, the mathematical and the hydraulic model may be used to determine the size of the chamber required to achieve desired levels of solids removal. Ordinarily this will not be feasible and the flow criteria developed by the hydraulic model will be used to design the facility and predict removal efficiencies.

In order to evaluate the efficiency of the chamber, facilities should be provided for sampling the inflow, foul sewer flow and overflow. Settleable solids should be delineated in all these flows. The quantity of inflow and foul sewer flow should also be measured. Difficulties in obtaining representative samples from any of the flows may make evaluation difficult. However, the treatment plant or combined sewer overflow

treatment facility, if used, should provide an excellent means of making a gross evaluation as to the effectiveness of the chamber.

Provision of a means to measure the depth of flow over the weir should act to give a reliable measurement of the flow when added to the quantity of flow to the foul sewer.

Data from many full-scale operations, operating with various flow conditions and solid loadings will be necessary to properly evaluate the usefulness of the swirl concentrator as a combined sewer overflow regulator.

Cost of Facility. The cost of construction of the swirl concentrator will vary with the length of inlet pipe which must be reconstructed, the depth of the chamber and the nature of the material to be excavated, the need for a roof, and the general site conditions under which the work will be conducted. The materials of construction will usually be concrete and steel and elaborate form work will not be required.

For the Lancaster, Pennsylvania, application where a 36-ft-diameter chamber in limestone is contemplated, the preliminary estimate of cost was $100,000 in 1972 costs. This cost estimate included a roof, foul sewer outlet control and a wash-down system. Site construction problems are minimized in as much as the construction will be off of the street right-of-way.

SECTION VI
POTENTIAL USES AND RESEARCH NEEDS

POTENTIAL APPLICATIONS

The principle which has been demonstrated in this study project should have application to facilities (other than combined sewer regulators) which are involved in, and affected by, liquid flows and the presence of solid particles of various diameters and specific gravities which must be concentrated and removed from the liquid flowfield. In the sanitary engineering field, this could relate to sanitary sewer flows, storm sewer flows, primary treatment requirements for sewage treatment plants, and concentration of settleable solids from industrial and commercial wastes.

Each of the above applications in the sanitary engineering spectrum may involve less arduous conditions of operation than the combined sewer regulator application. Both the hydraulic laboratory and the mathematical model investigation have indicated that greater efficiency of solids separation may be experienced if the device operates under steady flow conditions, and if a specific range of solids size and specific gravity is to be removed. The hydraulic laboratory studies concluded that the device appears to exhibit preferential limits of grain sizes separated according to the elements being tested.

Future research should be directed at narrower grain size bands. For example, a chamber which was designed to separate only the fines might do so with much greater efficiency than the regulator device which was designed to remove grit as well. Similarly, the mathematical investigation report states, "It is not clear whether better efficiencies can be achieved with two half-size chambers or one full-size unit. With two units, one chamber could be used for all flows lower than 100 cfs . . (at the site of the proposed prototype regulator where 165 cfs was the design flow) . . . and the second would be required if the storm flow exceeded that value. This might provide better separation at both higher and lower flow rates. This example corresponds to operating two chambers in parallel and the concept can readily be extended to an arbitrary number of units. The possibility also exists of operating units in series to improve, i.e., classify, the solids particles to be removed."

The following applications of the swirl concentrator are not proven, but appear to be rational in light of the experience of the current studies, basic hydraulics, and available information from water and wastewater systems.

Primary Treatment Plant Application. In the primary sewage treatment process floating, suspended settleable solids in untreated sewage are reduced by plain sedimentation, or fine screening. Therefore the principal elements of primary treatment are devices which assist in the physical separation of sewage solids from their flow. This is the specific purpose for which the swirl concentrator is intended. The principal elements of primary treatment facilities which could be considered include grit chambers, primary clarifiers, and sludge thickeners. In each of these applications, the range of material sizes and inflow variation can be reduced, increasing the probability of efficient performance.

Grit Chamber. In the application of the swirl concentrator as a grit chamber, two design features are desirable. First, the device should separate grit only; second, it should be self cleansing under design operating conditions. As the specific gravity of grit is 2.65, the ratio of design inflow to the foul sewer outflow would be greater than that of combined sewer overflow regulator design, so that rotational velocities in the chamber would be sufficient to move all the heavier denser material to the foul sewer, and so great that all the lighter solids fraction would overflow to further treatment devices. Based on current laboratory experiments, the device could be sized so that shoaling of grit would not be a problem. No mechanical collection and removal would be required.

The grit fraction removed from the sanitary sewage would require dewatering.

This could be achieved by using conventional grit collectors of the screw or cleaning bucket variety. The advantage of this application is the speed with which the grit can be removed, and the reduced size or quantity of conventional grit collection devices required at the plant. No attempt should be made to recover floating solids in this operation; they would overflow to further treatment.

Primary Clarifier. The primary clarifier is a sedimentation basin which normally operates on a continuous flow basis. Considering that the grit has been removed, as described above, the function of the swirl concentrator as a primary clarifier is the removal of organic suspended settleable solids and floating solids.

Removal of settleable solids would be accomplished by reducing the rotational velocity in the chamber sufficiently to promote their settlement to the bottom. Floatables could be separated by using a scum ring and floatables deflector, sized and located as in the regulator application, with the optimum point of collection and concentration of floatables determined by further studies. It may be advantageous to use coagulant aids to assist in the removal of particles in suspension.

In a prototype sized primary clarifier being tested in England, one of the most serious difficulties encountered has been how to ensure the continuous removal of sludge. The greater the separation efficiency in the chamber, the more difficult this became. It was virtually impossible to operate the clarifier continuously with a low foul sewer flow without mechanical cleaning in the England application. Base scrapers had to be used and they were vane driven by the rotational flow of the sewage.

Data developed by Smisson in England indicate that a solution to this problem may be to operate two swirl concentrator clarifiers in series with sludge thickeners of the same type, and with a percentage of the overflow returned to the inlet. A significant decrease in sludge shoaling has been achieved with a return flow of less than 25 percent.

The principal advantage of the use of the swirl concentrator as a primary clarifier is the great reduction in time required to effect the settlement as compared to standard sedimentation basins. The standard separation time is 120 minutes. The swirl concentrator should achieve similar separation efficiencies in less than 15 minutes. Thus the size and space requirement of the swirl concentrator would be 12.5 percent of current needs. This application would reduce the area of the plant, the construction materials required, and the mechancial equipment and energy required to move and collect solids. Consequently, the capital, operating and maintenance costs of primary treatment facilities would be similarly reduced.

Sludge Thickener. The object of this third potential application of the swirl concentrator principle in primary treatment is to separate and concentrate all solids delivered from the primary clarifier so that the volume to be handled in the digestor or other sludge disposal facilities will be reduced. The specific gravity of sludge particles approaches unity, and the purpose of sludge thickening is to stir sludge for prolonged periods for the purpose of agglomerating the mass to form larger and more rapidly settling aggregates of sludge floc with less water content. To achieve this phenomena in a swirl concentrator, it will be necessary to operate the device with a very gentle rotary motion under steady flow conditions, so that the floc will not be broken. The advantage of this application of the swirl concentrator is that thickened sludge at the foul outlet should be available in considerably less than the hours normally ascribed to the process of sludge thickening by standard stirring methods, thus reducing the size requirement of a comparable swirl sludge concentrator. Although the need for mechanical equipment may be reduced in the device, the use of a bottom sludge collector mechanism may be necessary.

OTHER APPLICATIONS

Other potential applications of the swirl concentrator offer rational possibilities in related liquid-solids handling in the hydraulic sanitary engineering field.

Wash Water Clarifier–Water Treatment Plant. Serious concern has been expressed

over the pollutional effect of discharging filtered wash water into watercourses. To overcome this hazard, these wash waters must be intercepted and treated. Concentration of the wash liquor in a swirl concentrator of appropriate design offers the possibility that approximately 80 percent of the wash water solids could be concentrated in three percent of the wash water flow, and be directed to a predetermined point of disposal. The balance of the flow would be permitted to overflow to the receiving water without creating a shock loading on the receiving waters.

Storm Sewer Pollution. A report entitled "Water Pollution Aspects of Urban Runoff," prepared by the American Public Works Association for the Federal Water Pollution Control Administration, concluded that the coarse or crude materials in street litter have a marked pollutional impact on receiving waters. These suspended solids are washed into street inlets of storm sewers and can create objectionable conditions at storm sewer outlets, where they float or shoal in receiving waters. In addition, organic materials may decompose and produce tangible oxygen demand upon receiving waters while the cost of reducing pollution of surface drainage water from urban areas may be very high, it may become necessary in some areas to treat storm water runoff before it is discharged into receiving waters.

In such case, the foul sewer discharge could be directed into an available interceptor sewer for treatment either by gravity or pumping, as required.

Improvement in the quality of such separate storm sewer discharges could be accomplished by swirl concentrator facilities much in the same manner used for combined sewer flows as described by the current study.

Soil Conservation. Sediment carried by erosion represents the greatest volume of waste entering surface waters.[6] The volume of such suspended solids reaching watersources is at least 700 times greater than the total of sewage wastes. One estimate is that the average siltation yield at construction sites during rainstorms is about ten times that for cultivated land, 200 times that for grass areas, and 2,000 times that for forest areas, depending on the rainfall, land slope and exposure.

Many agencies now require that special precautions be taken by developers during subdivision construction and by road construction contractors. In spite of these regulations, erosion of silt and topsoil from construction sites can infuse downstream receiving waters with suspended and settleable solids, and make it necessary for new landscaping material to be hauled to the construction site, increasing the cost of land development and other projects.

In subdivision construction, installation of storm water utility services is one of the first phases of a project. A swirl concentrator could be placed at the downstream end of a drainage project. Silt and topsoil could be trapped at the site and used in landscaping, rather than being discharged to a receiving stream. Even if it is a temporary installation, its cost may represent a minor part of the overall value of the development.

Similarly, mine tailing wastes, particularly from strip mines, have been allowed to run off to receiving streams creating excessive dredging costs and endangering downstream reservoirs because of siltation. These tailings could be concentrated in a swirl concentrator and rehandled for backfilling at the mine site.

RESEARCH NEEDS

In order to evaluate these and other applications, it will be necessary to demonstrate by pilot studies the value of the swirl concentrator principle outside the combined sewer regulator field. Because of the limitations of the tests carried out in the current combined sewer study, ranges of particle sizes and their specific gravities, which produce greater separation efficiencies are unknown. The size limitations of the swirl device for the suggested purpose are also unknown. It is understood that different rotational velocities produce maximum separation efficiency of specific particle size and specific gravity ranges, but the relationships are not yet defined. It has been demonstrated that the concentrator can produce maximum efficiencies when operating under steady flow conditions, but

in the sanitary engineering field this hydraulic condition is rarely possible. Consequently, it will be necessary to determine by research what fluctuation in flow can be tolerated to achieve an acceptable level of efficiency and what inlet to foul sewer outlet ratio produces the greatest separation efficiency, consistent with self-cleansing velocity and for what type particle.

These criteria must be answered through continuing research aimed at examining such applications and developing of design nomographs and simple parametric formula which will enable designers to exploit the swirl concentrator to its fullest potential.

SECTION VII

The American Public Works Association is deeply indebted to the following persons and their organizations for the services they have rendered to the APWA Research Foundation in carrying out this study for the City of Lancaster, Pennsylvania, and the Environmental Protection Agency.

City of Lancaster

Lester R. Andes, Director of Public Works

Consultants

Dr. Morris M. Cohn, Consulting Engineer
J. Peter Coombes, Consulting Engineer
Bernard S. Smisson, Bristol, England

Alexander Potter Associates, Consulting Engineers

Morris H. Klegerman
James E. Ure

General Electric Company, Re-entry and Environmental Systems Division

Harold D. Gilman
Dr. Ralph R. Boericke
Carl M. Koch

LaSalle Hydraulic Laboratory, Ltd.

F. E. Parkinson

U. S. Environmental Protection Agency

Richard Field, Project Officer, Chief, Storm and Combined Sewer Technology Branch, Edison Water Quality Research Divison, National Environmental Research Center

William A. Rosenkranz, Chief, Municipal Technology Branch, Office of Research and Monitoring

Darwin R. Wright, Chief, System Control and Optimization Section, Office of Research and Monitoring

Meridian Engineering, Inc.

T. R. Darmody

University of Florida

Dr. Wayne C. Huber

SECTION VIII
GLOSSARY OF PERTINENT TERMS
(as applied to the report on the swirl concentrator)

Deflector—A plate or plane structure which diverts and directs flows in a swirl concentrator chamber into desired patterns and thus prevent flow kinetic conditions which would interfere with optimum swirl motion.

Combined Sewer—A pipe or conduit which collects and conducts sanitary sewage, with its component commercial and industrial wastes and inflow and infiltration waters at all times, and which in addition, serves as the collector and conveyor of storm water runoff flows from street and other sources during precipitation and thaw periods, thus handling all of these types of waste waters in a "combined" facility.

Depth of Chamber—The vertical distance between the floor level in the swirl concentrator chamber and the crest of the overflow weir at the central downdraft structure.

Exterior Liquid Mass—The liquid induced to flow in the outer zone of the circular swirl concentrator chamber, by use of the skirt, wall structural configuration or other built-in devices, where the higher velocities of flow produce a longer liquid trajectory which allows adequate time for heavier solids to settle to the floor of the chamber.

Floatable Solids—Solids and congealed liquid matter which are lighter than water and float on the surface of the waste water flowing in the swirl concentrator chamber.

Floatables Trap—A device or structural configuration in a swirl concentrator chamber which intercepts floatable solids, prevents them from overflowing from the chamber with clarified waste water, and retains these materials at a desired location until removed and disposed of by predetermined means.

Foul Sewer—The sewer carrying the mixture of combined sewage and concentrated settleable solids to the interceptor sewer.

Grit—Heavier and larger solids which, because of their size and specific gravity, settle more readily to the floor of the swirl concentrator chamber by the phenomenon of gravity classification.

Gutter—A structural configuration in the floor of a swirl concentrator chamber which serves as a channel for the desired flow of dry-weather sanitary sewage flow from the inlet to the foul sewer outlet, and for conducting any other waste water components to predetermined points of concentration and exit from the chamber.

Interior Liquid Mass—The liquid induced to flow in the inner zone of the circular swirl concentrator chamber—by use of the same skirt, wall structural configuration or other built-in devices which induce exterior liquid mass flows—where the lower velocity permits lighter solids to settle out of the waste water flow and to deposit on the chamber floor and to be drawn to the foul sewer outlet. The principle of the swirl concentrator is to organize the flow patterns and cause the liquid mass to pass through the exterior and interior liquid mass zones to optimize solids separation and removal.

Overflow Weir—The structural member of the swirl chamber, which is built as a central circular wall with a proper form of overflow edge over which the clarified waste water can discharge to the downdraft outlet leading to receiving waters or to holding or treatment facilities.

Regulator—A device or apparatus for controlling the quantity and quality of admixtures of sewage and storm water admitted from a combined sewer collector sewer into an interceptor sewer or pumping or treatment facility, thereby determining the amount and quality of the flows discharged through an overflow device to receiving waters, or to retention or treatment facilities.

Scaling—The principle of ascertaining dimensions and capacities of hydraulic test units and mathematical analysis systems to

evaluate the performance of swirl concentrator chambers, and to up-scale such sizes to provide actual field design and construction criteria or parameters.

Scum Ring—A circular plate or baffle encircling the overflow weir, located at a predetermined distance from the weir and at a depth which will serve to retain floating or scum material and other floatables and prevent them from passing over the effluent weir with the overflow liquid.

Settleable Solids—That portion of the solids contained in the waste water flow into a swirl concentrator chamber which will subside and be collected in the chamber due to gravity and other liquid-solids kinetic conditions induced by the controlled swirl flow pattern. (Note: Not all suspended solids are settleable solids, nor are so-called colloidal solids or other finely dispersed solids settleable solids.)

Spoiler (Energy Dissipating Baffle)—A plate or structural plane constructed from the scum ring to the weir plate in a swirl concentrator chamber for the purpose of preventing or dampening the development of free vortex flow conditions and minimizing agitation and rotational flow over the discharge weir.

Static Regulator—A regulator device which has no moving parts, or has movable parts which are insensitive to hydraulic conditions at the point of installation and which are not capable of adjusting themselves to meet varying flow or level conditions in the regulator-overflow structure.

Storage Silo—A holding chamber, constructed in the form of a "silo," for the Lancaster, Pennsylvania overflow management project, which will collect, store and aerate overflow waste waters from the combined sewer regulator facilities until these liquids can be pumped back into the interceptor sewer system or treated prior to being discharged into nearby receiving waters.

Storm Frequency—The time interval between major storms of predetermined intensity and volumes of runoff for which storm sewers and combined sewers, and such appurtenant structures as swirl concentrator chambers, are designed and constructed to handle flows hydraulically without surcharging and back-flooding; i.e., a five-year, ten-year or twenty-year storm.

Swirl Concentrator—In the context involved in this study and report, a device or chamber with necessary appurtenant structural configurations which will kinetically induce a rotary motion to the entering waste water flow from a combined sewer, resulting in secondary motion phenomena which will cause a concentration of solid pollutional materials at a predetermined location, from which it can be diverted into the foul sewer, thereby producing a partially clarified waste for decantation or overflow into receiving or storm overflow treatment facilities.

Vortex Separator—A device of general structural configuration similar to the swirl concentrator studied in the current project, but which involves flow patterns that produce less effective solids separation because of turbulence and other uncontrolled liquid-solids flow conditions.

Weir Plate—A plate or surface constructed contiguous with the outlet overflow weir of a swirl concentrator chamber, and a skirt hanging below the weir, under which floatables will be trapped and held until released for removal from the chamber.

Weir Skirt—A plate hanging below the swirl concentrator chamber overflow weir, to assist in retaining floatable solids under the weir plate and in inducing the shearing of the chamber flow into an exterior liquid mass and an interior liquid mass, thereby optimizing the solids separation effectiveness of the swirl concentrator principle.

SECTION IX
REFERENCES

1. American Public Works Association, *Combined Sewer Regulation and Management,* 11022DMU 08/70, U.S. Environmental Protection Agency, 1970, pp. 134.
2. American Public Works Association, *Combined Sewer Regulator Overflow Facilities,* 11022DMU 07/70, U.S. Environmental Protection Agency, 1970, pp. 139.
3. Smisson, B., *Design Construction, and Performances of Vortex Overflows,* [Proceedings, Symposium on Storm Sewage Overflows, Institution of Civil Engineers, May 4, 1967], pp. 99.
4. Ackers, P., Harrison, A.J.M., and Brewer, A.J., *Laboratory Studies of Storm Overflows with Unsteady Flow,* [Proceedings, Symposium on Storm Sewage Overflows, Institution of Civil Engineers, May 4, 1972], p. 37.
5. Prus-Chacinski, T.M., and Wielgorski, J.W., *Secondary Motions Applied to Storm Sewage Overflows.*

SECTION X
INDEX TO TABLES AND FIGURES IN APPENDICES

Appendix 1 – Hydraulic Model Study

Appendix 2 – Mathematical Model Study

APPENDIX 1
HYDRAULIC MODEL STUDY

The hydraulic model study described in this appendix was undertaken with the object of developing the basic geometry for a swirl concentrator best adapted to North American conditions. Guidance was provided in this work by earlier research carried out in Bristol, England, by Mr. Bernard Smisson.

PRINCIPLES AND SCOPE OF STUDY

The general principle which Mr. Smisson had developed did not fit into the definition of known laws of either vortex or simple settlement separation, but rather appeared to be a controlled combination of the two. Basically, his approach consisted of introducing the combined sewer flows into a cylindrical chamber, so that a rotational flow was created in the chamber. A significant portion of the heavier solid particles settled to the floor, then migrated toward the center of the chamber. The foul sewer outlet was located to intercept this concentration of pollutant materials, so that they could be directed to the interceptor and thence to the treatment plant. The clearer liquid overflowed a central circular weir, to the outfall and receiving waters.

Mr. Smisson's publications covered his work up to 1967, and the first tests served as a verification of these principles. Since 1967, his research led him to modify slightly the chamber geometry. The test program was laid out to carry on from there, adapting his principles to North American requirements.

The main difference in European and North American conditions was the discharge/chamber volume ratio. The aim was to use a similarly sized chamber as Mr. Smisson, but to treat from four to six times as much flow.

The first model geometry selected was based on the latest Smisson test data. This was a flat floored chamber with central column one-sixth the chamber diameter supporting a weir approximately five-sixths of the chamber diameter. A weir and weir skirt plate were attached to the outer circumference of the weir plate. The research program investigated the importance of chamber depth, shape of the entrance to the chamber, and various weir diameters to obtain the optimum recovery of settleable solids through the foul outlet.

Mr. Smisson's latest work had also included use of an oblique entry to the chamber. With the flow directed across the chamber from the chamber wall toward the central shaft, it became possible to trap floatables. He found that a skirt hanging below the weir would retain the floatables under the weir plate. When the water level dropped in the chamber, these trapped floatables descended on the water surface to be evacuated through the foul sewer outlet.

The skirt also served the purpose of creating a shear zone which effectively divided the chamber into two parts; an exterior liquid mass in which the flow moved rapidly, and an interior mass which rotated slowly Optimum separation could be obtained by the proper exploitation of these two zones; the longer trajectory in the outside section would allow sufficient time for larger particles to settle to the floor, and the slower movement in the interior mass would permit settling of finer material. Manipulation of these research parameters was directed toward organizing the flow in the chamber to pass continuously through the two zones so as to take maximum advantage of their respective characteristics.

Dimensioning of the model and scale-up were based partly on the White Ladies Road project[1] in Bristol, with the object of using it in a project being built in Lancaster, Pennsylvania. At the same time all the testing and results were treated as being applicable to other installations at other locations, on the basis that this type of device would be adaptable, over a wide range of scale-up ratios, to amenable projects anywhere.

Model Description

The swirl concentrator took the form of a vertical cylinder 36 inches in diameter and 40 inches high, made of 1/2-inch plexiglass as

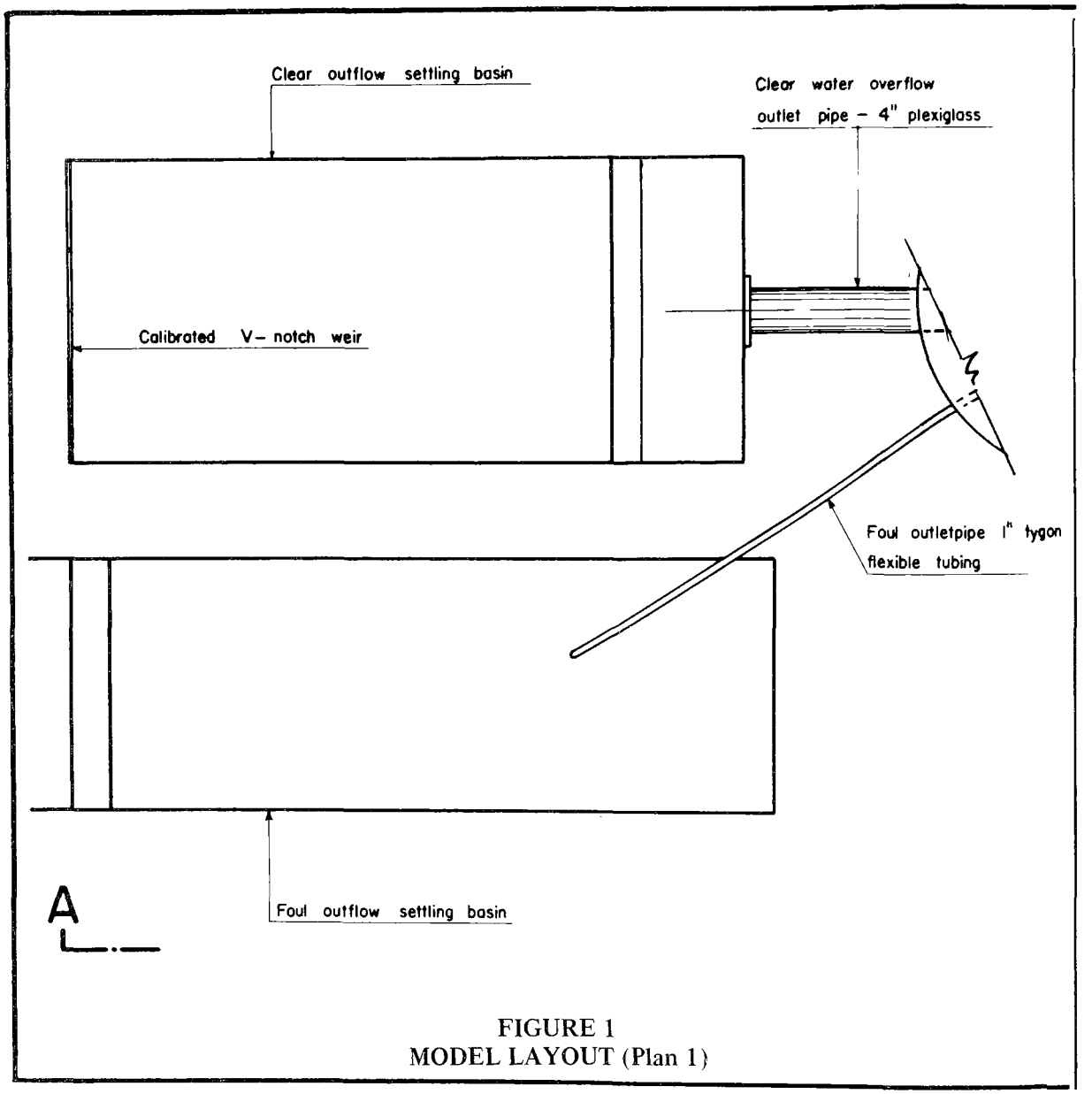

FIGURE 1
MODEL LAYOUT (Plan 1)

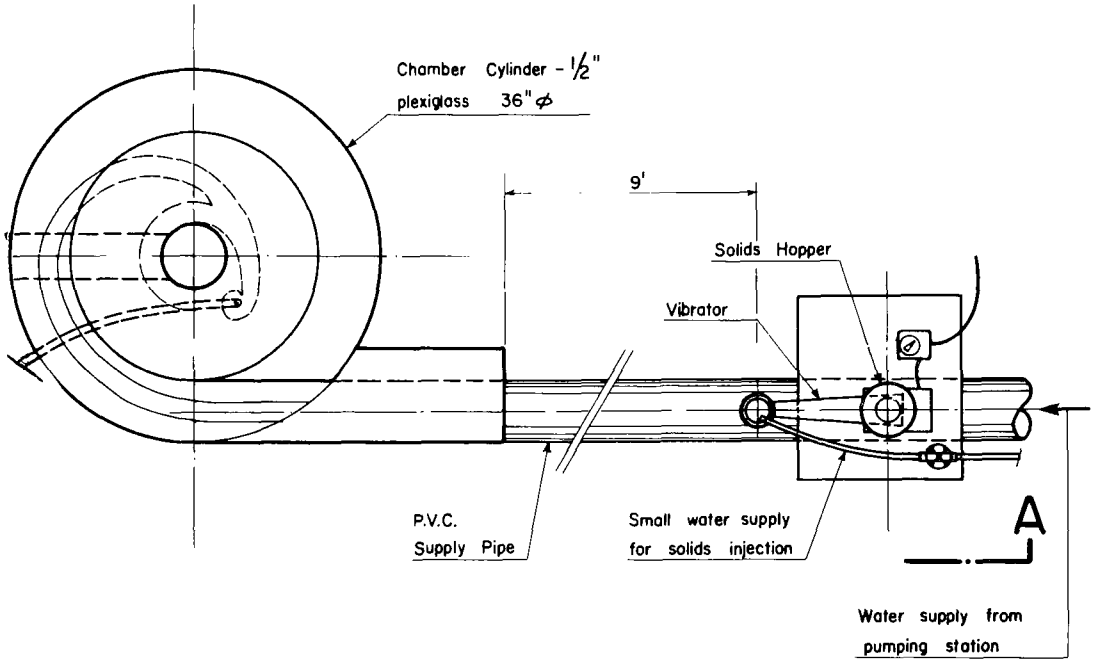

FIGURE 1
MODEL LAYOUT (Plan 2)

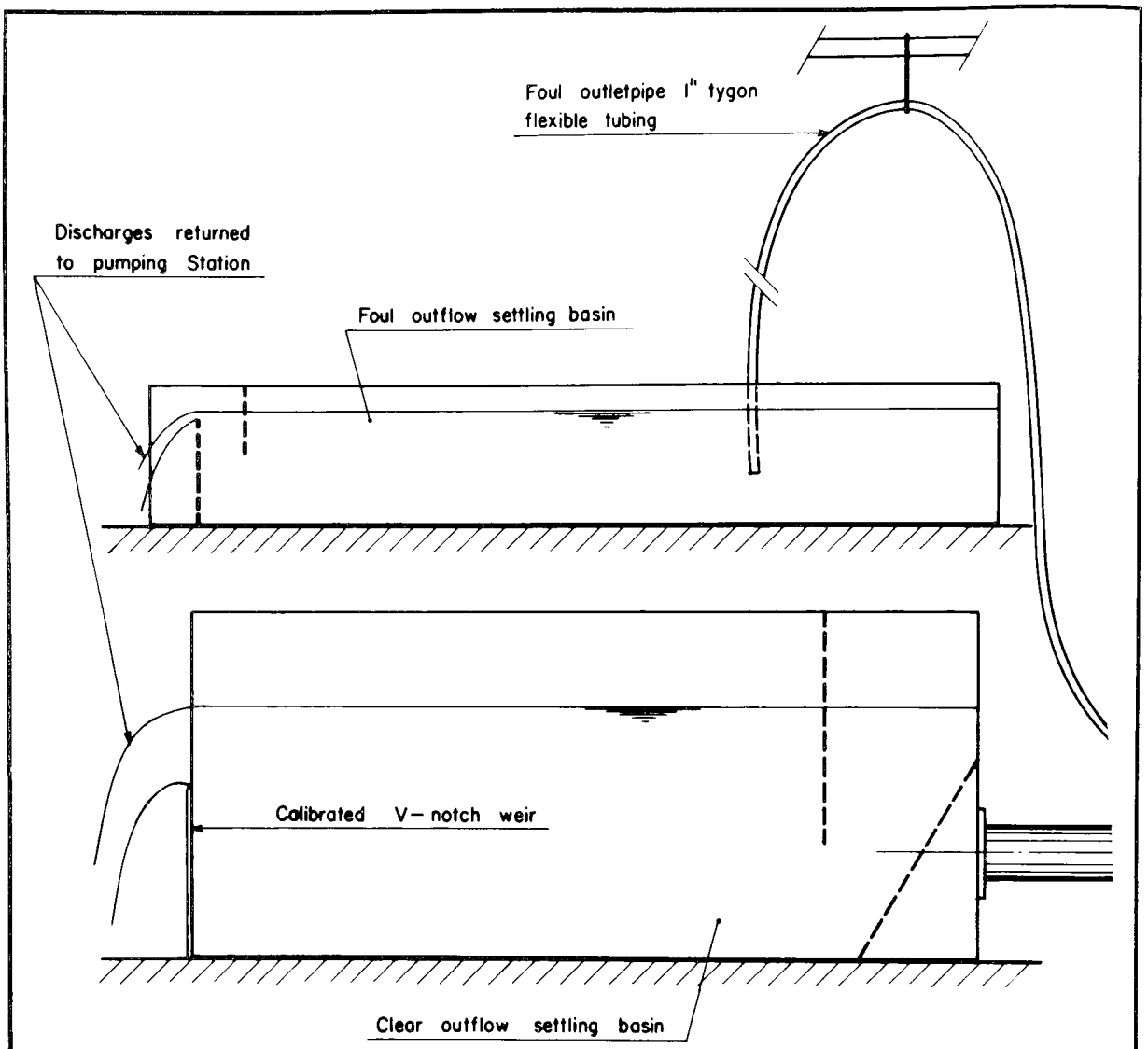

FIGURE 1
MODEL LAYOUT (Section 1)

shown in Figure 1, Model Layout. The inlet was a six-inch diameter polyvinyl chloride (PVC) pipe, set at an arbitrary level with respect to the chamber, and at a slope of 1:1000. A vibrating solids injection system was placed on this supply pipe, nine feet upstream of the chamber. Water supply to the model through the pipe was taken directly from the constant level tank in one of the laboratory permanent pumping stations.

A movable one-inch diameter tygon tube was placed inside the cylinder, beneath the floor of the test chambers to pick up the foul flow. The tube was led out the bottom of the cylinder, and its free end could be raised or lowered at will to control the discharge drawn off through the foul outlet.

The overflow water outlet came up from the base, on the centerline of the cylinder in the form of a six-inch-diameter P.V.C. pipe. Its level could be changed easily either by adding or removing elements of the same

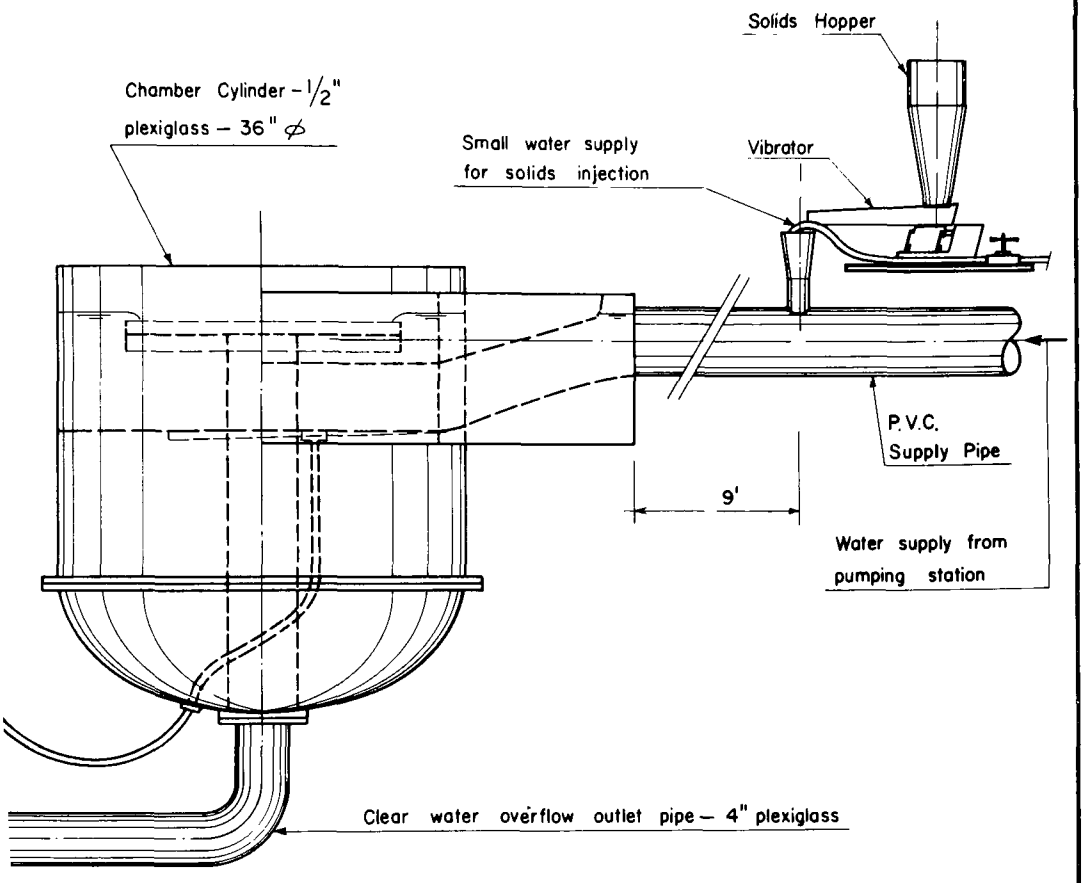

FIGURE 1
MODEL LAYOUT (Section 2)

diameter pipe, or with adaptors to provide either larger or smaller diameter downshafts.

Outflow from this pipe, which in operation represents the major part of the total discharge through the structure, was led to a large settling basin equipped with a calibrated V-notch weir. The basin allowed sufficient time for most of the solids contained in the clarified overflow to settle out. A manometer was used to read the level within the basin. The clear discharge over the circular weir in the chamber was determined with a V-notch weir.

As mentioned above, the central clearwater downshaft could have its upper elevation modified with elements of P.V.C. pipe. Similarly, different diameters or configurations of weir could be adjusted and held in place on top of the shaft by a simple threaded brass rod coming up the center of the shaft.

As the model was originally built, the

inlet pipe with its round cross section was built undeviatingly to the circular chamber wall, directing flow around the chamber periphery as shown by Figure 2, White Ladies Road Configuration. A later modification provided a wider and deeper enclosure in which variations to the entrance form could be fitted and tried.

Solids Simulation Relationships

Project consultants specified the materials in prototype combined sewage that were desired to be removed with the swirl concentrator:

Solids	Specific Gravity	Diameter (mm)	Concentration (-mg/1)
Grit	2.65	0.2-2.0	20-360
Setteable Solids	1.2	0.2-5.0	200-1150
Floatables	0.9-0.998	5-25	10-80

A further definition was provided for the organic settleable solids material with specific gravity 1.2, by specifying its grain size distribution as follows and as shown on Figure 3, Model Simulation of Prototype Solids:

Diameter–(mm)	0.2	0.5	1.0	2.5	5.0
Cumulative Total – %	10	20	35	60	100

Simulation of these materials on the model was considered on the basis of settling velocities according to Stokes equation:

$$V = \frac{\partial w\, d^2}{18\,\mu} \quad (\partial s - \partial w)$$

where: V = settling velocity
d = particle diameter
μ = water viscosity
∂w = specific gravity of water
∂s = specific gravity of solids

The material most used in the testing was gilsonite, a natural hydrocarbon with specific gravity 1.06 and grain sizes between one and three mm. Following the Stokes relation at 1/12 scale, this material reproduces grit between 0.36 and 1.06 mm, and settleable solids between one and three mm.

Reference to Figure 3 indicates that this grit range leaves a small part of the fines unrepresented, as well as a wide part of the coarser particles. The coarser end of the scale was assumed to be covered, since any larger particles would obviously settle out if those represented had settled. The fines at the lower end were simulated with Petrothene®, a compounded plastic with grain sizes between two and four mm and specific gravity of 1.01.

Similar reasoning was followed concerning the settleable solids. The large gilsonite covered much of the middle size range, and the larger particles were assumed to have better settling characteristics than the gilsonite. Therefore the large gilsonite represented 65 percent by volume of the settleable solids in the specified prototype combined sewage. Two finer fractions of ground gilsonite were tested to cover the fines. The first, which passed 25 mesh and was retained on 30 mesh, had a mean particle diameter of 0.5 mm. The second, retained on 50 mesh had a mean particle diameter of 0.3 mm, thereby practically attaining the finest particles specified of 0.2 mm.

The rates of solids injection normally used corresponded to the 50-300 mg/l range in prototype for the development tests. Proving tests later raised the solids injection rate up to 1,550 mg/l, prototype.

Tests for removal efficiency of floatables were carried out using uniformly sized polythene particles 4 mm in diameter with specific gravity 0.92 and Alathon®, another plastic compound, with particles 3 mm in diameter and specific gravity of 0.96. Injection rates were varied from 30 to 150 mg/l at prototype scale.

Testing Procedures

Although the basis for utilization of a swirl concentrator involves its operation with a continuously varying discharge over a storm hydrograph, for testing purposes, quantity steady state discharges were used. The maximum discharge for which an appreciable degree of solids removal could be attained for the Lancaster application was taken as 165

cfs. Optimum solids removal for flows of 103 cfs was desired at an actual flow of 0.32 cfs. A few control tests were also carried out for 50 and 15 cfs. The development tests consisted of putting the particular chamber form on the model, then running steady discharges simulating 100 cfs and 165 cfs. A few control tests simulated flood passage with variable discharge hydrographs.

Two forms of measurement were used to provide quantitative means of comparison between the succeeding chamber modifications. These were solids separation and rotational flow velocity in the chamber.

Solids Separation Efficiency

The first measurements used various light specific gravity solids which were selected to simulate as nearly as possible the settleable solids in combined sewers. This allowed observation of the particle flow path within the chamber, at the same time giving a definite measure of the amounts of the material which overflowed or were deposited on the chamber floor, or were taken out the foul sewer outlet. Observations on several of the earlier configurations indicated that the separating process was not always uniform in time, indicating that measuring solids concentrations was not a complete form of measurement.

A system using a constant volumetric measurement was devised. This consisted of ejecting, at a predetermined rate, one liter of the solid material into the given steady state discharge. The test was continued until all solids had been removed from the water in the chamber; solids had either passed over the weir, through the foul sewer outlet, or had been deposited on the chamber floor. Measurements were then made of the removal efficiency which was defined as the total quality of the solid material by volume which was separated to the bottom foul sewer outlet, plus all that deposited on the chamber floor, the total expressed as a percentage of the original full liter introduced.

Rotational Velocity Measurement

The second form of comparison was measurement of the rotational velocity in the outer, faster moving flow section of the chamber. Only three points were taken regularly—at the surface, in the middle and at the bottom of the flow on a vertical line in the center of the annular section between the weir and the chamber wall at the 180° position (see Fig. 2).

Study of these velocities served as an indication of any tendencies to approach the higher velocity ranges which had been found earlier to cut down the removal efficiency. Once the acceptable geometry of the chamber had been developed, detailed velocity contours were measured on four predetermined radii. All velocity measurements were made using a small propellor current meter.

DEVELOPMENT PROGRAM

The testing procedures described in this chapter follow the various steps through which the different chamber characteristics were investigated, leading up to the final optimum structure. Each basic form that was tested is discussed, along with the various alterations that were tried. Observations and comments on each of these intermediate steps are also included in order to aid future researchers. Throughout the following discussion, the flow given is the clear overflow volume.

A. White Ladies Road Configuration—The layout shown on Figure 2 was adapted from Mr. Smisson's 1967 publication of a project he had built in Bristol, England. Tests were carried out first without any deflectors in the chamber, and gilsonite with specific gravity 1.06 and particle sizes between one and three mm was used.

Visual observation of flows in the chamber immediately classed the conditions as a free vortex. Velocity measurements indicated velocities in the chamber in excess of that at the inlet for the 100 cfs case, with practically undisturbed rotational flow lines. Very few gilsonite particles settled to the bottom to be drawn off through the foul sewer outlet; the rest remained in suspension in the rotating water mass for several turns before overflowing.

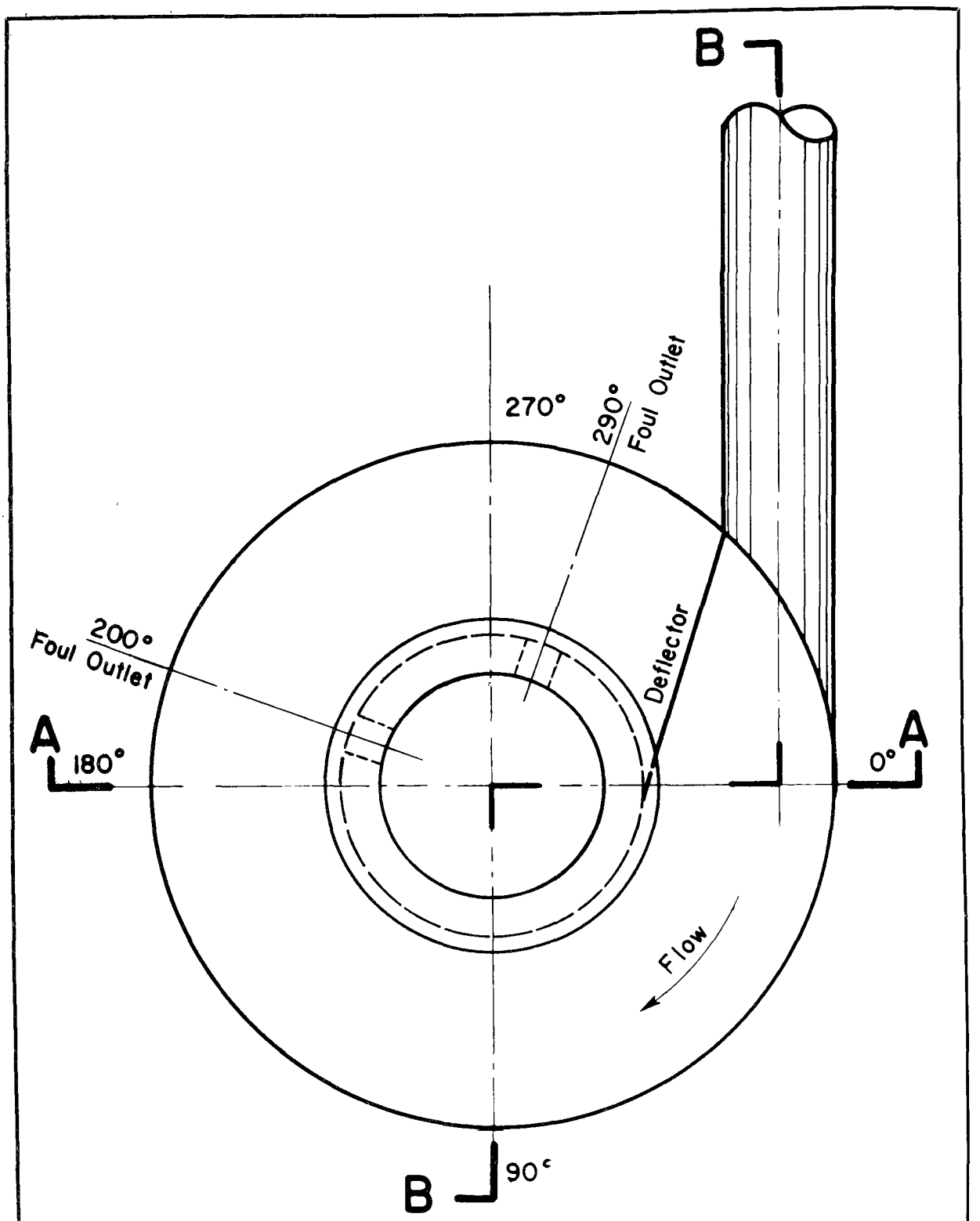

FIGURE 2
WHITE LADIES ROAD CONFIGURATION (Plan)

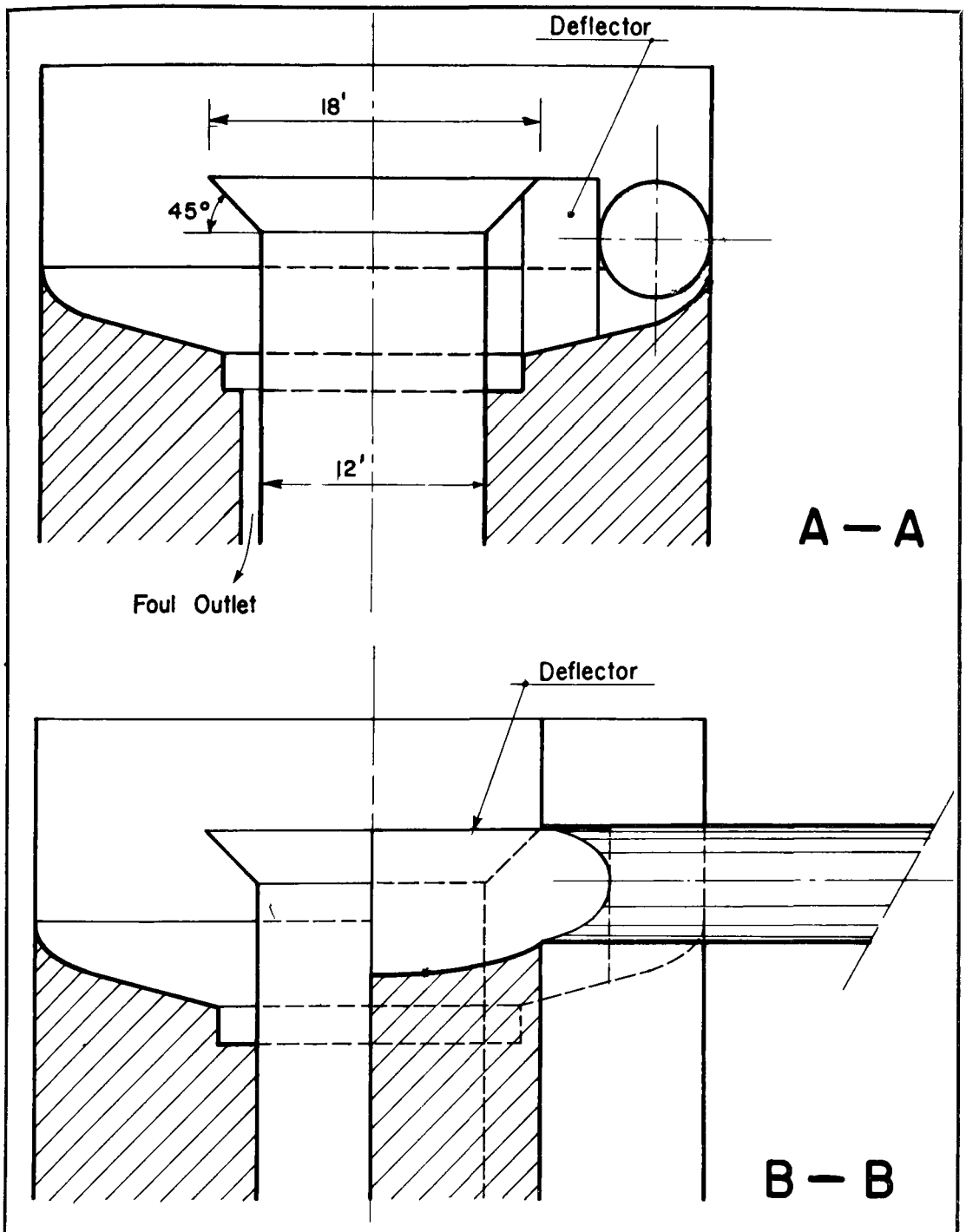

FIGURE 2
WHITE LADIES ROAD CONFIGURATION (Sections)

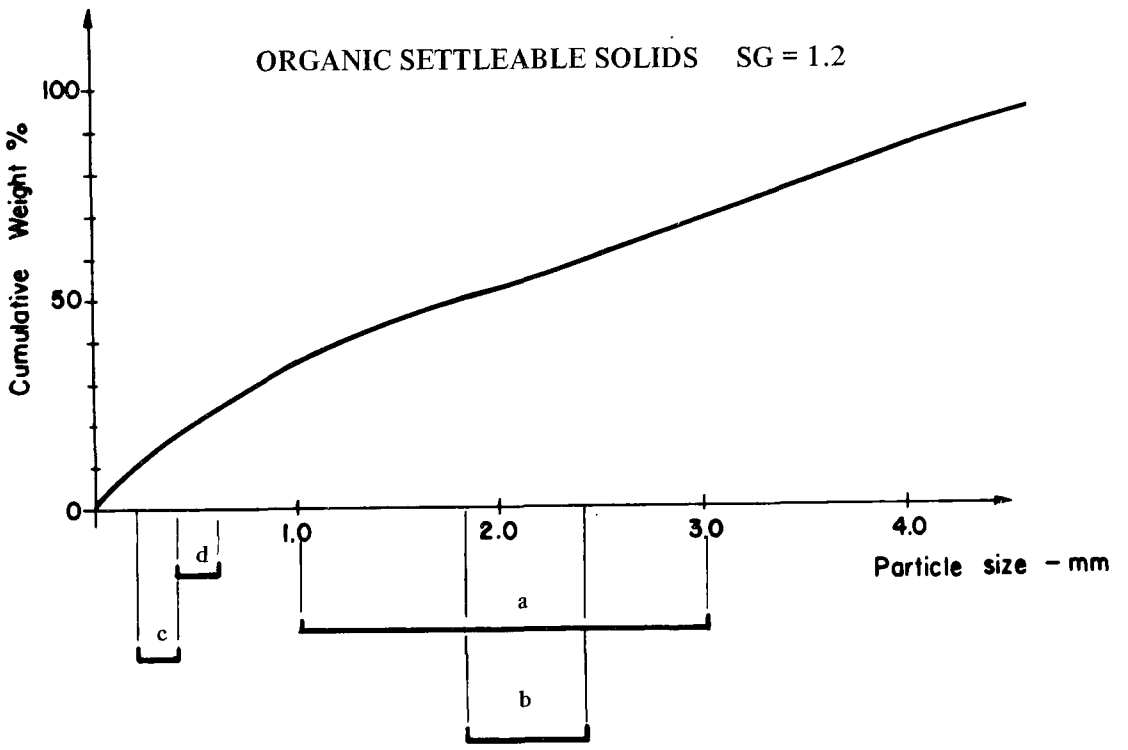

			Particle size—mm
MODEL MATERIALS	(a)	Gilsonite 1-3 mm	SG = 1.06
AND SIZE	(b)	Gilsonite on 30 mesh	SG = 1.06
SIMULATIONS AT	(c)	Gilsonite on 45 mesh	SG = 1.06
PROTOTYPE SCALE	(d)	Petrothene 2-4 mm	SG = 1.01

FIGURE 3
MODEL SIMULATION OF PROTOTYPE SOLIDS

Also shown on Figure 2 is the location of the flow deflector which was put into the chamber adjacent to the inlet. The flow conditions were vastly changed immediately, with the free vortex being eliminated. Some rotational movement remained, but in the form of a *gentle swirl,* such that water entering the chamber from the inlet pipe was slowed down and diffused with very little turbulence.

This effect was particularly evident when gilsonite was injected into the flow As particles entered the basin, they spread over the larger cross section of the chamber and settled rapidly. Particles were entrained along the bottom around the chamber and concentrated by two secondary vortices located under the lip of the weir, at approximately positions 200° and 290° from the inlet point. Foul sewer outlets at each of these positions did not draw off all the gilsonite: the greater part remained in deposits on the chamber floor, out from the central shaft. Volumetric measurements of the total gilsonite recovery from both the foul outlet and the floor deposit, for three tests yielded the following results:

Storm Discharger	Gilsonite Removal Efficiency
50 cfs	97%
100 cfs	87%
162 cfs	65%

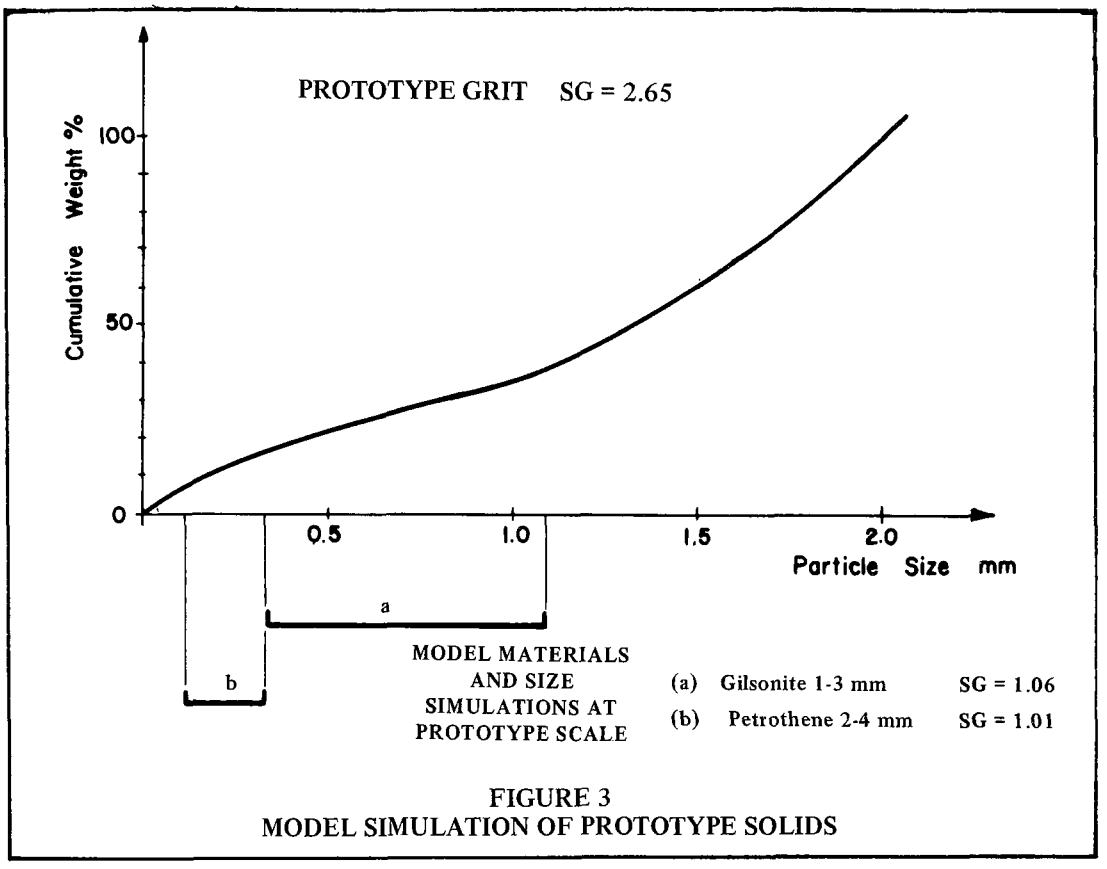

FIGURE 3
MODEL SIMULATION OF PROTOTYPE SOLIDS

Mr. Bernard Smisson reviewed the two tests described, and indicated that these findings agreed entirely with his own earlier work. He also pointed out the direction his most recent research was following and proposed a means by which he felt the study could be advanced rapidly.

Mr. Smisson had found that large diameter weirs, with horizontal undersides but no deflector walls gave light solids removal efficiency even better than the smaller diameter, sloping underside weir with deflector wall, as used in our second test series. He also suggested that a smaller diameter storm water down shaft would improve efficiency.

In order to advance development as rapidly as possible, full advantage of Mr. Smisson's experience was taken, including adoption of the following criteria:

- use a 6-ft-diameter central shaft
- use a spiral gutter from the inlet sewer to the foul outlet for dry-weather flow
- concentrate on flat, large diameter weirs without any deflectors underneath
- try to avoid drowning the inlet sewer
- test flat bottomed chamber

B. Stage I Modifications—As the first departure from the original layout, the central shaft was reduced to six feet in diameter. On the model it was made up of stacked elements to allow for easy changing of the weir elevations, and the original sloping floor was retained, as shown on Figure 4, Stage I Modifications.

Operating with this basic shape, tests were carried out on three different weir elevations, but with only the 24-ft-diameter

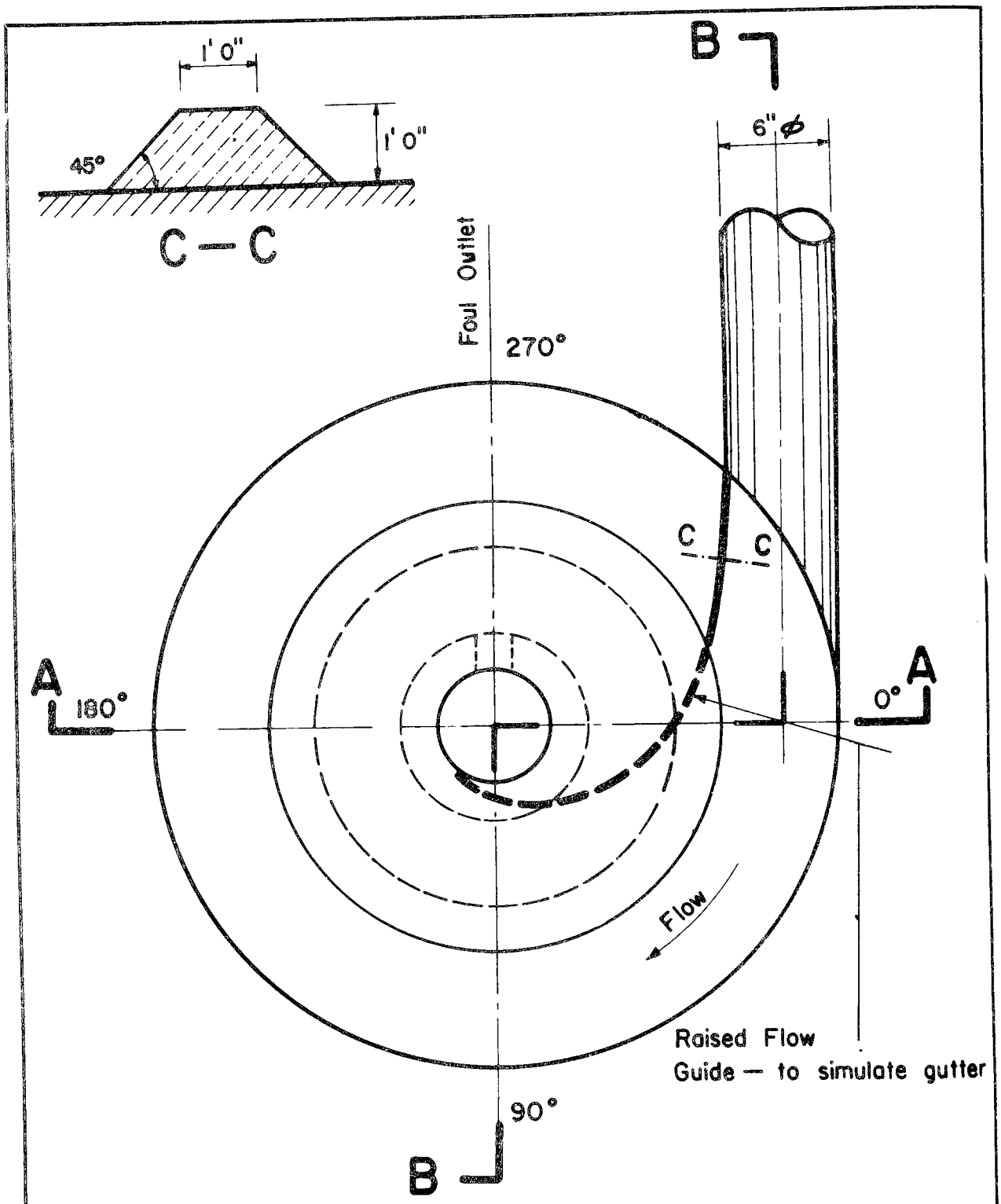

FIGURE 4
STAGE I MODIFICATIONS (Plan)

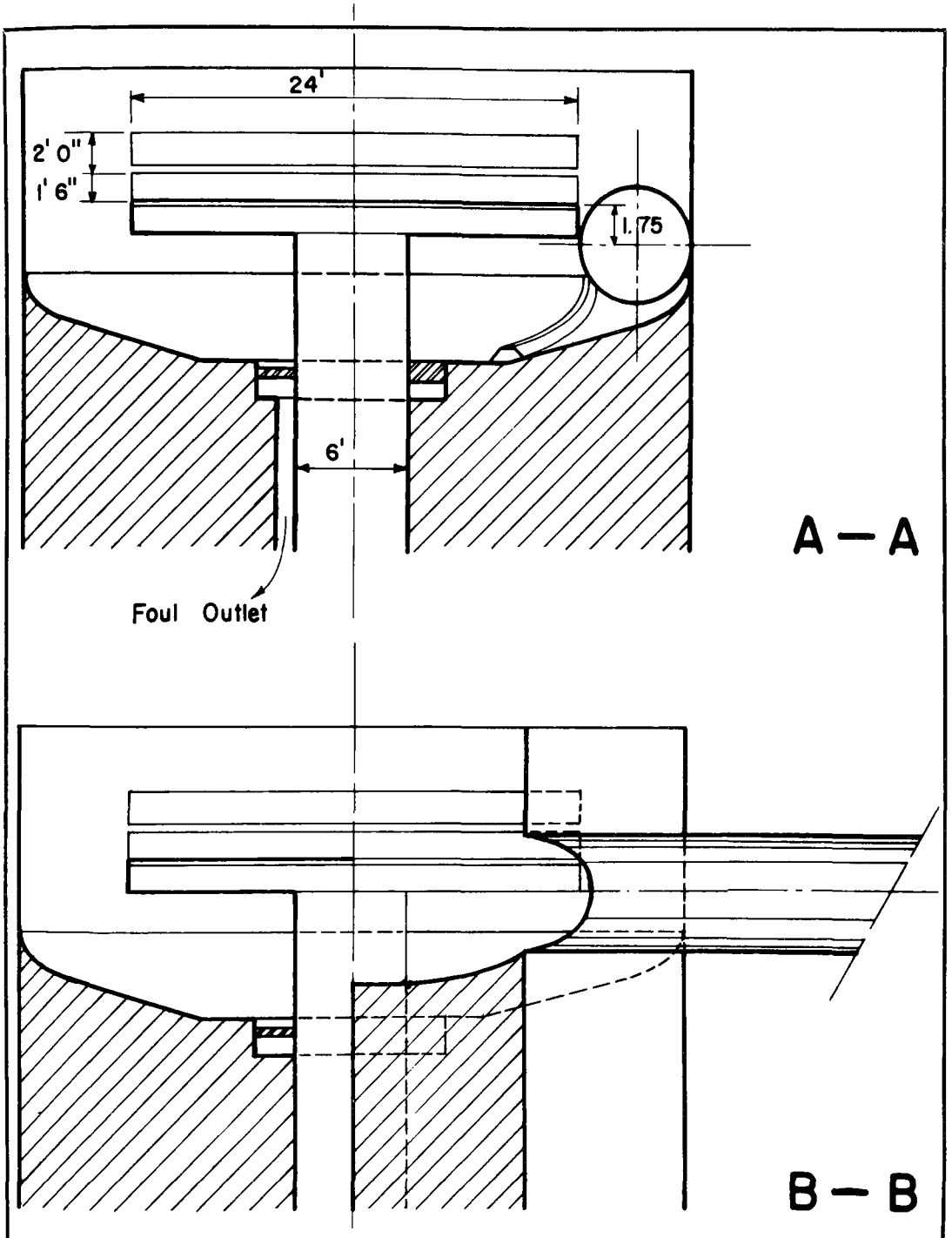

FIGURE 4
STAGE I MODIFICATIONS (Sections)

weir, and various floor configurations to simulate a spiral gutter placed above the existing floor.

Observations of the various tests, using one to three mm gilsonite representing grit between 0.3 and 1.1 mm, led to the following conclusions:

- need more depth in chamber;
- put spiral gutter in floor, below floor level, i.e., avoid any projections above floor level;
- inflow sewer should be directed along bottom of chamber;
- flat floor in chamber probably as good as sloping floor; and
- with greater depth and bottom inlet, try larger diameter weirs.

C. Stage II Modifications—As shown on Figure 5, Stage II Development, tests carried out in this series were concerned with the chamber depth, weir diameters, and elevations with respect to the inlet.

1. Chamber 13.75-15.75 Feet Deep—For the first tests, the chamber floor was dropped to a point nine feet below the inlet pipe invert. The inlet itself was not modified because of the importance of the relative levels of the weir lips with respect to the inlet and the chamber floor.

The 24-ft weir was first set +1.75 feet above the pipe center line (depth = 7.75 ft) giving free surface flow in the inlet pipe for 100 cfs, and just submerged for 162 cfs. The flow impinged directly on the weir periphery, and the resulting turbulence combined with the low water surface level (relative to the inlet) allowed a higher portion of the gilsonite rise and spill over the weir. Recovery of gilsonite through the foul sewer outlet dropped to 75 percent for 100 cfs and 60 percent for 165 cfs.

Following this finding, the weir was raised two feet (depth 9.75 ft) and the gilsonite recovery efficiencies were 100 percent for 100 cfs and 75 percent for 165 cfs. At this new elevation, the 32-ft weir was tested and found to give slightly less efficiency at 100 cfs (95%), but more at 162 cfs (87.5%). Deposits remained on the chamber floor, so different positions of the foul outlet were tested to try to intercept more of the material as it settled; 290° seemed to be the best position.

2. Chamber 10 75-12.75 Feet Deep—Tests were run for the 12-ft-deep chamber, using both the 24-ft and 32-ft-diameter weirs, placed at the higher levels, submerging the pipe inlet. A spiral gutter was placed in the chamber floor to give some indication of its effect, as shown in Figure 5.

3 Chamber 7 75-10.75 Feet Deep—Exactly the same series of tests was carried out with the chamber nine feet deep.

Observations at this stage were:

a. Relative to each other, the weir must be above the inlet and shielded from the direct inflow. Tests should be made on a submerged inlet configuration which would leave free surface flow in the pipe upstream. In this approach, floatables should be caught under the weir, and settleables will reach the floor of the chamber, and thus migrate more directly to the foul outlet.
b. The greater depths of chamber, down to 15 feet, gave only marginal, even questionable, increases in gilsonite recovery. Therefore, consideration should be given to depths only to 12 feet for the inlet modification tests. It should be noted that with the submerged bottom inlet, the weirs would be lowered to give free surface flow in the pipe. This means that the water volume in the 12-ft chamber corresponds approximately to the water volume in the 9-ft chamber in the previous tests.
c. The 32-ft diameter weir was better for the 15-ft deep chamber only; the 24-ft weir was better for the others. It would be desirable to check a 28-ft weir as well in the next series of tests.
d. Grit sizes of solids carried toward the foul outlet just as well on the flat chamber floor as on the sloping floor.

The spiral gutter must be placed below the floor level.

e. The spiral gutter below floor level is a valuable element in generating and maintaining the circular motion in the chamber; it aids in clearing the grit deposits.

D. Stage III Developments—Modifications as shown in Figure 6, Submerged Horizontal Slot Inlet, include:

- a plexiglass enclosure at the entrance into the chamber in which various inlets could be fitted, and
- the floor of the chamber was set flat at a level of five feet below the invert of the inflow sewer

Working to this basic set of characteristics, different inlet shapes and weir diameters were tested, and their performances evaluated with the usual two clear water overflow discharges—100 and 162 cfs. At all times the foul outflow discharge maintained at three cfs.

Submerged Inlet Three Feet x Nine Feet—No Skirt on 24-ft. Weir—All of the previous tests had indicated that this form of inlet should solve most of the problems. However, as soon as it was put in operation, it became evident that it was disturbed by the rotating mass already in motion, and the ensuing turbulence rolled the incoming jet up the chamber wall. The gilsonite, which entered the chamber along the floor, rose into the upper layers of flow due to turbulence. From this position, a large proportion of it went over the weir before it had completed half a turn in the chamber.

Several different flow deflectors and ramps were tried in order to shield the incoming flow from the exterior liquid mass. The most efficient was the ramp shown shaded on Figure 6. This arrangement, with the 24-ft. weir produced 90-percent removal efficiency with 100-cfs clear flow, and 60 percent at 162 cfs. These figures in themselves were not as good as previous results, however, these were the first tests where all the material removed exited through the foul sewer outlet. There were no deposits left on the chamber floor.

Submerged Inlet Three Feet x Nine Feet with One and One-Half-Foot Skirt Below the Weir—Adding a skirt below the weir as suggested by Mr. Smisson's tests represented an effort to induce a flow pattern similar to that obtained with the ramp in the preceding tests. The results were most disappointing; for the 100-cfs clear flow discharge, both the 24-ft and 32-ft weirs gave 90 percent recovery efficiency of gilsonite, and both left significant portions deposited on the chamber floor.

The evaluation at this stage did not incriminate the skirt below the weir; to the contrary, it seemed to be working well. However, it was evident that efforts to direct the flow under the weir in order to trap floatables was the source of the problem. The flow entering the chamber obliquely, moved across under the weir, struck the opposite chamber wall and welled up to the surface and over the weir.

Once this problem was recognized, a series of brief tests were carried out trying different forms of vertical wall deflectors as shown in dotted lines on Figure 6. Use of these deflectors resulted in better removal efficiencies as the flow was brought back to a tangential entry.

This constituted the first major departure from Smisson's work. He had found he could use oblique inflows to great advantage to trap floatables under the weir and control the rate and location of deposition of the settleable solids. However, the fact that this was not reproduced can be easily explained by comparing discharges. The maximum discharge that Mr. Smisson had used, was 25 cfs, meaning that the LaSalle unit had to handle between four and six times as much energy in its chamber.

Vertical Slot Free Surface Inlets—In proposing the inlet forms shown on

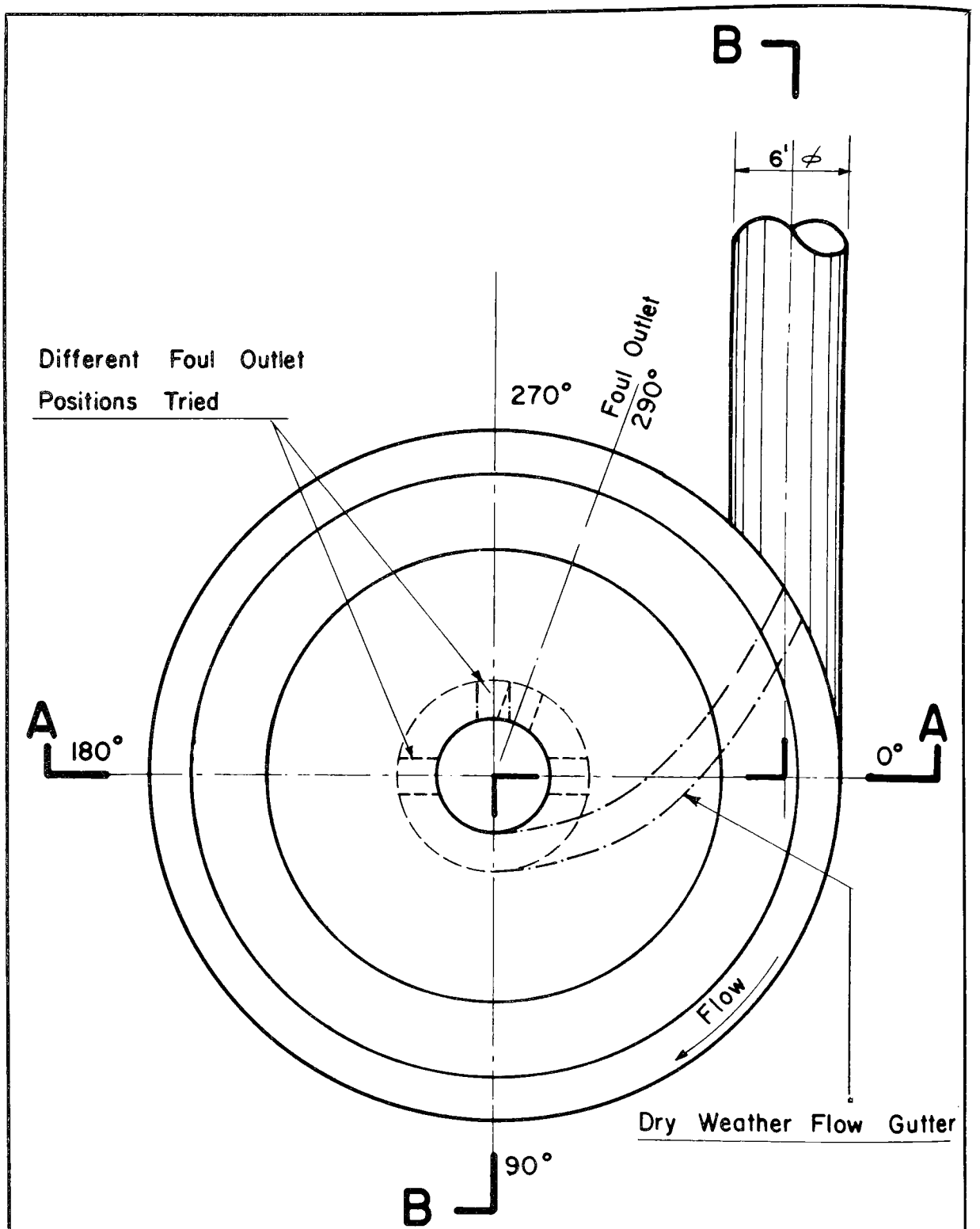

FIGURE 5
STAGE II DEVELOPMENT (Plan)

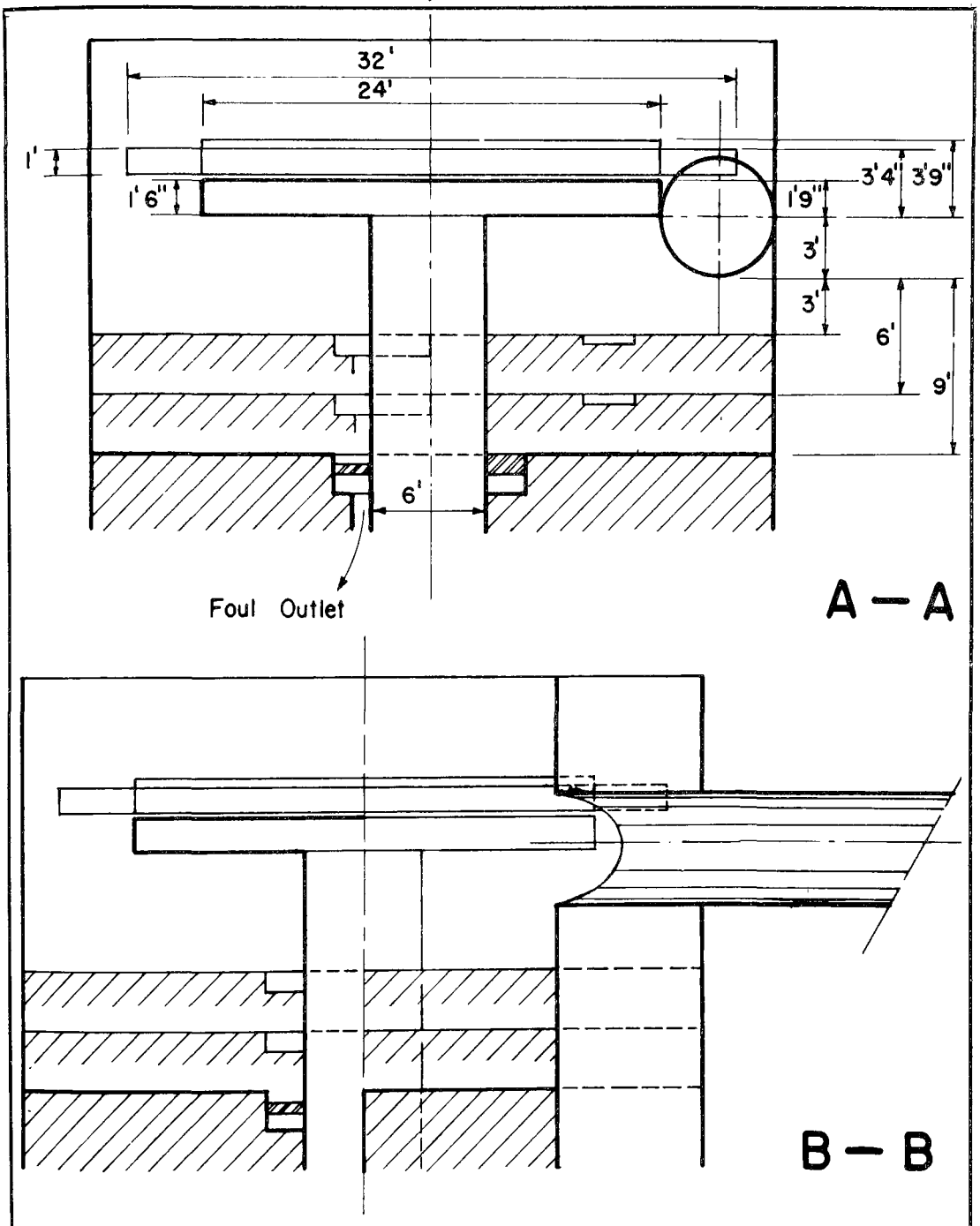

FIGURE 5
STAGE II DEVELOPMENT (Sections)

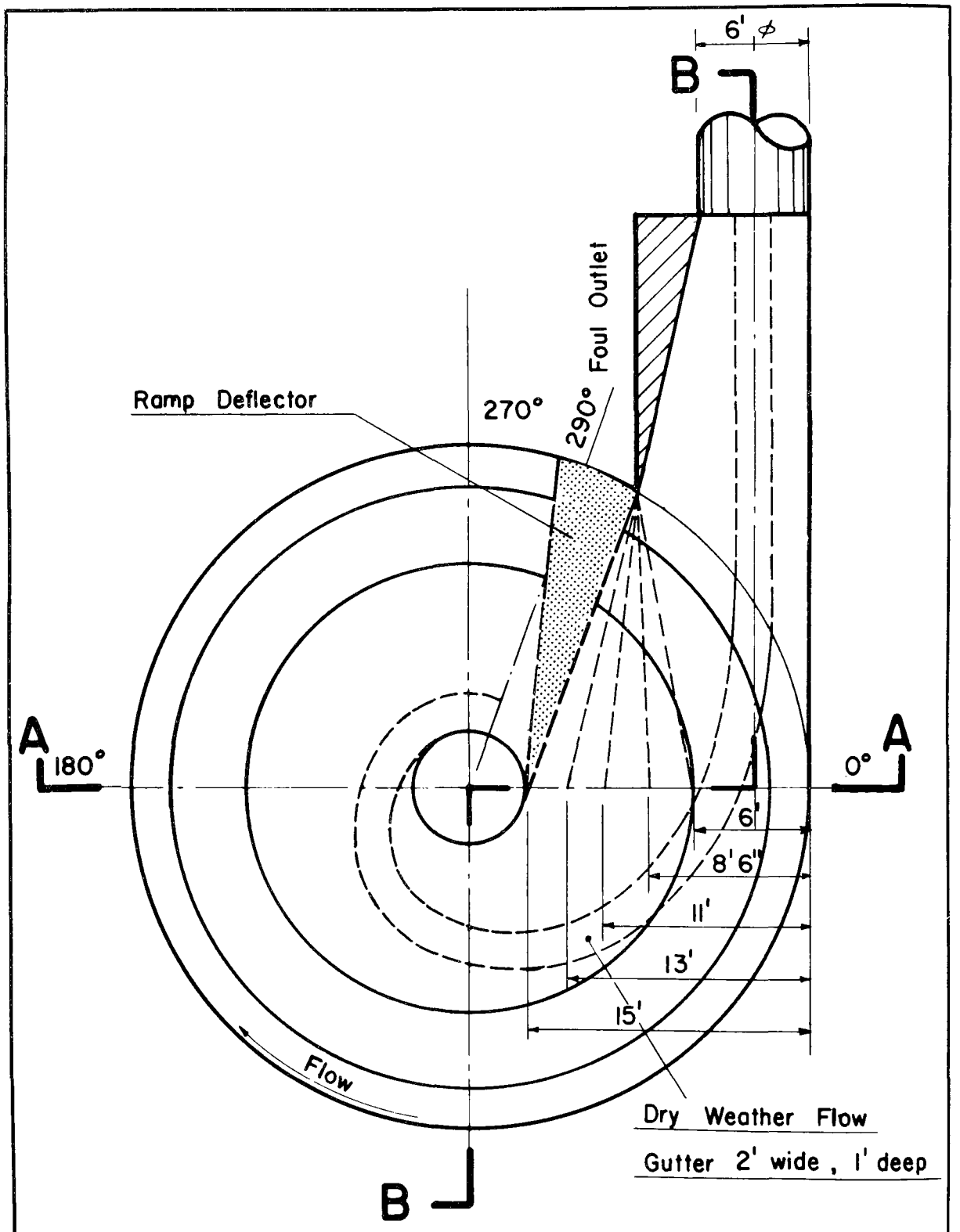

FIGURE 6
STAGE III DEVELOPMENT
Submerged Horizontal Slot Inlet (Plan)

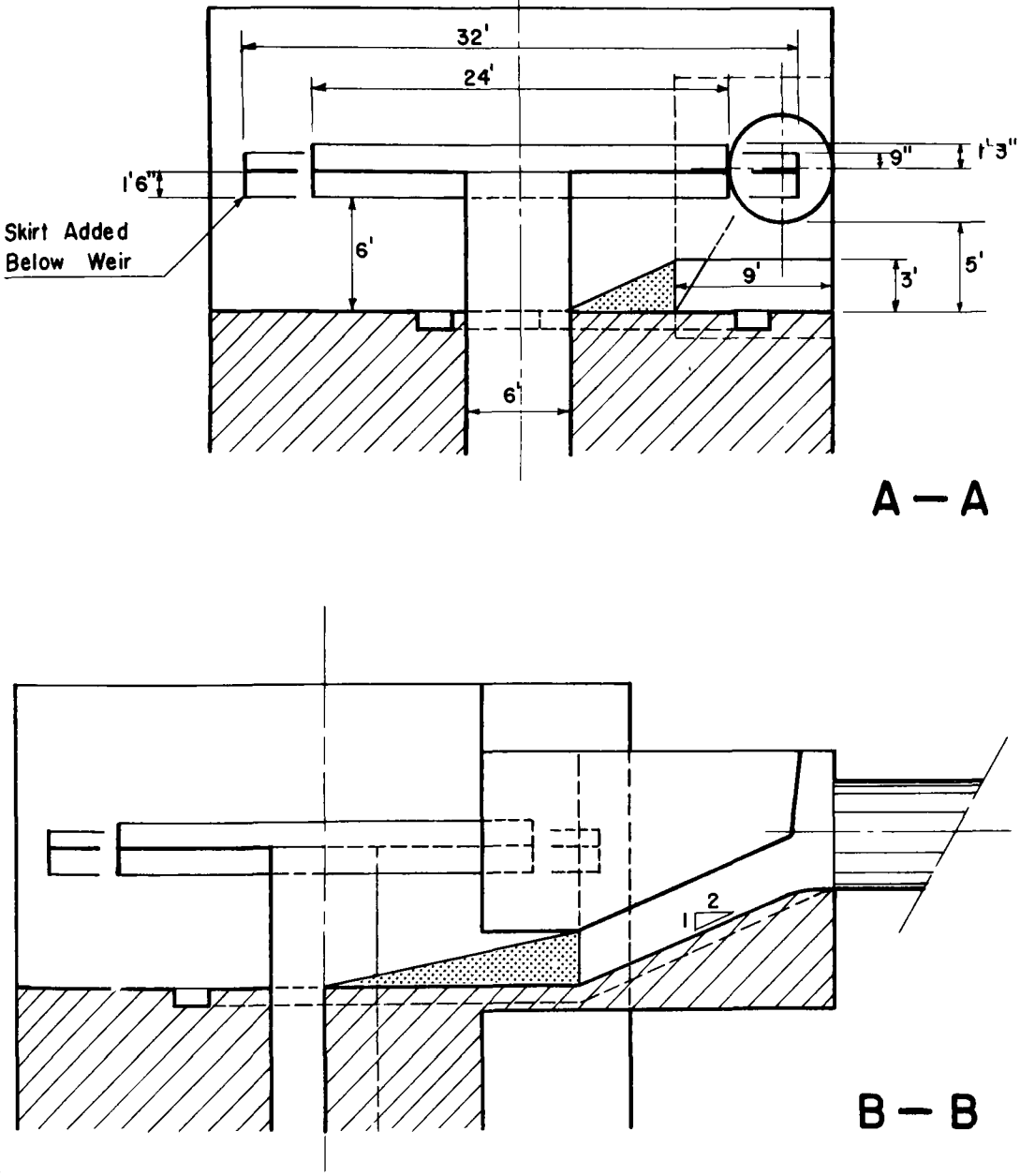

FIGURE 6
STAGE III DEVELOPMENT
Submerged Horizontal Slot Inlet (Sections)

Figure 7, Vertical Slot Inlet, the following characteristics were being sought:

- bring the flow into the chamber tangentially,
- keep free surface flow for ease of maintenance access,
- disregard floatables recovery, and
- avoid physical intrusion in the chamber.

Slot widths of two and one half, three, three and one-half and four feet were tried as a means of evaluating the importance of the inlet velocity. Brief preliminary tests quickly eliminated the 24-ft and 32-ft weirs, since the 28-ft. weir gave markedly better recovery efficiencies. Table 1 presents the pertinent results from these tests, using the 28-ft weir, with the one and one-half-foot skirt below it:

TABLE 1

Test Removal Efficiencies Using Various Slot Widths

Slot Width ft.	Discharge (cfs)	Vm at 180° (ft/s)	Gilsonite Recovery Efficiency	Floor Deposit
2 1/2	100	4.8	100%	10%
	162	7.2	90%	5%
3	100	4.4	93%	traces
	162	7.0	83%	none
3 1/2	100	4.3	82%	35%
	162	6.1	80%	30%
4	100	3.9	97%	37%
	162	6.7	75%	20%

The two and one-half-foot-wide slot gave very good separation of the gilsonite. The settlement to the floor immediately upon entry to the chamber, combined with concentration of the particles against the wall further around drew the gilsonite toward the foul outlet in two revolutions. However, the high velocity of rotation once again approached a vortex form of flow.

The wider slots appeared to offer smoother flow conditions in the chamber, but their gilsonite recovery efficiency fell off considerably.

Submerged Inlet, Six Feet x Six Feet—This final inlet shape was chosen as the means to combine the best characteristics from the preceding tests. First runs using the 28-ft weir with skirt, and without any deflector in the chamber, gave removal efficiencies of 95 percent and 75 percent for 100 and 162 cfs. These were encouraging results, but they both left significant deposits on the chamber floor—50 percent and 35 percent, respectively.

The 24-ft weir, with skirt but no deflector, was tested. This produced gilsonite removal efficiencies of 100 percent and 90 percent for 100 cfs and 162 cfs respectively; the first left 15 percent deposit, and the second left only traces in the chamber after the test.

Tests were then performed using Petrothene® granules, measuring between two and four mm with a sg of 1.01. These granules correspond in the prototype to grit in the 0.2 to 0.3 mm range, and to sg of 1.2 for material in the 1.5 to 2.5 mm range, as indicated by Figure 3.

With the 100 cfs discharge, and no deflectors in the chamber, 45 percent of the Petrothene® was recovered through the foul sewer outlet. After modifications were made as indicated by Figure 8, Submerged Six-ft x Six-ft Inlet, with a six-ft-high deflector, 65 percent removal efficiency was obtained.

Tests were then undertaken using ground gilsonite. The first fraction tested passed 25 mesh sieve and was retained on 30 mesh; i.e., a mean grain size of 0.5 mm corresponding in prototype to 0.2 mm grit or 0.5 mm material of sg = 1.2. Two successive tests with this fraction at 100 cfs gave 35 percent and 42 percent removal efficiency through the foul sewer outlet; deposits were five percent and ten percent respectively. Simulating 50 cfs gave an 80 percent removal efficiency, with 60 percent remaining in the form of a deposit.

The second gilsonite fraction passed the 30-mesh sieve and was retained on 45 mesh. The mean particle size of 0.3 mm corresponds to about 0.1 mm grit and 0.3 mm particles at sg = 1.2 in prototype. With a discharge of 50 cfs, 50 percent of

the material was evacuated through the foul outlet, with 38 percent as a deposit. At a discharge of 100 cfs, 28 percent of the material was removed, with six percent in the form of a deposit.

A series of point velocities was taken for the 100 and 162 cfs cases and the velocity contours drawn for the four selected cross sections as shown on Figures 9 and 10, Velocity Contour Cross Sections for 100-cfs Overflow and 162 cfs.

Velocity Contour Cross Sections for 100 cfs and 162 cfs Overflow—An effort was made to show the flow direction deviations from the purely tangential by means of thread tracers. A wire grid with one-inch squares was placed across the chamber at the 90° section. Thread tracers two inches long were tied to the wire intersections and photographed from three positions—from downstream normal to the flow, vertically down on the section and looking radially inward along the section. The threads were cut back to one inch long and photographed again. All photographs were taken with 100 cfs clear discharge and 3 cfs foul sewer discharge.

Scum Ring and Floatables Trap

The chamber layout as it had been developed at this stage was acceptable in its treatment of grit and settleable solids, but it had no means of separating floatables. All tests using an oblique entrance to the chamber had been unsuccessful in trapping floatables under the weir. Therefore, tests were performed with a scum ring 28 feet in diameter; this left two feet clear between the weir and the scum ring, and four feet between the scum ring and the chamber wall. Polythene® grains four mm in diameter and with sg = 0.92 were used as a test material.

Tests were carried out with the scum ring alone, first with its lower edge at the same level as the weir crest, then six inches lower. When the scum ring was at the same level as the weir, much of the Polythene® was drawn under the ring, escaping over the weir crest. With the ring six inches lower, the Polythene® was held outside the ring at first, but gradually was drawn under after several revolutions in the chamber.

Two concepts of floatables traps were tried. The first had a deflector across the annular channel outside the scum ring, and deflected the floating material through a hole cut in the exterior wall of the swirl chamber as shown in Figure 11, Floatables Trap Arrangements. The floatables were retained in the small ante-chamber on the model, while the excess water was evacuated through a low level opening back into the swirl chamber. This system worked well, but left the problem of what to do with the trapped floatables without adding a mechanical device.

As a second concept, the deflector was placed to bring the material into a 1-ft-wide channel cut through the scum ring and the weir. This channel arrived tangentially in a 2-ft-diameter vertical cylinder whose open bottom was cut through the weir disc as shown in Figure 11. As the floatables arrived, they were pushed by the flow along the deflector, through the channel, then were swept around in the vortex that formed in the cylinder and were drawn down under the weir disc. Two forms of this arrangement were tried; one with the vortex cylinder beside the weir crest, and the second with the cylinder half way between the crest and the clear water downshaft. Repeated tests with the second gave Polythene® recovery in the order of 80 percent for 100 cfs, and 40 percent for 162 cfs. The first worked equally as well for trapping the material, but allowed some to escape later. The second cylinder location, set at the 225° position in the chamber appeared desirable.

When the storm discharge was turned off, the floatable solids under the weir dropped with the receding water surface. The floor gutter and vortex foul sewer outlet shown in Figure 11 were developed as an efficient means of drawing off the floatables from the surface while there was still about one foot of water in the chamber. This did not remove all the floatables, and some remained scattered at random after draining.

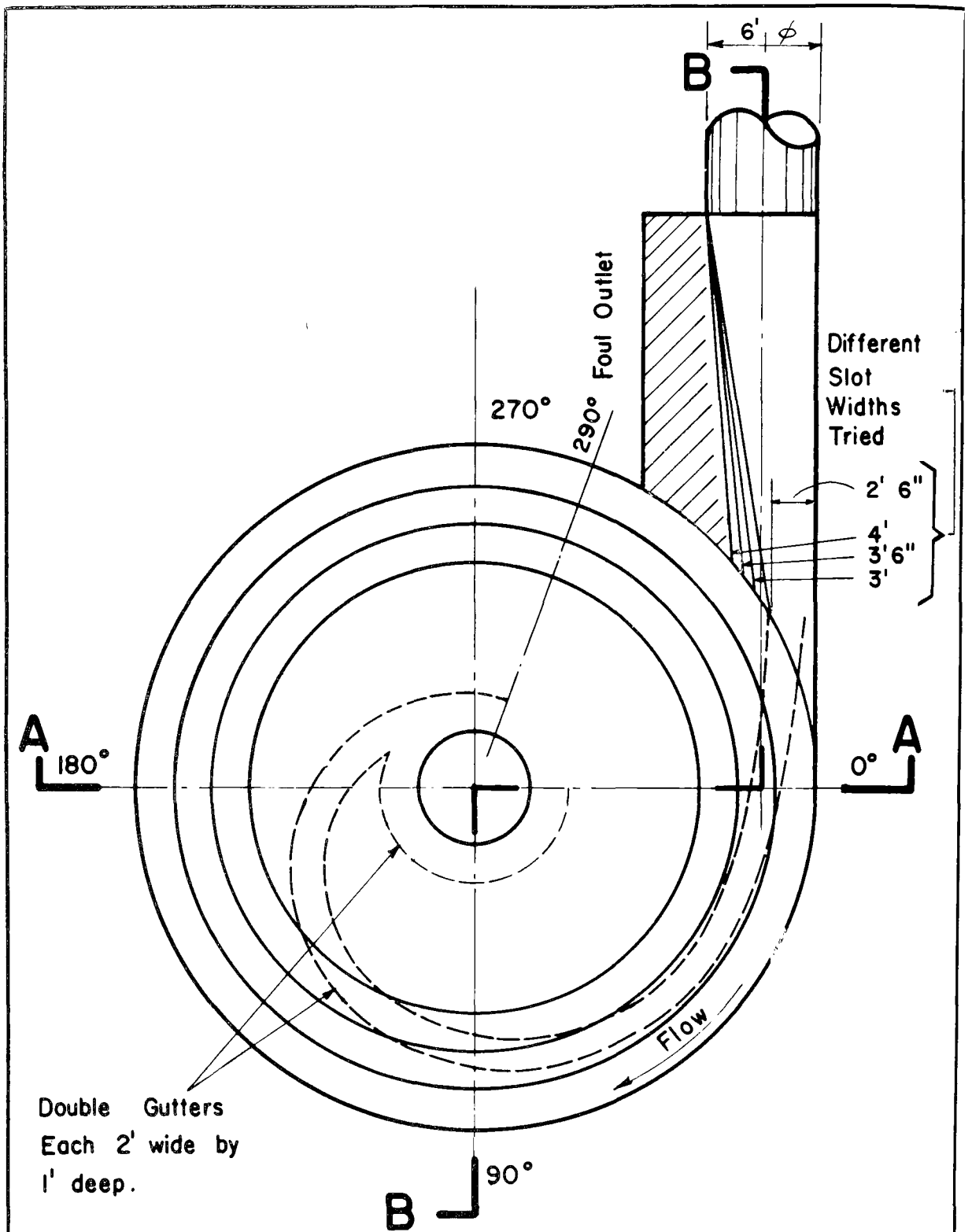

FIGURE 7
STAGE III DEVELOPMENT
Submerged Vertical Slot Inlet (Plan)

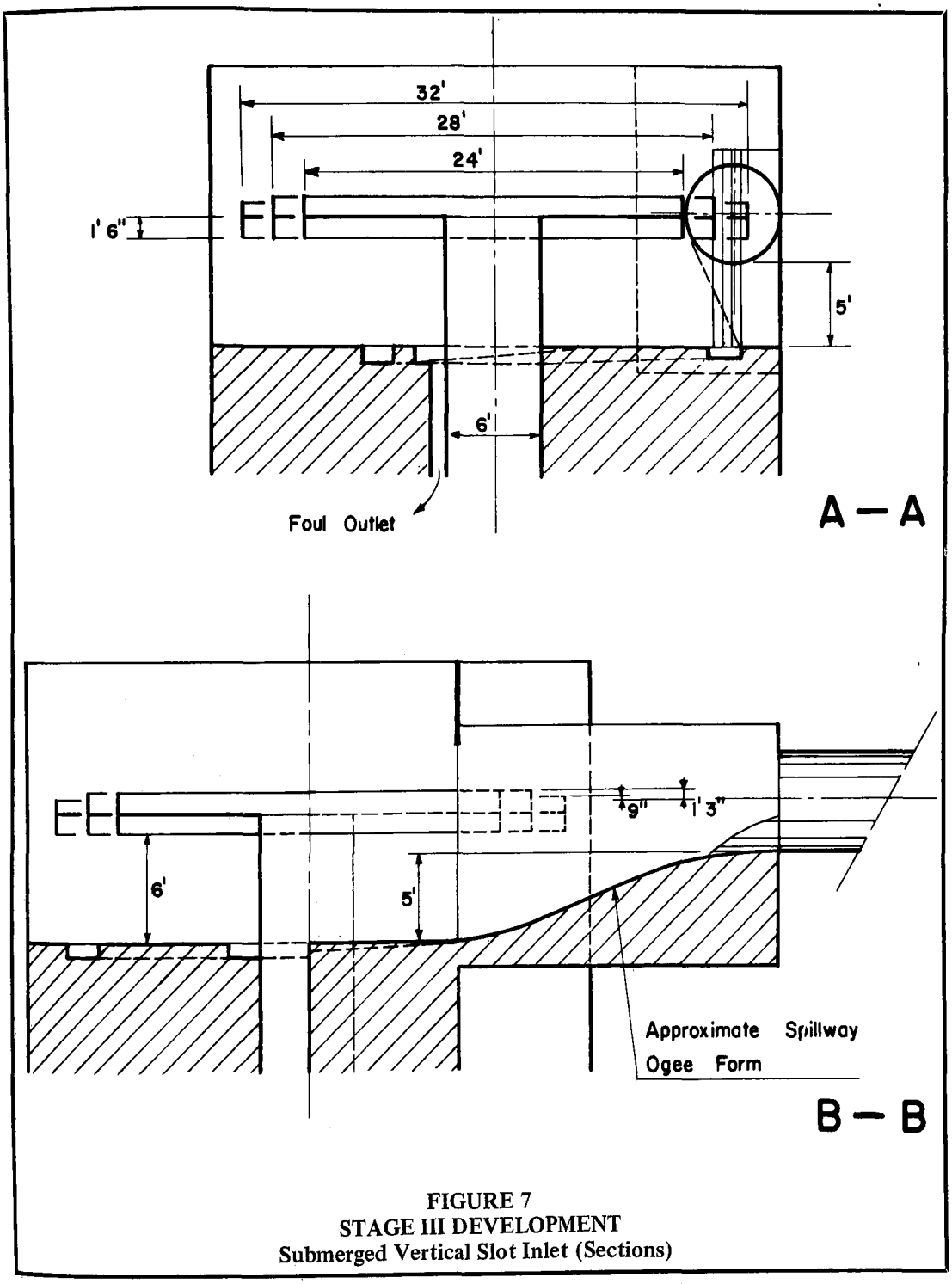

FIGURE 7
STAGE III DEVELOPMENT
Submerged Vertical Slot Inlet (Sections)

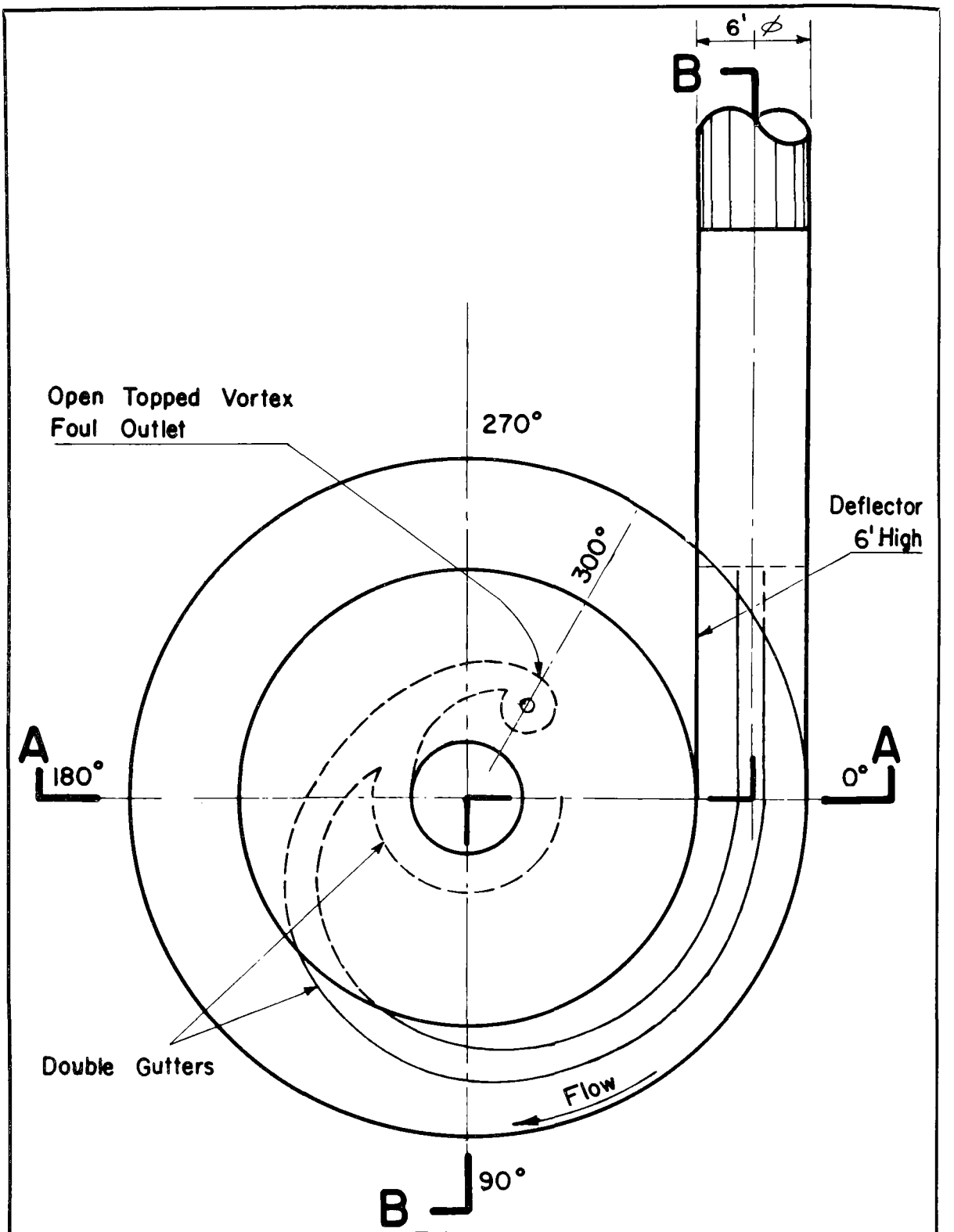

FIGURE 8
STAGE III DEVELOPMENT
Submerged 6 ft x 6 ft Inlet (Plan)

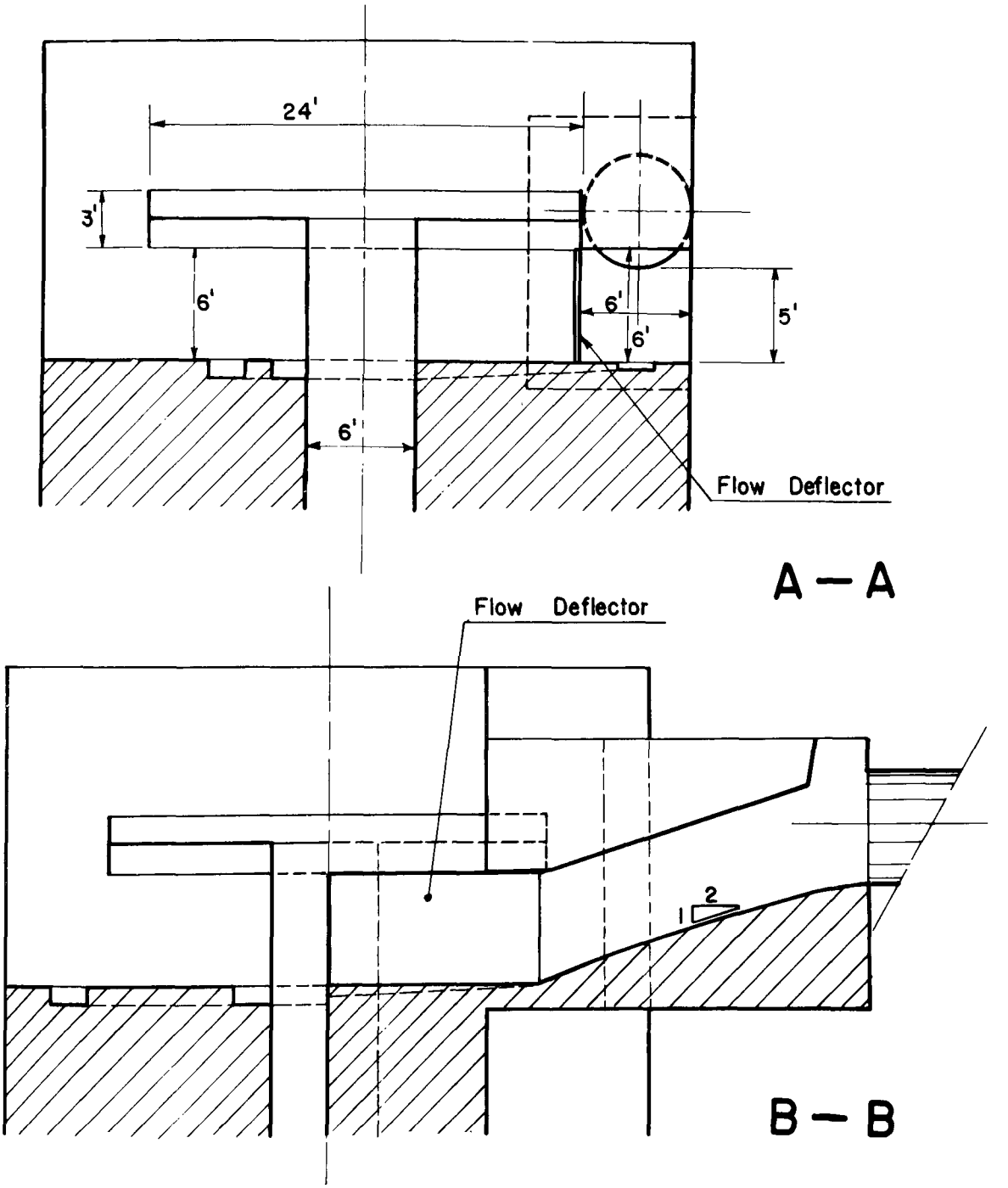

FIGURE 8
STAGE III DEVELOPMENT
Submerged 6 ft x 6 ft Inlet (Sections)

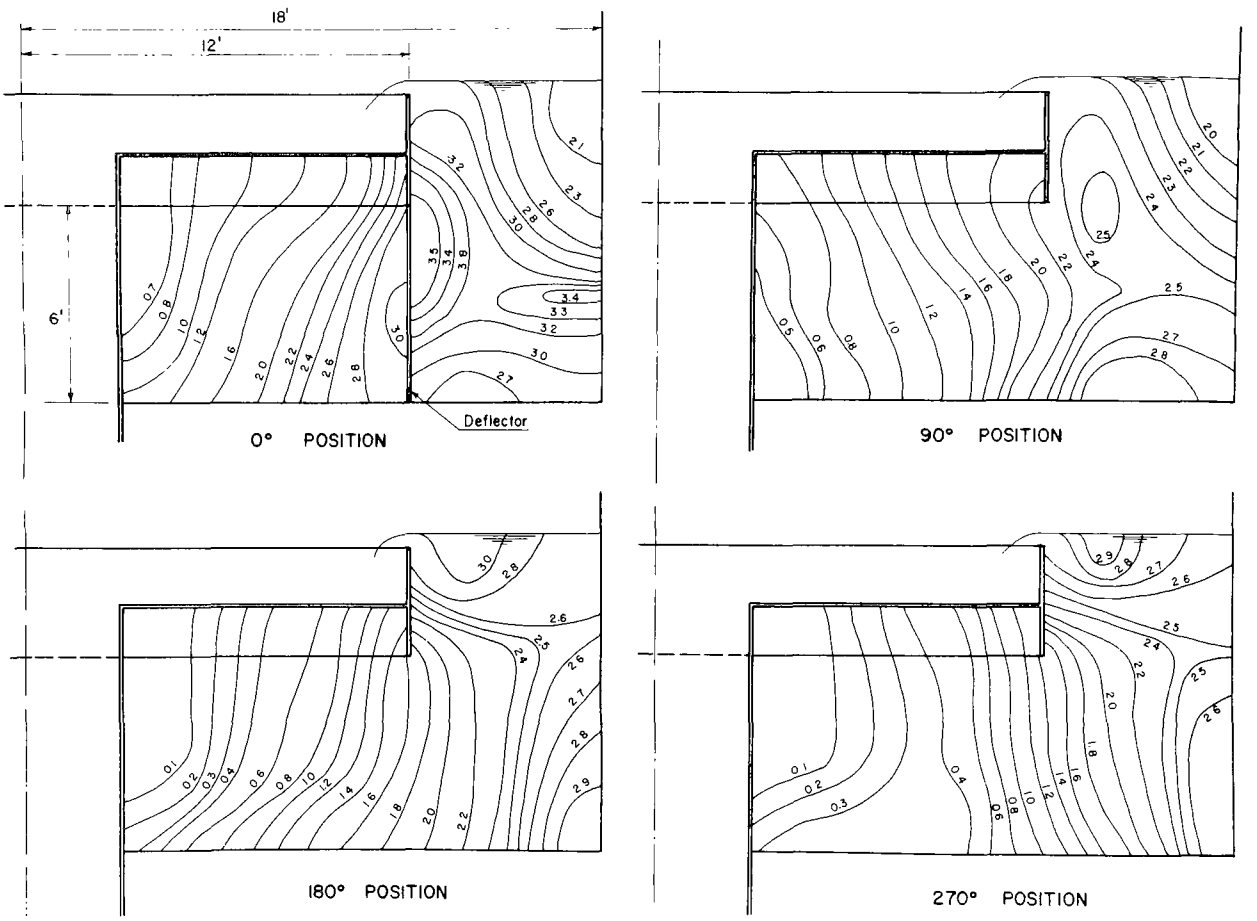

FIGURE 9
VELOCITY CONTOUR CROSS SECTIONS FOR 100 cfs OVERFLOW

Later tests on the recommended configuration showed that the 225° position for the floatables trap was disturbing the settleable solids movement on the chamber floor. Successive changes moved the floatables trap around to the 320° position. This was the location finally retained. It offered good floatables recovery (80% for 100 cfs), introduced a minimum of disturbance for the rest of the flow, and provides direct vertical access to the foul outlet, which could be a distinct advantage for visual inspection or maintenance. In the final arrangement, the vortex cylinder was moved in nearer the downshaft, to be concentrically located above the foul outlet.

Final Proof Tests–Stage IV Development

The 28-ft scum ring and floatables trap placed on the 24-ft weir had modified the flow conditions significantly, so a final series of tests was carried out to check the structure's overall operation.

A slope was put on the floor of the chamber, dropping one foot along a radius in the 15-feet distance from the chamber periphery to the central downshaft. The outside wall level was retained at the same position as in the preceding tests; i.e., five feet below the inlet sewer invert, and nine feet below the weir crest. This change was incorporated in an effort to improve the self-cleansing of remaining solids following a storm.

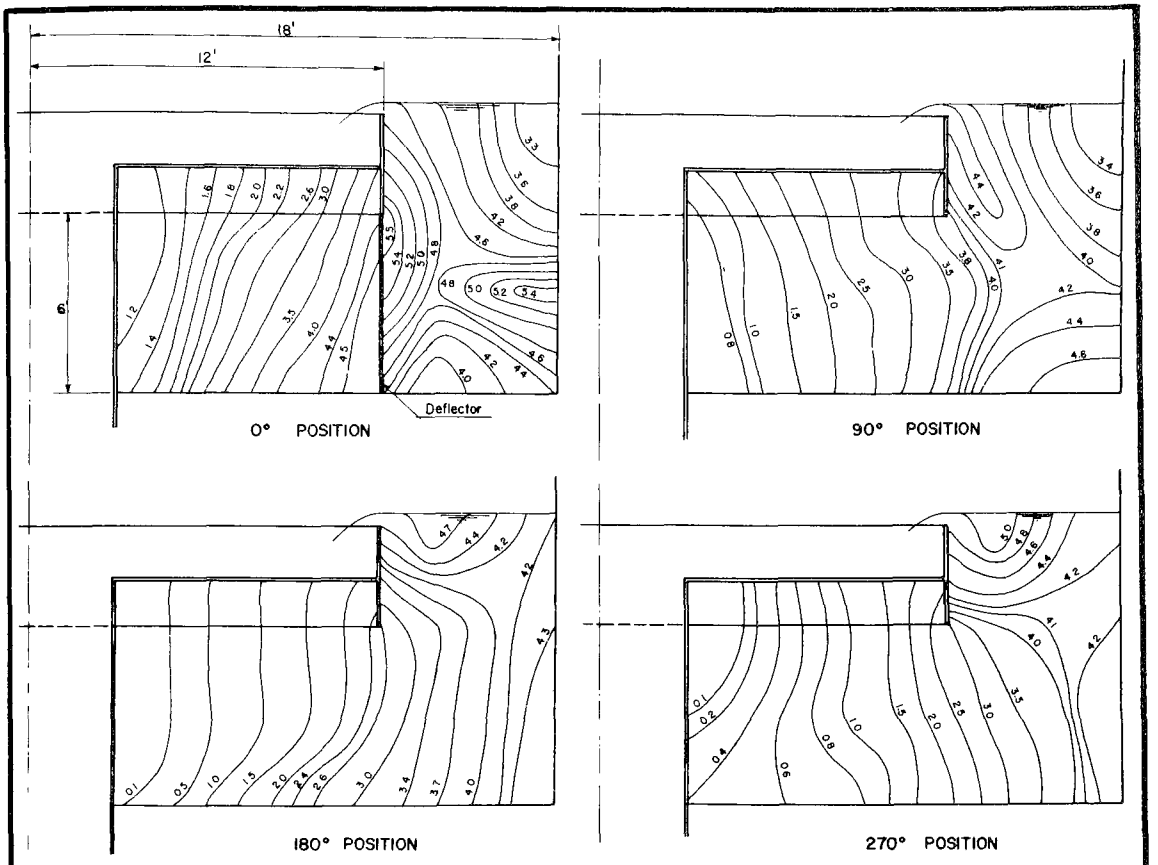

FIGURE 10
VELOCITY CONTOUR CROSS SECTIONS FOR 162 cfs OVERFLOW

Observation of the settleable solids trajectories in the flow led to trying the modified floor gutter layout shown in fine dotted lines on Figure 12, Stage IV Proof Tests; this proved to be inadvisable and after several further changes, the optimum layout was selected as shown in heavy solid and dotted lines.

Tests were run injecting Polythene®, Petrothene® and the large gilsonite. It was immediately evident that the gilsonite was settling out into significant deposits on the chamber floor, for the most part outside the gutters between the 90° and 270° positions. Analysis of the results indicated that the presence of the 28-ft scum ring was causing flow conditions the same as the 28-ft weir, which had been eliminated in earlier tests.

Attempts were made to get back to the efficiencies of the 24-ft weir alone by cutting off the skirt below the weir. A weir skirt of one foot deep produced the best test results, however, with this, a deposit of 15 percent of the solids remained at 100 cfs and 30 percent at 162 cfs.

In later tests the scum ring acted as the limit between the interior and exterior flow masses. Then the weir skirt could be lowered to three feet without adversely affecting flow characteristics in the chamber. The depth provided greater floatables recovery.

These tests indicated the desirability of a smaller diameter weir. The scum ring submerged to a depth only six inches below the weir crest imposed flow conditions similar to that for a solid skirt extending to three feet

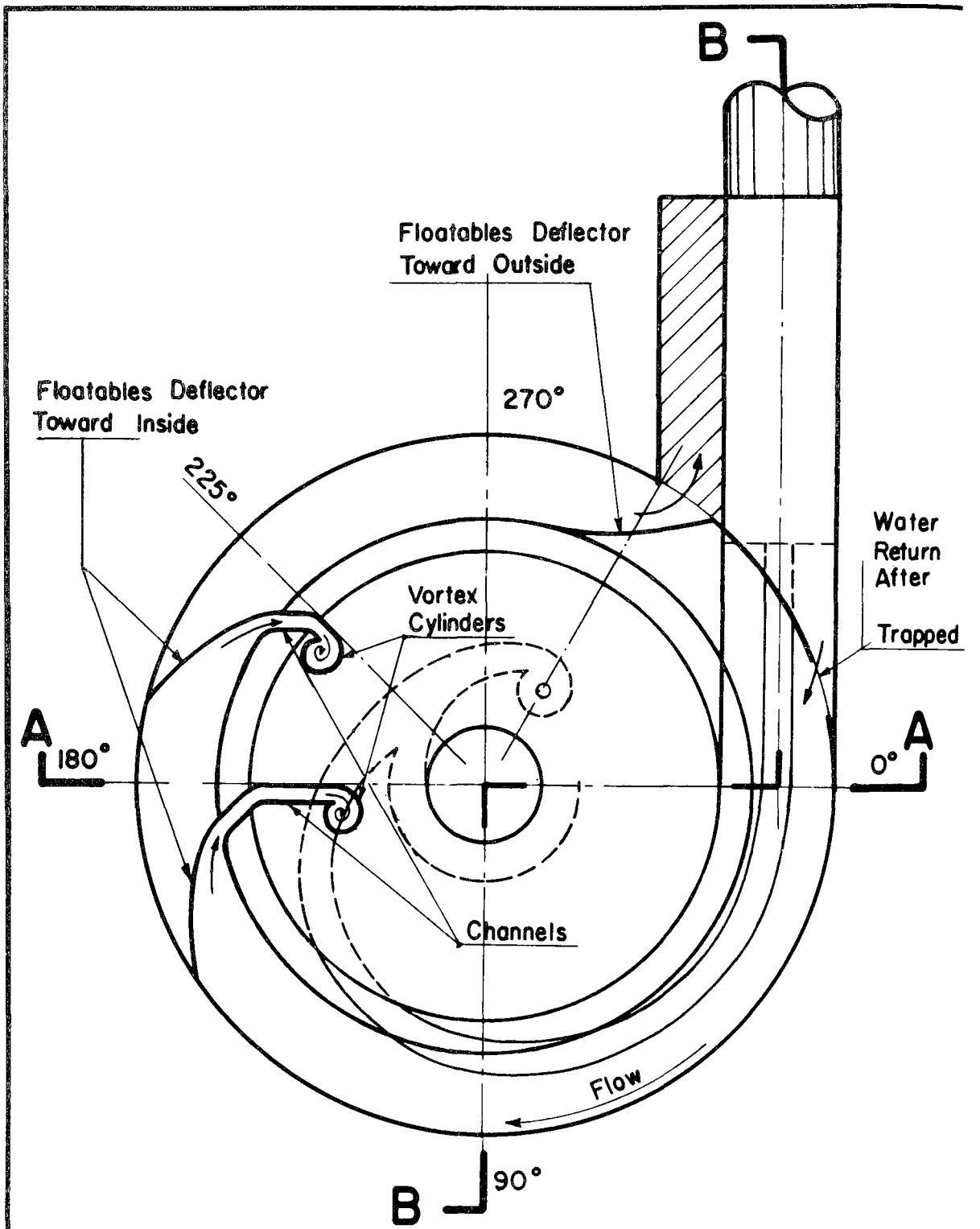

FIGURE 11
FLOATABLES TRAP ARRANGEMENTS (Plan)

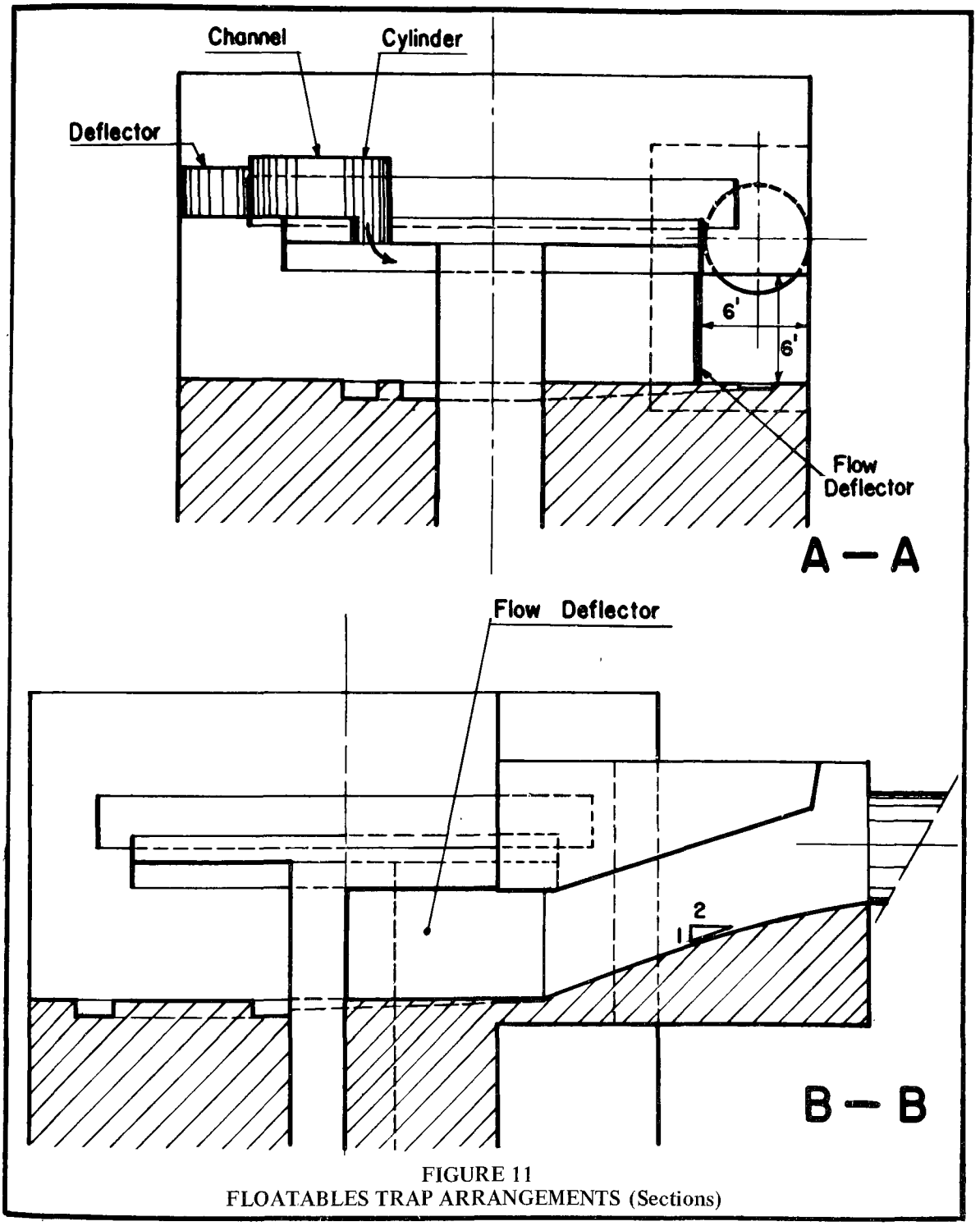

FIGURE 11
FLOATABLES TRAP ARRANGEMENTS (Sections)

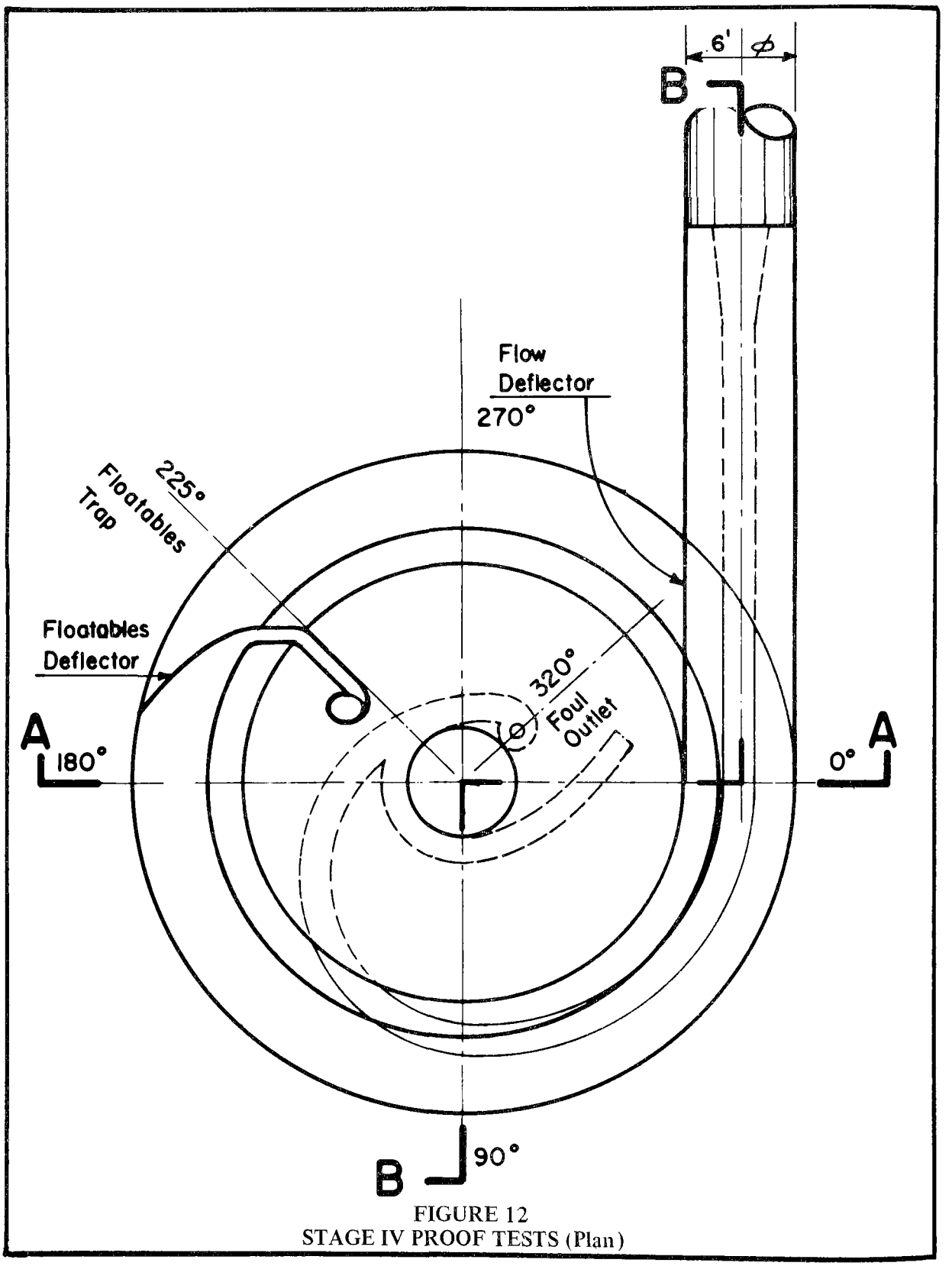

FIGURE 12
STAGE IV PROOF TESTS (Plan)

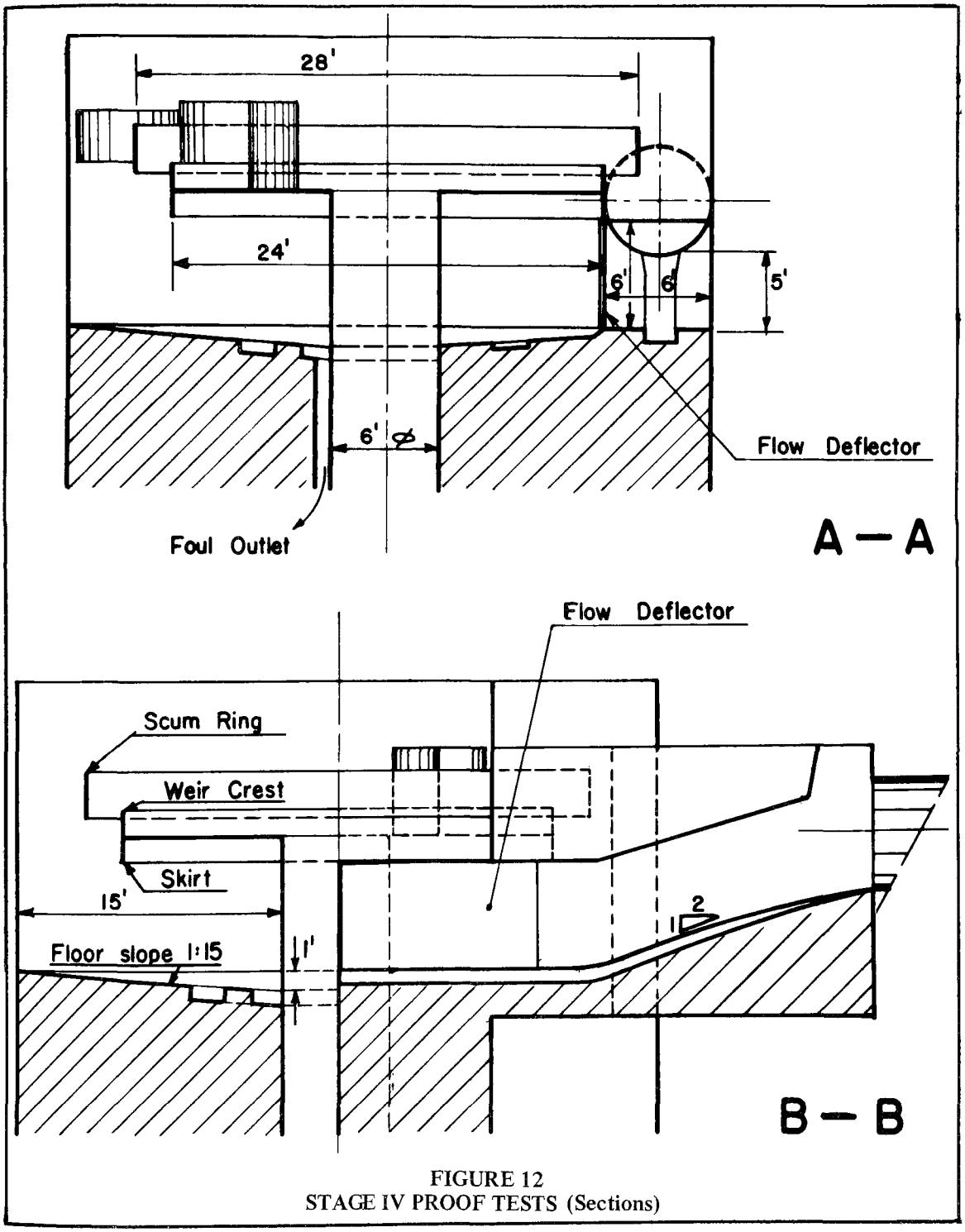

FIGURE 12
STAGE IV PROOF TESTS (Sections)

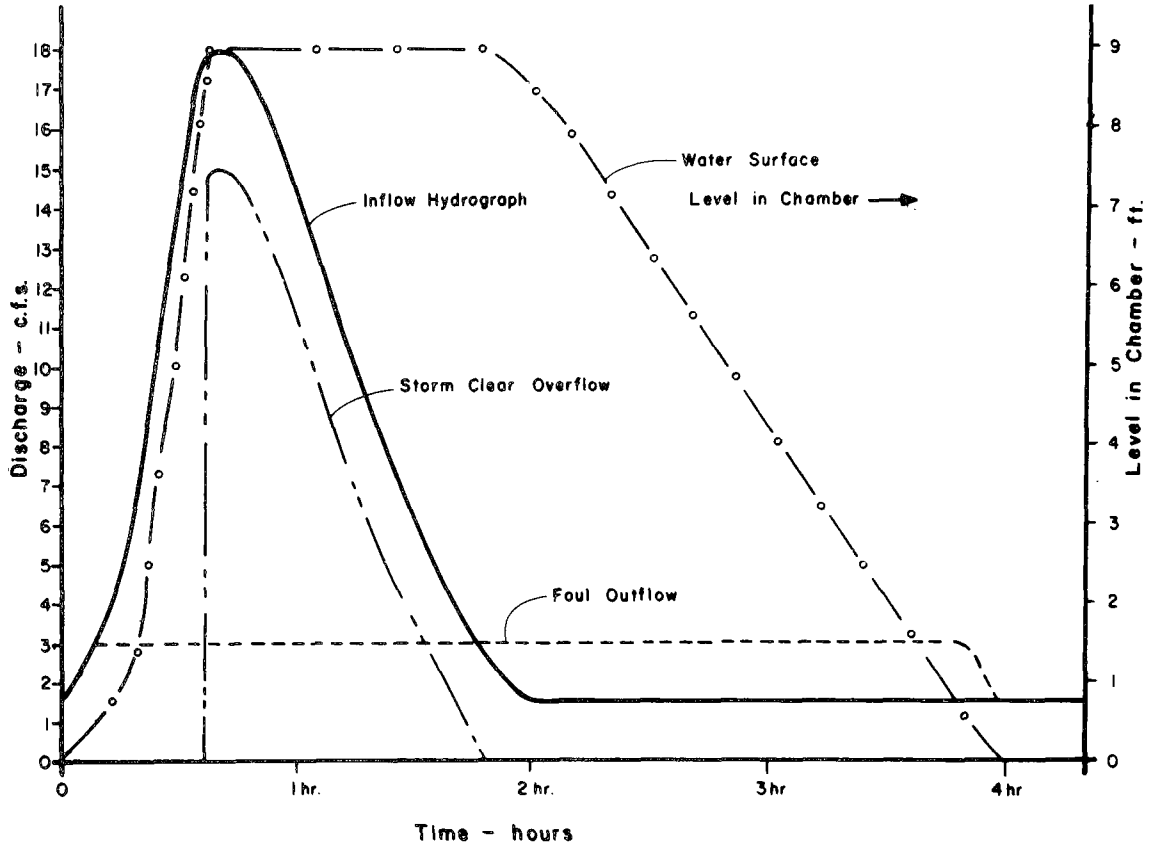

NOTE:

—Read all discharges on left hand ordinate scale
—Read chamber water level on right hand scale

FIGURE 13
15 cfs HYDROGRAPH WITH STAGE IV CONFIGURATION

below the weir around the scum ring diameter. Therefore, since the optimum weir alone from the earlier tests had been found at 24-ft diameter, a 20-ft-diameter weir and 24-ft-diameter scum ring were tested.

Confirmatory tests on this configuration showed flow conditions very similar to those for the 24-ft weir alone, and the large gilsonite recovery for 100 cfs was 100 percent, leaving just traces in the gutters, and for 162 cfs, 85 percent recovery with no deposit at all.

Short-Duration, Low-Discharge Storm Hydrograph Passage

Three tests were performed to reproduce the storm hydrograph relations shown on Figure 13, 15 cfs Hydrograph with the Stage IV Configuration. Gilsonite injection rates were used to reproduce an approximate prototype settleable solids concentration of 200 mg/l.

All these tests showed remarkably similar characteristics. Each test was different, although each adhered to the same general pattern.

As the discharge began rising from 1.5 to 3.0 cfs, all the gilsonite passed quickly through the chamber with the flow contained in the main gutter. As soon as the flow exceeded the capacity of the foul outlet, and began to extend out and cover the floor, the gilsonite movement slowed down quickly. With one foot depth in the chamber, gilsonite

was deposited in the gutter between the 60° and 90° positions. Through a depth of five feet, the gilsonite flowed into the chamber but was deposited in the vicinity of the inlet.

All of the gilsonite was deposited in the supply pipe as the level in the chamber rose from five feet up to the weir crest level at nine feet. The mass in the chamber was very quiescent, with only a very gentle rotation. This same characteristic continued until the flood peak had passed and the level began dropping.

As the flow went down, when the chamber level reached 5.5 feet, large slugs of gilsonite started coming out of the pipe, and before the 5.0-feet-level was reached, a large rush of gilsonite poured out of the pipe. The mass was carried as far as the inlet ramp, and was then redeposited. As the depth was lowered, the agitation of the 1.5-cfs discharge coming down the inlet gutter swept most of the gilsonite deposit down underwater.

When the water surface was at 1.3 to 1.0 foot, the three tests showed divergent results. The general pattern was for the incoming flow to stir up and carry the gilsonite around in the main gutter to the foul outlet. A large portion of the discharge also spilled out of the main gutter running across the chamber floor toward the secondary gutter, carrying along much of the gilsonite.

As the level dropped to the point where all of the discharge could be carried by the main gutter, the spill over the floor toward the secondary gutter was cut off, leaving significant deposits on the floor. The volume and location of these deposits differentiated the individual tests. Table 2, Comparative Volumes of Gilsonite Recovered, indicates amounts of gilsonite recovered through the foul outlet.

TABLE 2

Comparative Volumes of Gilsonite Recovered

Test	Rising Hydrograph	Natural Flush Falling Hydrograph	Manual Washout of Model
1	26	18	56
2	22	56	22
3	26	26	48

The data for Tests 1 and 3 should be considered as most representative, since Test 2 was artificially altered by temporary blockage of the main gutter just as the final flush was occurring. Figures 14 and 15, Deposition of Solids at Low Flows, show the deposits for Tests 1 and 3.

The tests showed that significant deposits may remain after low flow discharges. An automatic wash-out system should be incorporated in the chamber design, with jets directed to flush the inlet, the chamber perimeter walls and the floor, including the inside of the main gutter to minimize maintenance following operation of the concentrator.

It appeared that deposition in the sloping inlet ramp area could be avoided if the floor sides were sloped in toward the central gutter. Another solution might be to have a semi-circular lower half-pipe down the ramp and flaired into the chamber floor. Neither was tried on the model, but they could be accepted as a design detail for prototype construction.

7.5-Foot Deep Chamber Tests

As an added check to determine the necessity of the nine foot depth (measured from the weir crest to the floor level at the perimeter wall), two tests were run with the weir lowered to 7.5 feet.

The two standard steady flow discharges of 100 and 162 cfs were run with the 1-3 mm gilsonite injected at about the prototype 200 mg/l. rate, and Polythene® grains representing floatables.

For the 100 cfs tests, 90 percent of the gilsonite was recovered through the foul outlet, and 70 percent of the Polythene® was retained under the weir. With 162 cfs, only 60 percent of the gilsonite was recovered, and 50 percent of the Polythene® was trapped.

These efficiencies are less than the performance with a nine foot depth. The general impression gained from observation of the flows was that the turbulence for both discharges was greater, and more gilsonite and Polythene® were churned up into the upper layers and discharged over the weir crest.

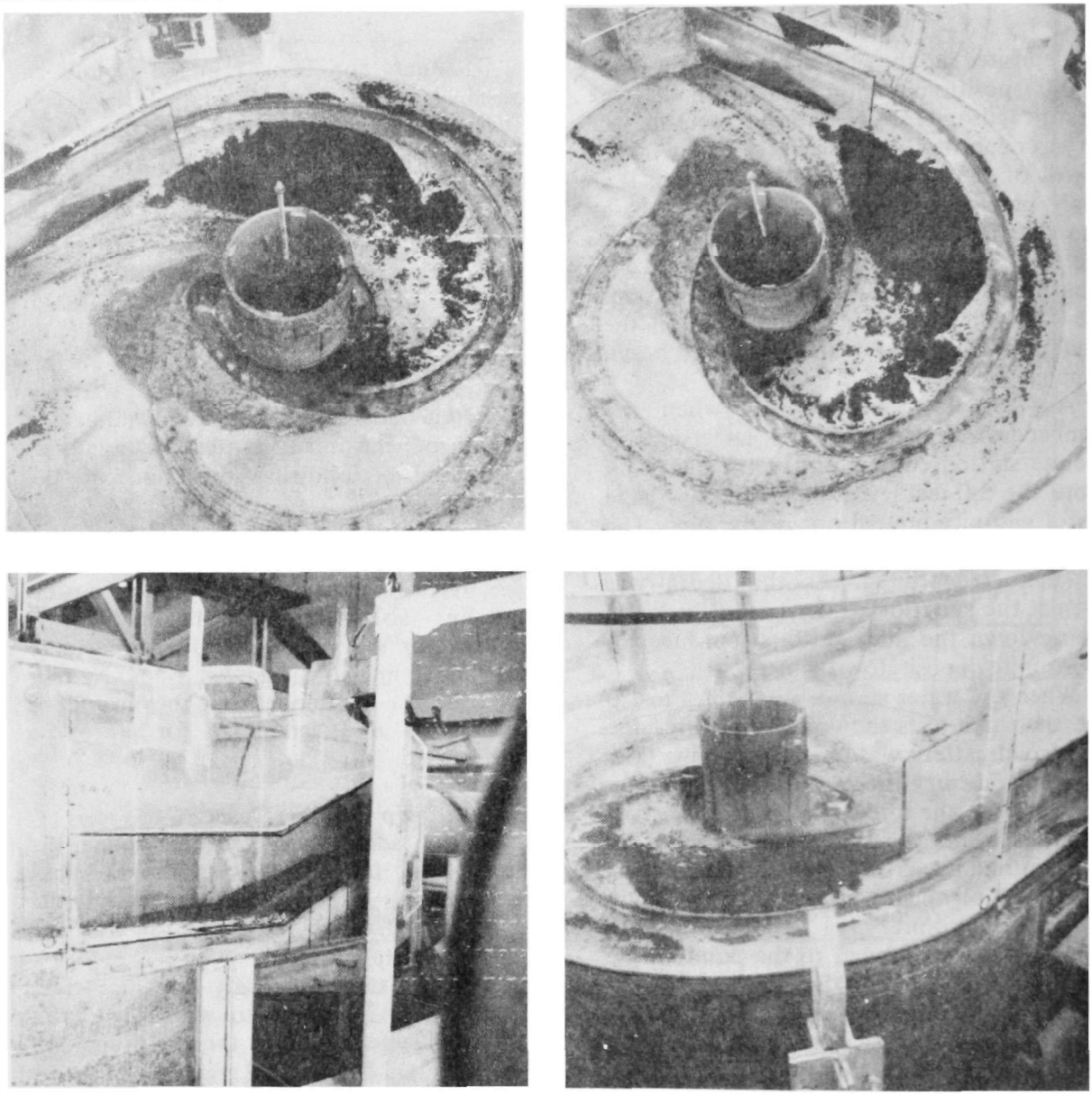

FIGURE 14
DEPOSITION OF SOLIDS AT LOW FLOWS, TEST 1

RECOMMENDED CONFIGURATION

Structural Layout

As shown on Figure 16, Recommended Configuration, the recommended layout incorporated a 36-ft diameter for the chamber, a 20-ft-diameter weir, a 1.5-ft weir skirt and a 224-ft-diameter scum ring, set so its lower edge is just six inches below the weir crest. The 6-ft x 6-ft-square submerged inlet was retained as well as a two gutter floor arrangement. Details of the open vortex foul sewer outlet are shown on Figure 17, Details of Special Structures, as well as the floatables trap and vortex cylinder. If desired, the weir skirt could be increased to as much as three feet to maximize floatables storage capacity.

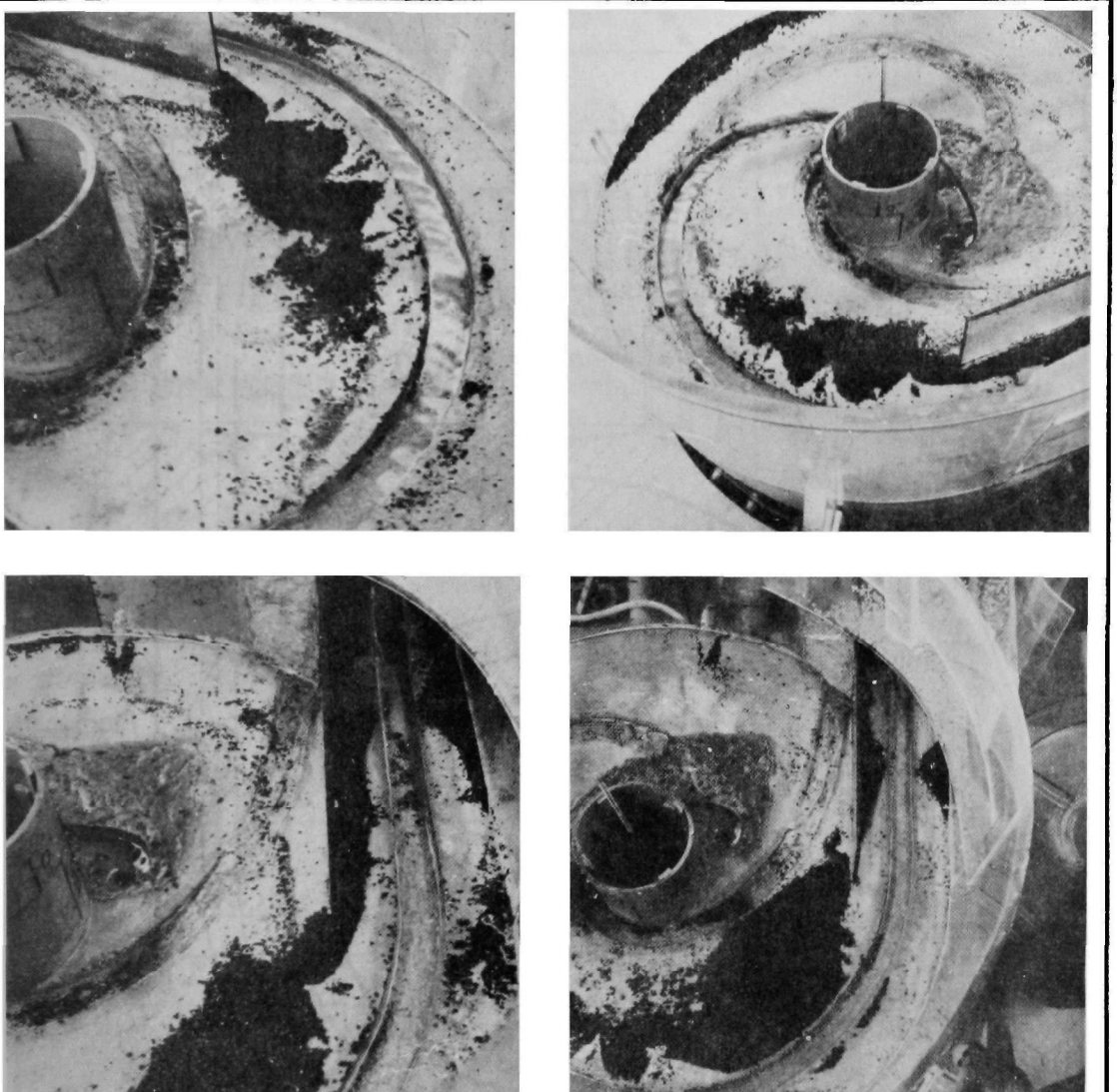

FIGURE 15
DEPOSITION OF SOLIDS AT LOW FLOWS, TEST 3

Figure 16 also indicates the 1-ft slope across the chamber radius. This slope appears desirable from a maintenance standpoint.

Expected Efficiencies

In the normal procedure for the model tests, a given volume of solids was introduced to a steady flow, and the recovery efficiency specified in terms of the original volume. Prototype operation will always be in the form of a hydrograph passage, with varying discharges and solids concentrations. In forecasting efficiencies for the prototype, a simple system similar to that used on the model was followed. Removal efficiencies are expressed in percentages, representing the amount of the various materials going out the foul sewer outlet with respect to the total

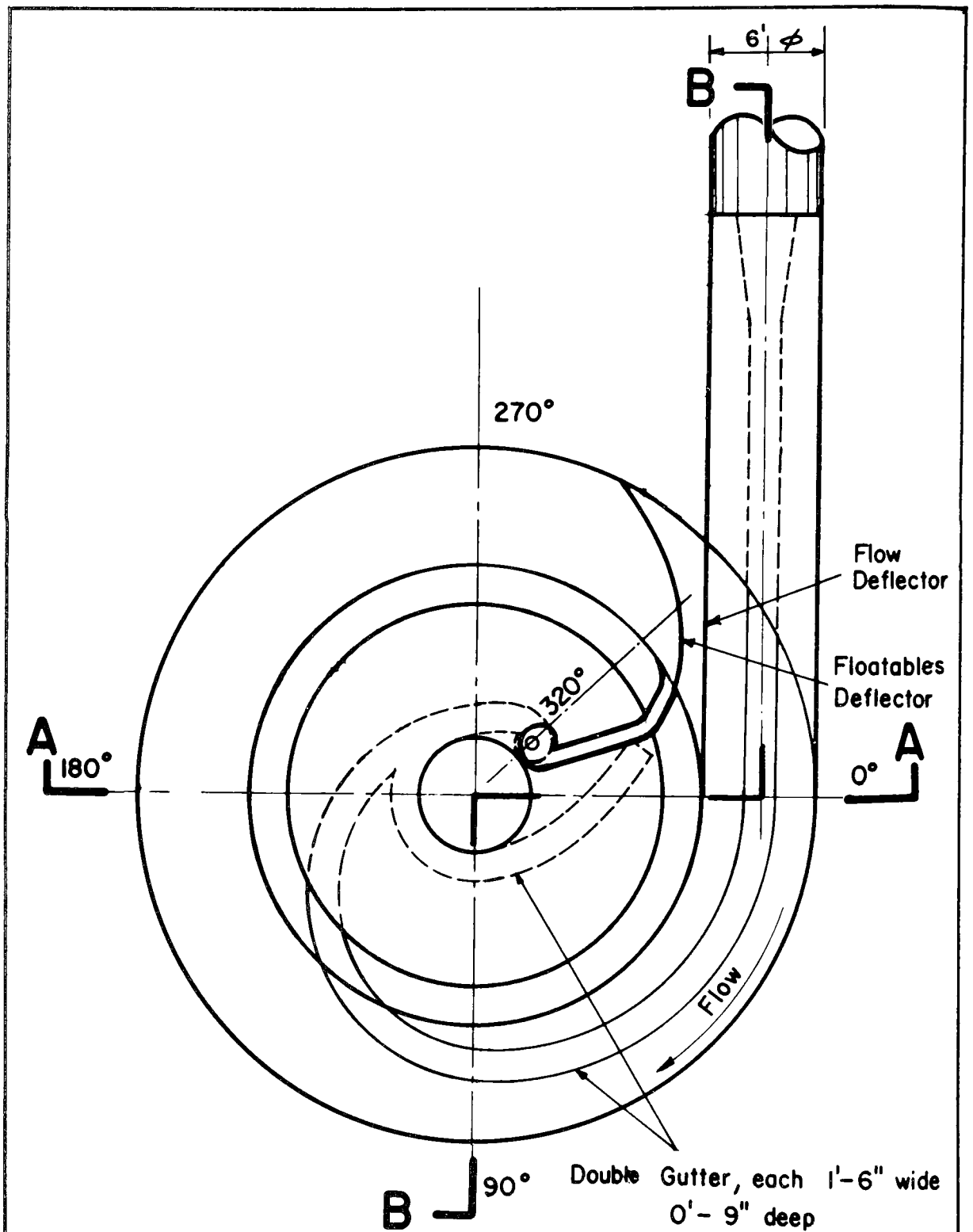

FIGURE 16
RECOMMENDED CONFIGURATION (Plan)

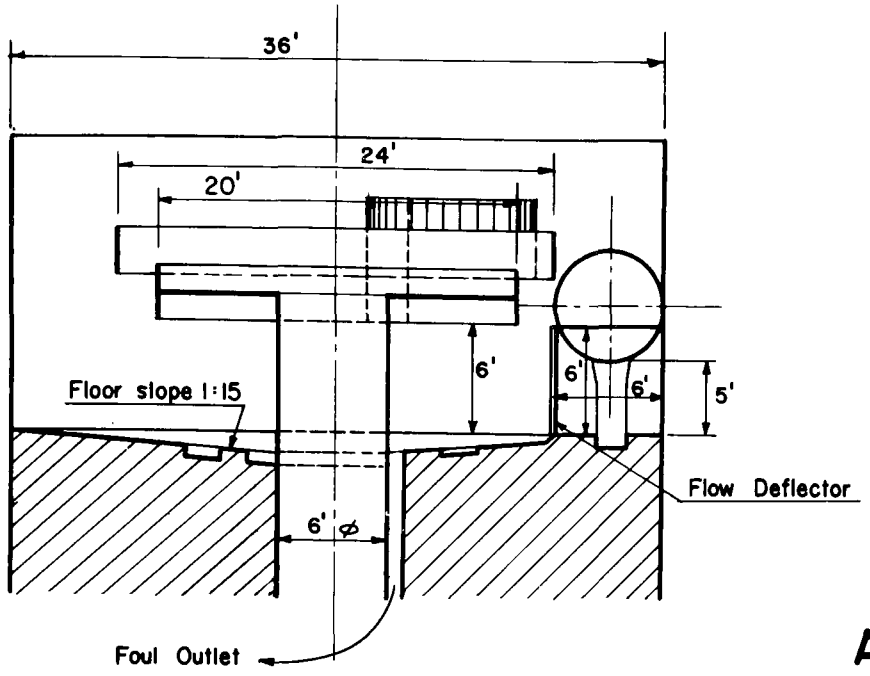

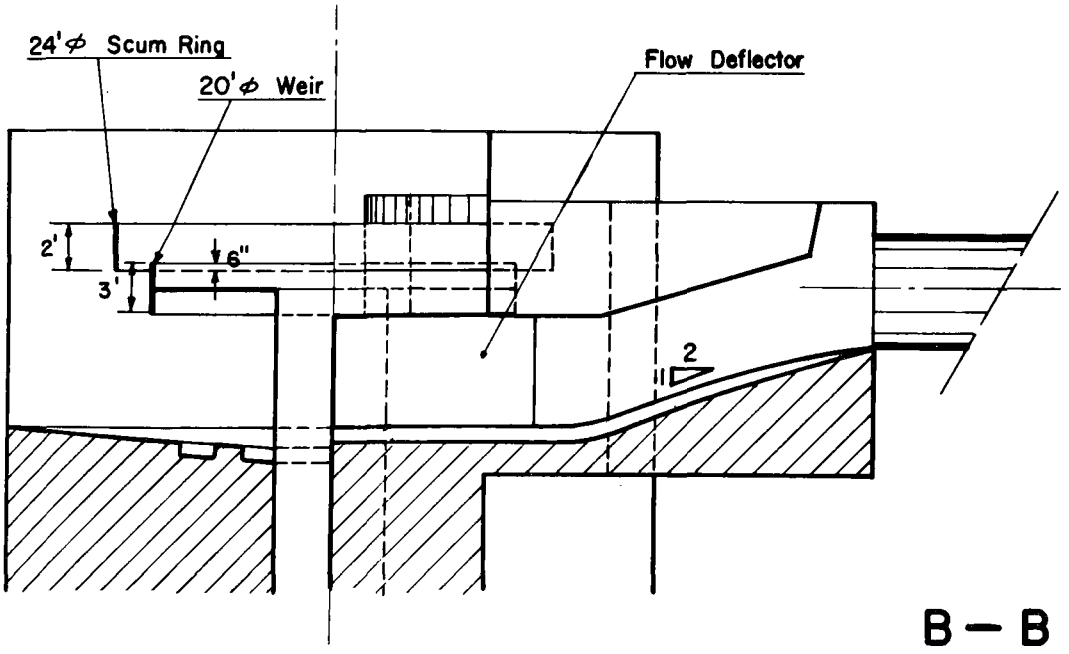

FIGURE 16
RECOMMENDED CONFIGURATION (Sections)

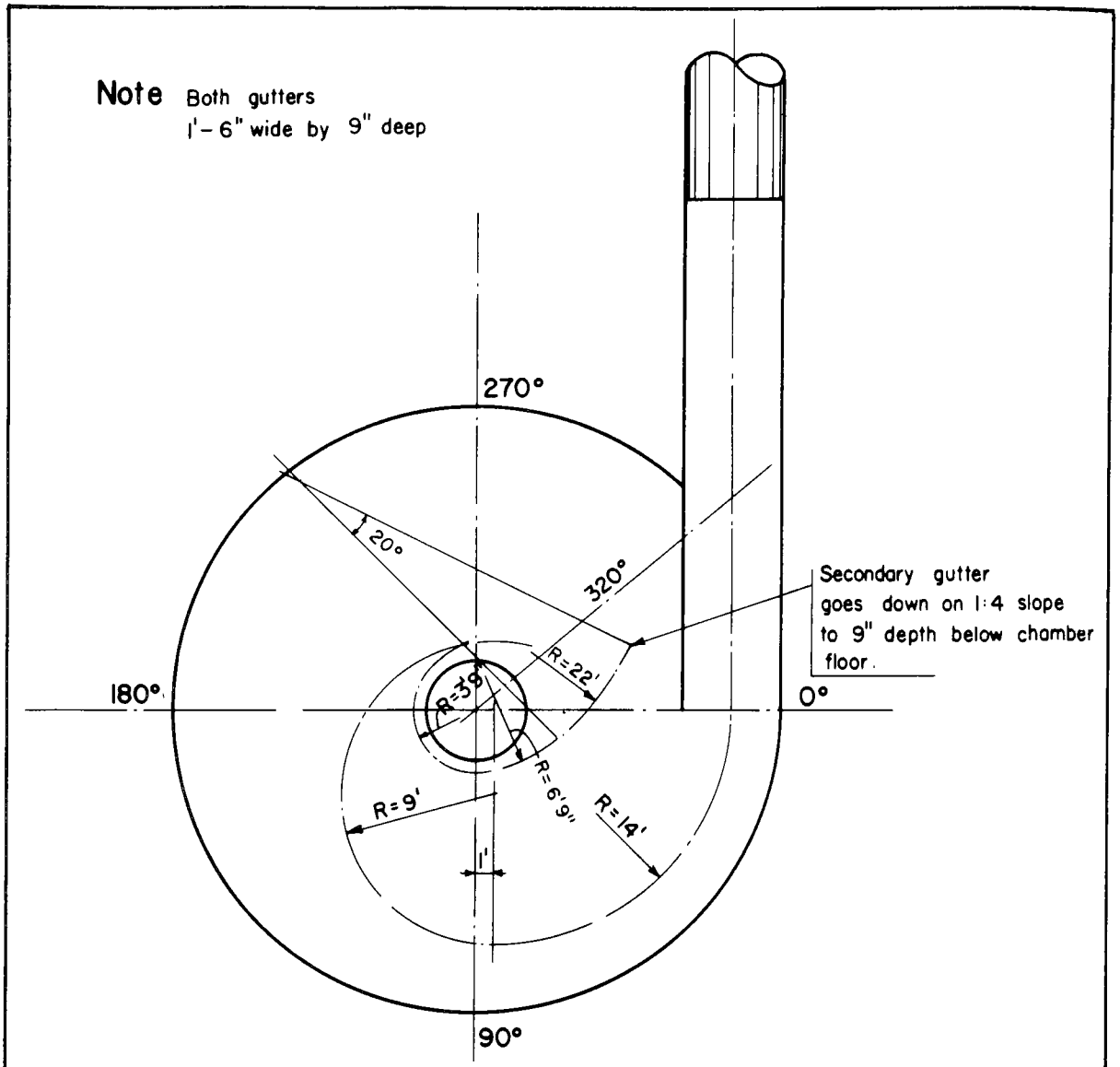

FIGURE 17a
DETAILS OF SPECIAL STRUCTURES
GUTTER LAYOUT

amount entering the chamber over the storm flow period.

1. Floatables: Specific Gravity 0.9-0.96. Particles sizes between five and 50 mm. The chamber should remove between 65 and 80 percent;

2. Grit: Specific Gravity 2.65. For particles larger than 0.3 mm, removal should be 90 to 100 percent with the possibility of some minor deposits confined to the gutters. Progressing towards smaller particles, the efficiency would drop, so that at 0.2 mm it would be about 75 percent, and at 0.1 mm, probably less than 50 percent;

3. Settleable Solids: Specific Gravity 1.2. For particles larger than .1 mm, the recovery efficiency should be between 80 and 100 percent. As shown on Figure 3, this fraction represents 65 percent of the

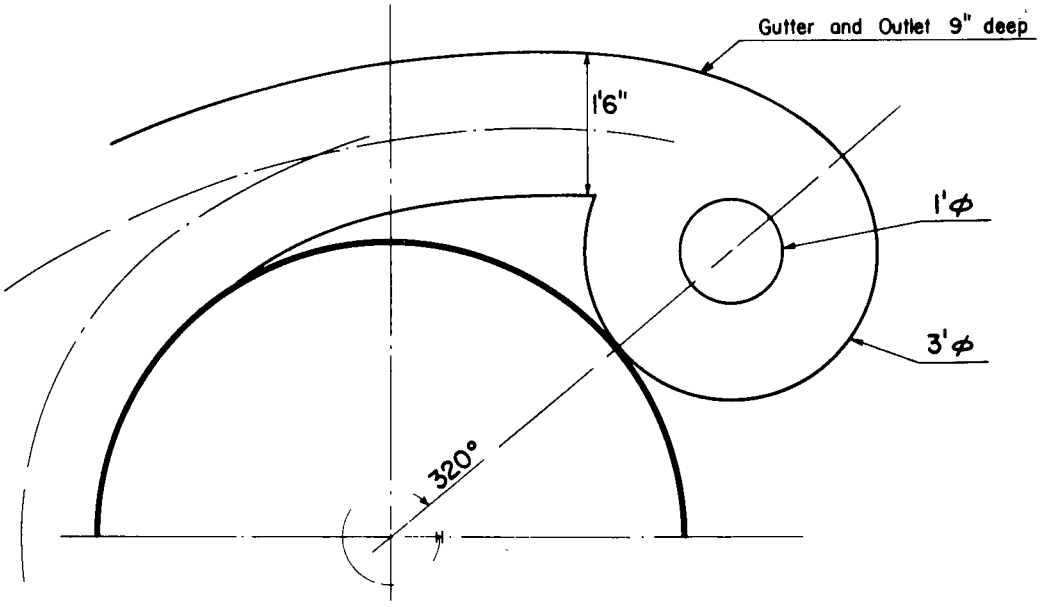

FIGURE 17b
DETAILS OF SPECIAL STRUCTURES
DETAILS OF OPEN VORTEX FOUL OUTLET

total amount of settleable solids in the design solids concentration. Progressing towards the finer particles, removal efficiency would fall off so that for 0.5 mm, it would be about 30 percent and for 0.3 mm, probably less than 20 percent.

Operation With Higher Discharges

It was proposed at a later stage in the study that discharges far exceeding the original design maximum of 162 cfs would be considered. Tests with higher discharges were carried out with both the 24-ft weir alone, and the 20-ft weir with 24-ft scum ring.

The stage-discharge curves are shown on Figure 18, Stage Discharge and Efficiency Curves. The ends of the curves in the 320-350 cfs range indicate the flow limits found for the model as it was constructed; the water level was just splashing over the top of the chamber. The water surface was very irregular, with rotating waves, but a free surface vortex was not developed due to the dampening effect of vertical baffles (spoilers) constructed on the weir plate which acted as energy dissipators.

Spot checks were carried out on separation efficiency by using the large gilsonite. The separating flow characteristics in the chamber remained remarkably steady up to about 250 cfs in each case, then they seemed to break up. The separation efficiencies, however, seemed to drop more consistently as shown on Figure 18.

Comments on Model Test Results

Evaluation of the experience gained on the model study of the swirl concentrator chamber strongly supports the validity of the basic principles of its operation. As was pointed out earlier by Mr. Smisson, the flow inside the chamber must not be allowed to accelerate to the point where vortex forces take control of the particle movements. The particles must be allowed to settle either through the water or along the perimeter wall onto the chamber floor, and to be drawn along by the swirl or the gutters towards the foul outlet.

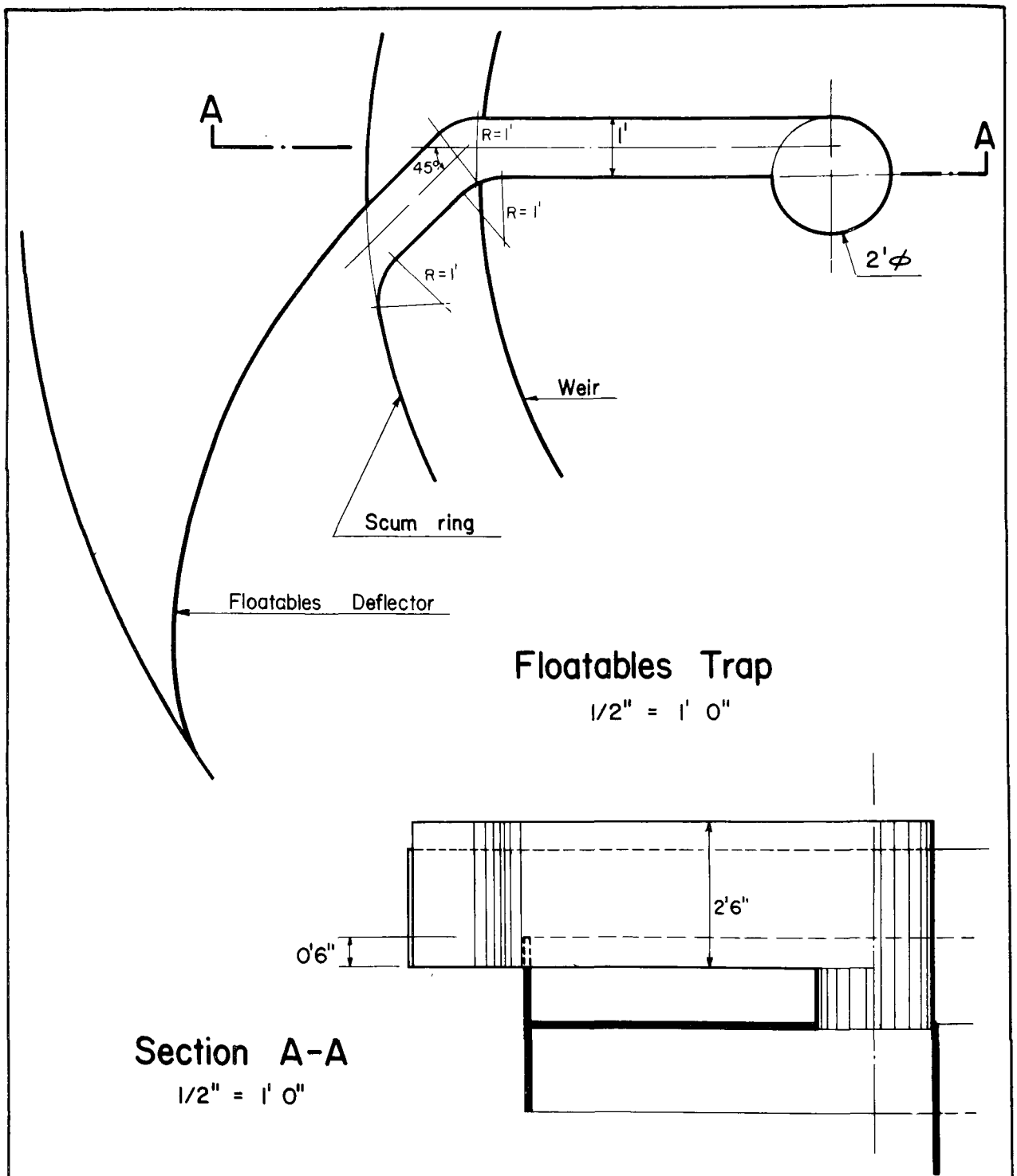

FIGURE 17c
DETAILS OF SPECIAL STRUCTURES
FLOATABLE TRAPS

Other chamber configurations may exist which could provide the required flow characteristics, but that selected in this study appeared the most practical as well as offering high recovery rates for solids.

The following comments are offered on the various elements in the chamber which were studied. Similar remarks appear from time to time in the Appendix, and in some cases the views which follow may contradict the earlier statements. This situation has been retained purposely to show the evolution of knowledge of the structure's operation, and it is always the latter opinion which indicates the latest state.

1. *Inlet Port:*
   - must introduce the flow tangentially;
   - with submerged inlets, top of inlet must be either at same level or below the lowest part of the scum ring;
   - the square inlet was retained on the model, but a round inlet with diameter equal to the square side, giving smooth, evenly distributed flow would also be acceptable;
   - inlet invert should come in on the floor of the chamber so solids tend to stay down and not be swirled up;
   - on the model, flow arrived at the inlet after dropping down a 1:2 slope, designed to keep free surface flow in the sewer upstream, this arrangement is not critical—what is required is smooth even flow; if a longer section at the lower level, which would be submerged under storm flows, can be provided, it would be better for the chamber's operation; the least possible turbulence in supply gives better concentration of solids near the bottom before entry to the chamber;
   - the narrow vertical slot entrance 2 1/2-ft wide showed much promise, and should be kept in mind for further development if a completely free surface flow system would be desired;
   - the inlet has a six-ft nominal dimension, either square or round, in the 36-ft-diameter chamber; it was arrived at through the testing program;
   - this six-ft inlet can be independent of the combined sewer diameter; if this latter is a different size, a transition would be necessary to introduce the flow into the chamber, evenly distributed through a six-ft inlet; and
   - in scaling up prototype sizes, this 1:6 ratio between the inlet dimension and the chamber diameter must be adhered to.
2. *Chamber Depth*
   - the nine-ft depth retained in the final structure was based partly on performance criteria, partly on practical considerations;
   - the two shallower chambers tested showed a slight drop off in solids removal efficiency; and
   - greater depths gave only marginally better removal, and that was not always consistent; these unpredictable advantages were judged so small that they did not justify the extra expense for the deeper construction.

Note: Chamber depth is the difference in elevation between the nominal floor and the overflow weir crest.

3. *Chamber Diameter*
   - the diameter was not varied, however, extrapolation of the depth studies indicates that greater diameters should give more efficient solids separation.
4. *Weir Diameter (Without Scum Ring)*
   - 32-ft-diameter weir was eliminated early as it created a very quiescent inside mass of water and deposits covered much of the chamber floor;
   - all inlet forms created jet impingment on weir or skirt, causing turbulence in the outer ring, allowing more solids rise to go over weir;
   - 28-ft weir had the same characteristics as the 32-ft, but to lesser degree;
   - only exception was with 2 1/2-ft-wide vertical slot, with the narrow slot; the 28-ft weir showed

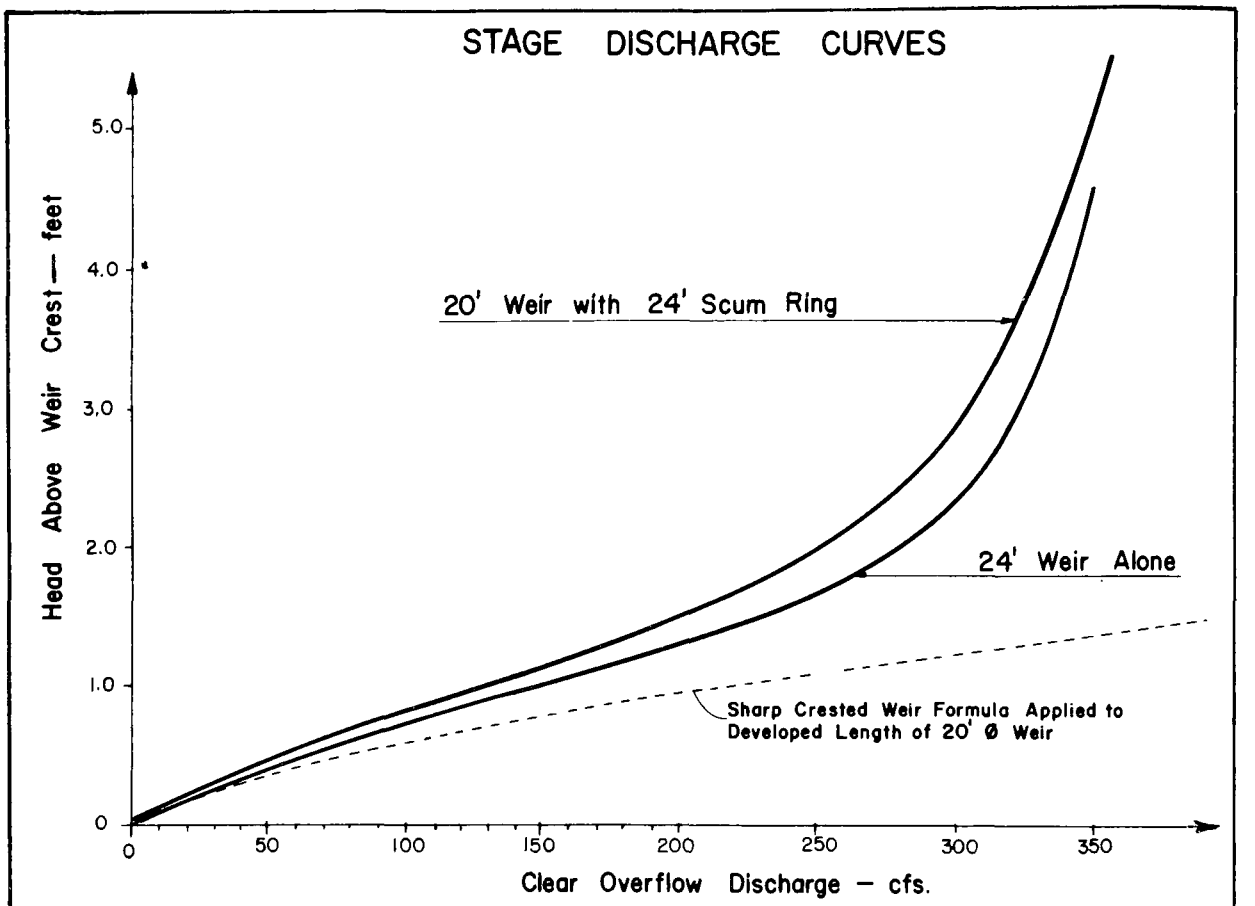

FIGURE 18
STAGE DISCHARGES AND EFFICIENCY CURVES

promise;

- if further research considers the vertical slot, the 28-ft weir should be investigated further;
- 24-ft weir when operating alone (i.e., no scum ring) offers optimum solids separation and good settling characteristics with still enough velocity to entrain particles to the foul sewer outlet;
- when used with 28-ft scum ring, the 24-ft weir reverted to conditions found for 28-ft weir, i.e., serious deposits on floor; and
- 20-ft weir in combination with 24-ft scum ring gave optimum solids separation, similar to the 24-ft weir alone, as shown in Figure 19, Details of Weir Scum Ring and Spoiler Assembly.

5. Weir Crest Shape

- only two crest shapes were tested in this study; the first had a sharp outer edge created by a horizontal cutoff of the 45° rising underside of the cone on the White Ladies Road configuration as shown in Figure 2; the second was the simple flat-topped vertical plate wrapped around the weir disc for all other tests;
- this latter form corresponded to a flat section 1 1/2 inches across on the prototype; with its vertical sides, this could be considered as a sharp crested weir;
- the stage–discharge curves for this weir crest on the two last weir diameters tested on the model are shown on Figure 18; also shown for

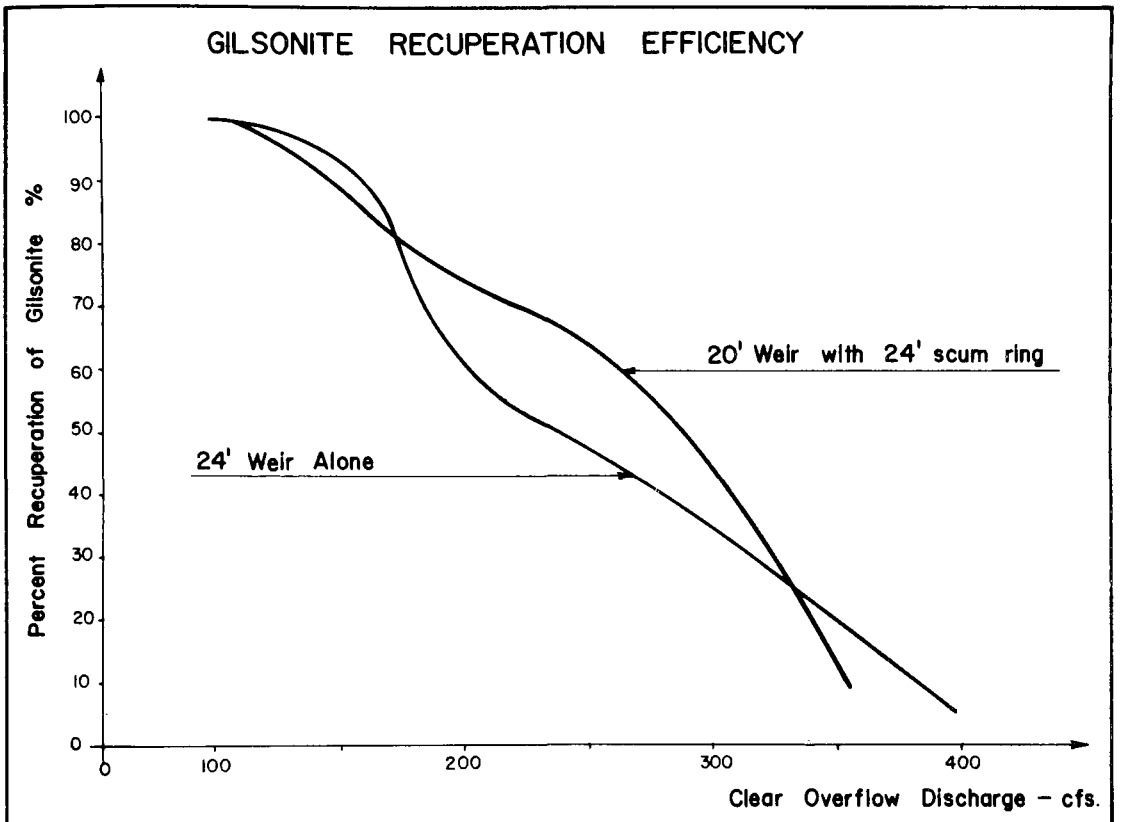

FIGURE 18
STAGE DISCHARGES AND EFFICIENCY CURVES

comparison is the curve for a straight sharp crested weir, 62.8 ft long, this being the perimeter length of the 20-ft weir;

- this crest shape could be made round topped for practical construction or operating reasons without affecting the chamber's separating characteristics; and
- more refined weir crest shapes were not investigated in the present study; they were considered of secondary importance as compared to the overall flow patterns in the chamber, but could be the subject of more detailed research.

6. *Flow Deflector*
   - fundamental approach to study was aimed at avoiding any auxiliary appurtenances in chamber; in spite of this, flow deflector was found necessary;
   - tests run without deflectors showed build-up of rotational velocity and reduction of solids separation;
   - the flow deflector was devised to be a continuation of the inlet, and serves two purposes; (1) it shields the incoming flow from the rotating mass in the chamber, hence avoids turbulence which would make the solids rise; (2) it guides the flow into the inner zone;
   - deflector must terminate at height of incoming channel to allow liquid mass in chamber to pass over incoming flow; this reduces tendency for upward incoming velocity;

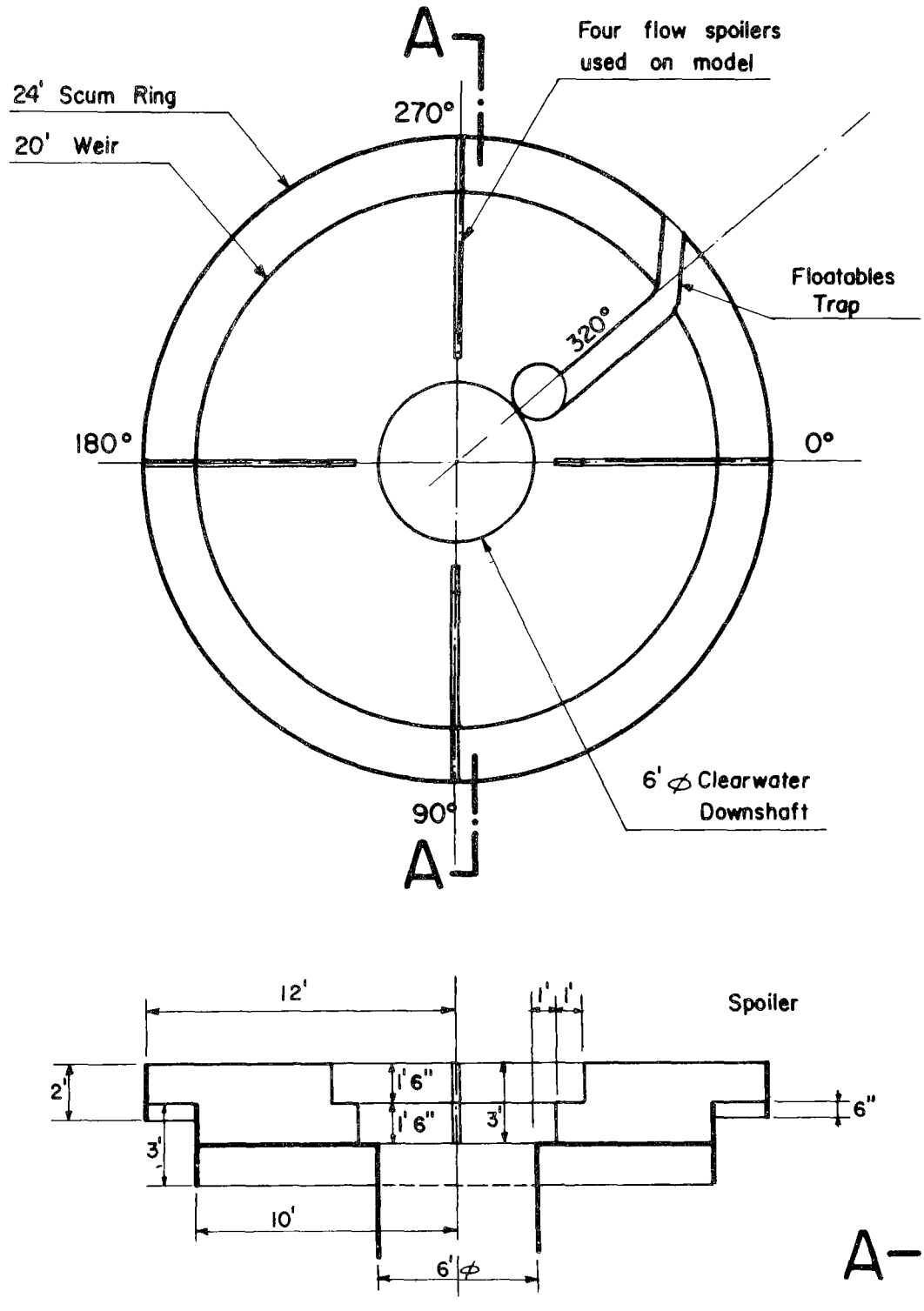

FIGURE 19
DETAILS OF WEIR, SCUM RING AND SPOILER ASSEMBLY

- in the final form, the deflector does not touch the weir, so must be free-standing, six feet high, reinforced at its base to withstand the thrust of guiding the rotating water into the interior water mass; and
- the downstream end of the deflector on the model was cut off square—it could be rounded or parabolic in plan if desired.

7. *Scum Ring*
   - only one location of scum ring tried; i.e., two feet outside overflow weir;
   - when rings were placed at same elevation as weir crest, serious loss of floatables occurred under ring, then over weir;
   - when rings placed six inches below weir crest elevation, good retention of floatables was obtained up to 100 cfs with some losses at 162 cfs;
   - depth six inches below weir is acceptable; and
   - scum ring is subjected to irregular hydrodynamic forces; head variations equivalent to three or four inches of water should be considered in designing structure that would remain rigid in place during operation and afford some measure of safety from large floating objects.
8. *Floor Gutter Layout*
   - extremely critical in reducing deposits;
   - plan shown was optimum evolved in this program of tests, and its layout should be adhered to with care and model studies should be conducted on any variations; for example, the primary gutter shown dotted on Figure 12 was laid out to follow the predominant solids trajectory along the floor: it proved very inefficient, causing serious deposits beyond the foul outlet, and stirring up the solids so more went over the weir;
   - gutter cross section 1.5-ft wide and nine-in. deep retained as adequate to pass dry-weather flow.
9. *Foul Sewer Outlet*
   - the position shown on the final configuration at 320° resulted from successive changes during the tests;
   - at times it appeared desirable to move back towards 270°, but when this was done, deposits remained on the floor against the downshaft between 270° and 360°;
   - first tests performed with horizontal opening at end of gutter, one-ft x two-ft were judged not as efficient, and more subject to blockage, and more difficult for visual inspection or maintenance;
   - open vertical outlet intercepted more solids moving along floor and provided easy visual and access maintenance;
   - vortex shape developed to draw surface down with dry-weather flow; also, after storm, floatables on surface would be drawn down while still about one foot of water remained in chamber; and
   - diameter of outlet should be capable of permitting twice the sanitary flow to prevent shoaling of deposits on the chamber floor; the actual discharge should be controlled by a gate.
10. *Floatables Trap*
    - bottom of the floatables deflector across exterior annular channel placed at same level as scum ring for best floatables diversion and minimum flow disturbance;
    - simple vertical deflector best, curved as it crosses annular channel to meet exterior wall; deflector should not extend more than one inch below water surface to prevent eddy currents from sweeping floatables under the deflector and scum ring;
    - canal and trap envisaged as simple shop fabricated unit, possibly of 1/4-in. steel plate;
    - location of vortex cylinder, which passes down through weir disc, is important; if too close to weir, loose floatables would flow in current out

under skirt; position as shown on Figure 16 was efficient in keeping floatables under weir and provided access to foul sewer outlet;
- location at 320° for floatables trap selected as optimum; and
- similar deflector approach possible to divert floatables out through exterior chamber wall; this was not pursued in this test program but would merit attention in any future studies if it were desired to retain them.

11. *Floor Shape*
- flat floors performed perfectly acceptably when flows are constant or operating; and
- 1-ft slope toward center across radius used to help clear floatables after storm introduces effect of directing some of the flow upward off the deflector.

12. *Spoilers*
- from the beginning, tests showed that discharge through the vertical downshaft was seriously reduced if rotational flow was allowed to build up on the weir plate;
- spoilers, or radial flow guides were constructed on the weir plate to dissipate the rotational energy components of the flow and to direct the flow to the center outlet;
- in the final form, four 3-ft. spoilers were adequate to control discharges up to 250 cfs as shown in Figure 19, Details of Weir Scum Ring and Spoiler Assembly; and
- no limiting number of spoilers was found on the model, but it would seem likely that a practical limit would be six to eight.

13. *Prototype Construction Standards*
- in the model, plexiglass and finished concrete were used to reproduce the chamber—they produce a Manning's of approximately 0.008.
- scaling up from this to a prototype 12 times larger would give "n" = 0.013;
- this degree of smoothness would correspond to a concrete finish inside the chamber, using either smooth wood forms or steel forms;
- care should be taken to avoid projections into the flow period.

DESIGN CRITERIA

The model separation chamber used in the present study had a diameter of three feet, and was operated according to Froude's scaling relations. Froude's law states that the discharge between two geometrically similar structures varies according to the five-halves power of the linear scale between the two structures:

$$Q \alpha \lambda^{5/2}$$

The design peak discharge used on the model was 0.322 cfs, so the scale-up relation between the chamber diameter, D_2, and the peak discharge, Q_d, can be expressed as:

$$D_2 = 3.0 \times \left(\frac{Q_d}{0.322}\right)^{2/5}$$

This equation was used to draw the curve shown on Figure 20, Storm Discharge vs Chamber Diameter, and is presented as a design curve for determining chamber sizes.

The design procedure is as follows:

1. The hydrological study for the given application would be carried out independently of this report. Resulting from that study would be a storm hydrograph giving the possibility of runoff from various sized storms.
2. Take either the peak discharge from the above hydrograph or determine from an economic study the flow which can economically be considered, say a two, five or ten year storm, and consider it as the Design Storm Discharge, Q_d.
3. Find this discharge, Q_d, on the abcissa of the graph on Figure 20., then move vertically upward to the design curve.
4. From this point, move horizontally to the left to read the corresponding Chamber Diameter, D_2, on the ordinate scale.
5. Using the D_2, go to Figure 21, General Design Details, first to find D_1, then to calculate the dimensions of the other

chamber elements.

6. The dry weather sanitary flow was taken as two percent of Q_d in the present model study. The same value was maintained as the foul outflow during storm operation. In practical design, this same order or ratio, two percent times Q_d, should be retained, and the main gutter designed to carry it through the chamber to the foul outlet during dry weather.

Figure 21 presents in simplified symbolic form the dimensions for the various internal elements of the separation chamber. Although the chamber diameter, D_2, is the basic dimension taken off the design curves on Figure 20, advantage was taken of the 6:1 ratio between this and the inlet dimension, D_1, and this latter was selected as the unit dimension. The resulting symbolic relations given on Figure 21 are:

D_1 = inlet dimension = unit
D_2 = diameter of Chamber = $6D_1$
D_3 = diameter of scum ring = $4D_1$
D_4 = diameter of overflow weir 3 1/3 D_1
h_1 = height of overflow weir = 1/2 D_1
h_2 = height of scum ring = 1/3 D_1
b_1 = distance between scum ring and overflow weir = 1/3 D_1
b_2 = offset distance to determine locations of gutter = 1/6 D_1
d_1 = depth from weir plate = 1 1/2 D_1
d_2 = distance from inlet invert to bottom of chamber = 5/6 D_1
R_1 = radius of gutter 0-90° = 2 1/3 D_1
R_2 = radius of gutter 90-180° = 1 1/2 D_1
R_3 = radius of inner gutter 90-270° = 5/8 D_1
R_4 = radius of inner gutter 45-90° = 1 1/8 D_1
R_5 = radius of inner gutter 315-45° = 3 2/3 D_1

For a chamber dimensioned on the basis of Q_d as shown on Figures 20 and 21, the efficiency of solids recovery over a storm period is given by the curve on Figure 22, Separation Efficiency Curve. Solids recovery is the volume of solids taken out through the foul outlet, divided by the total volume of solids entering the chamber during the complete storm hydrograph period, expressed as a percentage.

The solids described by the curve on Figure 22 are those which were represented by the 1-3 mm gilsonite on the model. It follows by reasoning that if that material was recovered, any larger particles would also settle. Therefore, Figure 22 may be used to include either all grit larger than 0.35 mm or all settleable solids larger than 1.0 mm. There would be less but still significant recovery of finer particles of both materials, but not enough data were taken in the present model study to allow its definition for generalized design use.

In following this scale-up procedure, considerable liberty has been taken in interpreting the model results. The structure dimensioning has been done simply on the basis of the Froude law. This procedure is categorically correct as concerns the hydraulic flow characteristics.

The grain size dimensioning, on the other hand, was developed following Stokes law, on the basis of settlement velocities. Over as wide a range of particle specific gravities and sizes, and scale-up ratios which have been suggested, it is certain that the limits of this law would be exceeded in some manner or another. However, it should be pointed out that the absolute definition of the operating laws still lies in the field of advanced fundamental particle movement research, hence, far beyond the scope of the present study. Therefore, in referring to the separation efficiencies given on Figure 22, it should be borne in mind that they are an attempt to give a useful, practical guide to the design engineer, rather than a presentation of clinically precise research data.

The abscissa scale on Figure 22 has been graduated non-dimensionally as a function of the Design Storm Discharge, Q_d. If a storm with peak discharge equal to Q_d occurs, 90 percent of all the grit and settleable solids larger than the sizes shown on the curve

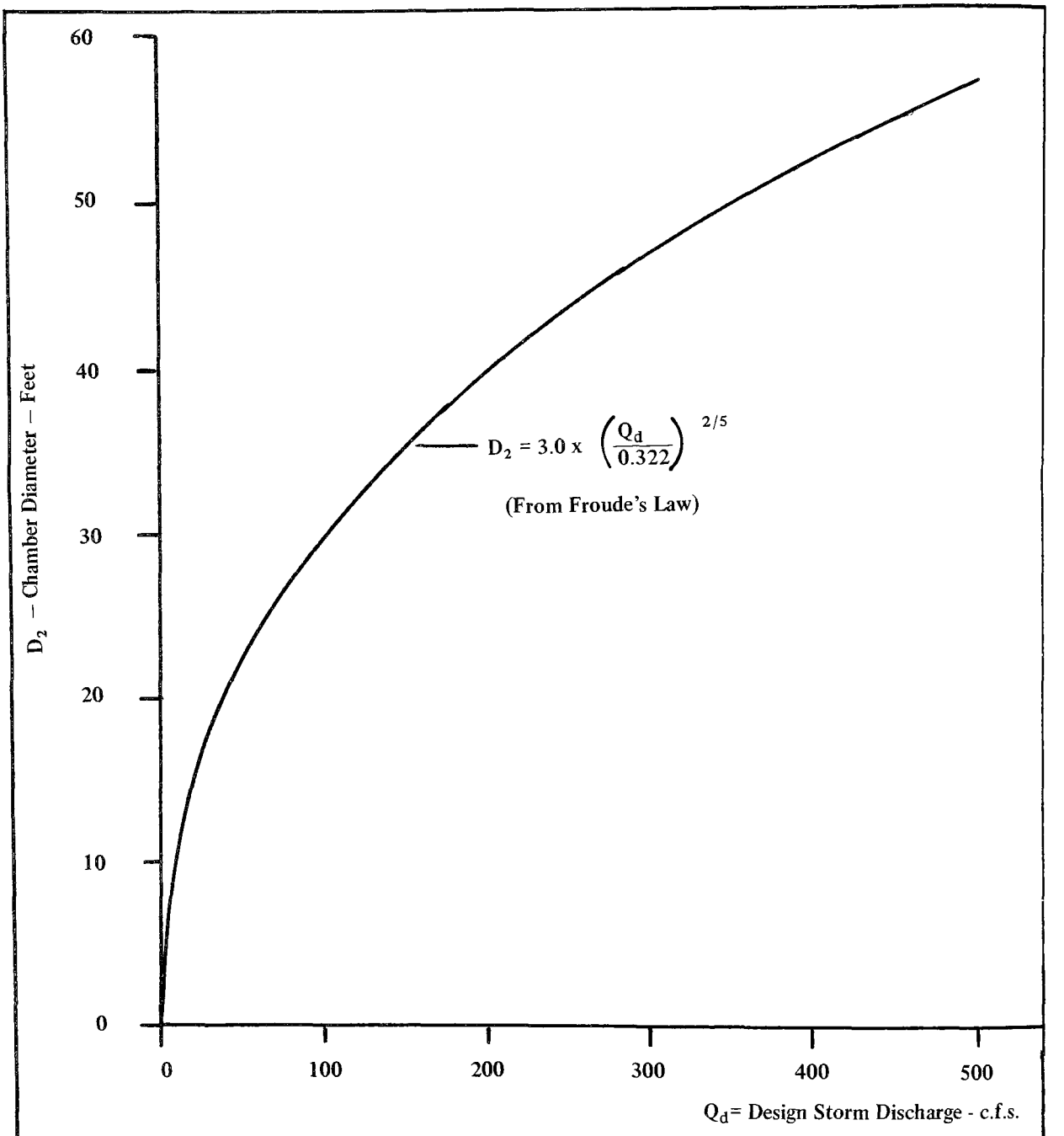

FIGURE 20
STORM DISCHARGE VS CHAMBER DIAMETER

DESIGN PROCEDURE

1. Select the peak discharge from the desired probability storm hydrograph and use this as the Design Storm Discharge, Q_d.
2. Enter the graph with Q_d, go up to the curve then read the corresponding chamber Diameter, D_2, on the ordinate scale at left.
3. Using this D_2, go to Fig. 18 to find first D_1, then calculate the dimensions of the other chamber elements.

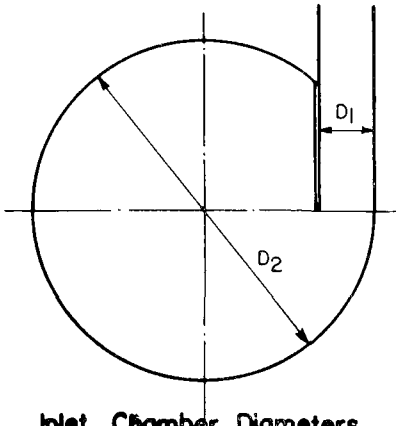

Inlet, Chamber Diameters

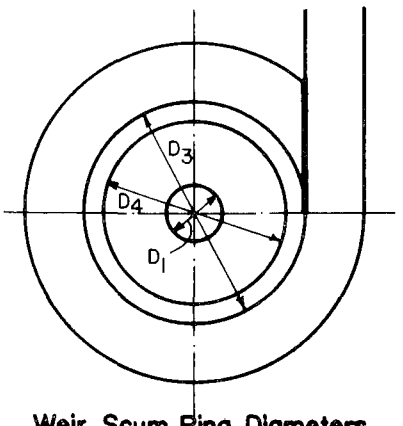

Weir, Scum Ring Diameters

D_1	= unit	D_2	= $6D_1$	D_3	= $4D_1$	D_4	= $3\ 1/3\ D_1$
h_1	= $D_1/2$	h_2	= $D_1/3$	b_1	$D_1/3$	d_1	= $1\ 1/2\ D_1$
d_2	= $5/6\ D_1$	R_1	= $2\ 1/3\ D_1$	R_2	= $1\ 1/2\ D_1$	R_3	= $5/8\ D_1$
R_4	= $1\ 1/8\ D_1$	R_5	$3\ 2/3\ D_1$	b_2	= $D_1/6$		

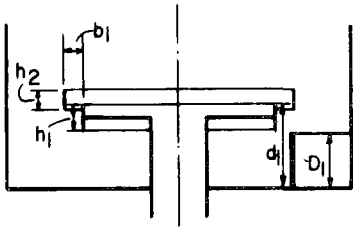

Weir, Scum Ring Details

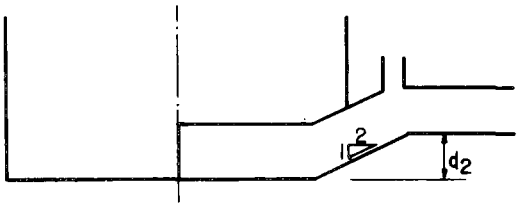

Inlet Detail

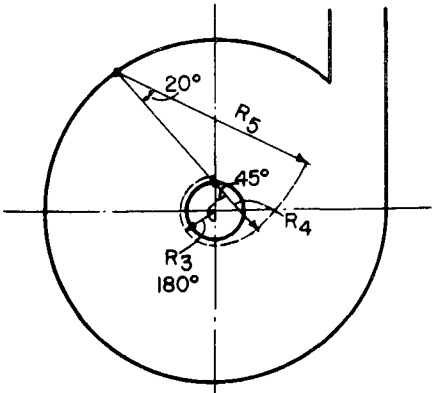

Centerline Secondary Gutter

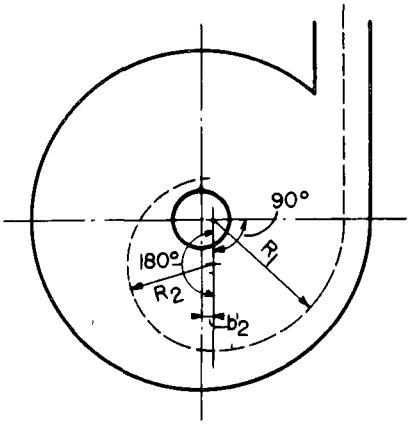

Centerline Primary Gutter

FIGURE 21
GENERAL DESIGN DETAILS

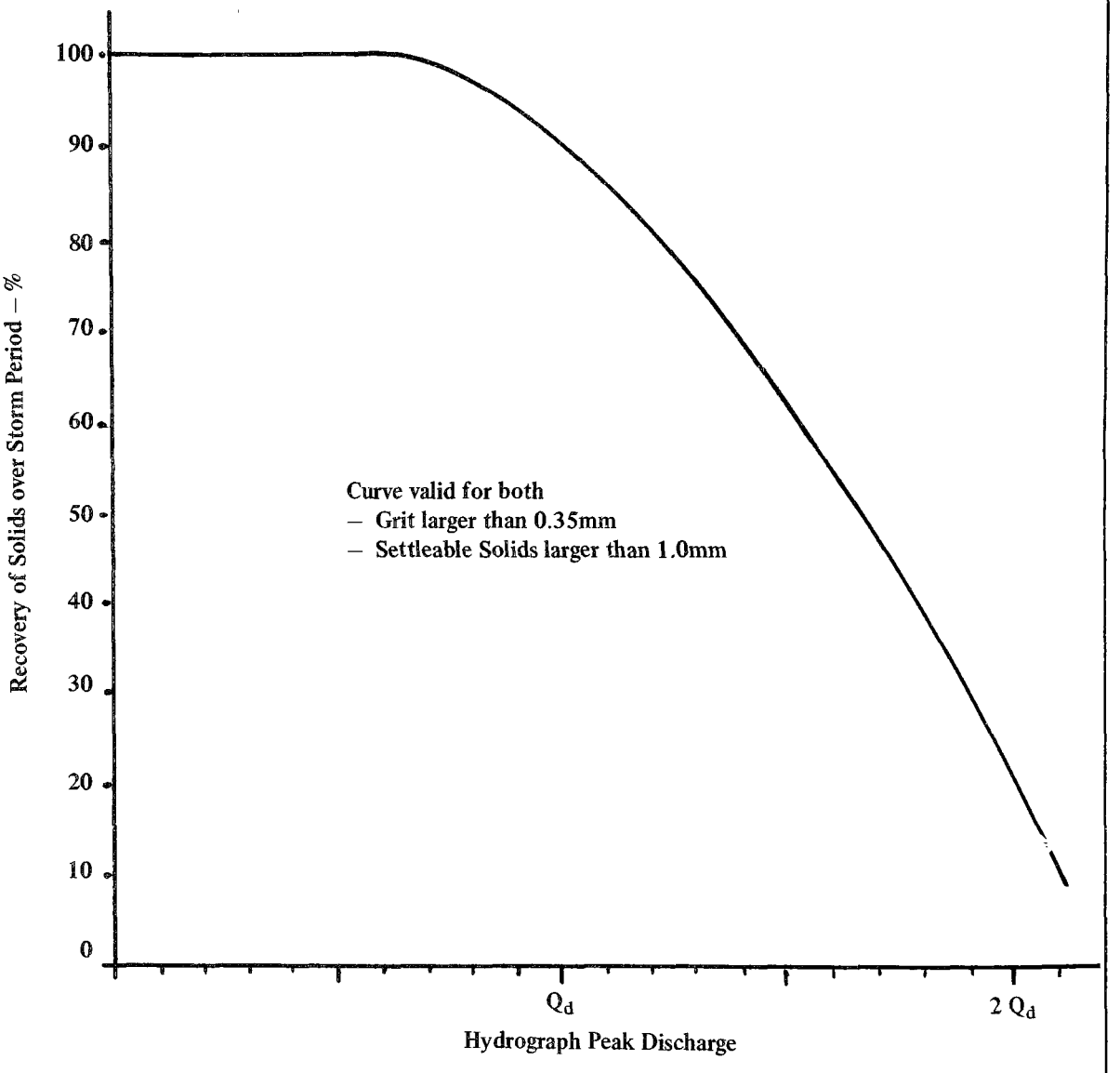

FIGURE 22
SEPARATION EFFICIENCY CURVE

NOTE:

1. Solids recovered are only those *larger* than the sizes shown on the curve; i.e., grit larger than 0.35mm, and settleable solids larger than 1.0mm. Smaller percentages of finer material would be removed, but are not defined by this curve.

2. Percentages of solids recoveries calculated as the volume of solids taken out through the foul outlet, with respect to the total volume of solids entering the chamber during the complete storm hydrograph period.

would be recovered through the foul sewer outlet. For storms with peak discharges greater or smaller than Q_d, the solids recovery over each particular storm period can be determined as a function of the ratio of the actual storm peak divided by Q_d. For example, for a storm peak equal to 1.5 Q_d, enter the curve on Figure 22 on the abscissa with this value. Move vertically upward to the curve, then horizontally to the left to read 62 percent on the ordinate scale. The chamber would therefore recover through the foul sewer outlet 62 percent of the solids larger than the sizes shown arriving in the chamber over the storm hydrograph.

DESIGN EXAMPLE

The hydrological study of a given urban area shows a peak storm discharge, Q_d, of 400 cfs. If it is desired to effectually treat this entire flow, reference to Figure 20 gives a chamber diameter of 52 feet. From Figure 21, the following main dimensions can be found:

a. Inlet Dimension, $D_1 = \frac{D_2}{6} = 8$ ft -8 in.

   for practical design, eight feet six inches or nine feet would be acceptable.

b. Weir Diameter, $D_4 = 3\ 1/3\ D_1 = 28$ ft 10 in.

   for practical design, take 29 ft

c. Scum Ring Diameter, $D_3 = 4\ D_1 = 34$ ft 8 in.

   for practical design, take 35 ft

d. Chamber Depth (weir crest to floor), $d_1 = 1\ 1/2\ D_1 = 13$ ft

With a structure built to these dimensions, reference to Figure 22 will show what efficiencies to expect. If the design storm discharge of 400 cfs occurred, 90 percent of all the grit and settleable solids larger than those mentioned previously would be removed from the clearer overflow. For flows of 240 cfs or less the concentrator would operate at maximum efficiency.

If a storm with peak of 500 cfs occurred, this would be:

$$\frac{500}{400} = 1.25 Q_d$$

Going into Figure 22 with this value on the abscissa, moving up to the curve, then to the left on the Recovery scale, would indicate that 78 percent of the solids would still be removed.

APPENDIX 2
MATHEMATICAL MODELING OF SWIRL CONCENTRATORS

INTRODUCTION

The objective of this study was to develop a mathematical model and computer simulation of a swirl concentrator device to separate grit and settleable solids from storm water overflows. The general features of the device were described in Appendix 1, Figure 12. The flow enters tangentially, setting up a swirling motion. Settleable solids sink to the bottom, and are carried by a secondary liquid flow to the center of the chamber where they are withdrawn, along with a fraction of the liquid flow to the foul sewer. Most of the flow proceeds over the circular weir mounted on the central standpipe. This clarified effluent (the overflow) is withdrawn through the central standpipe.

As described in Appendix 1, a deflector plate was installed parallel to the inlet flow as shown in Figure 12. The deflector plate forces the high energy liquid at the periphery of the tank to flow into the center, thus raising the tangential velocities under the weir. An additional effect of the deflector is to help scour the deposited particles and direct them into the foul sewer.

Near the conclusion of the present study, additional changes were introduced in the laboratory model in order to trap floating material. The changes included a vertical scum ring between the weir crest and the outer tank wall. Material floating to the surface between the scum ring and tank wall are thereby prevented from flowing over the weir. A surface deflector located at station 320° directs these floating particles into a channel across the weir and into a small vortex drain through the weir plate. The particles are drawn through this drain and are stored in the low velocity area under the weir. Due to schedule limitations, the mathematical model does not include the effects of the scum ring.

The swirl concentrator was first proposed by Smisson[1] in Bristol, England, and has since been further investigated by Smisson and other investigators.[2-4] This study is the first attempt to rationalize the design of such devices through development of an analytical model to predict the operating principles. In conjunction with the laboratory tests described in Appendix 1, the analytical model has been used to predict the variation in performance with the principal design variables, and so arrive at a valid configuration.

The present results are aimed specifically at optimizing the design of a unit to be installed at Lancaster, Pennsylvania, as part of a demonstration grant. In this application, up to 440 cfs flowrates may occur, with a nominal design value of 165 cfs. The laboratory unit is referred to as the model chamber. Although specific calculations were performed for the model and prototype chambers, the results are applicable to a broad range of chamber sizes, flowrates, particle sizes and specific gravities. This broad applicability is achieved through a set of scaling laws based on the governing equations. With the scaling laws, the results of the lab tests and the computer calculations can be extended to chambers of other sizes and flowrates, *provided that geometric similarity is maintained.*

The general approach of this study has been to calculate the liquid flowfield within the swirl concentrator, neglecting the presence of the particles (i.e., assuming a dilute mixture). This is accomplished by using a relaxation procedure to numerically solve the equations for turbulent axisymmetric flow. A three-dimensional eddy viscosity model is used to relate the local turbulent Reynolds stresses to the gradients of the mean flow properties. Once the liquid flow has been calculated, the particle flow through the liquid is computed. At each point at which the liquid flow was computed, the three particle momentum equations, and the equation of continuity are solved to determine the particle velocities and concentration. The equations include turbulent diffusion terms, virtual mass effects, gravity forces, and drag. The equations are solved with a time dependant scheme, integrating forward in time until a steady state is achieved.

The liquid flow calculation has been calibrated by adjusting the mixing length and friction coefficient to provide the best match with the experimental data. The agreement is generally good, but limited by non-axisymmetric flow effects in the physical model due to the inlet jet and deflector plate. Using the calibrated liquid flow, particle flows were calculated for several flow rates, particle sizes, and chamber sizes. The results generally show favorable agreement with the laboratory data for prototype overflow rates up to 162 cfs on a 36-ft diameter computer model.

ANALYSIS SUMMARY

Liquid Flow Calculation

The calculation of the liquid flowfield within the swirl concentrator requires making several simplifying assumptions. The two chief assumptions are that the flow is axisymmetric, and that its turbulent character can be modeled as described in the following section. The axisymmetric assumption means that the flow can be described with only two independent variables (r, radius and z, depth), and is independent of the angular position. This assumption requires that the inlet flow, which in the actual device enters tangentially through a square duct be represented by a circumferential region of the wall through which the inflow occurs. The inlet flow through the wall is assumed to have a quartic velocity profile as illustrated in Figure 1, Cross Section of Swirl Concentrator, with the magnitude adjusted to give the proper mass flowrate. The tangential velocity of the incoming flow is assumed to be constant, and equal to the mean velocity in the entrance channel. These assumptions give the correct tangential velocity near the outer wall. Also, since the inflow is spread over a large area, the radial inflow velocity is small, and does not differ appreciably from the actual case in which the radial velocity vanishes at the wall. The axisymmetric model thus approximates well the average behavior of the flow at most radial locations.

There are three principal non-axisymmetric effects in the physical model:

a) The tangential velocity near the center of the tank is increased due to the deflection of the outer flow under the weir by the deflector plate.

b) A local vortex is created above the foul sewer outlet by the deflector plate.

c) The inlet flow exhibits a jet-like behavior.

The first of these effects has been simulated in the mathematical model by adjusting two arbitrary constants (mixing length and wall skin friction coefficients) to match the average observed tangential velocities under the weir. The second of the effects listed is very important in determining the scouring properties of the chambers. The location of the foul sewer outlet has been carefully adjusted in the physical model to take advantage of the scouring properties of the local vortex induced by the deflector. Without the local vortex, the separated solids may remain as deposits on the floor of the chamber. An auxiliary device (mechanical scraper or flushing jet) is then required to cleanse the chamber after a storm. In the mathematical model, however, all particles hitting the bottom are assumed to eventually be withdrawn through the foul sewer. The mathematical model does not determine whether these particles form deposits or are swept into the foul sewer outlet. This distinction is not required to predict the overall separation efficiency because the local vortex does not appreciably affect the separation ability of the chamber, only its self-cleaning capability.

The third non-axisymmetric effect (jet-like inlet flow) is most important at high flowrates. At low flowrates (100 cfs or lower in the present case), the inlet jet has largely diffused vertically and laterally before the liquid reaches the 90° station, without creating serious non-axisymmetric distortions. At these low flowrates, the water surface appears relatively smooth and axisymmetric. At high flowrates (250 cfs and above), the entrance jet persists further into the chamber and tends to surface as a plume, creating waves and turbulence at the surface. Since the mathematical model is limited to axisymmetric flow, there is a gradual breakdown in its ability to describe the

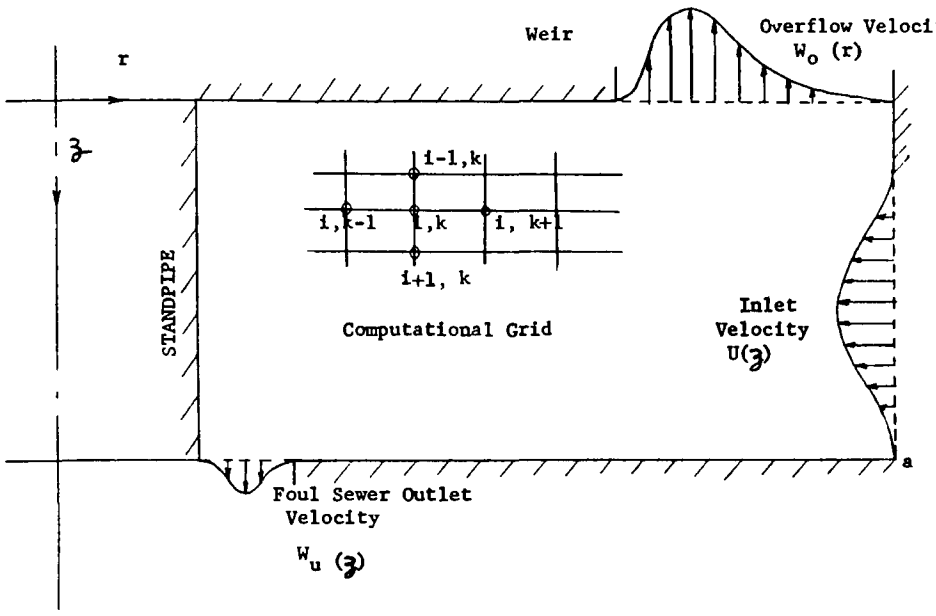

FIGURE 1
CROSS SECTION OF SWIRL CONCENTRATOR

physical flow above 100 cfs. At high flowrates, the mathematical model will overestimate the separation efficiency because the transport of particles to the surface by the entrance jet and by excess turbulence has not been accounted for.

Even at low flowrates where the axisymmetric approximation applies, the flow is turbulent and quite complex. The art of turbulent flow calculation is not far advanced, and even for the simpler case of a boundary layer flow, two different models can give results which differ by as much as 50 percent in some respects. The present model uses an elementary eddy viscosity approach which relates the turbulence to the gradients of the mean velocities through the use of a mixing length concept. This approximation cannot duplicate the finer details of the turbulent, time varying flow structure. However, at low flowrates, the main features of the internal flow are reproduced reasonably well, and the results give considerable insight into the behavior of the streamlines within the swirl concentrator.

Also, in keeping with the axisymmetric nature of the model, the outflow velocities are specified as uniform around the circumference of the weir. This is accomplished by using smooth power series profiles, as illustrated in Figure 1. This procedure represents the overflow velocity fairly well, except near the inlet where disturbances due to the deflector plate occur. The overflow velocity is specified along a horizontal line at the same height as the underside of the weir, as shown in Figure 1. This procedure is used in order to maintain a rectangular computational mesh. The actual depth of liquid in the tank is higher by about 1.5 ft (prototype scale) due to the projection of the weir crest above the weir plate. For consistency with the hydraulic model report, the depths in this report refer to the distance from the bottom of the chamber to the weir crest, even though the computational region did not extend beyond the underside of the weir plate.

The foul sewer flow is also represented as an annular discharge in the mathematical

model. In reality, the foul sewer flow is withdrawn through a single port in the bottom of the concentrator. For small values of the foul sewer fraction, the differences resulting from the annular approximation will not be large. For sizeable foul sewer flows, significant non-axisymmetric effects could be anticipated.

An additional detail of the actual swirl concentrator which could not be modeled, was the skirt which hangs below the weir to trap floatables. The computational mesh used for the present calculation was too coarse to permit this detail to be modeled without causing numerical instabilities. However, the present results seem satisfactory without the complication. The ultimate test of the reasonableness of this and the other approximations discussed previously, is how well the mathematical model predicted the actual behavior of the concentrator. Based on the comparisons to be discussed later, the model appears to be satisfactory in its present form at overflow rates up to 162 cfs.

Equations of Motion

The basic equations for the steady-state flow of a viscous incompressible fluid in tensor notation are[5]

Continuity:

$$U^{j}_{,j} = 0 \tag{1}$$

Momentum:

$$(\rho U^{j} U_{i})_{,j} = -\frac{\partial p}{\partial x}_{i} + \tau^{j}{}_{i,j} \tag{2}$$

where

$$\tau_{ij} = \mu (U_{i,j} + U_{j,i}) \tag{3}$$

To obtain equations for the mean motion, $\bar{U}_i$, in the presence of fluctuations in velocity and pressure (U'_i, and p') whose averages are zero, one can substitute

$$U_i = \bar{U}_i + u'_i$$

$$p = \bar{p} + p'$$

into Equations (1) and (2) and perform an averaging in time. The result is the well-known Reynolds equations for the mean motion:

$$\bar{U}^{j}_{,j} \tag{4}$$

$$(\rho \bar{U}^{j} \bar{U}_{i})_{,j} = \frac{\partial \bar{p}}{\partial x^{i}} + (\bar{\tau}^{j}{}_{i} \quad \overline{\rho u'^{j} u'_{i}})_{,j} \tag{5}$$

In Equation (5) the viscous shear term

$$\bar{\tau}^{j}_{i} = g^{jk} \mu (\bar{U}_{i,k} + \bar{U}_{k,i}) \tag{6}$$

is due to the viscosity of the fluid, whereas the Reynolds stress

$$T_{ij} = \overline{\rho u'_{i} u'_{j}} \tag{7}$$

arises from the correlation between the fluctuating velocities u'_i and u'_j.

For this project, the Reynolds stress terms have been modeled by relating the local stress to properties of the mean flow, retaining the proper tensor character of the equation.[5] In particular

$$T_{ij} = -\rho \epsilon (\bar{U}_{i,j} + \bar{U}_{j,i}) \tag{8}$$

where ϵ is an eddy viscosity defined by

$$\epsilon = \ell^{2} \Phi^{1/2} \tag{9}$$

in which ℓ is a mixing length, and Φ is the local dissipation function

$$\Phi = \tfrac{1}{2} S^{ij} S_{ij} \tag{10}$$

where

$$S_{ij} = \bar{U}_{i,j} + \bar{U}_{j,i} \tag{11}$$

Written in the cylindrical coordinate system of Figure 1, Equations (4) and (5) become, for axisymmetric flow:

$$\frac{\partial \bar{u}}{\partial r} + \frac{\bar{u}}{r} + \frac{\partial \bar{w}}{\partial z} = 0 \tag{12}$$

$$\bar{u} \frac{\partial \bar{u}}{\partial r} + \bar{w} \frac{\partial \bar{u}}{\partial z} - \frac{\bar{v}^{2}}{r} = \frac{-1}{\rho} \frac{\partial \bar{p}}{\partial r} + (\epsilon + \nu) \left(\frac{\partial^{2} \bar{u}}{\partial r^{2}} + \frac{1}{r} \frac{\partial \bar{u}}{\partial r} - \frac{\bar{u}}{r^{2}} \quad \frac{\partial^{2} \bar{u}}{\partial z^{2}} \right) + 2 \frac{\partial \bar{u}}{\partial r} \quad \frac{\partial \epsilon}{\partial z} + \left(\frac{\partial \bar{w}}{\partial r} + \frac{\partial \bar{u}}{\partial z} \right) \frac{\partial \epsilon}{\partial z} \tag{13}$$

$$\bar{u}\frac{\partial\bar{v}}{\partial r}+\bar{w}\frac{\partial\bar{v}}{\partial z}+\frac{\bar{u}\bar{v}}{r}=(\epsilon+\nu)\left(\frac{\partial^2\bar{v}}{\partial r^2}+\frac{1}{r}\frac{\partial\bar{v}}{\partial r}-\frac{\bar{v}}{r^2}+\frac{\partial^2\bar{v}}{\partial z^2}\right)+\frac{\partial\bar{v}}{\partial z}\frac{\partial\epsilon}{\partial z}+\left(\frac{\partial\bar{v}}{\partial r}-\frac{\bar{v}}{r}\right)\frac{\partial\epsilon}{\partial r} \tag{14}$$

$$\bar{u}\frac{\partial\bar{w}}{\partial r}+\bar{w}\frac{\partial\bar{w}}{\partial z}=-\frac{1}{\rho}\frac{\partial\bar{p}}{\partial z}+(\epsilon+\nu)\left(\frac{\partial^2\bar{w}}{\partial r^2}+\frac{1}{r}\frac{\partial\bar{w}}{\partial r}+\frac{\partial^2\bar{w}}{\partial z^2}\right)+\left(\frac{\partial\bar{w}}{\partial r}+\frac{\partial\bar{u}}{\partial z}\right)\frac{\partial\epsilon}{\partial r}+2\frac{\partial\bar{w}}{\partial z}\frac{\partial\epsilon}{\partial z} \tag{15}$$

Following the technique of Reference 6, Equations (12)-(15) are put in a more convenient form for computation as outlined below. The continuity equation (Eq. 12) is identically satisfied by introducing a stream function, ψ such that

$$\bar{u}=\frac{1}{r}\frac{\partial\psi}{\partial z},\quad \bar{w}=-\frac{1}{r}\frac{\partial\psi}{\partial r} \tag{16}$$

The pressure is then eliminated by differentiating Equation (13) with respect to z, and Equation (15) with respect to r, and then subtracting one from the other. The results are then written in terms of the non-dimensional variables

$$\zeta=z/s \tag{17a}$$

$$\xi=r/s \tag{17b}$$

$$G=\frac{\bar{v}}{\xi\omega s} \tag{17c}$$

$$\Omega=\frac{s}{\omega r}\left(\frac{\partial\bar{u}}{\partial z}-\frac{\partial\bar{w}}{\partial r}\right) \tag{17d}$$

$$f=\frac{\psi}{\omega s r^2} \tag{17e}$$

$$\hat{u}=\bar{u}/\omega s \tag{17f}$$

$$\hat{w}=\bar{w}/\omega s \tag{17g}$$

where s is a reference length (chosen equal to the concentrator depth), and ω is a reference frequency (chosen to be $Q/r_o A$ where Q is the inlet flowrate and A is the area of the inlet channel).

The final equations are as follows:

$$\frac{\partial^2 f}{\partial\zeta^2}+\frac{\partial^2 f}{\partial\xi^2}+\frac{3}{\xi}\frac{\partial f}{\partial\xi}=\Omega \tag{18}$$

$$\frac{\partial^2\Omega}{\partial\xi^2}+\frac{\partial^2\Omega}{\partial\zeta^2}+\frac{3}{\xi}\frac{\partial\Omega}{\partial\xi}=\frac{1}{\bar{\epsilon}}\left[\left(\hat{u}-\frac{\partial\bar{\epsilon}}{\partial\xi}\right)\frac{\partial\Omega}{\partial\xi}+\left(\hat{w}-\frac{\partial\bar{\epsilon}}{\partial\zeta}\right)\frac{\partial\Omega}{\partial\zeta}-\frac{\Omega}{\xi}\frac{\partial\bar{\epsilon}}{\partial\xi}-\frac{\partial G^2}{\partial\zeta}-\frac{2}{\xi}\left(\frac{\partial\hat{u}}{\partial\xi}-\frac{\partial\hat{w}}{\partial\zeta}\right)\frac{\partial^2\epsilon}{\partial\zeta\partial\xi}-\frac{1}{\xi}\left(\frac{\partial\hat{w}}{\partial\xi}+\frac{\partial\hat{u}}{\partial\zeta}\right)\left(\frac{\partial^2\hat{\epsilon}}{\partial\zeta^2}-\frac{\partial^2\hat{\epsilon}}{\partial\xi^2}\right)-\frac{1}{\xi}\frac{\partial\hat{\epsilon}}{\partial\zeta}\left(\frac{\partial^2\hat{u}}{\partial\xi^2}+\frac{1}{\xi}\frac{\partial\hat{u}}{\partial\xi}-\frac{u}{\xi^2}+\frac{\partial^2\hat{u}}{\partial\zeta^2}\right)+\frac{1}{\xi}\frac{\partial\hat{\epsilon}}{\partial\xi}\left(\frac{\partial^2\hat{w}}{\partial\xi^2}+\frac{1}{\xi}\frac{\partial\hat{w}}{\partial\xi}+\frac{\partial^2\hat{w}}{\partial\zeta^2}\right)\right] \tag{19}$$

$$\frac{\partial^2 G}{\partial\xi^2}+\frac{\partial^2 G}{\partial\zeta^2}+\frac{3}{\xi}\frac{\partial G}{\partial\xi}=\frac{1}{\hat{\epsilon}}\left[\left(\hat{u}-\frac{\partial\hat{\epsilon}}{\partial\xi}\right)\frac{\partial G}{\partial\xi}+\left(\hat{w}-\frac{\partial\hat{\epsilon}}{\partial\zeta}\right)\frac{\partial G}{\partial\zeta}+2G\frac{\partial f}{\partial\zeta}\right] \tag{20}$$

$$\hat{u}=\xi\frac{\partial f}{\partial\zeta} \tag{21a}$$

$$\hat{w}=-\xi\frac{\partial f}{\partial\zeta}+2f \tag{21b}$$

$$\hat{\epsilon}=\epsilon+\frac{\nu}{\omega s^2} \tag{21c}$$

The eddy viscosity ϵ is computed from the mean motion with Equation (9). The quantity Φ in Equation (9), expanded in axisymmetric cylindrical coordinates becomes, in non-dimensional variables.

$$\Phi = 2\left(\frac{\partial \hat{u}}{\partial \xi}\right)^2 + 2\left(\frac{\partial \hat{w}}{\partial \zeta}\right)^2 \quad 2\left(\frac{\hat{u}}{\xi}\right)^2 + \left[\xi \frac{\partial G}{\partial \xi}\right]^2 + \left(\frac{\partial \hat{w}}{\partial \xi} + \frac{\partial \hat{u}}{\partial \xi}\right) + \left(\xi \frac{\partial G}{\partial \zeta}\right)^2 \quad (22)$$

The mixing length is assumed to be of the form

$$\hat{\ell} = \aleph \zeta (1-\zeta)(\xi_0 - \xi)(\xi - \xi_i) \quad (23)$$

so that $\hat{\ell}$ vanishes at all boundaries. The constant $\aleph$ is chosen to give the best match with test data.

Boundary Conditions

In keeping with the axisymmetric approximation to the flow the inlet region is treated as a porous wall rotating at the mean inlet velocity. Thus the flow is assumed to enter uniformly around the circumference at the mean tangential velocity of the entrance pipe as illustrated in Figure 1. In the overflow and foul sewer outlet shown in Figure 1, the vertical velocity of the flow leaving the concentrator is specified, and the tangential velocity is obtained by extrapolation from the interior region, assuming no tangential shear stress to act in these regions. On the solid boundaries, the two velocity components parallel to the surface are obtained by setting the local shear stress at the wall equal to an average skin friction coefficient times the local dynamic pressure. The skin friction coefficient is selected to give good agreement with test data.

Translated into equations for the non-dimensional stream function (f), vorticity (Ω), and tangential velocity (G), on the boundaries, these conditions are expressed as follows:

a) Inlet

$\hat{u}_o(\zeta)$ and $\hat{v}_o(\xi)$ are specified. Then from Equation (21a)

$$f(\xi_o, \zeta) = \int_a^{\zeta} \frac{\hat{u}_o(\zeta)}{\xi_o} d\zeta + c \quad (24)$$

and from Equation (17c)

$$G(\xi_o \zeta) = \frac{\hat{v}_o(\zeta)}{\xi_o} \quad (25)$$

To obtain a boundary condition for Ω, the stream function is expanded into a third order Taylor Series, and the required derivatives are evaluated from the specified velocity, and from Equation (18) which defines Ω. This procedure is substantially as outlined in Reference 2, modified to allow for the inflow of fluid. The resulting equation for Ω on the boundary at the inlet region is

$$\Omega_b = \left[f_{b+1} - \left(1 + \frac{2\Delta\xi}{\xi} + \frac{3\Delta\xi^2}{\xi^2} + \frac{4\Delta\xi^3}{\xi^3}\right) f_b + \frac{\hat{u}(\zeta)}{\xi} \frac{\Delta\xi^2}{2}\left(1 + \frac{5}{3}\frac{\Delta\xi}{\xi}\right) - \frac{\Delta\xi^2}{6}\Omega_{b+1}\right] \frac{3}{\Delta\xi^2\left(1+\frac{3}{2}\frac{\Delta\xi}{\xi}\right)} \quad (26)$$

where the subscript "b" refers to the value on the boundary, while "b + 1" refers to the point immediately interior.

b) Overflow and Foul Sewer Outlet Flow

In the overflow region, $\hat{w}_o(\xi)$ is specified. Then from Equation (21b), we obtain

$$f(o,\xi) = \frac{1}{\xi^2}\left[f(\xi_o)\xi_o^2 - \int_{\xi_o}^{\xi} \hat{w}_o(\xi)\,\xi\, d\xi \right] \quad (27)$$

which defines f in the overflow region, and a similar equation applies to the foul sewer outlet.

The boundary value of G is obtained by noting that for zero tangential shear stress, $\frac{\partial G}{\partial \zeta} = 0$ so that

$$G_b = G_{b+1}. \quad (28)$$

As in the inlet region, the boundary

condition for Ω is found by the procedure given in Reference 2. The result is

$$\Omega_b = \frac{3}{\Delta\zeta^2}(f_{b+1} - f_b) - \frac{1}{2}\Omega_{b+1} - \frac{3}{2}\hat{w}_o'(\xi) \quad (29)$$

with a similar equation for the foul sewer outlet.

c) **Solid Boundaries**

On solid boundaries, the expression for the wall shear stress in terms of the skin friction coefficient, C_f', and dynamic pressure is

$$\tau_\theta = C_f'\left(\frac{1}{2}\rho v^2\right) \quad (30)$$

For a Newtonian fluid, the shear stress can also be expressed in terms of the velocity gradient. For example, on the bottom

$$\tau_\theta = -\mu\frac{\partial v}{\partial z} \cong \mu\frac{v_b - v_{b+1}}{\Delta z} \quad (31)$$

Combining Equations (30) and (31), and rewriting the result in terms of the non-dimensional tangential velocity function, G, the resulting boundary condition is

$$G_b = \frac{-\nu}{\omega s^2 \xi C_f' \Delta\xi} + \sqrt{\left(\frac{\nu}{\omega s^2 \xi C_f' \Delta\xi}\right)^2 + \frac{2\nu}{\omega s^2 \xi C_f' \Delta\xi} G_{b+1}} \quad (32)$$

Similar expressions can be found for G on the top and sides.

The boundary condition for Ω is of a simpler form than used in Reference 6. For example, on the bottom, the radial component of shear is

$$\tau_r = -\mu\frac{\partial u}{\partial z} \quad (33)$$

From the definition of Ω (Equation 17a), on the bottom where $\frac{\partial w}{\partial r} = 0$, we have

$$\Omega(\zeta_o, \xi) = \frac{s}{\omega r}\frac{\partial u}{\partial z} \quad (34)$$

For small values of u/v, the radial shear can also be written in terms of the tangential shear

$$\tau_r \cong \frac{u}{v}\tau_\theta = \frac{u}{v}C_f'\left(\frac{1}{2}\rho v^2\right) \quad (35)$$

Combining (33) to (35) and using Equation (21a) gives for the vorticity on the bottom

$$\Omega_b = \frac{C_f'}{2}\frac{G_b}{(\nu/\omega s^2)\xi}\left[\frac{f_b - f_{b+1}}{\Delta\zeta}\right] \quad (36)$$

Numerical Method

Equations (18), (19) and (20), together with the auxiliary equations (21)-(23) and boundary conditions defined above, are solved numerically on a uniform grid, subdividing the cross section of the swirl concentrator as shown in Figure 1. Each of the principal equations is of the general form

$$\frac{\partial^2\phi}{\partial\zeta^2} + \frac{\partial^2\phi}{\partial\xi^2} + A\frac{\partial\phi}{\partial\xi} + B\frac{\partial\phi}{\partial\zeta} + C\phi + D = 0 \quad (37)$$

where θ represents f,Ω or G in Equation (18), (19) and (20) respectively. By writing centered finite difference approximations for the derivatives, i.e.,

$$\frac{\partial\phi}{\partial\zeta} \cong \frac{(\phi_{i+1,k} - \phi_{i-1,k})}{2\Delta\zeta} \quad (38)$$

and

$$\frac{\partial^2\phi}{\partial\zeta^2} \cong \frac{(\phi_{i+1,k} - 2\phi_{i,k} + \phi_{i-1,k})}{\Delta\zeta^2} \quad (39)$$

Equation (37) can be solved for $\phi_{i,k}$ in terms of the surrounding four points. The numerical procedure consists of sweeping through the mesh repeatedly, replacing each value of $\phi_{i,k}$ with an updated value found from Equation (37). In performing this calculation for Ω the new-found value is averaged with the previous value to provide additional stability. This relaxation process is repeated until successive changes in the function are less than some preassigned value.

In performing the numerical calculation, it was found that numerical instability occurred whenever the kinematic viscosity appearing in Equation (21) was made too small. With a mesh spacing of 1/2 inch (model

scale), these difficulties occurred at about $\nu = 4 \times 10^{-4}$ ft^2/sec, whereas the viscosity of water is 1×10^{-5} ft^2/sec. This is a common difficulty in viscous flow calculation, and occurs when the Reynolds number based on mesh spacing and kinematic viscosity

$$\left(\frac{V\triangle r}{\hat{\epsilon}}\right)$$

becomes too large. The problems can be solved by using a smaller mesh spacing (thereby lowering the Reynolds number). However this is a costly solution. To use the viscosity of water (1×10^{-5} ft^2/sec) would require that the mesh spacing be reduced by a factor of 40 in each direction, with a consequent large increase in the computer storage and computational time.

The numerical difficulties arise near the walls where the turbulent eddy viscosity ϵ vanishes (note that the mixing length, Eq. 23, is zero at all boundaries), leaving only the kinematic viscosity contribution to $\hat{\epsilon}$ (see Eq. 21c).

Away from the walls, the eddy viscosity is several orders of magnitude larger than the kinematic viscosity and the Reynolds number is correspondingly small. The mesh therefore needs to be refined only near the walls. However, this requires a non-uniform mesh and presents considerable complications in the program logic. For the present study, the kinematic viscosity was simply maintained large enough to avoid instability, and the resulting inaccuracy near the wall was considered acceptable. All of the results were obtained with $\nu = 4 \times 10^{-4}$ ft^2/sec or 8×10^{-4} ft^2/sec. These results therefore exhibit a higher viscous laminar-like flow behavior in the immediate vicinity of the wall. However, two or more mesh points away from the wall where the eddy viscosity is dominant, the results are unaffected by these boundary effects.

Liquid Flow Summary

The equations developed in the preceeding section makes it possible to numerically compute the turbulent axisymmetric flow within the swirl concentrator. The turbulence in the flow gives rise to local fluctuations in the velocities which cause apparent stresses (Reynolds stresses) similar to those induced by viscosity. In the present study an eddy viscosity model is used to relate these Reynolds stresses to gradients of the mean flow properties through the use of a mixing length concept.

For the numerical calculation, a stream function is introduced to satisfy the continuity equation, and the vertical and radial momentum equation are combined to give a single equation for the vorticity, Ω. By assuming axial symmetry, the dependance of the flow on angular position is eliminated and the number of independant variables is reduced to two: the non-dimensional radial coordinate ξ, and the non-dimensional radial coordinate ζ. The final result is three partial differential equations for the stream function, f, the vorticity, Ω, and the tangential velocity function, G(Eq. 18, 19, and 20, respectively). These three principal equations are supplemented by auxiliary relations for computing the non-dimensional velocities $\hat{u}$ and $\hat{w}$ (Eq. 21a, 21b) and eddy viscosity (Eq. 21c, 9, 22, and 23). These equations and appropriate boundary conditions are solved with a numerical relaxation procedure.

The ability of the mathematical model to describe the actual flow phenomena is limited by the approximate eddy viscosity model, and by non-axisymmetric flow effects in the physical model. At low flowrates, the mathematical model should give reasonably good agreement with the physical model, within the limits of the eddy viscosity approximation. The mathematical model results are independent of the angular position, and thus represent the average behavior of the flow of any cross-section. At these low flowrates, the chief non-axisymmetric effect of the laboratory model deflector is to increase the velocity of the liquid under the weir. The velocity increase is simulated in the model by adjusting the mixing length and skin friction coefficients to give results in agreement with laboratory data. The local vortex induced by the deflector cannot be duplicated in the

axisymmetric approximation. However, the local vortex affects primarily the self-scouring ability of the concentrator, and is not critical to the overall separation efficiency.

At high flowrates (250 cfs), large asymmetries appear in the physical flow due to the jet-like behavior of the inlet flow Turbulence and waves are visible on the surface. The axisymmetric model cannot duplicate these phenomena, and so the usefulness of the numerical results is restricted to flows lower than 250 cfs for the tested configuration.

Particle Flow Calculations

The particle flow within the swirl concentrator is calculated assuming sufficiently low concentrations so that particle collisions and coalescence can be neglected. The effect of the particles on the structure of the liquid flowfield is also neglected. These assumptions are both valid for particle concentrations less than 1,000 mg/l as demonstrated by data on settling rate versus concentration given by Camp.[7] Additional approximations are required to calculate the particle flow. The most significant approximation concerns the effect of turbulence. The turbulent fluctuating liquid velocity induces fluctuations in the particle velocities. In addition, and more importantly, it also causes a diffusion of particles away from the paths they would follow for a laminar motion.[7,8] The modeling of this effect is crucial because in the absence of turbulence, the particles in many cases would sink directly to the bottom. The turbulence, however, scatters the particles into the vicinity of the weir where they are entrained with the overflow For this study, the effect of the turbulence was accounted for by adding the approximate diffusion terms to the equations of motion and continuity (see following section for details). The eddy diffusion coefficient was modeled in the same way as the eddy viscosity for the liquid flow [8]

In addition to turbulence, the following factors also contribute to uncertainties in the particle motion:

non-spherical shape
offset center of gravity and/or buoyancy
acceleration effects
Magnus effects
previous motion history

The non-spherical shape of both the actual sewage particles and the simulated sewage used in the laboratory tests introduces uncertainties into the particle's drag, although the differences due to the shape are small at the low settling rates involved.[7,9] The uncertainty in the drag was minimized by measuring the settling velocities of the test particles. The measured velocities are compared in Figure 2, Comparison of Predicted Particle Settling Rates with Measured Settling Rates, to the values calculated for spherical particles of various diameters and specific gravities. The differences are not large, but the data shows considerable scatter.

The effect of offset center of gravity or center of buoyancy is to induce oscillations in the particle orientation. For non-spherical particles, the changing orientation will cause variations in the particle trajectory due to lift forces perpendicular to the trajectory. Even for spherical particles only a very small center of gravity offset can cause wandering from the nominal trajectory due to asymmetric vortex shedding.[10,11] The ultimate effect of the center of gravity offset is to introduce additional uncertainties into the trajectory of a given particle. Statistically, this is equivalent to having a larger dispersion, and the effect can be included in the eddy diffusion coefficient. The Magnus effect can also be accounted for in this way. The Magnus effect is the lift perpendicular to the trajectory associated with a spinning particle.[9,12] The classic example is the baseball pitcher's curve ball. Since the sewage particles are moving through a highly rotational liquid flow, the fluid shear will cause some particles to spin, and thus increase their dispersion.

Studies have also shown that the drag of an accelerating sphere is not the same as the drag of the same sphere at constant velocity. The difference is believed due to asymmetric

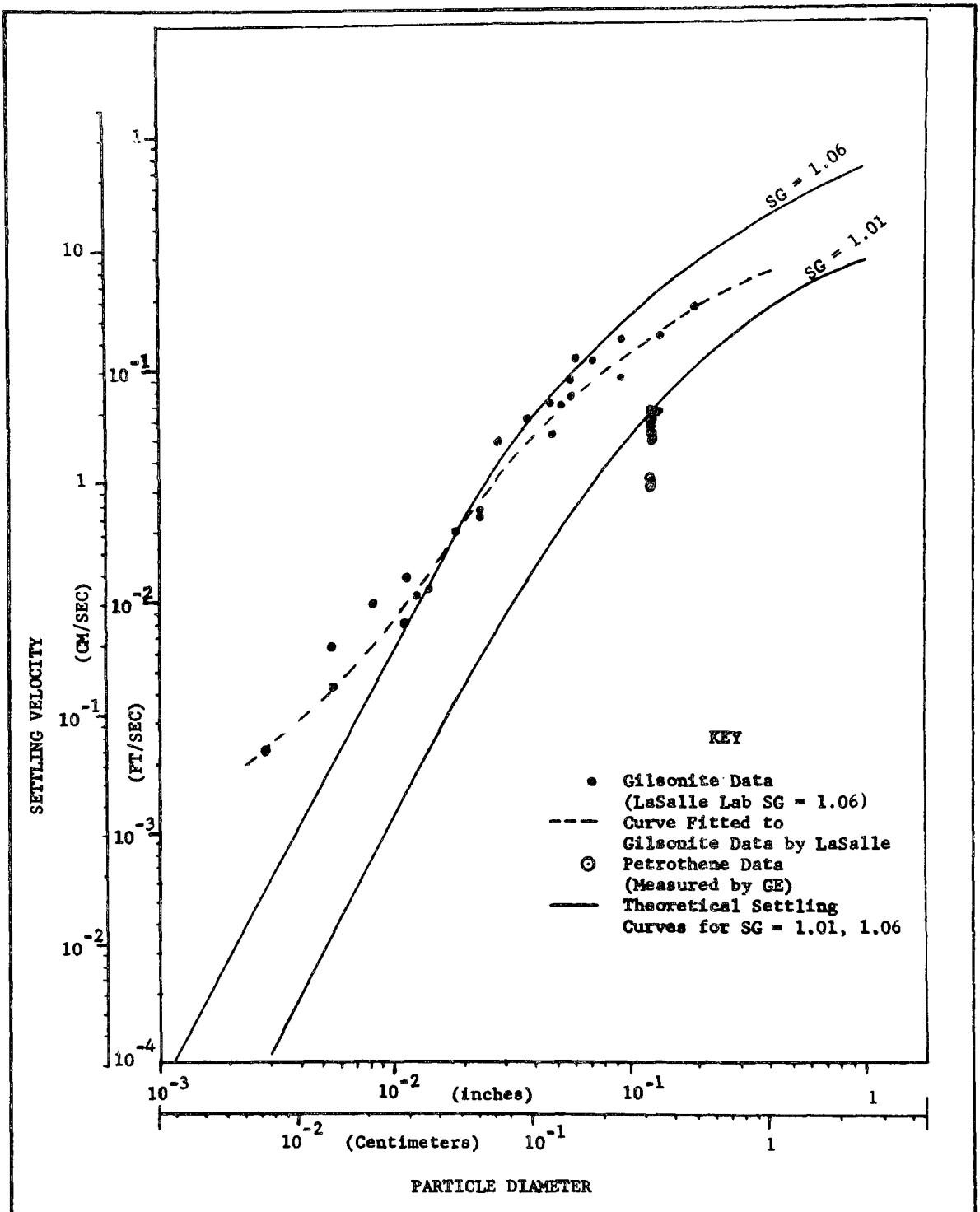

FIGURE 2
COMPARISON OF PREDICTED PARTICLE SETTLING RATES
WITH MEASURED SETTLING RATES

shedding of vortices behind the particle.[11] At very low Reynolds number (creeping motion), there is also an influence due to the previous history of motion.[8] This unsteady viscous effect appears to represent a drag due to momentum transfered back to the particle as a "shear wave" from fluid previously accelerated.[13] Both of these effects are relatively small, and their influence on drag has been neglected in the present study.

Another area of uncertainty in the particle flow calculation is the behavior of particles near solid boundaries. Heavy particles, for example, sink rapidly to the bottom. However, a detailed study of the interaction of the particle with the boundary layer is required to determine whether the particle actually hits the bottom or is deflected and carried away by the secondary flow. If the particle does hit the bottom, it may form a deposit, or it may subsequently be either re-entrained by the flow, or rolled along the bottom to a new location. In the physical model, all of these mechanisms are at work, but modeling them properly is a very difficult task, requiring a detailed description of the flow on the bottom. In fact, an accurate analysis of the scouring and re-entrainment phenomena would require a description of the non-axisymmetric local vortex induced by the deflector plate. This vortex cannot be modeled with the present axisymmetric liquid flow model.

Rather than attempt a detailed local boundary layer analysis, the present particle flow model assumes that particles hitting the bottom simply pass through it and out of the chamber (in computing the separation efficiency, all such particles are assumed to be entrained in the foul sewer flow). The particle concentration at the bottom is therefore the same as at the adjacent interior points, and no deposits build up. Since the deposition and re-entrainment of particles are not accounted for, the particle concentrations near the bottom will be underestimated. For very shallow chambers the particle concentrations near the overflow may also be lower than they should be, and the model will therefore tend to underestimate the number of particles entrained in the overflow (thereby overpredicting the efficiency). This effect is minimized with deeper chambers, and does not appear to be a problem with the nominal 9-ft. depth.

Particle Equations of Motion

The time-dependant equations of motion for spherical particles can be written in tensor notation as:

$$\text{Continuity:} \quad \frac{\partial N}{\partial t} + (N V^i)_{,i} = 0 \tag{40}$$

$$\text{Momentum:} \quad (S_g + \eta)\left(\frac{\partial V_i}{\partial t} + V^j V_{i,j}\right) = -\frac{1}{\rho}\frac{\partial p_2}{\partial x^i} + \eta\,(V^j U_{i,j}) + (S_g - 1)\, g\vec{e}_g \quad \frac{A_p C_D}{2 \nu_p} \left|\vec{V} - \vec{U}\right| (V_i - U_i) \tag{41}$$

In Equation (40), N is the local number density of particles with volume ν_p, moving at velocity $\vec{V}$ in liquid which is moving with the (different) velocity $\vec{U}$. In Equation (41), the left hand side represents the mass times acceleration of the particle. On the right hand side are the various forces acting on the particle. The first term is the integrated effect of pressure acting over the surface of the particle where p_2 is the pressure, as obtained from the liquid flow solution, but without the hydrostatic term. The latter has been included in the third term. The second term on the right is the "induced mass" effect, which arises from the acceleration of surrounding fluid in response to alterations in particle motion. The coefficient of virtual mass, η, depends on the particle shape, and is equal to 1/2 for a sphere. The third term on the right is the buoyancy force, and the last term is the viscous drag due to relative motion between the particle and liquid. The drag coefficient, C_D, is a function of the Reynolds number for flow over the particle, based on the difference between particle and liquid velocities. This dependence can be adequately represented for spheres by the empirical relation[14]

$$C_D = \frac{24}{R_e} + \frac{3}{\sqrt{R_e}} + 0.34 \tag{42}$$

Equations (40) and (41) are modified for turbulent flow with fluctuations v_i in particle velocity, u_i in liquid velocity, and n in number density by substituting

$$\begin{aligned} V_i &= \bar{V}_i + v_i \\ U_i &= \bar{U}_i + u_i \\ N &= \bar{N} + n \end{aligned} \tag{43}$$

and taking a time average. This is essentially the same procedure as followed in deriving the Reynolds equation for liquid flow as previously described. As before, the correlation between the fluctuating velocities $\overline{v_i v_j}$, and between the velocity and number density $\overline{nv_j}$ appear as additional terms in the equation for the mean motion. Neglecting the effect of turbulent fluctuations on the mean value of the drag, the result of this averaging process is

$$\frac{\partial \bar{N}}{\partial t} + (\bar{N}\,\bar{V}^i)_{,i} + (\overline{nv^i})_{,i} = 0 \tag{44}$$

$$(S_g + \eta)\left[\frac{\partial \bar{V}_j}{\partial t} + \bar{V}^i\,\bar{V}_{i,j} + (\overline{v^i v_i})_{,j}\right] =$$

$$-\frac{1}{\rho}\frac{\partial \bar{p}_2}{\partial x^i} + \eta\left[\bar{V}^i\,\bar{U}_{i,j} + (\overline{v^i u_i})_{,j}\right] + (S_g - 1) g\,\vec{e}_g - \frac{A_p C_D}{2\nu_p}\left|\vec{V} - \vec{U}\right|(\bar{V}_i - \bar{U}_i) \tag{45}$$

As in the case of the liquid turbulent fluctuation, the correlations between the fluctuating quantities are modeled with an eddy viscosity/mixing length approach. Thus, it has been assumed that

$$\overline{v_i v_j} = -\epsilon_p\,(\bar{V}_{i,j} + \bar{V}_{j,i}) \tag{46}$$

$$\overline{v_i u_j} = -\alpha\,\epsilon_p\,(\bar{V}_{i,j} + \bar{V}_{j,i}) \tag{47}$$

and

$$\overline{n v_i} = -\epsilon_p\,\frac{\partial \bar{N}}{\partial x^i} \tag{48}$$

The constant, α, represents the ratio of the rms fluctuation in the liquid velocity, to that of the particle, i.e.,

$$\alpha = \frac{|u|}{|v|} \tag{49}$$

For large, heavy particles, one would expect small fluctuations in particle velocity so $|v| < |u|$. However for small particles with specific gravities near that of water $|v| \approx |u|$ and thus for all the calculations in this report $\alpha = 1$ is used. Substituting these approximations into (44) and (45), and rearranging yields for the mean particle flow quantities

$$\frac{\partial \bar{N}}{\partial t} + (\bar{N}\,\bar{V}^i)_{,i} = (\epsilon_p \frac{\partial \bar{N}}{\partial x^i})_{,i} \tag{50}$$

$$(S_g + \eta)\left[\frac{\partial \bar{V}}{\partial t} i + \bar{V}^j\,\bar{V}_{i,j}\right] =$$

$$(S_g + \eta\,(1 \quad \alpha))\left[\epsilon_p\,(\bar{V}_{i,}^{\ j} + \bar{V}^j_{,i})\right], j - \frac{1}{\rho}\overset{+}{\frac{\partial p_2}{\partial x^i}} +$$

$$\eta\,\bar{V}^j\,\bar{U}_{i,j} + (S_g - 1)\,g\,\vec{e}_g - \frac{A_p C_D}{2\nu_p}\left|\vec{V} \quad \vec{U}\right|(\bar{V}_i - \bar{U}_i) \tag{51}$$

The pressure gradient is found from the solution of the liquid equations of motion. For the calculations of this study, it is assumed that the eddy viscosities for the particles were identical with those computed for the liquid. This assumption is believed valid for the present case, especially for particles close to water in specific gravity. This point is discussed further by Hinze in Reference 8. It is important to note that Equation (51) reduces to the liquid flow equation for the special case of a small particle with specific gravity of unity. In that case the gravity term vanishes, and both the drag and the virtual mass terms drop out if, as supposed $\vec{V} \to \vec{U}$. Then, since $\alpha = 1$, Equation (51) becomes formally identical with Equation (5) for steady flow, provided $\epsilon_p = \epsilon + \nu$.

Equations (50) and (51) can be expanded for axismmetric flow in cylindrical coordinates. The resulting form of the equations, dropping the overbars for mean quantities, is:

$$\frac{\partial N}{\partial t} + u\frac{\partial N}{\partial r} + w\frac{\partial N}{\partial z} =$$

$$-N\left(\frac{\partial u}{\partial r} + \frac{u}{r} + \frac{\partial w}{\partial z}\right) + \epsilon_p\left(\frac{\partial^2 N}{\partial r^2} + \frac{1}{r}\frac{\partial N}{\partial r} + \frac{\partial^2 N}{\partial z^2}\right) +$$

$$\frac{\partial \epsilon_p}{\partial r}\frac{\partial N}{\partial r} + \frac{\partial \epsilon_p}{\partial z}\frac{\partial N}{\partial z} \tag{52}$$

$$\frac{\partial u}{\partial t} + u\frac{\partial u}{\partial r} + w\frac{\partial u}{\partial z} = \frac{v^2}{r} + \frac{1}{S_g+\eta}$$

$$\left\{ -\frac{1}{\rho}\frac{\partial p_2}{\partial r} + \eta\left(u\frac{\partial u_L}{\partial r} + \frac{\partial u_L}{\partial z} - \frac{vv_L}{r}\right) \frac{3C_D}{4d_p} \right.$$

$$\left| \triangle \vec{V} \right| (u - u_L) + (S_g + (1-\alpha)\eta)$$

$$\left[\epsilon_p \left(\frac{\partial^2 u}{\partial r^2} + \frac{1}{r}\frac{\partial u}{\partial r} - \frac{u}{r^2} + \frac{\partial^2 u}{\partial z^2} \right) + \right.$$

$$\left. \left. 2\frac{\partial u}{\partial r}\frac{\partial \epsilon_p}{\partial r} + \left(\frac{\partial w}{\partial r} + \frac{\partial u}{\partial z}\right)\frac{\partial \epsilon_p}{\partial z} \right] \right\} \tag{53}$$

$$\frac{\partial v}{\partial t} + u\frac{\partial v}{\partial r} + w\frac{\partial v}{\partial z} = \frac{-uv}{r} + \frac{1}{(S_g+\eta)}$$

$$\left\{ \eta\left(u\frac{\partial v_L}{\partial r} + w\frac{\partial v_L}{\partial z} + \frac{vu_L}{r}\right) - \frac{3C_D}{4d_p}\left|\triangle \vec{V}\right| \right.$$

$$(v - v_L) + (S_g + (1-\alpha)\eta)\left[\epsilon_p \left(\frac{\partial^2 v}{\partial r^2} + \right. \right.$$

$$\left. \frac{1}{r}\frac{\partial v}{\partial r} - \frac{v}{r^2} + \frac{\partial^2 v}{\partial z^2} \right) + \left(\frac{\partial v}{\partial r} - \frac{v}{r} \right)\frac{\partial \epsilon_p}{\partial r} +$$

$$\left. \left. \frac{\partial v}{\partial z}\frac{\partial \epsilon_p}{\partial z} \right] \right\} \tag{54}$$

$$\frac{\partial w}{\partial t} + u\frac{\partial w}{\partial r} + w\frac{\partial w}{\partial z} = \frac{1}{(S_g+\eta)}$$

$$\left\{ \frac{1}{\rho}\frac{\partial p_2}{\partial z} + (S_g - 1)g + \eta\left(u\frac{\partial w_L}{\partial r} + w\frac{\partial w_L}{\partial z}\right) - \right.$$

$$\frac{3C_D}{4d_p}\left|\triangle \vec{V}\right|(w - w_L) + (S_g + (1-\alpha)\eta)$$

$$\left[\epsilon_p \left(\frac{\partial^2 w}{\partial r^2} + \frac{1}{r}\frac{\partial w}{\partial r} + \frac{\partial^2 w}{\partial z^2} \right) + \left(\frac{\partial w}{\partial r} + \frac{\partial u}{\partial z} \right)\frac{\partial \epsilon_p}{\partial r} + \right.$$

$$\left. \left. 2\frac{\partial w}{\partial z}\frac{\partial \epsilon_p}{\partial z} \right] \right\} \tag{55}$$

Numerical Method for Particle Flow

Equations (52) to (55) all contain the same directional derivative on their left-hand side. This fact makes the method of characteristics a natural choice for integrating these equations. The method of characteristics consists of integrating each equation along this characteristic direction at each mesh point for each time step, and evaluating the right-hand side from the known (or initially assumed) solution at the previous time step. Thus, for example, assume that the solution (N,u,v,w) is known at each mesh point at time t_o, and it is desirable to find the solution at mesh point 1 at time $t_o + \Delta t$ [corresponding to point 6 of Figure 3]. As an initial guess, the quantities (N, u, v, w) at point 6 are assumed equal to the corresponding values at point 1. (This will be exactly true in the steady state). The "Characteristic" line $-(u\,\vec{e}_r + w\,\vec{e}_z)$ shown dotted in Figure 3, Illustration of the Method of Characteristics, is then extended back from time plane $(t_o + \Delta t)$] to time t_o, where it intersects at point 5. Since all the functions are known at time t_o, the right hand sides of (52) to (55) can be determined at point 5 by interpolation. Each equation can then be integrated forward in time using the finite difference approximation

$$\phi_6 = \phi_5 + \Delta t\,[\mathrm{RHS}]_5 \tag{56}$$

where ϕ represents any of the functions (N,u,v, or w), and $[\mathrm{RHS}]_5$ refers to the right side of the appropriate equation evaluated at point 5. The entire process described above is then repeated with the updated values for u and w averaged with those at point 5, to determine the characteristics direction.

Equation (52) through (55) can be integrated forward in time to provide a time-dependent history of particle number density, N, and velocity (u,v, and w) for particles with diameter, d_p, at each mesh point for which the liquid flow has been determined. These equations must be resolved for each particle size of interest. For steady liquid flow and constant boundary conditions a steady state is reached in which N, u,v, and w remain constant. This is the desired solution to the problem.

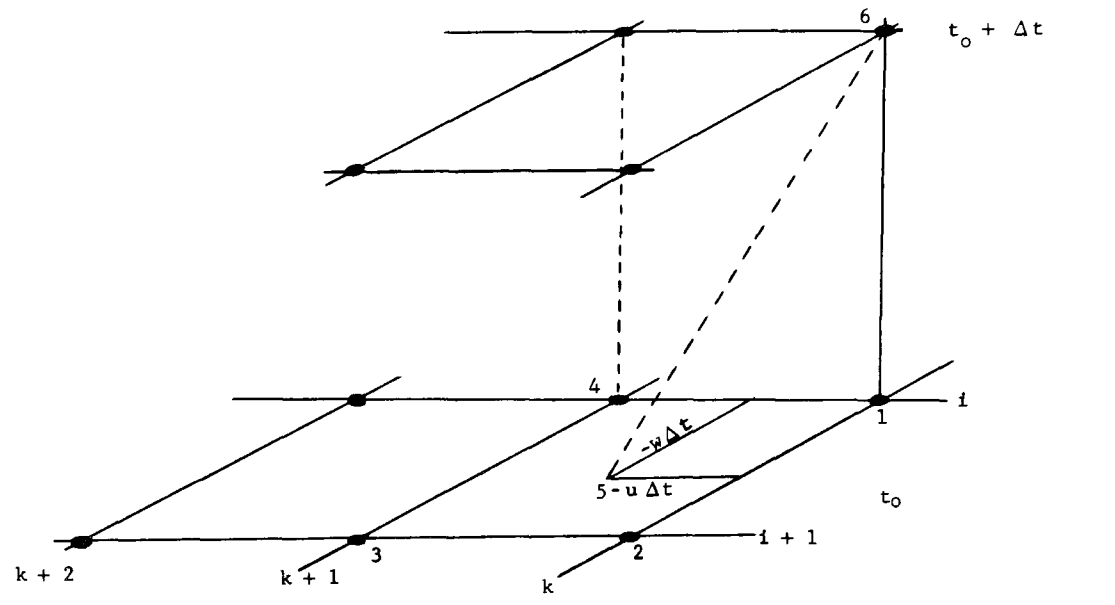

FIGURE 3
ILLUSTRATION OF THE METHOD OF CHARACTERISTICS

Boundary Conditions for Particle Flow

The procedure previously outlined serves to determine the values of N,*u*,*v*, and *w* at all interior mesh points. At the boundaries of the mesh, special conditions must be applied, and these boundary conditions are not so straightforward as those for the liquid flow The boundary conditions given below were found to be reasonably successful.

The number density of particles in the incoming flow can be specified arbitrarily as a function of the vertical coordinate, *z*. Since no interaction between particles is considered, the actual concentration is unimportant and only the relative concentration need be determined. Therefore the number density was set equal to unity over the entire inlet region. Stratification of the sediment near the bottom of the inlet channel could be readily simulated but was not attempted for this study. The velocities of particles at the inlet were assumed to be the same as those of the liquid.

The boundary conditions on the vertical sides (except in the inlet region) were set so that the derivative of the number density normal to the wall was always zero, as evaluated from a second order Taylor series expansion. Thus, the number density at the wall was taken as

$$N_b = \frac{4N_{b+1} - N_{b+2}}{3} \tag{57}$$

where N_b is the number density on the boundary, N_{b+1} is the next point inward, etc. The particle velocity normal to the wall was held at zero, and the velocity parallel to the wall was set to the local liquid velocity, plus the particle settling velocity.

At the underside of the weir plate, particle velocities are always downward for particles with a specific gravity greater than one. Any particles which exist at the underside of the weir, thus fall away towards the center of the chamber. Therefore, the number density is zero on the underside of the weir and also across the overflow at those points where the settling velocity exceeds the liquid outflow velocity. At such points, the particle velocities were set so that

$$u_p = u_L$$
$$v_p = v_L$$

and

$$w_p = w_L + V_S$$

At points along the overflow where the settling velocity was less than the local outflow velocity (so that particles were leaving the concentrator), the solution was found from the method of characteristics procedure. The method of characteristics was also used to determine the solution at all points on the bottom boundary, because the particles always flowed into the bottom, and not upward through it. All particles hitting the bottom were assumed to pass along it and out of the concentrator. This assumption is required in order to achieve a steady-state solution without having the number density grow indefinitely large due to deposition. In practice, this assumed boundary condition is closely matched due to the removal of particles on the bottom by the inward secondary flow.

The separation efficiency of the swirl concentrator for a given particle size can be readily determined from the numerical solution of Equations (52)-(55), by integrating the mass flux entering and leaving the concentrator. For this purpose, all particles hitting the bottom of the concentrator were assumed to be entrained in the underflow. The various particle fluxes, in units of number of particles per second are:

$$Q_{p_{in}} = -\int_{0}^{b} 2\pi r_o \, N_o \, (r_o, z) \, u_p \, (r_o, z) dz \tag{58}$$

$$Q_{p\ overflow} = \int_{r_o - \Delta r_o}^{r_o} 2\pi r \, N \, (r, o) \, w_p \, (r, o) \, dr \tag{59}$$

$$Q_{p\ bottom} = -\int_{ri}^{ro + \Delta ri} 2\pi r N \, (r, z_{max}) \, w_p \, (r, z_{max}) \, dr \tag{60}$$

The units of these particle fluxes, $Q_{p_{in}}$, Q_{p_o}, and Q_{pb}, are "number of particles per second," for an inlet concentration of one particle per cubic foot (because the number density has been normalized to unity at the entrance). For actual concentrations greater than one particle/cu ft, the particle fluxes are simply scaled up in direct proportion. The influx, $Q_{p_{in}}$, is positive for particle inflow. The other fluxes above are positive for an outward flux of particles.

In principle, the sum of the particle fluxes hitting the bottom and leaving through the overflow should equal the total influx, $Q_{p_{in}}$. However, due to numerical inaccuracies, this was not always the case. Consequently the chamber efficiency was always defined in terms of the actual sum of Q_{p_o} and Q_{p_b}. The fraction of particles removed is thus

$$E = \frac{Q_{p_o}}{Q_{p_o} + Q_{p_b}}$$

Particle Flow Summary

The equations developed for the particle flow provide a numerical solution for the particle concentration N and the three particle velocity components u, v, and w at each mesh point. From these velocities and concentrations, the flux of particles leaving the concentrator in both the overflow and in the foul sewer flow are calculated, in order to determine the separator efficiency. Since the concentrations and velocities are different for each particle size and specific gravity, the equations must be resolved for each particle class of interest.

The particle flow equations include the effects of turbulent diffusion, virtual mass, gravity, and drag. The turbulent diffusion is modeled in the same way as in the liquid flow calculation, assuming that the eddy diffusion coefficient is numerically equal to that of the liquid. The effect of turbulence is to scatter particles from regions of high concentration into regions of low concentration. The turbulence tends to decrease the concentrator performance because particles which might otherwise sink directly to the bottom are instead scattered to the top of the chamber and become entrained in the overflow.

As in the liquid flow case, the particle flow is assumed to be axisymmetric. The results are therefore accurate only at flowrates below 250 cfs where the axisymmetric approximation is reasonable. The particle flow equations also neglect interactions between particles, and therefore apply only to low concentrations (less than 1000 mg/l). At higher concentrations, agglomeration of particles and the interaction

between the particles and the liquid flow become important.

Scaling Laws

The governing equations for both the liquid and particle flow must be examined to deduce appropriate scaling laws. There are two aspects to the scaling problem. One is to determine what approximations are involved in representing the prototype concentrator chamber by a smaller scale laboratory device. The other aspect is to derive relationships for scaling the calculated results to the prototype system. By using these scaling laws, the results calculated for a few special cases can be extended to other flowrates, chamber sizes, particle diameters, and particle specific gravities. Scaling ,therefore,greatly reduces the amount of computation to be performed and extends the usefulness of both the mathematical and physical model results.

Scaling of the Liquid Flow

Equations (18)-(20) for the liquid flow are in non-dimensional form, such that all lengths are referred to the reference length "s," and velocities to the product of the reference frequency, ω, and length, s, etc. Therefore, the same equations apply to any combination of flowrate and concentrator size. A solution to these equations for any special case can therefore represent the solution for other flows and sizes, provided that:

(a) boundary conditions on f, Ω, and G must be the same

(b) the eddy viscosity, $\hat{\epsilon}$, must be the same.

Condition (a) is ensured by maintaining geometric similarity and a given overflow fraction. Condition (b), however, can only be satisfied approximately. From Equation (21c), (9), (22), and (23), the non-dimensional viscosity is:

$$\hat{\epsilon} = \hat{\ell}^2 \hat{\Phi}^{1/2} + \frac{\nu}{\omega s^2} \qquad (62$$

The first term on the right is the eddy viscosity arising from the Reynolds stresses while the second term represents the molecular viscosity. For the model chosen, the eddy viscosity is independent of scale size and flowrate since neither ω nor s appear explicitly in the first term. Thus, as the size of the chamber is increased, or the flowrate, the turbulence level increases so that the same non-dimensional eddy viscosity results. The second term on the right however, depends on both the flowrate and size. This term is the inverse of a Reynolds number based on reference length s, reference velocity (ω s), and liquid kinematic viscosity ν. Since this molecular viscosity term is very much smaller than the eddy viscosity term (provided the flow remains turbulent) it can be neglected for practical purposes, permitting scaling of the liquid flow calculation. It is noted, however, that as the concentrator size becomes very small (small s), or the flowrate becomes very small (low reference velocity, ωs), that this term can no longer be neglected, thus restricting the range of sizes and flows which can be represented by a single solution.

In practice, if the size of the chamber or flowrate is low enough to result in laminar flow, the turbulent flow solution will no longer apply. For the present case, interest is primarily focused toward scaling the results for the laboratory scale model to larger prototype sizes. Provided that the scale model has turbulent flow, upward scaling is feasible within the accuracy of the eddy viscosity model.

In summary, the non-dimensional equations show that two swirl concentrators of the same shape but of different sizes and flowrates will nevertheless have identical flowfields if a) all dimensions are divided by a reference dimension (the depth of the concentrator for example) and, b) if all velocities are divided by a reference velocity $V = \omega s$ (the inlet velocity for example).

It is important to observe that the gravitational term does not appear in the liquid flow equations. Gravity will not affect the calculated flow velocities, but it will influence the pressure. The actual pressure $p(r, z)$ can be written

$$p(r,z) = \rho g z + p_2 (r,z) \qquad (63)$$

where $p_2(r,z)$ is the pressure determined from solving the liquid flow equations. Thus, the hydrostatic term is not needed in calculating the internal liquid flow, but it can be added later if necessary. However, the action of gravity (through both the hydrostatic pressure and the weight) is crucial to the particle flow, and hence the separation efficiency of the concentrator, as will be discussed further. The effect of gravity is also important in determining the shape of the free surface at the overflow, although this effect has not been modeled in the present study. The importance of gravity dictates that the Froude number

$$\left(\frac{V}{\sqrt{gs}}\right)$$

be used as a scaling parameter between the model and prototype swirl concentrators. For a fixed size relationship $(s_{model}/\ s_{prototype})$, the flowrate in the model must then be adjusted so that

$$\frac{V_{model}}{V_{prototype}} = \sqrt{\frac{s_{model}}{s_{prototype}}} \qquad (64)$$

Maintaining the same Froude number in model and prototype ensures that the ratio of gravitational and inertial effects remains unchanged. Using the Froude number to determine the velocity ratio from Equation (64), the results calculated for the laboratory model can be applied to the prototype case equally well by scaling the results with

$$s = s_{prototype}$$

$$\omega = \omega_{model}\sqrt{\frac{s_{prototype}}{s_{model}}}$$

in equations 17 and 21.

The effect is to give larger dimensions and higher velocities, but the identical flow pattern. As an example, the present laboratory model represents the prototype swirl concentrator on a 1:12 scale. To represent the prototype concentrator operating at 100 cfs, the scale model velocities were reduced by:

$$V_m = V_p \sqrt{\frac{s_m}{s_p}}$$

Since flowrate is proportional to vs^2, the laboratory model was operated at a flowrate of

$$Q_m = Q_p \frac{(Vs^2)_m}{(Vs^2)_p}$$

$$= Q_p \left(\frac{s_m}{s_p}\right)^{5/2}$$

$$= \frac{100}{12^{5/2}} = 0.20037\ cfs$$

Equations (18)-(20) for the liquid flow condition were solved for the flowfield within the laboratory model, resulting in specific values for f, Ω, and G at each mesh point. To determine the actual flow velocities at any point, the non-dimensional variables were scaled according to Equation (17). Thus the tangential velocity at a general point (i,k) is

$$v_{i,k} = \omega s \xi_k\ G_{i,k} \qquad (65)$$

The reference length, s, is taken as the chamber depth, and the reference frequency is taken as (v_o/r_o) where v_o is the average tangential entrance velocity at the outer radius r_o.

$$s = 9 \text{ ft.}$$

and

$$\omega = \frac{v_o}{r_o} = \frac{Q}{Ar_o}$$

$$= \frac{100\ cfs}{(6\text{ ft} \times 6\text{ ft})(18\text{ ft})} = 0.154\ \text{sec.}^{-1}$$

Here A is the area of the 6-ft.-square entrance channel. If at point (i,k), $G_{i,k} = 0.500$ and $\xi_k = 0.800$, then the tangential velocity in the prototype at that location is, from (65),

$$(v_{i,k})_p = (0.154)(9)(0.8)(0.5)$$
$$= 0.556 \text{ ft/sec}$$

The same calculated solution can also be applied to the model by altering s and ω. For the model

$$s = 9/12 = 0.75 \text{ ft}$$

and

$$\omega = \frac{v_o}{r_o} = \frac{Q}{Ar_o}$$

$$= \frac{0.200\ cfs}{(0.5\text{ ft} \times 0.5\text{ ft})(1.5\text{ft})} = 0.535\ \text{sec.}^{-1}$$

The tangential velocity in the model at

point (i,k) is then

$$(v_{i,k})_{model} = (0.535\ \text{sec}^{-1})(0.75\ \text{ft})(0.8)(0.5)$$
$$= 0.1605\ \text{ft/sec.}$$

Note that from this numerical example

$$\frac{(v_{i,k})_{prototype}}{(v_{i,k})_{model}} = \frac{0.556}{0.165} = 3.47$$

so that these velocities are in proportion to $\sqrt{12}$ as demanded by the Froude number scaling (equation (64)).

Scaling of the Particle Flow

Equations (50) and (51) for the particle flow can be put in non-dimensional form by dividing all number densities by a reference value, N_o, all velocities by V_o and all lengths by s. If the pressure, p_2 is normalized by $e_w V_o s^2$, and time by s/V_o, the resulting equations with non-dimensional variables denoted with a caret are

$$\frac{\partial \hat{N}}{\partial \hat{t}} + (\hat{N}\ \hat{V}^i)_{,i} = \left(\hat{\epsilon}_p \frac{\partial \hat{N}}{\partial \hat{x}^i}\right)_{,i} \qquad (66)$$

$$(S_g + \eta)\left[\frac{\partial \hat{V}_i}{\partial \hat{t}} + \hat{V}^j\ \hat{V}_{i,j}\right] =$$

$$(S_g + \eta\,(1-\alpha))\left[\hat{\epsilon}_p\,(\hat{V}_{i,}{}^{j} + \hat{V}_{,i}{}^{j})\right]_{,j} - \frac{\partial \hat{p}_2}{\partial \hat{x}^i} +$$

$$\eta\,\hat{V}^j\,\hat{U}_{i,j} + (S_g - 1)\left(\frac{gs}{V_o^2}\right)\vec{e}_g - \left(\frac{A_p C_D s}{2\nu_p}\right)$$

$$\left|\hat{\vec{V}}\ \ \hat{\vec{U}}\right|(\hat{V}_i\ \ \hat{U}_i) \qquad (67)$$

The solution to Equations (66) and (67) in terms of the non-dimensional variables $\hat{V}$, $\hat{x}$ etc., will be identical for all cases for which the following dimensionless groups are the same:

$$\hat{\epsilon}_p\ ,\ \eta\ ,\ S_g\ ,\ (S_g - 1)\frac{gs}{V_o^2}\ ,\ \left(\frac{A_p C_D s}{\nu_p}\right) \qquad (68)$$

The particle eddy viscosity, $\hat{\epsilon}_p$, is assumed to be equal to the liquid eddy viscosity, which is independent of scale size and velocity, as has been discussed. Therefore, $\hat{\epsilon}_p$ will be the same for all flows within geometrically similar swirl concentrators.

The quantity η is the virtual mass coefficient, which is the same for all particles of the same shape. The coefficient η depends on orientation for non-spherical particles, but in this study an average value has been used to avoid the necessity to calculate the orientation. The effect of using an average value will be small, and within the accuracy of the other assumptions, η has a numerical value of 0.5 for a sphere and generally lies between zero and one.

The coefficient $(Sg\text{-}1)\ gs/V^2{}_o$ is the inverse of the square of the Froude number, modified by the factor (Sg-1). As noted in the previous section, the Froude number represents the ratio of inertial to gravitational forces, and must be maintained constant to properly model the liquid flow.

For a fixed particle shape, the remaining dimensionless group

$$\frac{A_p C_D s}{\nu_p}$$

is equivalent to the simpler form

$$\frac{s C_D}{d}$$

where d is a characteristic particle dimension. This group must be constant to insure that the drag forces are of the same magnitude (relative to the inertia, buoyancy, and gravitational forces) in the model and full size chambers. The drag coefficient, C_D, is a function of the particle shape and Reynolds number, as given in Equation (42).

Exact simulation of the prototype performance with a scale model is possible, provided that all of the dimensionless quantities mentioned

$$\left(S_g,\ \eta,\ (S_g - 1)\ \frac{gs}{V_o^2}\ ,\ \hat{\epsilon}_p,\ \text{and}\ \frac{sC_D}{d}\right)$$

are held constant. However, this is in general not possible if gravity and the liquid properties are not varied. There is no difficulty with $\hat{\epsilon}_p$, because this quantity is automatically properly scaled with the size and flowrate. But, if the specific gravity and Froude number are held constant, then the remaining ratio sC_D/d must also be constant. However, the drag coefficient is a

function of the Reynolds number which is proportional to the product of the scale velocity and particle size, Vd. If the particle size, d, is adjusted to give the proper Reynolds number at the scaled velocity, V, then the drag coefficient, C_D, will have the same value in model and prototype, but the grouping

$$\left(\frac{s\,C_D}{d}\right)$$

will not be correct. Similarly, if the ratio s/d is held constant, then the particle Reynolds number, and hence C_D will be wrong.

It is possible to arrive at an approximate scaling procedure by assuming that the particles always move at their equilibrium settling velocity with respect to the fluid. Then, it is always possible to vary the particle diameter, d, or specific gravity, Sg to obtain the proper scaled settling velocity. In fact, an infite varity of combinations of Sg and d will give the proper settling velocity. Scaling of the settling velocity is only valid, however, so long as the principal mode of separation is the settling of particles under the influence of gravity. This will be the case, provided the particle accelerations due to motion within the chamber are much smaller than the acceleration of gravity, so that the inertial terms in Equation (67) are negligible compared with the drag and buoyancy.

To determine the applicability of scaling the settling velocity in the present case, the magnitude of the inertial accelerations appearing in Equations (53) to (55) can be estimated. Because changes in velocities occur smoothly over the chamber cross section, terms such as

$$u\frac{du}{dr} \text{ can be approximated by } \frac{cu^2_{max}}{r_o}$$

where c is a constant of order one. Furthermore, in solving these equations for the swirl concentrator, it is found u_{max} and w_{max} are smaller than v_{max}, the inlet tangential velocity. Therefore the largest inertial acceleration term in (53)-(55) is the centrifugal acceleration $\frac{v^2}{r}$

For the prototype chamber operating at 100 cfs, this acceleration is approximately

$$\frac{v^2}{r} \cong \left[\frac{100\,cfs}{36ft^2}\right]^2 \left[\frac{1}{18\,ft}\right] = 0.43 \text{ ft/sec}^2$$

Since this acceleration is two orders of magnitude smaller than the gravitational acceleration, its effect on the particles should be negligible, and scaling the settling velocities is justified.

Summary of Scaling Laws

The liquid flow velocities (from either the mathematical model or physical model) for a swirl concentrator of size s_1, can be scaled to represent the flow in a geometrically similar concentrator of size s_2 using Froude number scaling. This requires that velocities and dimensions in the two concentrators be related so that

$$\frac{V_2}{V_1} = \sqrt{\frac{s_2}{s_1}}$$

As a corollary, since the flowrate is proportional to the velocity and to the reference length squared, the flowrates in these two concentrators are related by

$$\frac{Q_2}{Q_1} = \left(\frac{s_2}{s_1}\right)^{5/2}$$

For example, the flow in a swirl concentrator 36 ft. in diameter with an entrance velocity of 3 fps (corresponding to an inlet flowrate of 108 cfs in a 6-ft x 6-ft entrance channel) is equivalent to the flow in a swirl concentrator only three ft in diameter with an entrance velocity

$$V_2 = V_1\sqrt{\frac{s_2}{s_1}}$$

$$= (3)\sqrt{\frac{3}{36}}$$

$$= 0.866\,fps$$

The corresponding flowrate in the second concentrator is

$$Q_2 = Q_1\left(\frac{s_2}{s_1}\right)^{5/2}$$

$$Q_2 = \left(108\right)\left(\frac{3}{36}\right)^{5/2} = 0.217\,cfs$$

At this flowrate, the fluid motion and the balance between the gravitational and inertial forces will be identical in both concentrators. However, the foul sewer flow fraction must be the same in both cases.

The equations of motion also show that the flow velocities at any point in a given concentrator are proportional to the flowrate provided the fraction of flow in the foul sewer is maintained constant. For the example given above if the flowrate in the 36-ft concentrator is halved to 54 cfs, the entrance velocity will be half of its original value or 1.5 fps. While it is obvious that this rule applies to the entrance velocity, the equations show that the velocity at every point in the concentrator also scales in the same fasion. At very high flowrates, however, the equations are no longer applicable, due to the increasing importance of non-axisymmetric effects. Therefore the proportionality between local velocities and flowrate is only valid below about 250 cfs. This restriction does not limit the applicability of Froude number scaling. Since Froude scaling preserves the balance between gravitational and inertial forces, exactly the same non-axisymmetric effects will appear in both model and prototype concentrators.

The analysis of the particle flow equations discussed under the Scaling of the Particle Flow shows that it is not possible to reproduce in the laboratory the three-way balance between inertial, gravitational, and drag forces in the full size swirl concentrator. However, the inertial forces are shown to be much smaller than the gravitational and drag terms. By neglecting the inertial forces altogether, representation of the full scale particle flow in the laboratory is possible by preserving only the balance between gravity and drag forces. To achieve this balance it is only necessary to scale the particle settling velocities according to the Froude number, as for the liquid velocities. The separation efficiency of the concentrator will be the same for all combinations of particle size and specific gravity which give the same settling velocity.

Using the example above, suppose it is desired to represent in the scale model the behavior of 0.1 inch (0.254 mm) particles with specific gravity of 1.05 moving in the 36-ft chamber. These particles have a settling rate of 0.145 ft/sec (see Fig. 30). They can be represented in the 3-ft laboratory concentrator by particles with settling velocity V_{s2} scaled by the Froude number:

$$V_{s_2} = V_{s_1}\sqrt{\frac{s_2}{s_1}} =$$

$$(0.146)\sqrt{\frac{3}{36}} = 0.0420\ ft/sec$$

This scaled settling velocity can be achieved with 0.034-in. particles with specific gravity 1.05, or 0.080-in. particles with specific gravity of 1.01, or any other combination of diameter and specific gravity yielding the same settling velocity. The movement and separation efficiency of these scaled particles in the laboratory scale concentrator will duplicate closely the movement and separation efficiency of the full size particles in the full size concentrator.

In a similar fashion, once the separation efficiency for particles with a settling velocity of 0.0420 fps is measured in the laboratory, the same efficiency applies to all particles with a settling rate of 0.146 ft/sec in the 36-ft-diameter concentrator. The same measurement can also be applied to other concentrator sizes (say 20 ft.) by scaling the flowrate and settling velocity according to the Froude number.

RESULTS

Comparison of Mathematical Model With Test Data for Nominal Case

A detailed comparison has been made of the mathematical model results with data from LaSalle Hydraulics Laboratory. The comparison was made for the "nominal" concentrator configuration. This laboratory-scale concentrator is nine inches deep, 36 inches in diameter, and has a square 6-in. x 6-in. inlet channel at floor level. Due to schedule limitations, the results for the final laboratory model configuration which included the scum ring, could not be used in this comparison. However the performance of this final configuration is nearly identical to the performance of the nominal case. As will be described, the mathematical model was exercised using a range of mixing length and skin friction coefficients. These results were then compared with the measured velocity profiles. The final values for these two

constants were selected to give the best match between the mathematical and physical model velocity profiles for the nominal concentrator configuration at 100 cfs and 162 cfs. In this fashion, therefore, the mathematical model was "calibrated" against the laboratory scale concentrator. Additional calculations for both the liquid and particle flowfields were then carried out, retaining these values for the empirical constants.

Comparison of Predicted Liquid Flowfield with Laboratory Data

The velocity contours obtained from the LaSalle Hydraulics Laboratory model were used to calibrate the mathematical model liquid flowfield solution. These velocities were measured, in the laboratory at four tank cross sections, corresponding to angles of O°, 90°, 180°, and 270°, as measured from the inlet point. Measurements were made at two inlet flowrates corresponding to prototype overflow rates of 100 and 162 cfs. Thus, eight velocity profiles were available for calibration of the mathematical model liquid flowfield solution.

At this point it is important to note the geometric dissimilarities between the LaSalle Hydraulic model and the mathematical configuration. Due to the axisymmetric approximation, the mathematical model assumes that the inflow is introduced uniformly around the circumference of the chamber. Consequently, only minor local alterations in the liquid flowfield are imparted by the inflow In the axisymmetric mathematical model, therefore, the velocity contours are identical for any cross section.

The LaSalle Hydraulics Laboratory velocity profile data on the other hand, was obtained for a configuration which included a deflector plate at the inlet to direct the flow under the weir at the 360° location. The inflow was also given a downward direction to force the inflow beneath the overflow weir. These physical modifications resulted in a non-axisymmetric flow pattern as indicated by the differences in the velocity profiles between the 0°, 90°, 180°, and 270° cross sections shown in Figures 4-7, Tangential Velocities for 0°, 90°, 180°, and 270° Position.

For example, the location of the 0.8-fps velocity contour varies from one to three feet from the standpipe at the 90° (Fig. 5) cross section to seven feet from the standpipe at the 270° position. (Fig. 7) This variation in the velocity profiles between sections necessitates that an average profile be used to compare with the predicted axisymmetric mathematical model solution. Since the 180° section represents a situation somewhere between the other cross sections it was used for the data comparison. The 180° cross section also is located the fartherest away from the deflector plate, and as such should provide the closest approximation to the axisymmetric case.

The velocity profiles obtained for the 180° cross section were redrawn to the same scale utilizing the same velocity contours that were plotted by the mathematical model, Fig. 12, Comparison of Predicted Mathematical Model Velocity Profile With LaSalle Data. This yielded simplified velocity comparisons since the laboratory data could be superimposed directly upon the computer output plots.

As a result of the eddy viscosity and skin friction assumptions which have been discussed, the mathematical model contains two empirical constants which must be determined from the laboratory data. One of these is the skin friction coefficient which determines the velocity slip at the wall. The other constant is the mixing length which determines the scale of turbulence.

The effect of the skin friction constant in the velocity and streamline functions can be noted in Figures 8 and 9, Effect of Skin Friction Coefficient on Streamlines and Effect of Skin Friction Coefficient on Velocity Profiles. In Figure 8, the streamline patterns are plotted for the cases which are identical in every respect except for the value of the skin friction coefficient. For the lower skin friction coefficient the 50 percent and 60 percent streamlines are not as close to the bottom wall. This is a result of the relaxation of the velocity constraint along the wall imparted by the lower friction term.

This effect is even more pronounced in

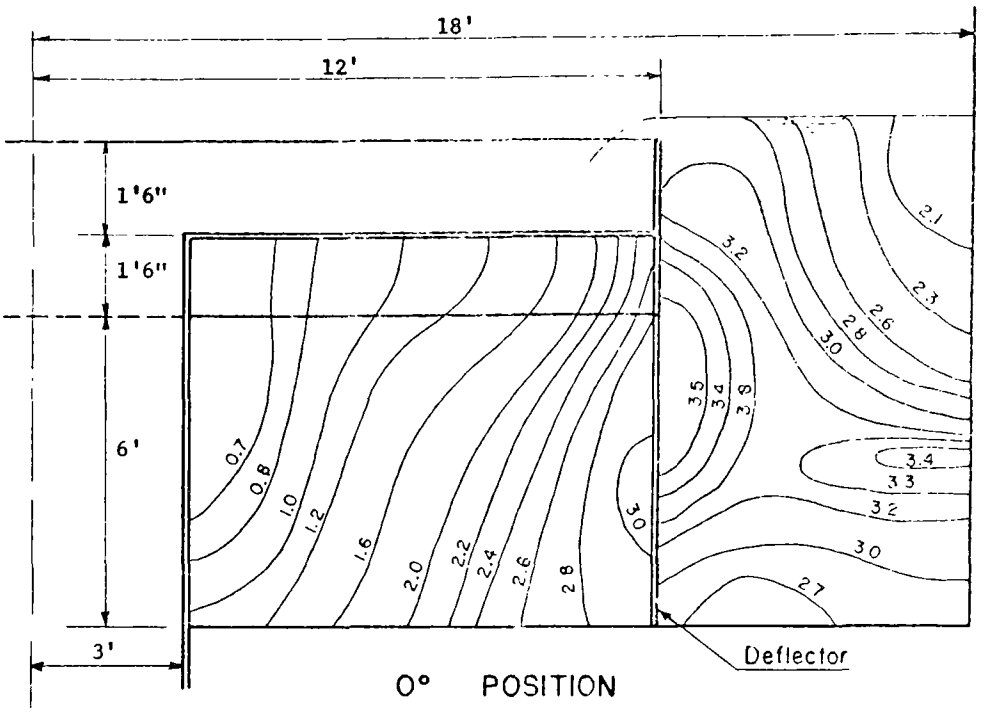

0° POSITION

FIGURE 4

TANGENTIAL VELOCITIES IN HYDRAULIC MODEL OF APWA SWIRL SEPARATION CHAMBER, 0° POSITION, FEET PER SECOND

Clear Overflow Discharge: 100 cfs (prototype)

Foul Bottom Outflow: 3 cfs (prototype)

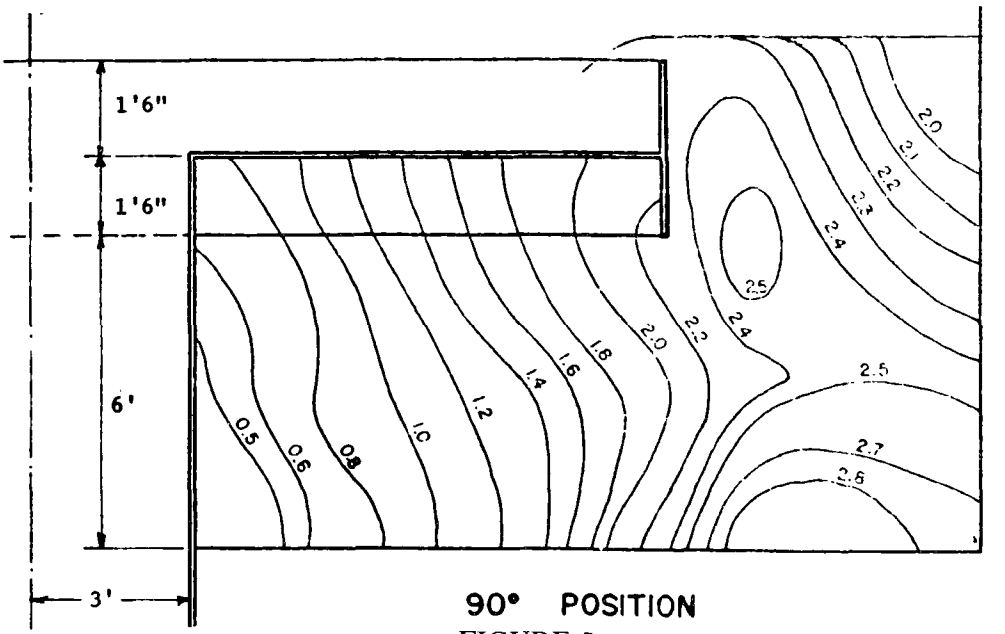

90° POSITION

FIGURE 5

TANGENTIAL VELOCITIES IN HYDRAULIC MODEL OF APWA SWIRL SEPARATION CHAMBER, 90° POSITION, FEET PER SECOND

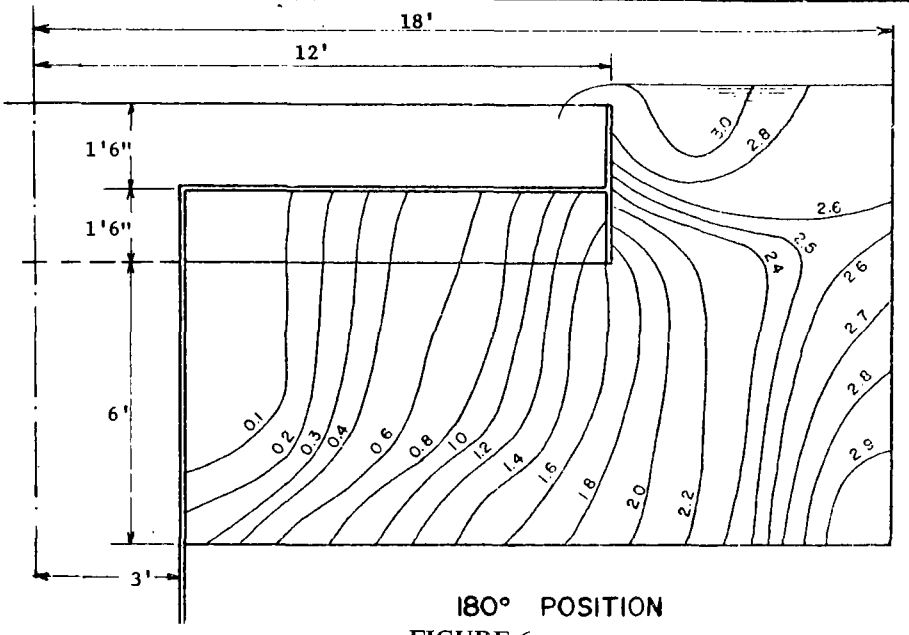

180° POSITION

FIGURE 6

TANGENTIAL VELOCITIES IN HYDRAULIC MODEL OF APWA SWIRL SEPARATION CHAMBER, 180° POSITION, FEET PER SECOND

Clear Overflow Discharge: 100 cfs (prototype)

Foul Bottom Outflow: 3 cfs (prototype)

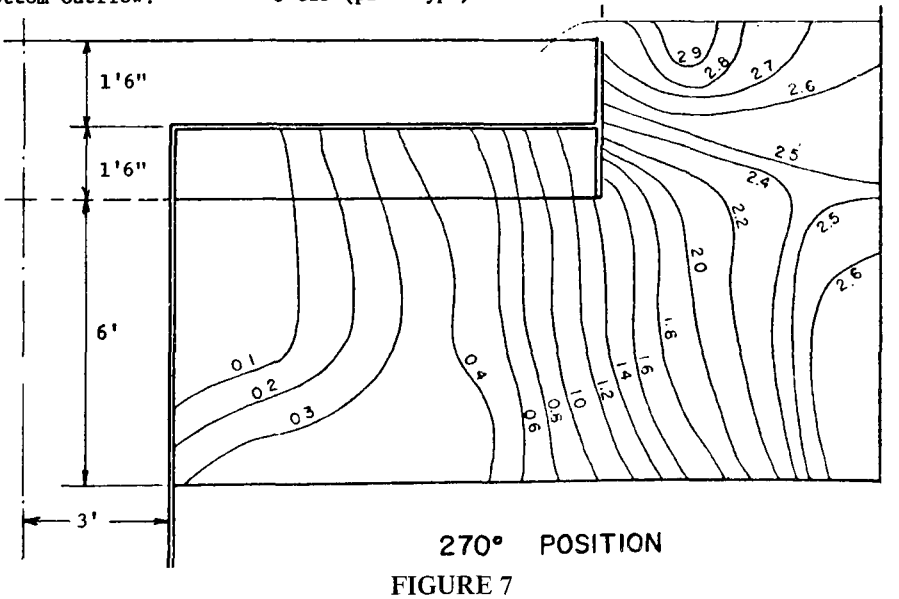

270° POSITION

FIGURE 7

TANGENTIAL VELOCITIES IN HYDRAULIC MODEL OF APWA SWIRL SEPARATION CHAMBER, 270° POSITION, FEET PER SECOND

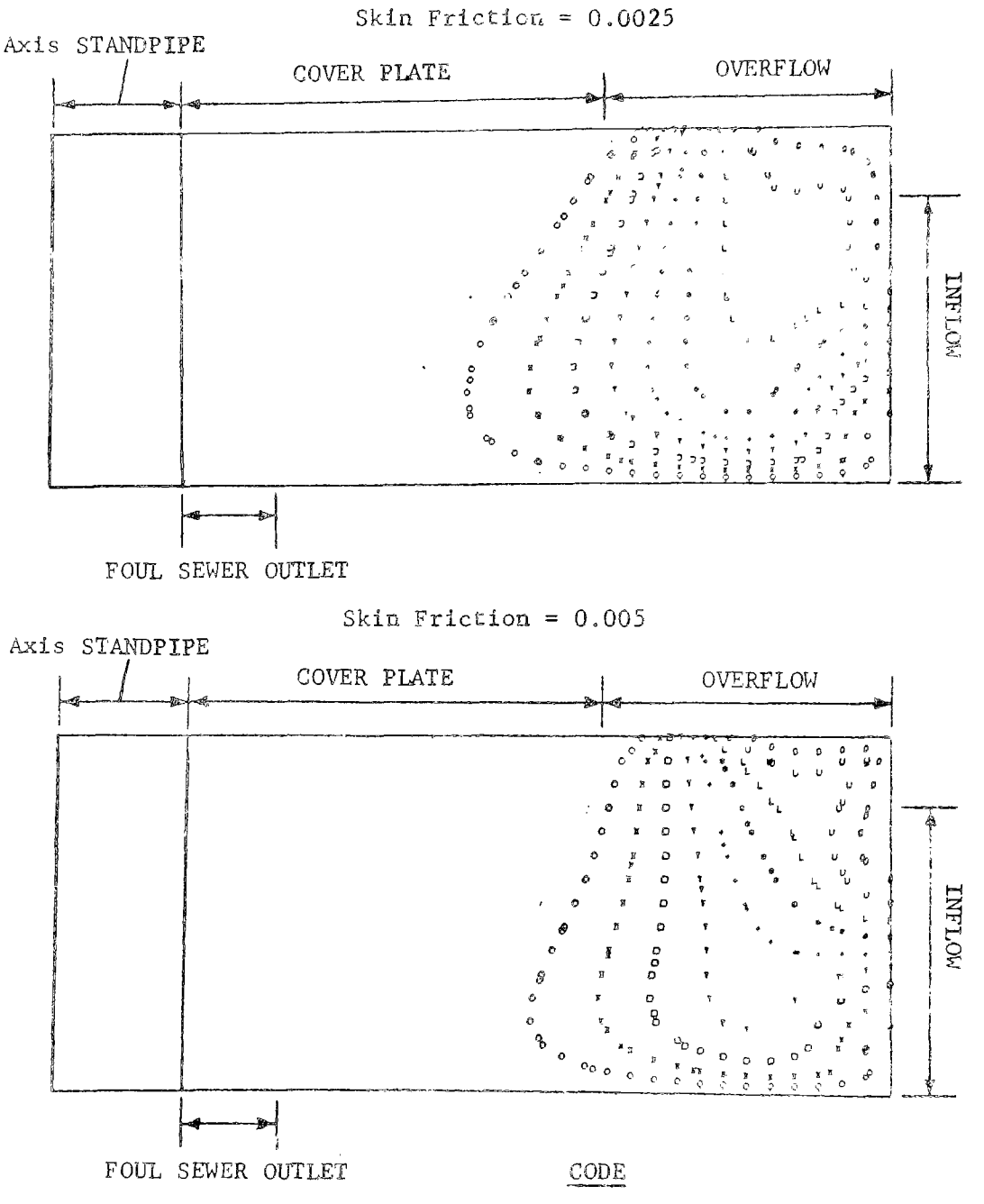

FIGURE 8
EFFECT OF SKIN FRICTION COEFFICIENT ON STREAMLINES

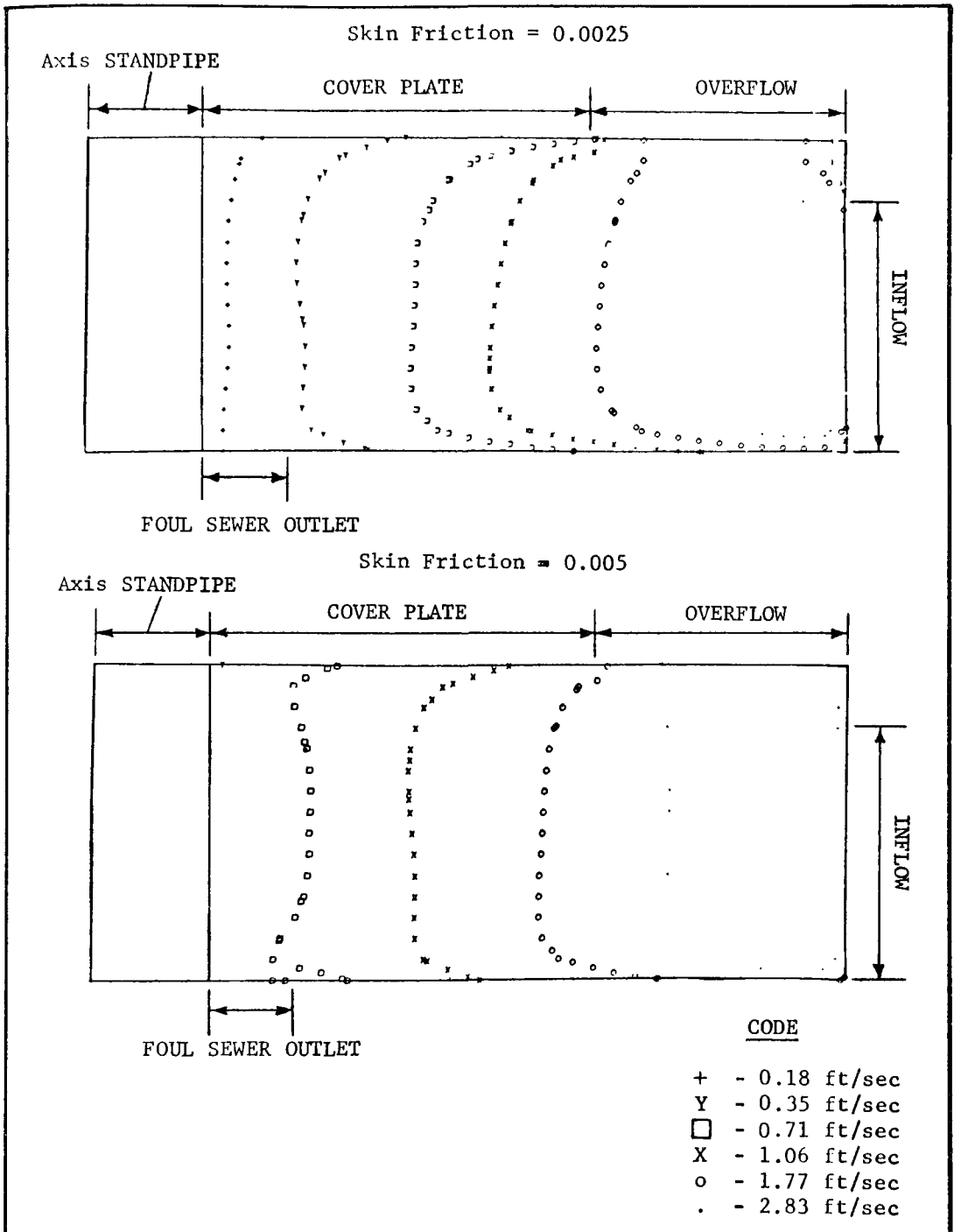

FIGURE 9
EFFECT OF SKIN FRICTION COEFFICIENT ON VELOCITY PROFILES

the velocity profiles in Figure 9. The 0.71-ft/sec velocity contour is shifted toward the center of the chamber as a result of the lowering of the skin friction coefficient. This is a result of increasing the velocities at the wall due to the velocity slip along the wall. The skin friction constant, therefore, tends to control the position of the velocity contours while maintaining the general shape of the streamline contours intact.

The effect of the mixing length constant, ℓ, is illustrated in Figure 10, Effect of Mixing Length Constant on Streamlines, and Figure 11, Effect of Mixing Length Constant on Velocity Profiles. Figures 10 and 11 represent flows with values of the mixing length constant differing by a factor of two with all other factors the same. Figure 10 illustrates how the general pattern of the streamlines is markedly affected by the mixing length. A higher mixing length constant increases the scale of turbulence, giving a more viscous solution. As a result of the greater shear stresses, the streamlines are shifted toward the outer chamber walls, and do not penetrate as far under the weir.

This effect can also be observed in the velocity contours in Figure 11. For the lower value of the mixing length constant the velocity contours more closely follow the direction that was imparted to them along the wall. For the higher mixing length case, the effect of the viscous shear along the wall is more rapidly damped out and the velocity contours take on a vertical orientation as they reflect the turbulence-dominated shear.

The mixing length, thus, tends to control the shape of the individual streamline and velocity contours.

The values of the mixing length constant and eddy viscosity coefficient were adjusted to provide the best fit of the mathematical model with the 100-cfs LaSalle data.

A mixing length constant of 1.0 and a skin friction constant of 0.0025 provided the best fit. The mathematical model was then operated for a flow of 162 cfs and the velocity profiles were compared to the LaSalle data at the higher flowrate, for the same 180° cross section. Figure 12 summarizes the results of these velocity comparisons for both 100 and 162 cfs.

The velocity profiles compare quite closely, especially under the degree of variation in the LaSalle data observed between the four sampling sections. The discrepancy between the predicted profiles and the observed profiles near the wall can be partially attributed to the higher viscosity near the wall in the mathematical model required to stabilize the computational procedure. In theory, the velocities must decline toward the walls as depicted by the mathematical model in order to satisfy the boundary conditions. However, the distance over which this occurs is smaller than indicated by the calculated results and would not be observed in the laboratory data. Furthermore, the laboratory data itself are not reliable at the walls as a result of limitations in the measuring equipment. Velocities were measured in the laboratory with a 1.5-in. diameter turbine meter which can only be placed at a minimum distance from the wall of about 0.75 in.

Another factor which could contribute to discrepancies in the velocity profiles near the upper wall is the presence of the skirt around the overflow weir. This structural detail could not be modeled with the relatively coarse computational grid of the present model.

Comparison with the laboratory velocity profiles near the outer wall was not attempted due to large variations in the contours at the various cross sections indicated by the LaSalle data. However, the average velocities observed in this region are of the same order of magnitude as predicted.

The crossflow streamline pattern for the selected baseline case (100 cfs) is shown in Figure 13, Streamline Pattern for Base Case. For the present choice of eddy viscosity model, the flow patterns are independent of flowrate. The flowfield at 162 cfs can be obtained by scaling up the velocity profiles for 100 cfs. The accuracy of this scaling procedure is demonstrated by the previous comparison with laboratory data (Fig. 12). The crossflow streamline pattern shown in Figure 13, therefore, applies to both flowrates.

It is interesting to compare the streamlines predicted by the mathematical

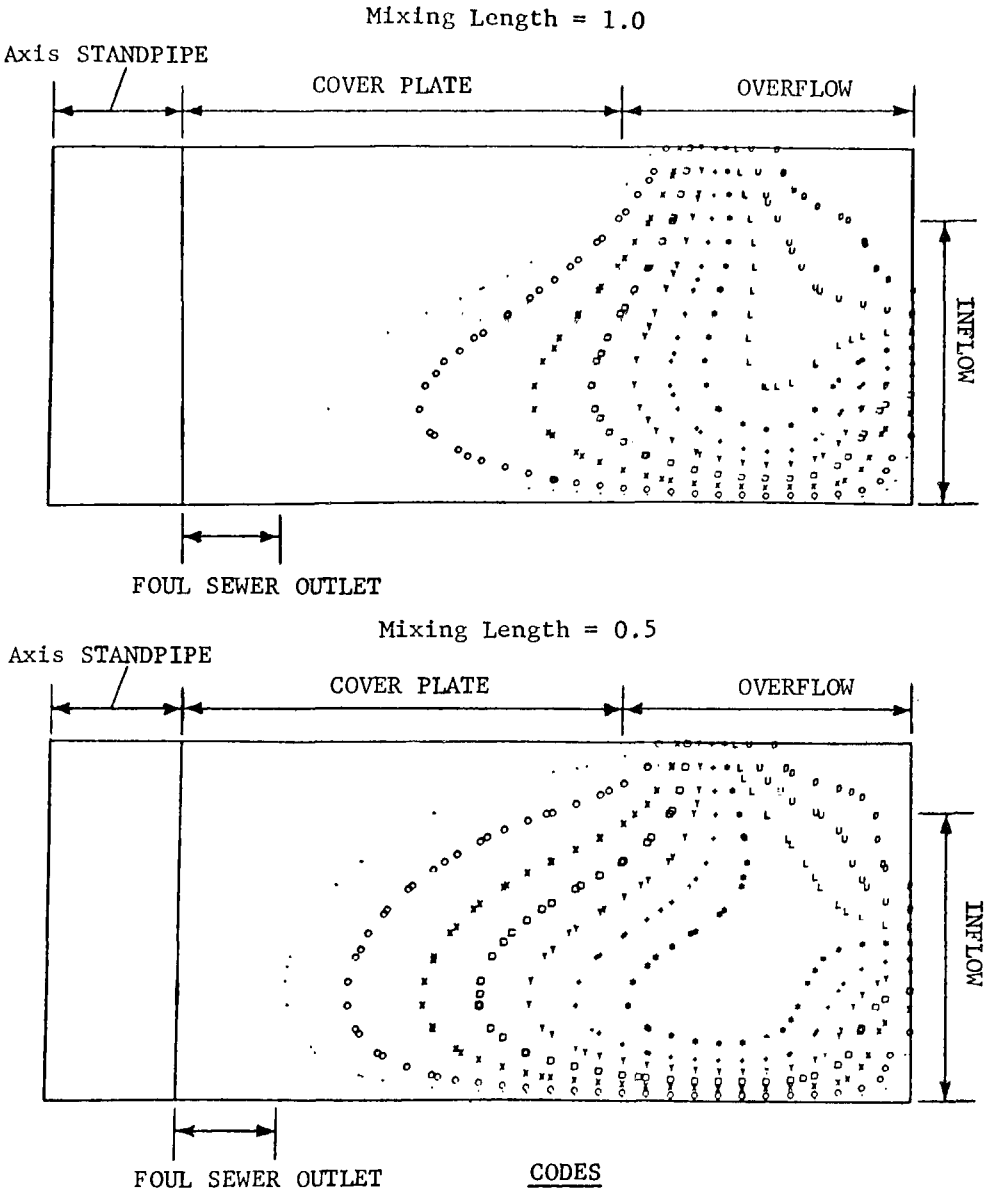

FIGURE 10
EFFECT OF MIXING LENGTH CONSTANT ON STREAMLINES

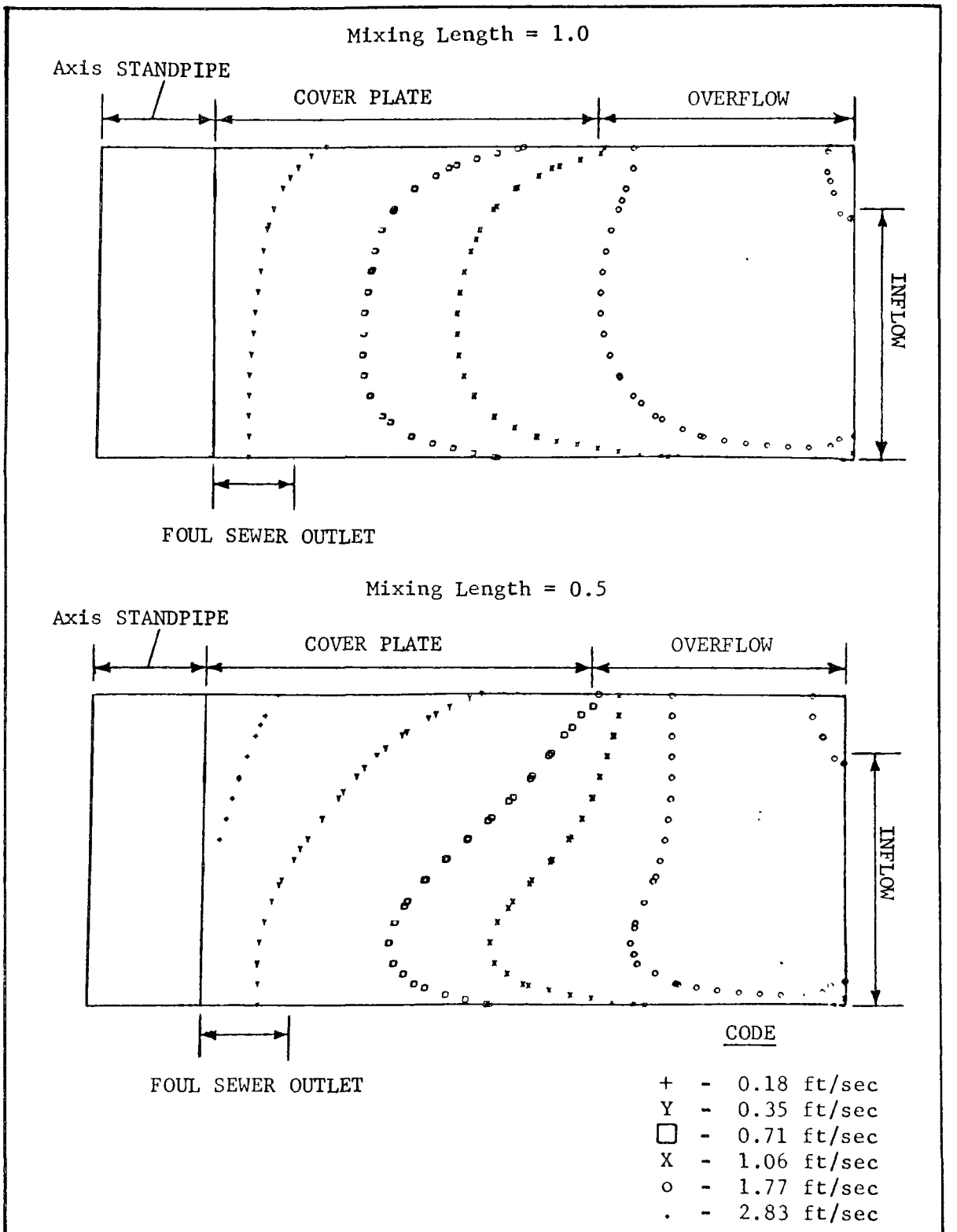

FIGURE 11
EFFECT OF MIXING LENGTH CONSTANT ON VELOCITY PROFILES

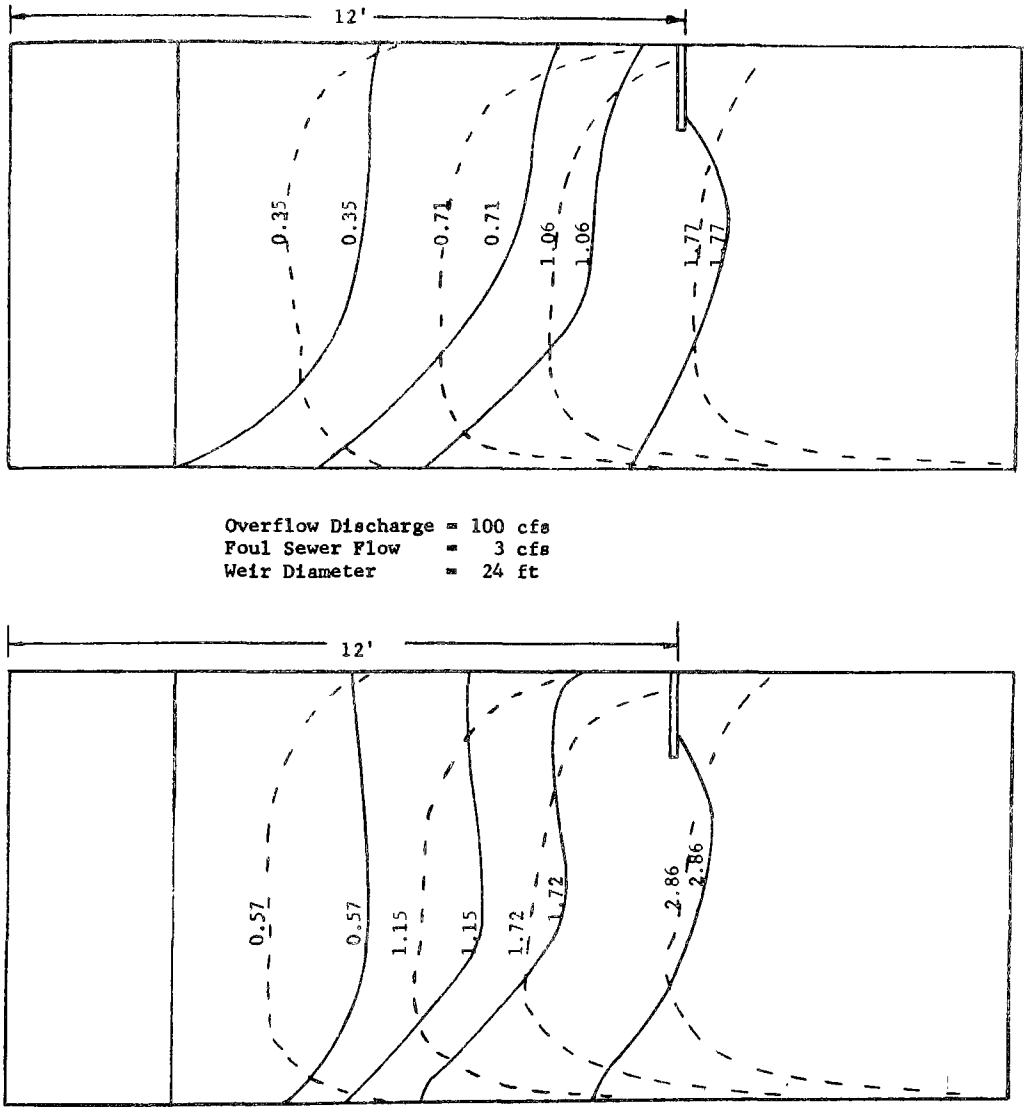

FIGURE 12
COMPARISON OF PREDICTED MATHEMATICAL MODEL VELOCITY PROFILE WITH LASALLE DATA

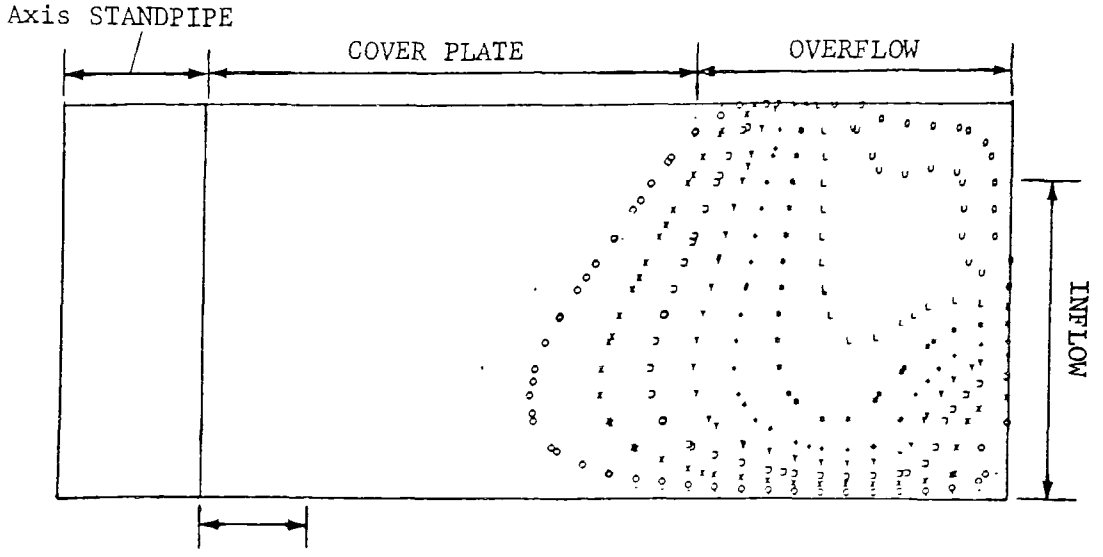

(THE PERCENTAGE OF FLOW PASSING TO THE LEFT OF EACH STREAMLINE IS INDICATED BY THE CODE BELOW)

CODE

.	-	5% of Inflow	+	-	50% of Inflow
o	-	10% of Inflow	*	-	60% of Inflow
X	-	20% of Inflow	L	-	70% of Inflow
□	-	30% of Inflow	U	-	80% of Inflow
Y	-	40% of Inflow	0	-	90% of Inflow

FIGURE 13
STREAMLINE PATTERNS FOR BASE CASE

model (Fig. 13) with photographs of the flow patterns observed by the laboratory. The LaSalle Laboratory performed two experiments in which a wire grid with threads attached was placed across the 90° cross section of the chamber. It was intended that the direction taken by the string would provide an approximation of the streamline pattern. Figures 14 and 15, Details of Special Structures and Photograph of Flow Direction Utilizing One-Inch Threads in Laboratory Model, illustrate the results of these experiments for both 1/2-in. and 1-in. long threads. LaSalle noted that the tests were complicated by violent fluctuations in the string position as a result of the high turbulence. The pictures are also distorted towards the outer chamber wall as a result of the chamber curvature.

Nevertheless, a few observations can be made. In Figure 15, toward the outer wall at points 1 and 2, toward the top of the chamber, the threads are directed upward. At point 3 in the same vertical line but toward the bottom of the chamber, the threads are directed downward. In Figure 13, the mathematical model indicates that toward the outer wall, the streamlines above the inlet will be directed upward while those below the inlet will be directed downward. Thus there is general agreement between the laboratory data and the mathematical model close to the outer wall. According to Figure 13, 70 to 80 percent of the flow never passes under the weir, thus to the left of the weir the flow is predominately in the

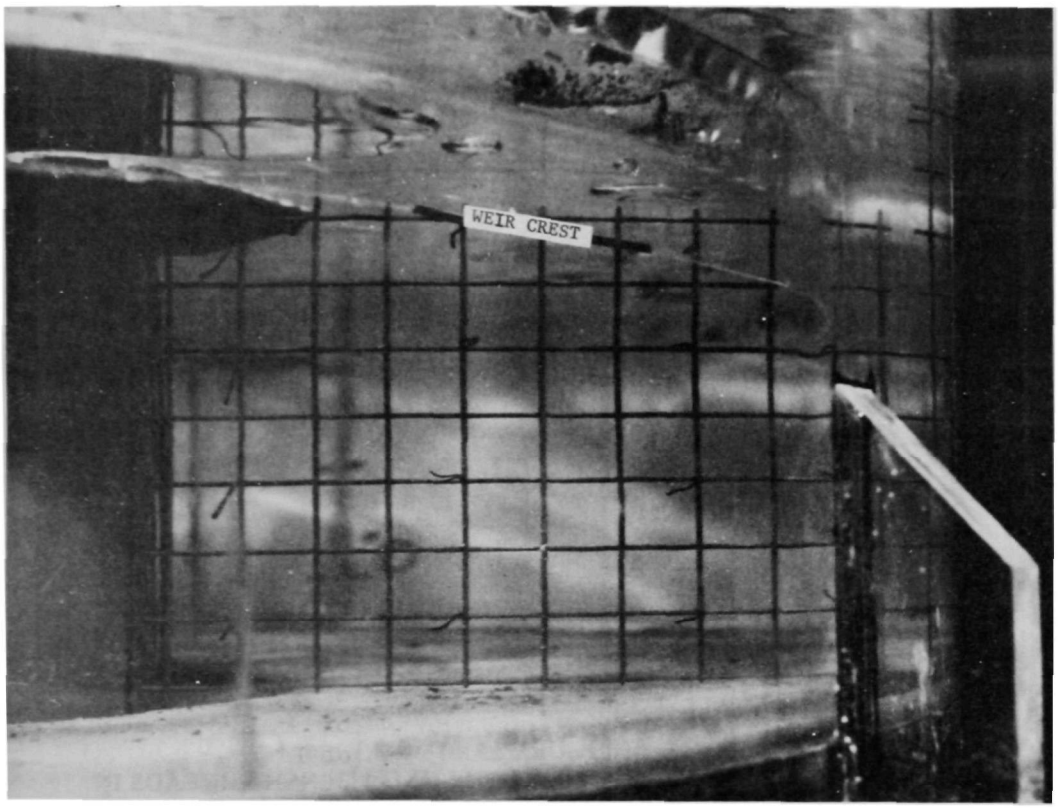

FIGURE 14
DETAILS OF SPECIAL STRUCTURES

tangential direction so that attempts to measure the streamlines would be complicated by the low radial velocities. At the weir (see Figs. 14 and 15) the threads are directed in an upward direction. This is also in agreement with the mathematical model. A more refined comparison of Figure 13 with Figures 14 and 15 is not warranted because of the high degree of uncertainty in the thread position as a result of the violent fluctuations in these positions observed by LaSalle.

Comparison of Mathematical Model Particle Flow With Test Data

Particle calculations were made for the five particle size and specific gravity combinations given in Table 1, Particle Sizes and Specific Gravity. Particle numbers one, three, four and five were chosen to represent gilsonite with specific gravity of 1.06, having equivalent spherical diameters of 2 mm 0.5 mm, 0.3 mm and 0.019 mm, respectively. Particle number two was selected to represent Petrothene® with specific gravity of 1.01, and diameter of 3.175 mm. These particle sizes give settling velocities which span the range of interest. Test data were available from LaSalle Hydraulics Laboratory for particle numbers one through four at 50 cfs, 100 cfs, and 162 cfs. The results for particle number five were used to establish trends at very low settling rates.

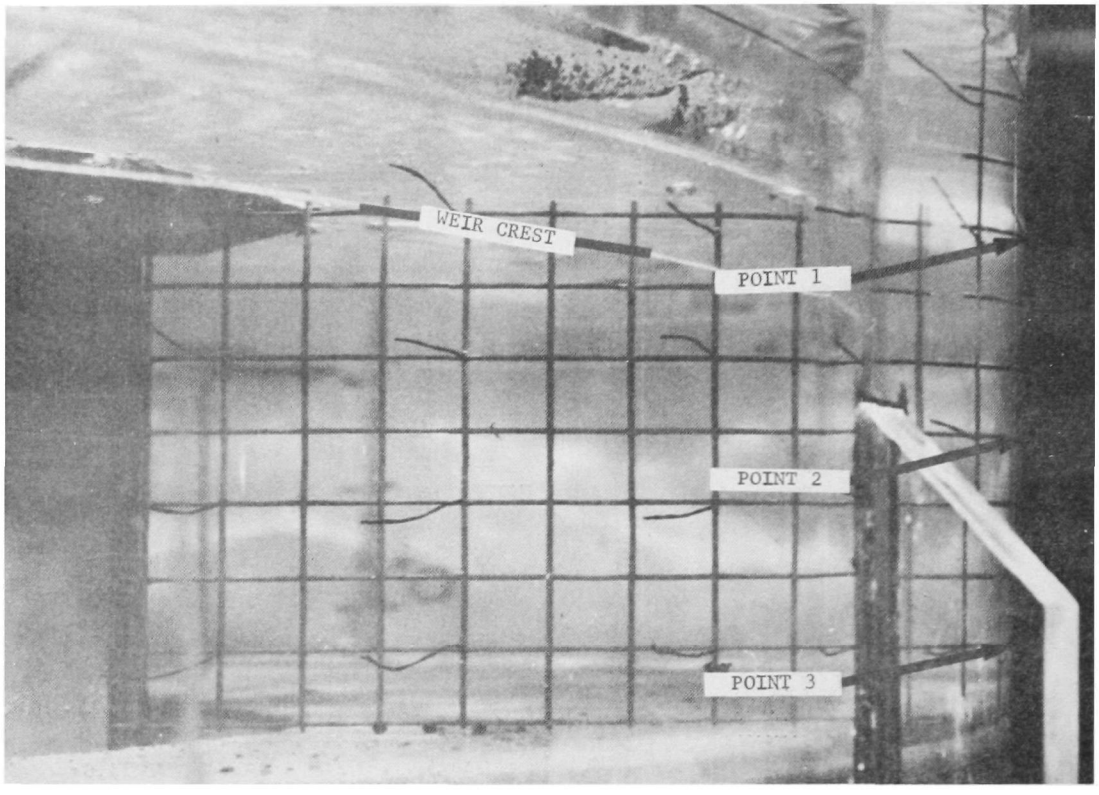

FIGURE 15
PHOTOGRAPH OF FLOW DIRECTION UTILIZING 1/2-INCH THREADS IN LABORATORY MODEL (provided by LaSalle Laboratory)

Particle flow calculations for all five particles were made for 100 cfs flowrate. The results are presented in Figure 16, Comparison of Particle Flow Mathematical Model Results with Test Data, as a graph depicting the percent of removal through the foul sewer outlet as a function of settling velocity. A smooth curve has been drawn through the five calculated points. The applicability of the scaling laws was tested next, by calculating a flowfield for particle number three at a flowrate of 162 cfs. This calculation was compared with a prediction made by scaling the 100-cfs results. Thus, particle number three, with settling velocity of 0.0717 fps (prototype scale), is separated with an

TABLE 1
Particle Sizes and Specific Gravity

	Particle Diameter	Sg	Settling Velocity (fps) Model Scale	Prototype Scale
1. Gilsonite	0.0787 in. (2mm)	1.06	0.1248	0.432
2. Petrothene®	0.125 in. (3.175 mm)	1.01	0.06112	0.212
3. Gilsonite	0.0197 in. (0.5mm)	1.06	0.0207	0.0717
4. Gilsonite	0.0118 in. (0.3mm)	1.06	0.00795	0.0275
5. Gilsonite	0.0075 in. (0.019mm)	1.06	0.00347	0.0100

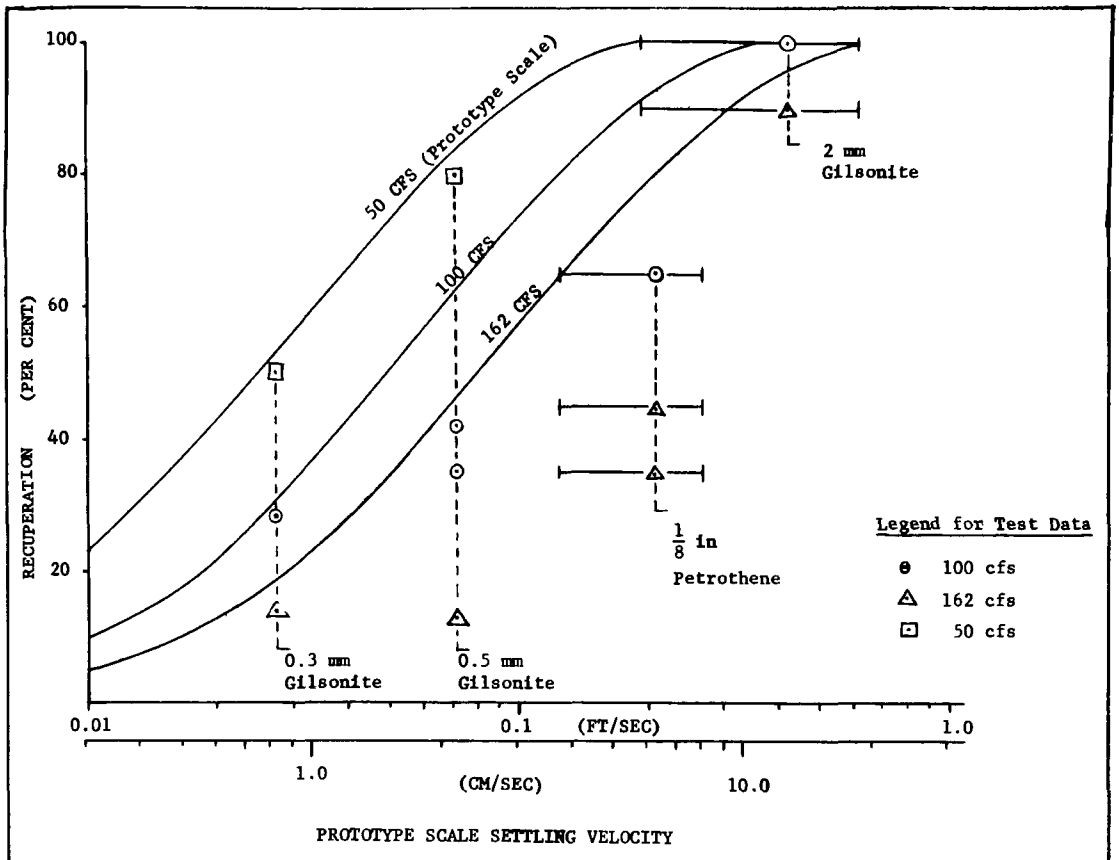

FIGURE 16
COMPARISON OF PARTICLE FLOW MATHEMATICAL MODEL RESULTS WITH TEST DATA

efficiency of 63.4 percent at 100 cfs. The separation efficiency for this particle at 162 cfs should be the same as for a particle with settling rate

$$V_{S_2} = V_{S_1} \frac{(Q_1)}{Q_2}$$

$$= (0.0717) \frac{100}{162} = 0.0442 fps$$

at 100 cfs. From the 100 cfs curve in Figure 16 this efficiency is 46 percent.

The mathematical model calculation for a particle with settling velocity of 0.0717 fps at 162 cfs, gave an efficiency of 46.2 percent, which is within the accuracy with which Figure 16 can be read. With the accuracy of the scaling procedure established, the separation efficiency results calculated for 100 cfs were scaled to 50 cfs and 162 cfs flowrates. The results are also shown as smooth curves in Figure 16.

The test data from LaSalle Hydraulics Laboratory have also been plotted in Figure 16 for comparison with the mathematical model results. The spreader bars shown on the Petrothene® and 2 mm gilsonite data indicate the range in settling velocities corresponding to the spread in particle sizes. At the two smaller sizes, the gilsonite was screened to reduce the range of particle sizes. Two data points are shown for 0.5 mm gilsonite at 100 cfs, which gave separation efficiencies of 35 and 42 percent in two successive tests. This difference of seven percent is probably

indicative of the scatter to be expected in the remaining data. The settling velocities of all particles in Figure 16 have been scaled up to the prototype chamber size (a factor of $\sqrt{12}$ times their actual settling velocities).

The calculated efficiency curves generally agree very well with the test data at both high and low settling velocities, but they overestimate the measured efficiencies at intermediate settling rates. For 0.3 mm gilsonite, the agreement is very good at all three flowrates. The calculated results slightly overestimate the actual efficiency by three percent at 50 and 100 cfs, and by five percent at 162 cfs. In the limit of very small settling velocities, all of the calculated curves correctly approach a lower limit of three percent removal efficiency, corresponding to the fraction of liquid withdrawn through the foul sewer outlet.

At the highest settling rates tested, the calculated results correctly indicate where 100 percent removal efficiency will occur. At 100 cfs, both calculations and tests show 100 percent removal efficiency is obtained with two mm gilsonite. At 162 cfs, the calculated separation efficiency is 96 dercent for two mm gilsonite. The measured efficiency at 162 cfs was 90 percent, but this test included finer particles as indicated by the spreader bars. The calculated curve crosses these spreader bars a little to left of center, just as it does at 100 cfs.

At the intermediate settling rates corresponding to 0.5 mm gilsonite and 3.175 mm Petrothene®, the calculated efficiencies are substantially larger than those measured at 100 and 162 cfs, for example, the mathematical model predicts 80 percent recovery for the Petrothene® whereas the tests gave only 35 to 45 percent removal efficiency. The agreement is somewhat better at 100 cfs, with calculated removal efficiency of 93 percent compared with a measured removal efficiency of 65 percent. The reasons for these discrepancies are not clear, but several suggestions are offered.

First, it is surprising that the measured removal efficiency for Petrothene® is so much lower than for the gilsonite because the unsieved gilsonite contains some particles whose settling rates are in the same range as that of the Petrothene® (note the overlap in the spreader bars shown in Figure 16). Probably these fine particles are lost in the gilsonite tests without appreciably affecting the measured removal efficiency. Nevertheless, the very sharp decrease in performance attained with Petrothene® is surprising. One explanation lies in the possible non-uniformity of the Petrothene® particles. With a nominal specific gravity of only 1.01, very small changes in the composition could drastically affect the settling rate, which varies in proportion to (Sg-1). In fact, in some simple tests performed at General Electric, 12 to 20 percent of the particles were found to float, even after soaking overnight in a detergent solution. In the LaSalle tests, these floating particles were removed from the test mixture. Nevertheless, the presence of these floating particles indicates a larger range in settling velocities than shown in Figure 16. During testing, adhered gas bubbles may also cause some particles to rise and be entrained in the overflow. For these reasons, the observed removal efficiency with Petrothene® may have been influenced by the loss of particles with lower settling velocities than those for which the calculations were made. It is doubtful, however, whether the entire discrepancy can be attributed to this cause, because a large number of lightweight particles would be required to explain the difference.

An additional source of disagreement between the mathematical model and test results lies in the non-axisymmetric nature of the laboratory model, which must differ appreciably from the computed axisymmetric flow at the inlet and near the baffle. In fact, it could be expected that the jet created by the inlet channel could readily carry particles to the surface, a condition not accounted for in the mathematical model. It is reasonable that the smoother flow in the mathematical model (produced by smoothly spreading the inlet flow over the entire circumference), would give better removal efficiencies. This explanation also confirms the observation that agreement is better at 100 cfs than at 162 cfs. At the higher flowrate, the turbulence and

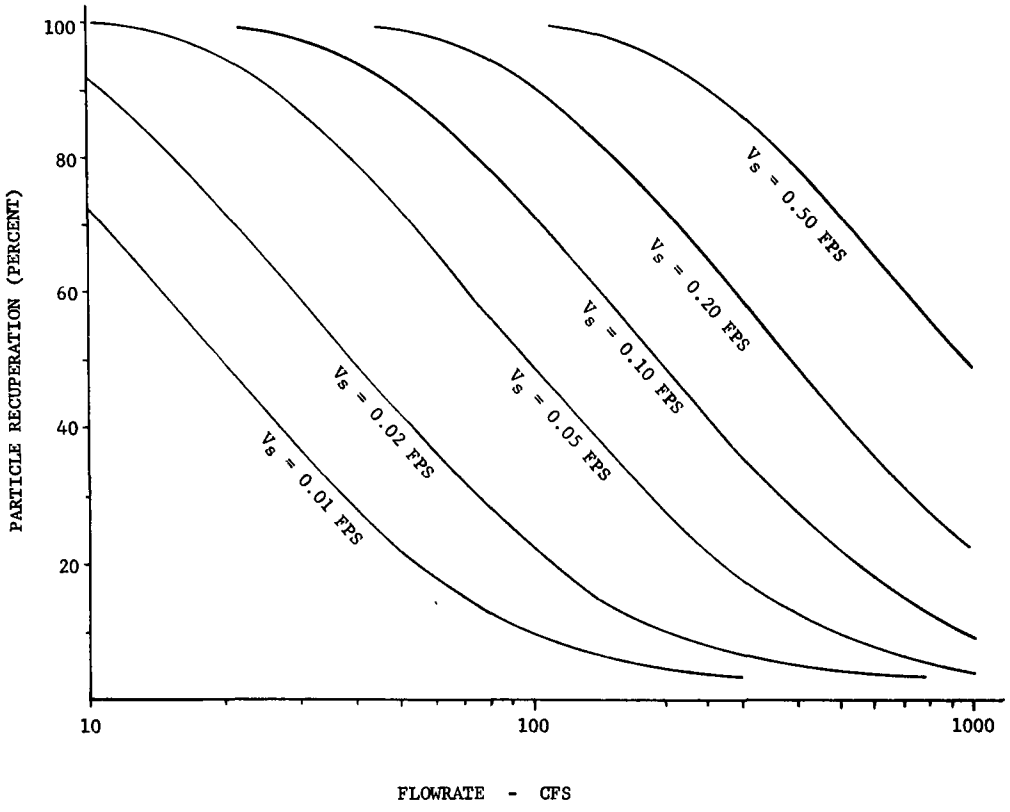

FIGURE 17
PREDICTED PERFORMANCE OF PROTOTYPE SWIRL CONCENTRATOR VS FLOWRATE
(36 ft Diameter)

non-axisymmetric effects are accentuated. Furthermore, at the lowest flowrate, agreement is quite good even at the intermediate settling rates. Thus, the predicted removal efficiency for 0.5 mm gilsonite at 50 cfs is 83 percent, whereas the measured removal efficiency was 80 percent.

In summary, it appears that the mathematical model correctly predicts the removal efficiency at the upper and lower ends of the efficiency curve. At intermediate settling rates, the model predicts the performance well at 50 cfs, but the agreement deteriorates at higher flows, probably due to non-axisymmetric flow effects.

Results for Nominal Case

The performance of the concentrator for several settling rates over a wide range of flowrates was determined through use of the scaling relationships. The results are shown in Figure 17. Predicted Performance of Prototype of Swirl Concentrator Versus Flowrate. The scaling of the calculated results to new flowrates requires that the flow patterns remain unchanged although the velocities increase in magnitude. The liquid flowfield will scale properly in this manner, provided the fraction of flow withdrawn through the foul sewer outlet is held constant. Therefore, Figure 17 applies to cases where the foul sewer flow is three percent of the total inflow. Because the foul sewer flow is so small, the results should also apply approximately to cases where the foul sewer fraction is still smaller or slightly larger. With

a different foul sewer fraction, the asymtotic lower limit of the separator performance will be altered from three percent to the new foul sewer value.

The results given in Figure 17 do not account for non-axisymmetric flow effects, or for changes in the flow pattern which may occur at high flowrates. Some evidence of non-axisymmetric effects is evident in the laboratory data at 100 and 162 cfs, and these effects may become more pronounced at still higher flows. Similarly, at the very large flows (250 cfs and higher) the nature of the flow could be altered due to the increasing restriction of the overflow weir and to the jet-like behavior of the inlet flow. The predicted results at large flowrates may, therefore, not be reliable and should be used cautiously. Within the range of the laboratory data (50 cfs-162 cfs) the scaling procedure has been shown to reliably predict the concentrator performance. The results should also be accurate at lower flows.

The physical mechanisms operating within the swirl concentrator are illustrated in Figures 18-21, Particle Trajectories and Concentration Profiles at 100 cfs for 2 mm, 0.25 mm, 0.5 mm and 0.3 mm Particles. Each of these figures shows the particle concentration (number density) profiles and typical particle trajectories for a given settling rate. The settling rates are 0.432 fps, 0.212 fps, 0.0717 fps, and 0.0275 fps respectively. In Figure 18, the very large settling rate results in high particle concentrations along the bottom, which decreases gradually toward the underside of the weir. These concentrations have been normalized by the inlet concentration and thus vary generally from zero to unity, with some local regions having concentrations greater than unity. The distortion of the concentration profiles by the upflow velocity near the overflow is interesting. The upflow increases the local concentration as evidenced by the lifting of the constant concentration lines in this region. Thus, at a given depth, the concentration is greater right under the overflow region than on either side, due to the transport of particles by the upward flow.

The particle trajectories in Figure 18 show very rapid fallout toward the bottom, with only slight deviations caused by the secondary liquid flow along the bottom. The trajectories were calculated for particles arbitrarily started at selected points in the flowfield as shown in Figure 18. It is not possible to determine concentrator performance by tracing particle paths from the inflow region alone, as one can for the liquid flow. For the case shown in Figure 18, for example, all the particles entering the concentrator at the periphery hit the bottom to the right of point B. Yet both the laboratory and mathematical model results show that particles in fact reach the inner region of the concentrator, as evidenced by the number density contours shown in Figure 18. The explanation of this seeming discrepancy lies in the turbulence of the flow The calculated trajectories only represent the mean particle motion. The liquid turbulence will cause the actual trajectories to differ randomly from those shown, thereby scattering particles from regions of high concentration into the low concentration regions.

As the particle settling velocity is decreased, the particle trajectories and concentration profiles change drastically. In Figure 19, Effect of Underflow Sewer Fraction on Removal Efficiency, particles with settling velocity of one-half those in Figure 18 show much more influence due to the secondary liquid flow in the chamber. This is evidenced by the large lateral excursions of the particles near the center, which move first outward and then inward as they fall. All particle trajectories shown, however, still reach the bottom indicating a very high efficiency (actually 93% for this case which represents the Petrothene®). The concentration profiles in Figure 19 indicate a much larger region with a concentration near unity. The N = 1 profile (marked by the symbol Y) is irregularly shaped, and generally covers the bottom two-thirds of the chamber. The random appearance of this profile is due to small variations in concentration about a nominal value of unity. Thus, adjacent points may have concentrations of 0.99 and 1.01 respectively The computer plotting

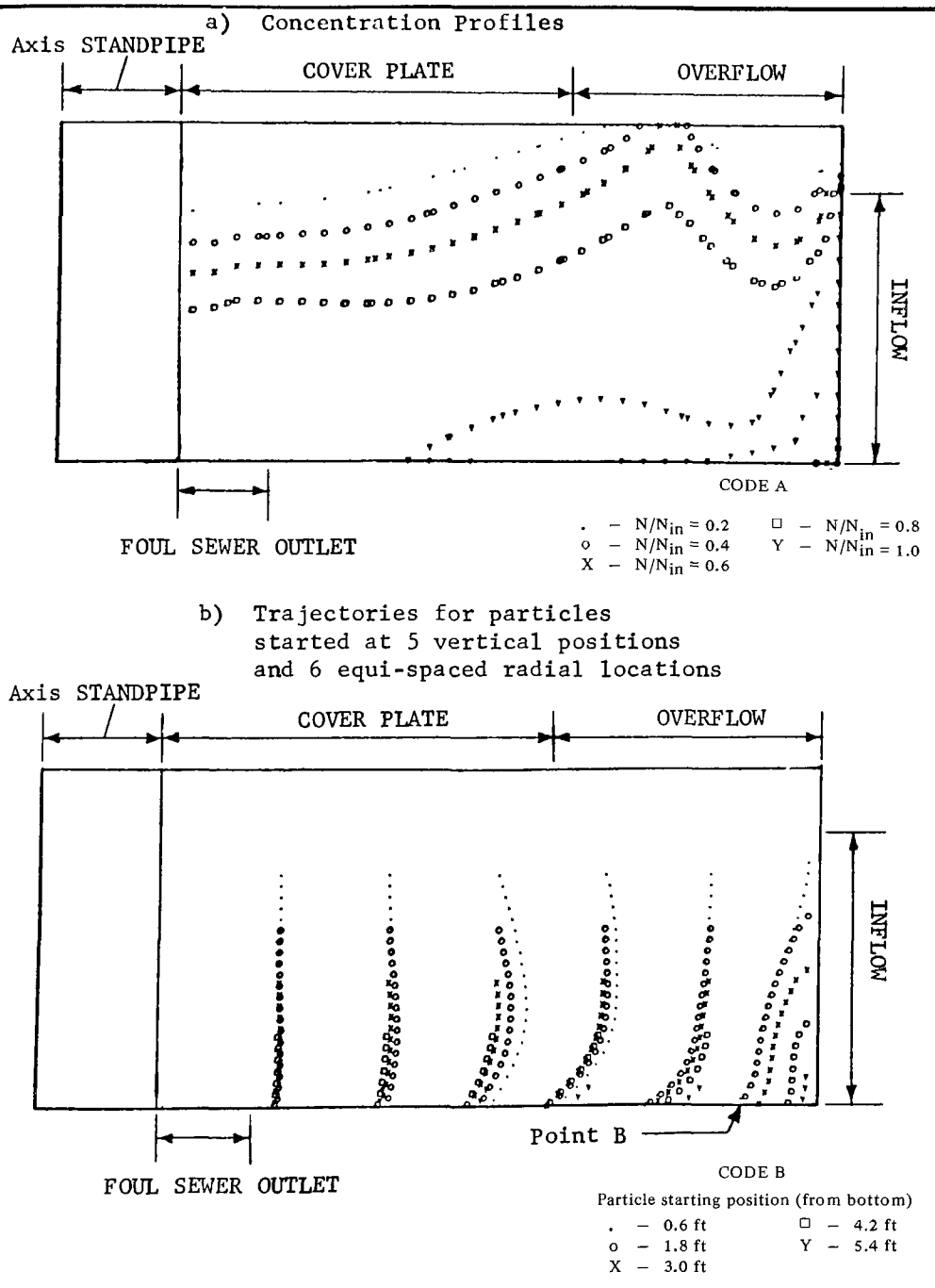

FIGURE 18
PARTICLE TRAJECTORIES AND CONCENTRATION PROFILES AT 100 cfs FOR 2 mm GILSONITE PARTICLES (prototype scale settling velocity of 0.432 fps)

a) Concentration Profiles

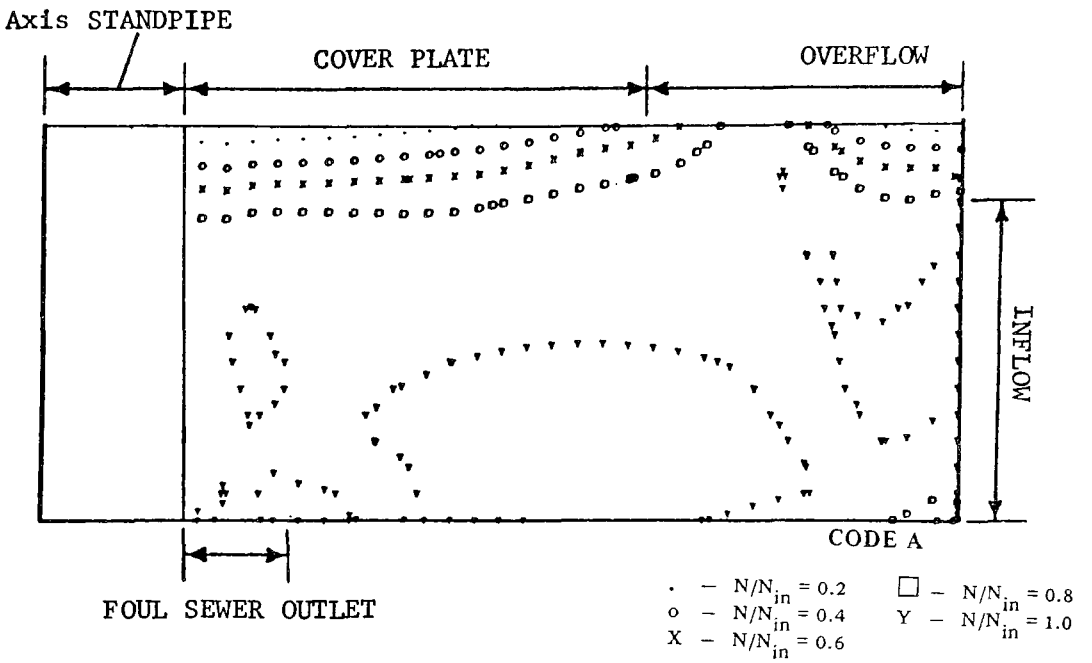

b) Trajectories for particles started at 5 vertical positions and 6 equi-spaced radial locations

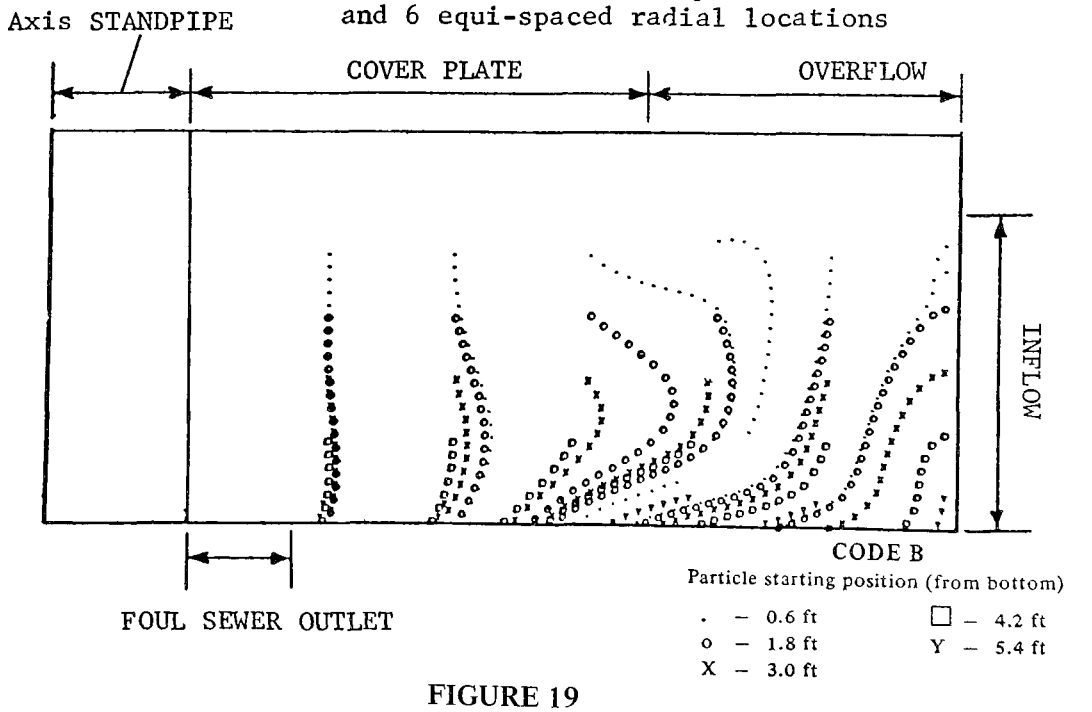

FIGURE 19

PARTICLE TRAJECTORY AND CONCENTRATION PROFILES AT 100 cfs FOR .25-INCH PETROTHENE® PARTICLES (prototype scale settling velocity of 0.212 fps)

procedure interpolates between these values to find the location of the N = 1 line. However such small variations are not physically significant, and the actual shape of this contour is not meaningful. What is significant is the volume of the chamber in which the concentration is near unity. For example, comparison of Figure 18 and 19 reveals that in the former case the N = 1 concentration profile is regular shaped, and confined to the region of the chamber near the bottom, due to the rapid settling rate. In contrast, the slower settling particles in Figure 19 are almost uniformly distributed (at the inlet concentration) over the entire bottom 2/3 of the chamber. The concentration gradient near the underside of the weir is also much greater in Figure 19, as evidenced by the closer spacing of the concentration profiles under the weir. As in Figure 18, the distortion due to the upward flow in the overflow region is evident in the concentration profiles of Figure 19.

Similar changes are evident in Figure 20, which corresponds to 0.5 mm Gilsonite. The concentration profiles show the particles are spread uniformly over most of the chamber, with a very steep gradient at the underside of the weir. The particle trajectories now indicate that a significant number of particles leave by the overflow. Some of the particles entering at the periphery are brought to the bottom by the downward flow, and are then dragged inward toward the center by the secondary liquid motion. As these particles reach the quiescent inner region they fall to the bottom and leave by the foul sewer outlet. It is noted that particles which are scattered by turbulence into the inner region near the standpipe, settle more or less straight to the bottom. A little further toward the outside, however, particles which start to settle to the bottom are entrained in the upward liquid flow and are carried out the overflow. The behavior of the particles near the top of the inlet region in Figure 20 is also interesting. These particles are brought to the surface by the upward liquid velocity, but then they settle again toward the bottom About half way down to the bottom, they are again re-entrained with the upflow and are carried out the overflow.

Finally, in Figure 21, which represents the very slow settling 0.3 mm gilsonite, the limit of the concentrator performance is quite evident. The concentration is essentially uniform over the cross section, and almost all of the particle trajectories exit by the overflow. Near the inner quiescent region by the standpipe, some settling is evident, but most of these particles are later entrained in the upflow. Some of the particles which reach the central region near the bottom are entrained in the liquid flow leaving the foul sewer outlet.

Taken together, Figures 18-21 provide a graphic illustration of the swirl concentrator operating mechanisms. The concentration profiles show clearly that particles are scattered into low concentration regions, and the trajectories illustrate the average motion of particles of different sizes within the concentrator. These average trajectories provide valuable insights into the concentrator operation which are not always possible with the physical model. In the laboratory tests, for example, turbulence and the rotational motion make it difficult to follow individual particles. And if an individual particle is tracked, its statistical significance is uncertain, because another particle started at the same location will follow a different path due to the influence of turbulence.

Effect of Scale Size on Concentrator Performance

Probably the most important use of the mathematical model is to predict how the prototype scale swirl concentrator will differ in performance from the laboratory model. This is a vital piece of information which cannot be obtained in the laboratory without constructing a full size unit. Usually, the answer cannot be obtained from field studies either, due to the difficulty of performing a controlled experiment under field conditions. Some differences are expected because it is impossible to correctly model all of the terms in the particle equations of motion in the laboratory. Consequently, the mathematical model was exercised for two cases: the nominal 100 cfs flow in the prototype scale concentrator, and the scaled flowrate of

a) Concentration Profiles

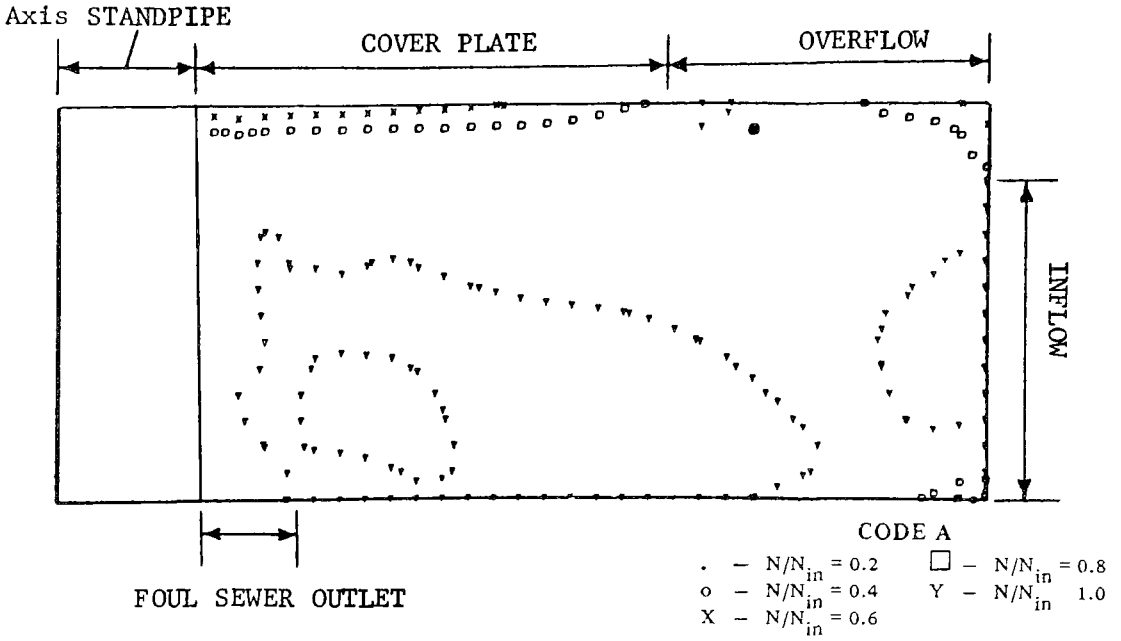

b) Trajectories for particles started at 5 vertical positions and 6 equi-spaced radial locations

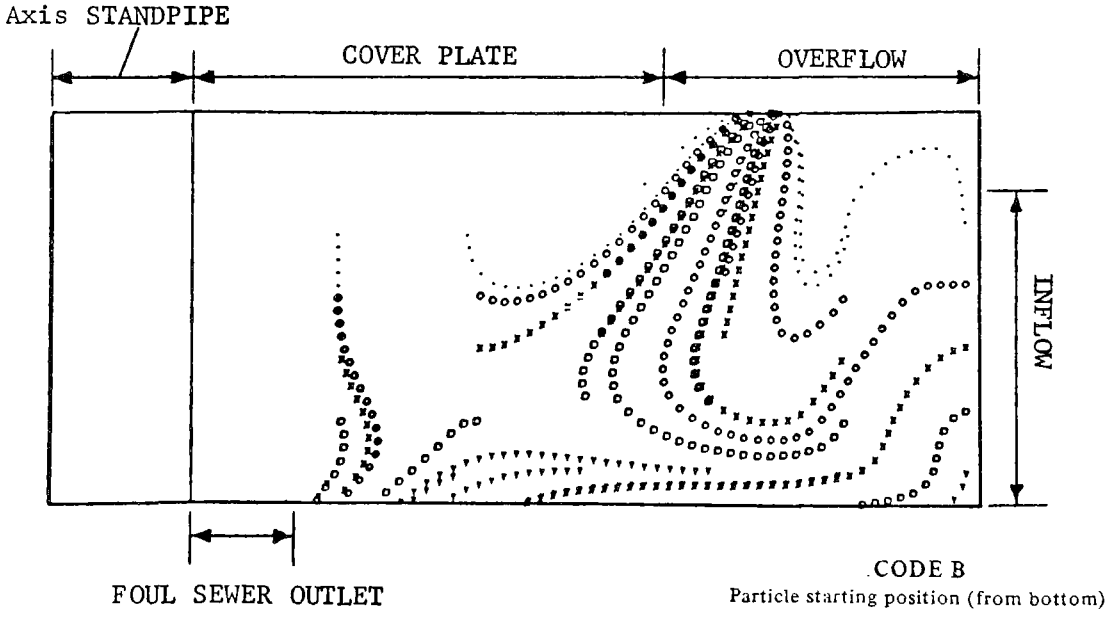

FIGURE 20
PARTICLE TRAJECTORIES AND CONCENTRATION PROFILES AT 100 cfs FOR 0.5 mm GILSONITE PARTICLES (prototype scale settling velocity of 0.0717 fps)

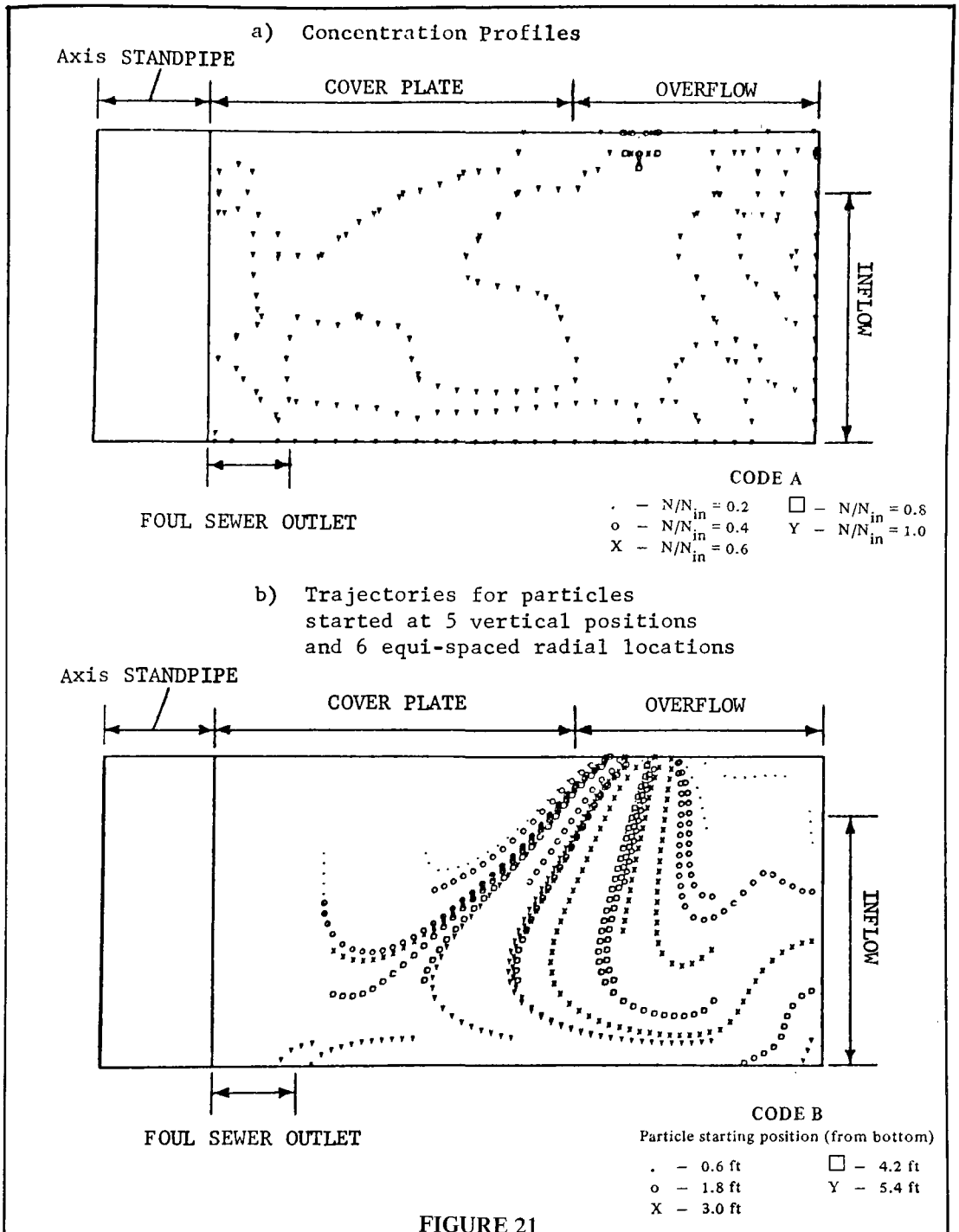

FIGURE 21
PARTICLE TRAJECTORIES AND CONCENTRATION PROFILES AT 100 cfs FOR 0.3 mm GILSONITE PARTICLES (prototype scale settling velocity of 0.275 fps)

0.20047 cfs flow in the model concentrator. Both calculations were performed for particle number 3 (Table 1) which represents 0.5 mm Gilsonite with settling velocity of 0.0207 fps on the model scale. The corresponding prototype scale settling velocity is

$$V_{s_p} = (0.0207)\sqrt{12} = 0.0717\ fps$$

which was obtained by using an 0.0238-in. particle with specific gravity of 1.2 (see Fig. 30). The results of these calculations are summarized as:

	Model Scale	Prototype Scale
Particle flux-		
Overflow (Q_{p_O})	0.0819 sec^{-1}	40.83 sec^{-1}
Particle flux-		
Bottom (Q_{pb})	0.1414 sec^{-1}	70.66 sec^{-1}
Efficiency Q_{pb}		
($Q_{pb} + Q_{po}$)	63.3%	63.3%

The equations from which Q_{po} and Q_{pb} are calculated have been given previously (Equations 59 and 60). The units are *number of particles per second* for an inlet concentration of one particle per cubic foot. The fluxes for higher inlet concentration are obtained by scaling them in direct proportion to the actual inlet concentration. Since both Q_{po} and Q_{pb} are scaled by the same factor, their ratio (and hence the efficiency) does not change with inlet concentration.

This numerical experiment demonstrates that the assumed scaling procedures are valid, and that the prototype concentrator performance can, in fact, be accurately predicted by adjusting the particle specific gravity and size so as to yield the proper scaled settling velocity. This conclusion is, of course, only valid to the extent that the liquid flow pattern is the same in the model and prototype. For the assumed eddy viscosity representation, this similarity is very close in the mathematical model. However, if the prototype scale were to be very much larger than the model (say a factor of 100 rather than 12 as in the present instance), it is possible for different flow effects to appear, which are not accounted for in the present mathematical model, specifically calibrated against the laboratory scale device.

It is noted that the scaling procedure only preserves the balance between the drag and the buoyancy if the particle motion relative to the fluid has exactly the settling velocity. At other relative velocities, this balance will be different for the model and prototype scales. Furthermore, the inertial acceleration terms are all multiplied by the specific gravity. Since different specific gravities have been used in the model and prototype calculations, these terms will not be correctly scaled. The fact that essentially the same results were obtained in both calculations demonstrates that the inertial terms in the equations of motion are, in fact, negligible compared with drag and buoyancy.

The results also indicate that, to a very good level of approximation, the particle velocities can be found by superimposing a uniform settling rate on the velocities obtained from the liquid flowfield. For example, at the randomly selected point i = 7, k = 17, in the model scale calculation, the following results were obtained:

	Flow Velocities (fps)	
	Liquid	Particle
Radial Velocity	0.02630	0.02620
Tangential Velocity	0.3130	0.3130
Vertical Velocity	-0.04979	-0.02827

The differences between the liquid and particle velocities are negligible for the radial and tangential components. For the vertical component, the difference is

$$V_p \quad V_1 = (-0.02878) - (-0.04979)$$
$$= 0.02101\ fps$$

which is very close to the calculated settling velocity of 0.0207 fps. Therefore, subsequent calculations for other cases were made with the particle velocities obtained by superimposing the settling rate on the liquid flow velocities as calculated for the given case.

Influence of Geometric Variables on Separator Performance

Weir Diameter

To determine the effect of the diameter of the overflow weir on the liquid flowfield and the particle removal efficiencies, the

mathematical model was operated at the same conditions of 100 cfs inflow and 3 cfs foul water outflow for two different weir sizes (24-ft diameter and 32-ft diameter, prototype scale).

The effect of the weir diameter on the liquid flowfield is summarized in Figures 22 and 23, Comparison of Crossflow Streamlines and Velocity Contours for 24-ft and 32-ft Weirs. It should again be emphasized that although the flowfields depicted in Figures 22 and 23 apply to any chamber cross section for the mathematical model, as a result of the axisymmetric approximation, they only predict conditions at the 180° cross section for the laboratory model. This is a consequence of the calibration of the mathematical model for the 180° laboratory cross section. Figure 22 shows the effect of the weir diameter on the crossflow streamlines. For the larger weir diameter, the streamline pattern is compressed near the surface of the chamber. This is a result of the smaller annular cross section through which the flow must pass. The streamlines toward the bottom of the chamber, on the other hand, retain the same position for both weir sizes.

This effect is also evident in the velocity contours for the two weir sizes depicted in Figure 23. As a result of the compression of the streamline pattern for the larger weir diameter, high velocities are experienced towards the outer wall of the swirl concentrator. The higher vertical velocities at the wall also cause the crossflow velocity contours to shift towards the outer wall. The net result of the larger weir diameter is therefore to cause larger vertical flow velocities towards the walls of the swirl concentrator.

The effect of the weir diameter on the particle removal efficiency is given in Table 2, Effect of Weir Size on Concentrator Efficiency.

The larger weir diameter yielded poorer removal efficiences for every particle settling velocity. The difference in the efficiency of the two weir sizes was lowest at both very high and very low particle settling velocities and largest at the settling velocity of 0.212 ft/sec. These results are in agreement with the tests performed by LaSalle. The Laboratory performed tests on 24, 28, and 32-ft (prototype scale) overflow weirs, and concluded that the 24-ft weir yielded the best removal efficiency. Recent tests performed by the Laboratory on a 20-ft weir with a 24-ft scum ring indicated removal efficiencies of the same order of magnitude as the 24-ft weir.

TABLE 2

Effect of Weir Size on Concentrator Efficiency

Particle Settling Velocity (Prototype Scale ft/sec)	Removal Efficiency % 24-ft Weir	32-ft Weir
0.0275	31.2	27.6
0.0717	63.1	51.6
0.212	93.2	79.4
0.432	100	90.3

Since both the mathematical and physical models predict better separation efficiencies for a 24-ft diameter weir than for a 32-ft one, it is possible that a still smaller weir diameter would give improved performance. The performance changes with weir diameter are related to the changing overflow velocity profile as illustrated in Figure 24, Effect of Weir Diameter Overflow Velocity Profile. For large weir diameters (Fig. 24a), the overflow velocity contains a high peak. Any particles entrained in this upflow will be readily carried out the overflow. As the weir diameter is decreased, the peak is reduced as a result of the increase in cross-sectional area through which the flow must pass (Fig. 24b). At this lower upward velocity, fewer particles will be carried out the overflow. In general, the lower the upflow velocity, the better the separator performance. Also, by withdrawing the flow nearer the center, more of the particles may be scattered by turbulence into the quiet region under the weir, from which they can settle to the bottom. As the weir diameter is reduced still further, as illustrated in Figure 24c, the peak upflow velocity may not be decreased any further because there is no upflow near the outside of the tank, and the smaller weir circumference demands a greater local velocity over the weir. Decreases in weir diameter below this point may reduce

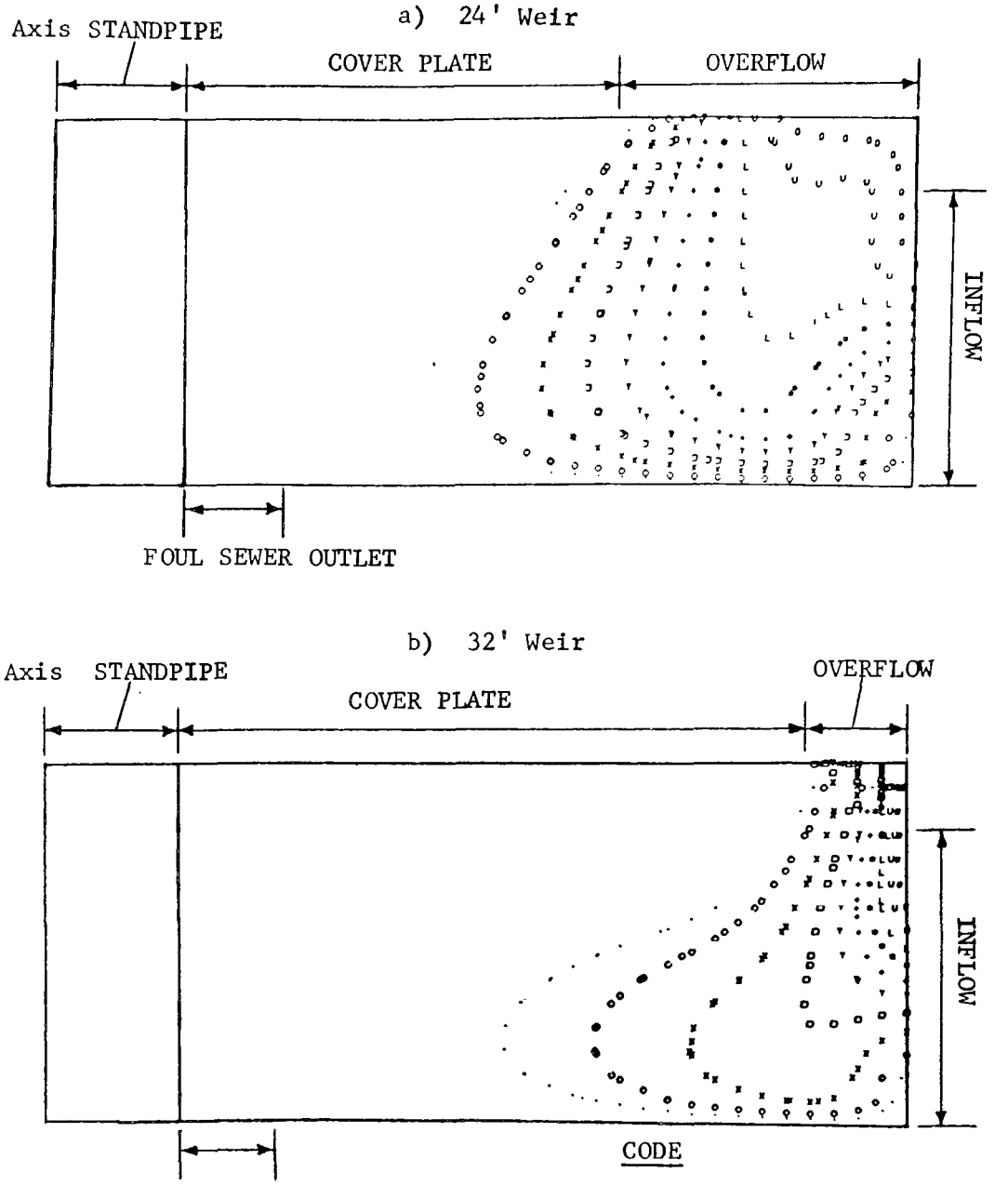

FIGURE 22
COMPARISON OF CROSSFLOW STREAMLINES FOR 24-FT AND 32-FT WEIR

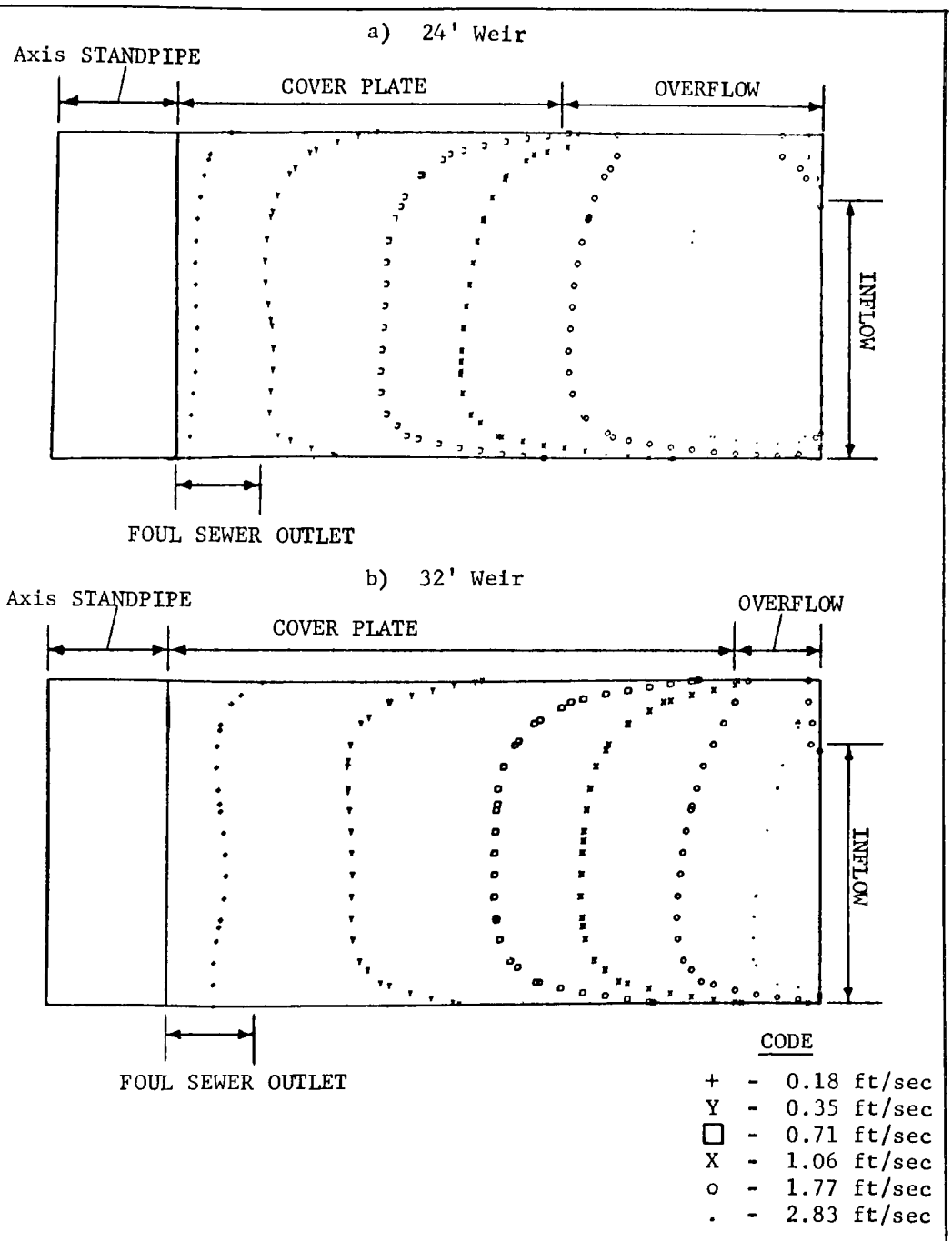

FIGURE 23
COMPARISON OF VELOCITY CONTOURS FOR 24-FT AND 32-FT WEIR

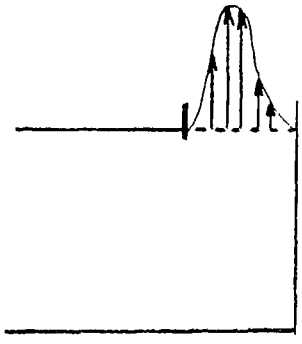

a) High peak velocity due to narrow overflow annulus

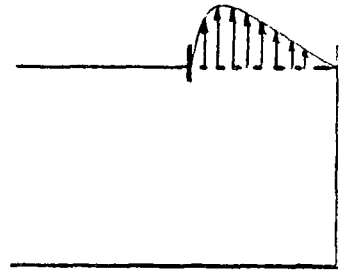

b) Lower peak velocity with wider overflow annulus

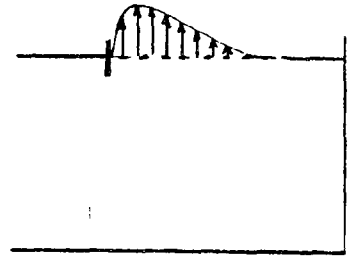

c) No additional reduction in peak velocity with further widening of annulus

FIGURE 24
EFFECT OF WEIR DIAMETER ON OVERFLOW VELOCITY PROFILE

removal efficiencies by reducing the size of the low velocity region beneath the weir in which much of the particle sedimentation occurs. The recent tests performed in the laboratory with a 20-ft weir and with a 24-ft scum ring indicated removal efficiencies approximately the same as those with the 24-ft weir. Thus 20 feet may be near this lower limit for improving efficiency by reducing weir diameter, although this conclusion is speculative and not supported by calculations or data. Further reduction in weir diameter would also have the undesirable effect of reducing the storage area available for floating solids.

Depth to Width Ratio

The effect of the depth to width ratio on the liquid flowfield and particle removal efficiency was determined by operating the mathematical model for two different chamber depths, with all other parameters held constant. The effect of the chamber depth on the liquid flowfield is shown in Figures 25 and 26.

Figure 25, Comparison of Crossflow Streamline Pattern for Different Tank Depths, illustrates the effect on the chamber crossflow streamlines. Although there is some difference in the position of a few of the streamlines between the 9-ft depth (7.5 ft to bottom of weir plate) and 10.5-ft depth (9.0 ft to bottom of weir plate), the general pattern and degree of penetration of the majority of the streamlines remain unchanged. This trend can also be noted in the velocity contours illustrated in Figure 26, Comparison of Velocity Contours for Different Tank Depths. As in the case of the streamlines, there is no marked difference between the general shape and location of the velocity contours.

With regard to the removal efficiencies, the mathematical model predicts a marginal improvement in the removal efficiencies for the larger tank depth as indicated in Table 3, Effect of Chamber Depth on Concentrator Efficiency. It should be emphasized that the results indicated in Table 3 are based upon the mathematical model and have not been verified by testing of the final laboratory configuration. However, laboratory tests

TABLE 3

Effect of Chamber Depth on Concentrator Performance

Particle Settling Velocity	Removal Efficiency	
	9.0 Ft Depth	10.5 Ft Depth
(prototype scale ft/sec)	0.25 depth/diameter	0.29 depth/diameter
0.0275	31.2	35.8
0.0717	63.4	67.1
0.212	93.2	96.0
0.432	100	99.5

utilizing earlier concentrator configurations, indicated that "marginal, even questionable," increases in performance were observed at depths down to 15 feet.

Foul Sewer Fraction

The 100 cfs nominal case was operated at three different foul sewer fractions to ascertain the effect of the foul sewer fraction on concentrator performance. Figures 27 and 28 depict the velocity contours and the crossflow streamlines for foul sewer fractions of 10 and 20 percent. The base case at a foul sewer fraction of three percent (see Fig. 26 for velocity profile and Fig. 25 for streamlines) provides a third point for comparisons.

The effect of the doubling of the foul sewer fraction from 10 to 20 percent is to move the ten percent streamline so that it provides for the increased flow out of the foul sewer outlet (Fig. 27, Comparison of Velocity Contours for Different Foul Sewer Fractions). The ten percent streamline for the higher foul sewer takes on the same shape as the five percent streamline for the lower foul sewer fraction. The remaining streamlines (for example the 60% streamline) are identical for both cases.

This localized change in the liquid flowfield is also evident in velocity profiles in Figure 28, Comparison of Crossflow Streamline Patterns for Different Foul Sewer Fractions. The velocity profiles near the outer wall are essentially unchanged for the two foul sewer fractions, while the velocity contours near the standpipe are shifted towards the foul sewer outlet. This effect is most pronounced for the 0.71 streamline which has a sharp deflection toward the base

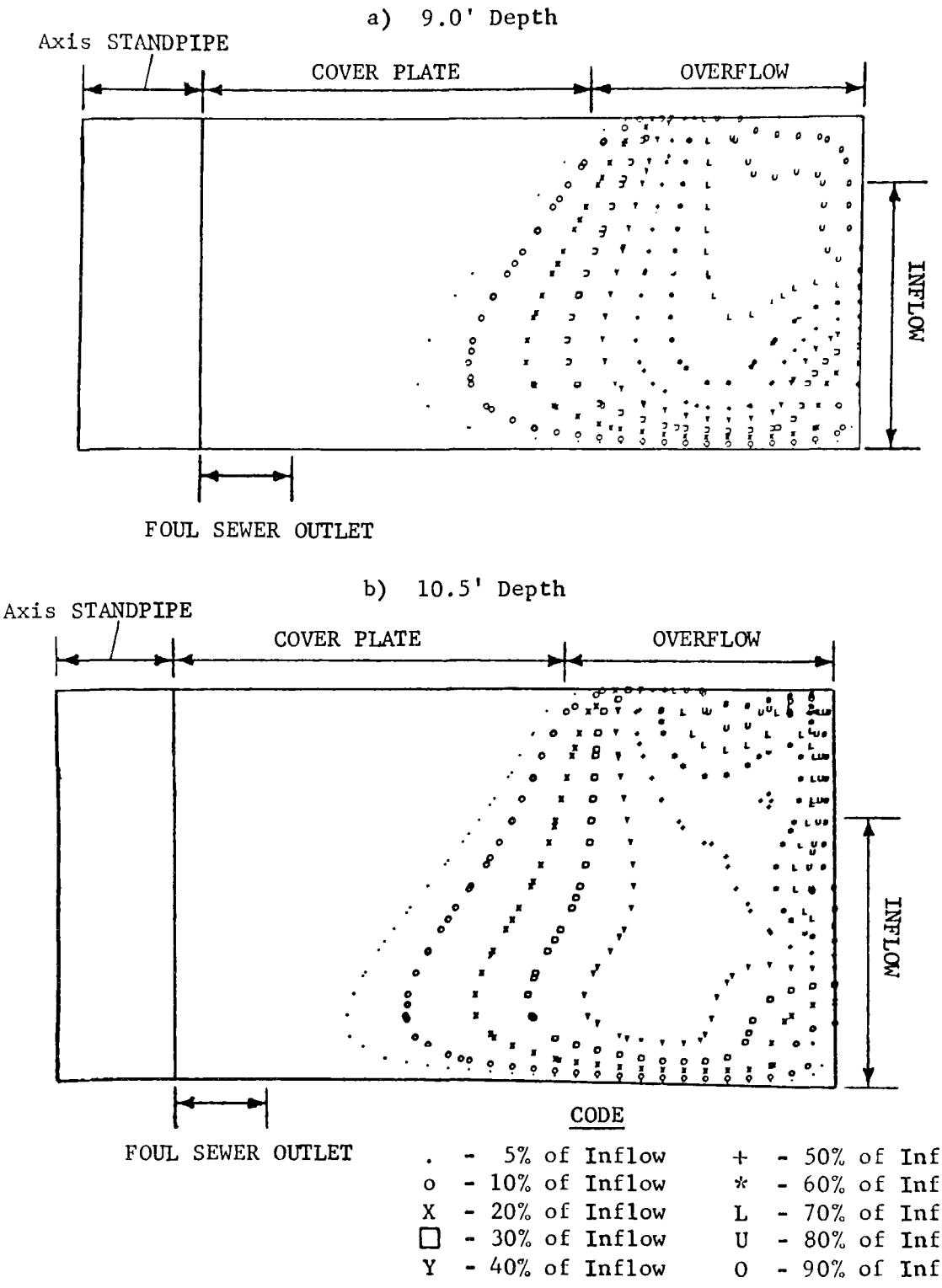

FIGURE 25
COMPARISON OF CROSSFLOW STREAMLINE PATTERNS FOR DIFFERENT TANK DEPTHS

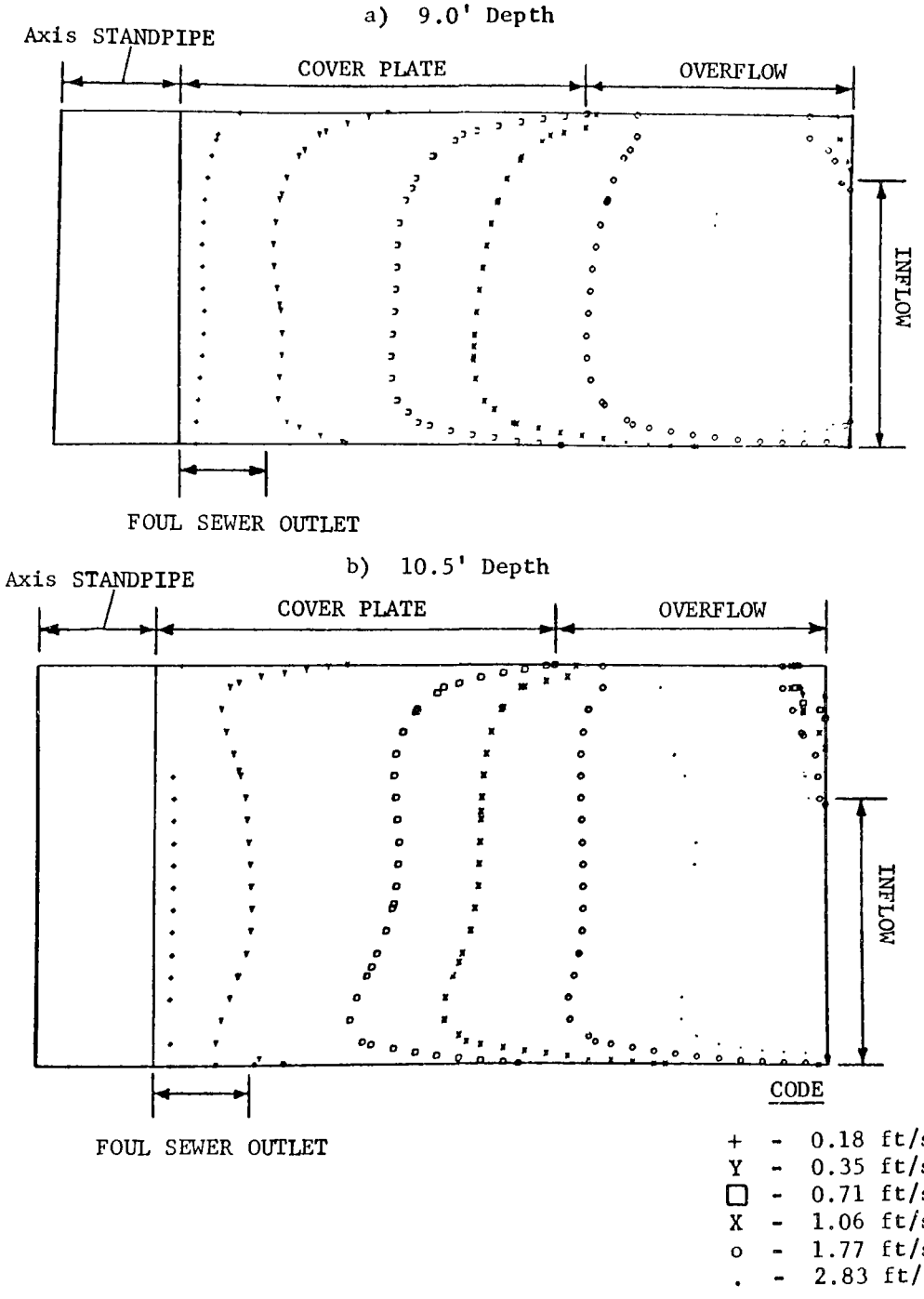

FIGURE 26
COMPARISON OF VELOCITY CONTOURS FOR DIFFERENT TANK DEPTHS

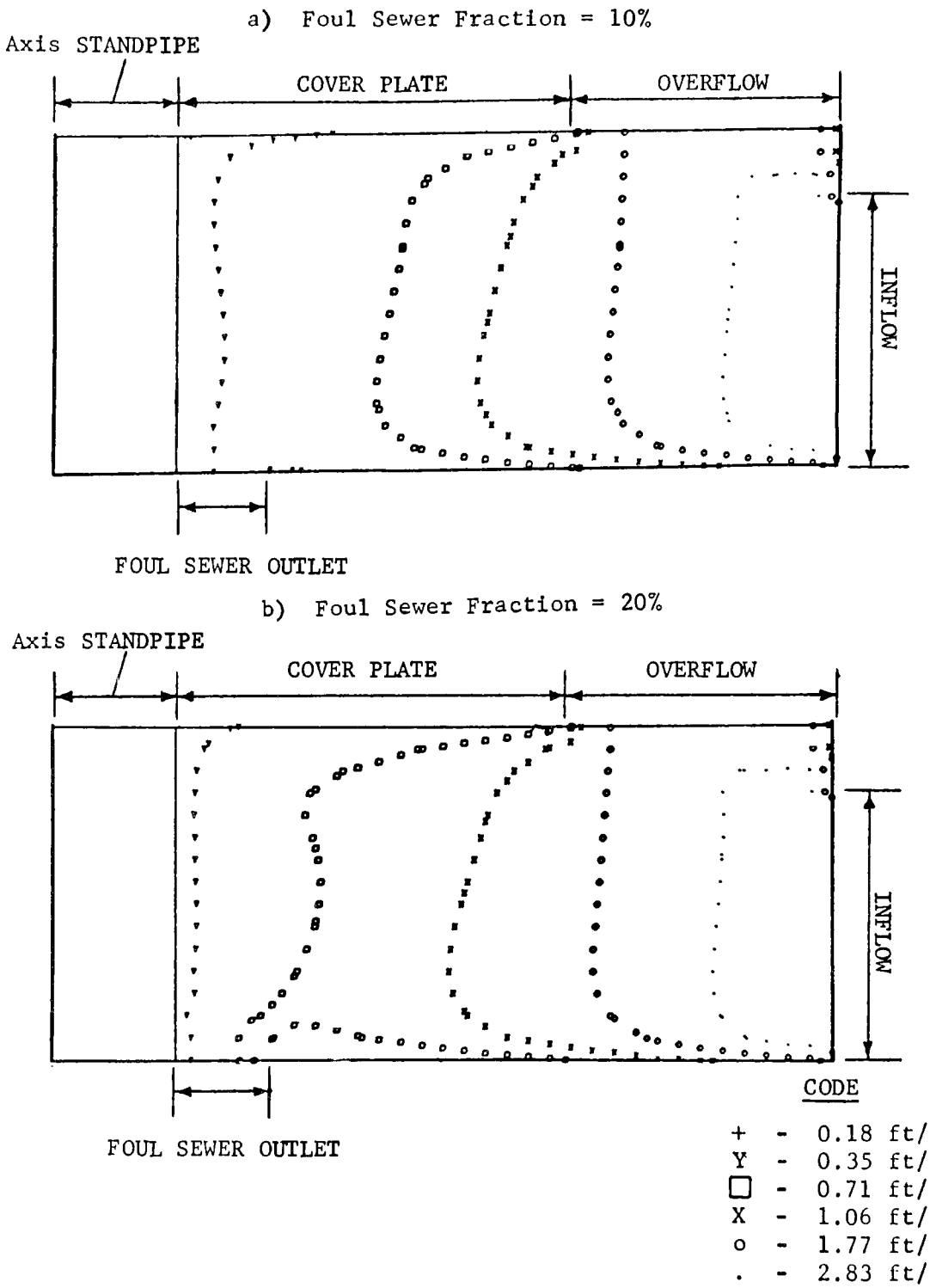

FIGURE 27
COMPARISON OF VELOCITY CONTOURS FOR DIFFERENT FOUL SEWER FRACTIONS

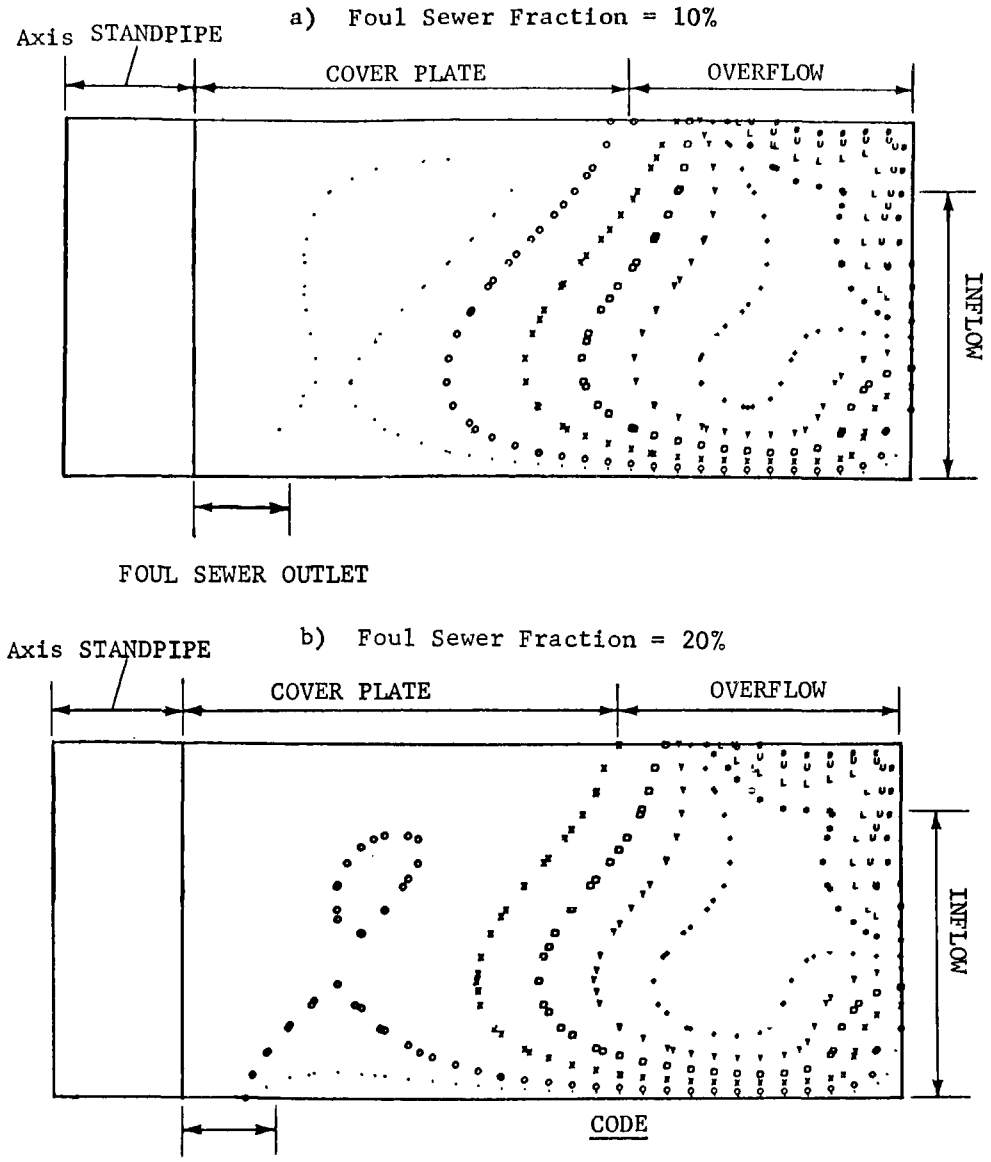

FIGURE 28
COMPARISON OF CROSSFLOW STREAMLINE PATTERN
FOR DIFFERENT FOUL SEWER FRACTIONS

of the chamber to account for the higher foul sewer velocity.

The removal efficiencies for the three foul sewer fractions are summarized in Table 4, Effect of Foul Sewer Fraction on Concentrator Performance.

It is apparent from Table 4 that the mathematical model predicts increased removal efficiencies for larger foul sewer fractions. The increased removal efficiencies can probably be attributed to the reduction in the vertical velocities at the overflow, thus allowing more particles to settle into the foul sewer outlet. Figure 29, Effect of Underflow Fraction on Removal Efficiency, represents a plot of the data from Table 4.

DESIGN RECOMMENDATIONS

The purpose of this section is to show how the results of the mathematical model can be utilized for designing a swirl concentrator from the model results. To illustrate the approach, a hypothetical design example will be used. Assume that a concentrator is to be designed for 80 percent removal of 1/4-in. particles having a specific gravity of 1.05 for a design storm which produces a chamber inflow of 200 cfs. The first step is to determine a design settling velocity of the particles from the particle size and specific gravity data. The settling velocity can be calculated by conventional methods, or from a graphical analysis such as Figure 30, Particle Settling Rates. Figure 30 was generated from Equation (42), which is valid for Reynolds numbers less than 10^4. Entering Figure 30 with a particle diameter of 0.25 in. and the S_g = 1.05 curve, a settling velocity of 0.3 ft/sec is obtained. If several particle sizes and specific gravities are involved, engineering judgment must be used to determine the design settling velocity for the particle mixture.

After determination of the particle settling velocity, the next step is to estimate the size of the required concentrator. This can be done by using a curve of the type shown in Figure 31, Scale Factor Diagram The constants θ, ψ, and ϕ represent intermediate variables which are used in the size calculation and are derived from Froude number scaling. (In actuality θ represents the model flowrate; ϕ, the model particle settling velocity; and ψ, the ratio of design flowrate to the fifth power of the design particle settling velocity.) For the chamber design, ψ can be computed from the relationship: $\psi = \frac{Q_{design}}{V_s^5}$

where

Q_{design} = design flowrate (200 cfs)

V_s = settling velocity of the particles to be removed (ft/sec).

For the hypothetical design example

$$V_s = \frac{200}{0.0026} = 8.22 \times 10^4$$

The designer can enter Figure 31 with the calculated values of ψ and interpolate to the ψ line representing the computed ψ value. The efficiency (E) line corresponding to the desired removal efficiency (E = 80%) is also selected. The coordinates of the intersection of the E and ψ lines specify the values of θ and ϕ associated with the design criteria. For the hypothetical example, the intersection of the $\psi = 8.22 \times 10^4$; E = 80% lines circled in Figure 31 yields the values of θ = 0.48 and ϕ = 0.09. The value of the scaling factor, S can now be computed from either the θ or ϕ value via either of the following equations.

$$S = \left(\frac{V_s}{\Phi}\right)^2$$

$$S = \left(\frac{Q_{Design}}{\theta}\right)^{0.4}$$

TABLE 4

Effect of Foul Sewer Fraction on Concentrator Performance

Particle Settling Velocities (ft/sec prototype scale)	3% Foul Sewer Fraction	10 % Foul Sewer Fraction	20% Foul Sewer Fraction
0.0275	31.2	41.9	51.6
0.0717	63.4	70.5	75.8
0.212	93.2	95.6	97.1

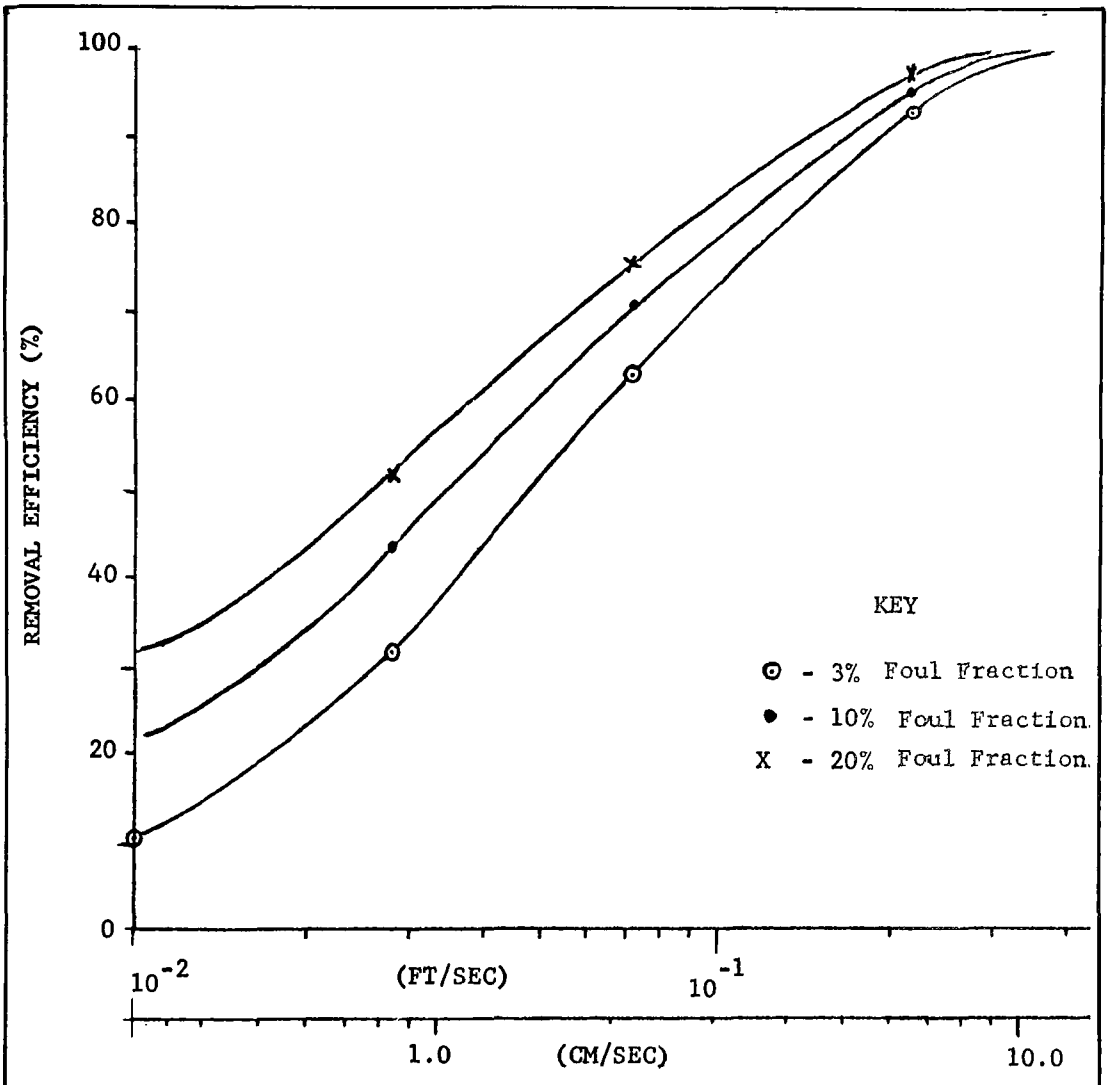

FIGURE 29
EFFECT OF UNDERFLOW SEWER FRACTION ON REMOVAL EFFICIENCY

For the hypothetical case, a value of S = 11.1 was obtained from either equation. An average scale factor of 11 will be used for the design example. The size of the chamber can now be determined by multiplying the dimensions of the LaSalle model concentrator by a factor of 11. Thus the 3-ft model concentrator diameter will result in a 33-ft design diameter. Likewise, the other model concentrator dimensions can be scaled up in a similar fashion.

The boxed region in Figure 31 indicates the model flowrates and particle settling velocities tested by La Salle Hydraulic Laboratory. Similarly the dotted ψ lines represent the scaling of the laboratory data to

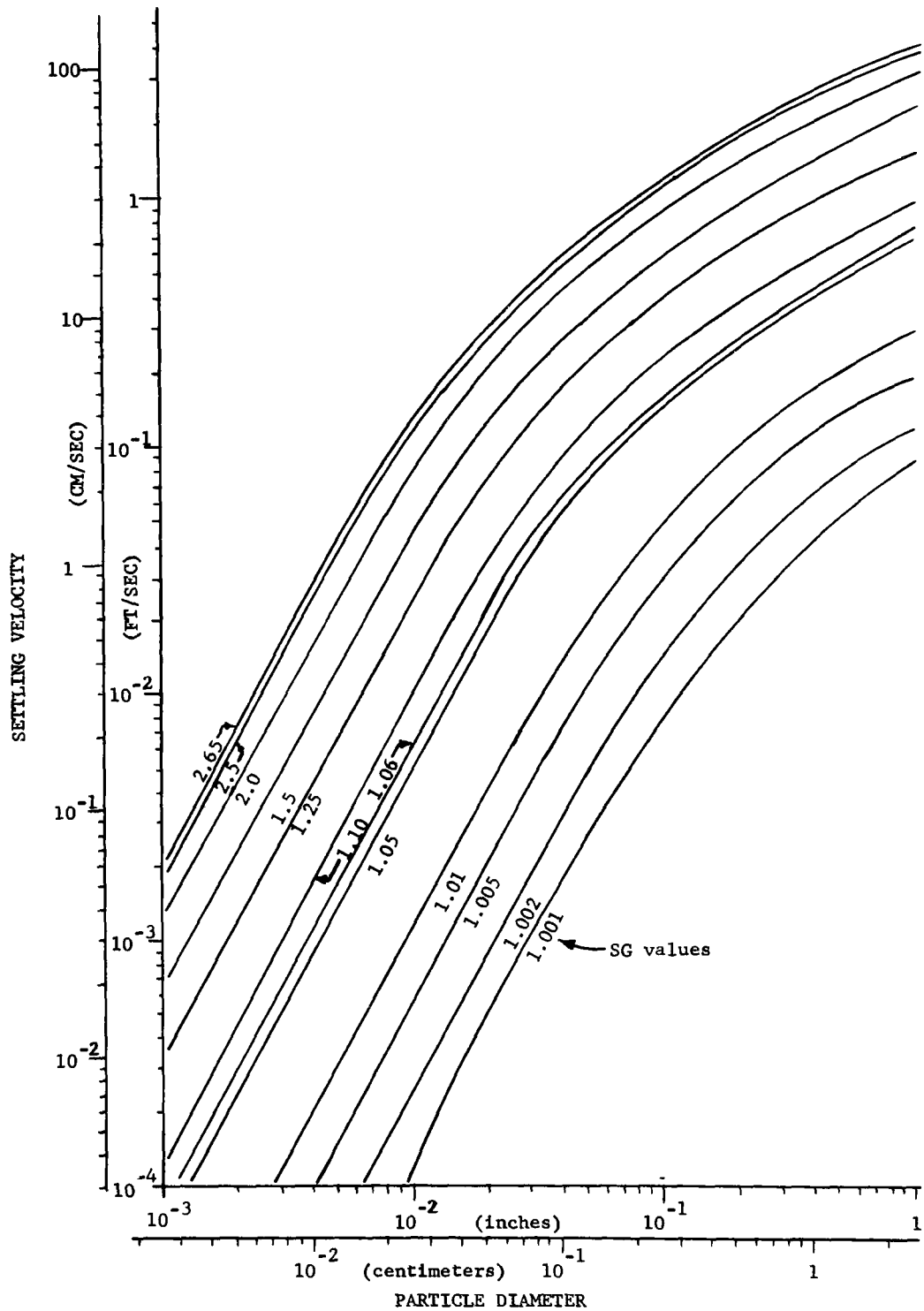

FIGURE 30
PARTICLE SETTLING RATES

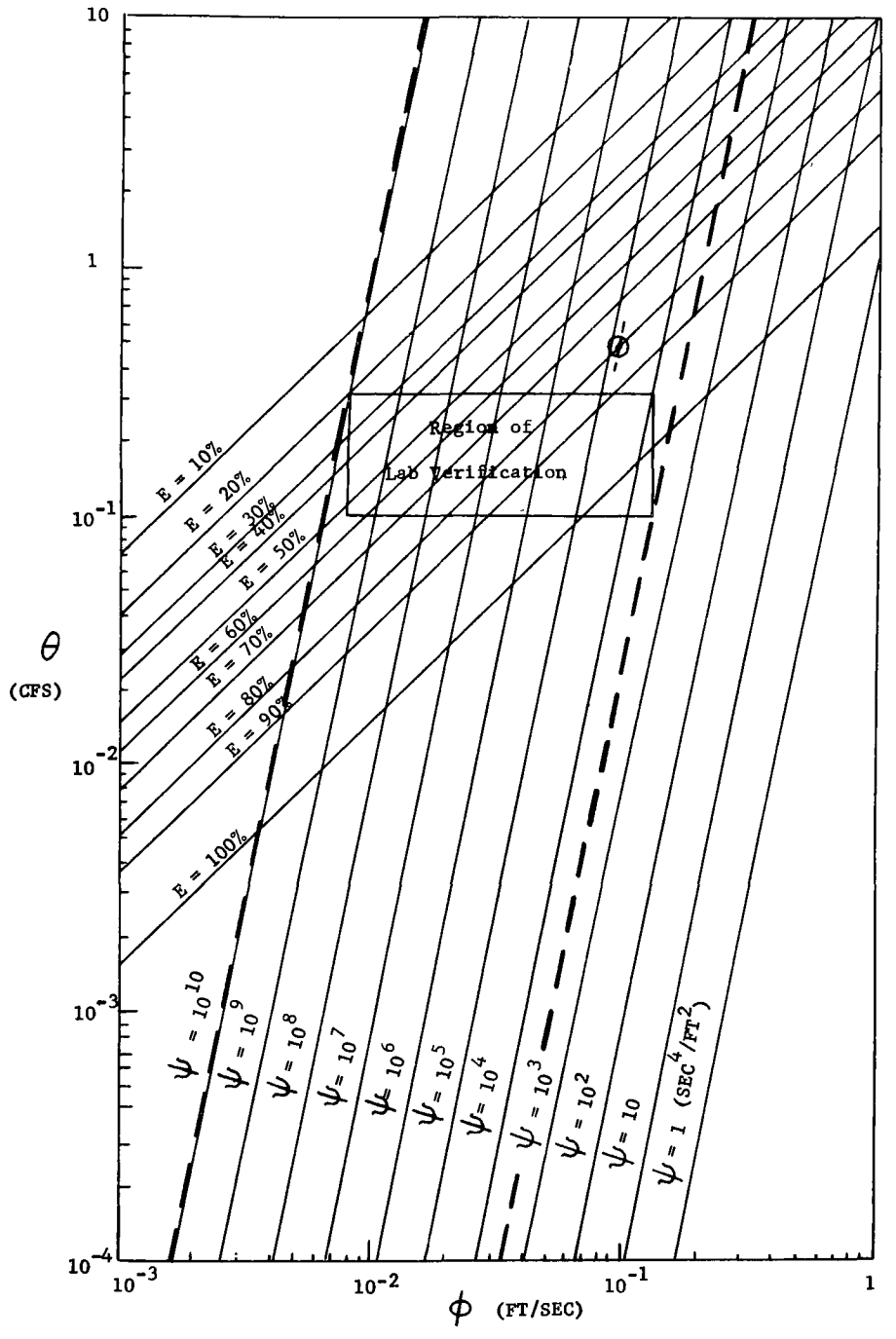

FIGURE 31
SCALE FACTOR DIAGRAM

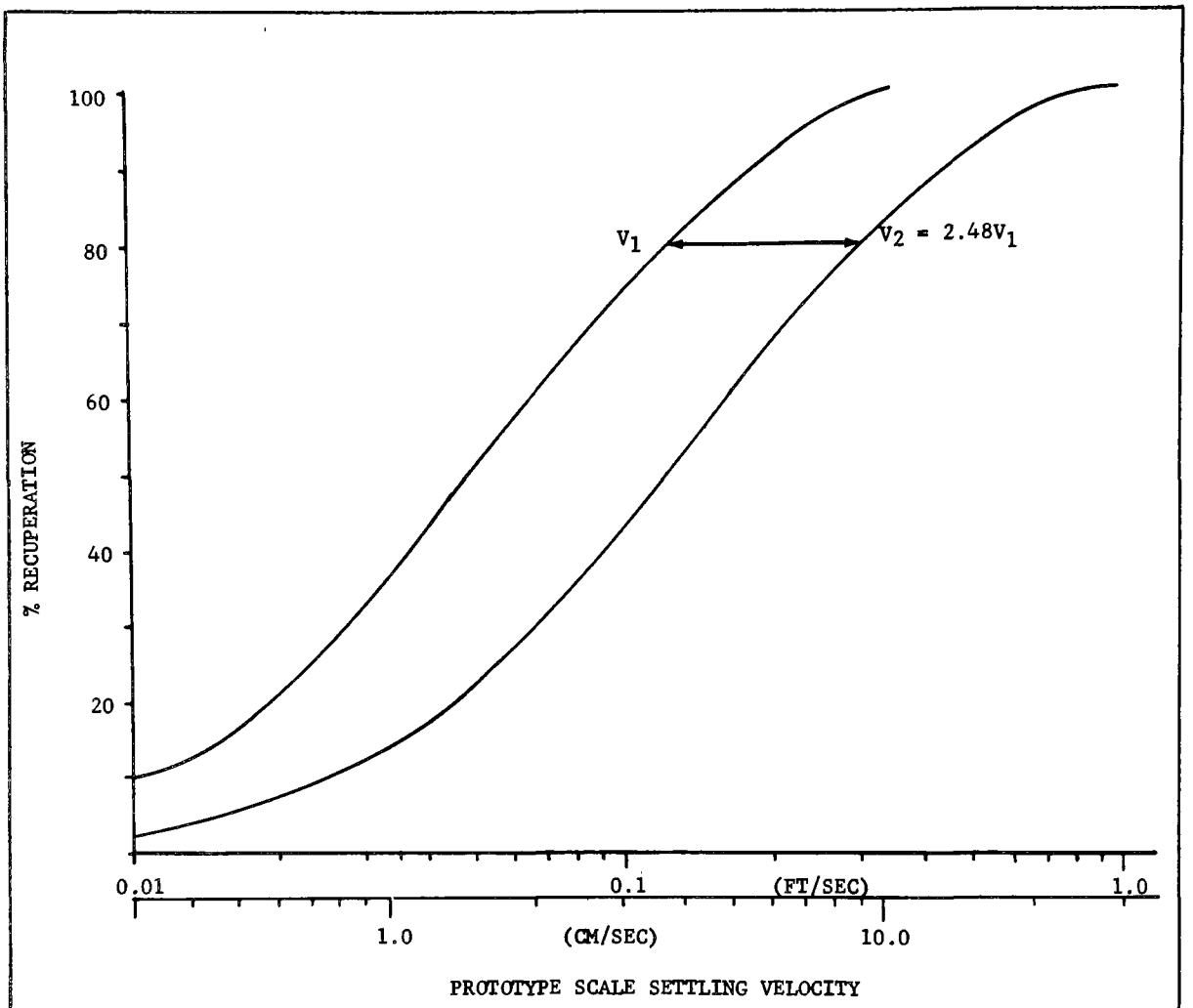

FIGURE 32
EFFICIENCY CURVE FOR PROTOTYPE SCALE (12:1)

other concentrator sizes. Only the regions within the dotted lines therefore represent laboratory verified testing. The use of Figure 31 in any other region involves extrapolation of the laboratory results beyond the range of parameters tested and must therefore be applied with cognizance of this fact.

With an estimation of the design size of the swirl concentrator, the removal efficiency, E, at flowrates other than the design flows and for particles sizes other than the design particles can be determined. This can best be accomplished by calculating the removal efficiency versus settling velocity for the 200 cfs design flow. This curve can be created from either the prototype efficiency curve fitted to the LaSalle data or the prototype efficiency curve determined by the mathematical model.

Consider the prototype curve shown in Figure 32, Efficiency Curve for Prototype Scale. This curve represents the prototype efficiencies as predicted by the mathematical model. To use this curve to extract information representing the 200 cfs flowrate for the design example, it is first necessary to determine the scale factor relating the two cases. Since the prototype curve represents a scale factor of 12 relative to the LaSalle Laboratory model, and the scale factor of the

design example represents a scale factor of 11 relative to the laboratory model, the scale factor of the design relative to the prototype case is equal to 11/12 or 0.915. To adjust the prototype curves shown in Figure 32, it is therefore necessary to adjust the flowrates and particle settling rates for the design example by the following factors:

$$Q_{ps} = \left(\frac{S_{ps}}{S_{Ds}}\right)^{5/2} Q_{Ds}$$

$$Q_{ps} = \left(\frac{12}{11}\right)^{5/2} Q_{Ds} = 1.24\, Q_{Ds}$$

$$V_{pps} = \left(\frac{S_{Ds}}{S_{ps}}\right)^{1/2} V_{pDs}$$

$$V_{pps} = \sqrt{\frac{12}{11}} \quad V_{pDs} = 1.04\, V_{pDs}$$

Where

Q_{Ds} = Flowrate for design scale
Q_{ps} = Flowrate at prototype scale
V_{pDs} = Particle settling velocity at design scale
V_{pps} = Particle settling velocity at protoscale
S_{Ds} = Design scale factor relative to model
S_{ps} = Prototype scale factor relative to model

Multiply the design flow by 1.24, (1.24 x 200 = 248) and the design particle settling velocity by 1.04 (1.04 x 0.3 = 0.312), and enter Figure 32 with these values to obtain the design removal efficiency of 80 percent. This compares with the initially specified 80 percent design value.

The removal curves for the prototype flowrate, Q_{PS} = 248 were created by shifting the given 100 cfs curve by a factor of (248/100) V along the settling velocity axis, (i.e., $V_2 = 2.48\, V_1$). The effect of different flowrates and particle settling velocities can also be determined on the design example. For instance, for a particle settling rate of 0.05 ft/sec, by entering Figure 32 at a Q_{PS} of 248 ft^3/cfs and a settling velocity of (1.04) (0.05) = 0.052 ft/sec, the designer obtains the removal efficiency of 23 percent, representing a particle having a settling velocity of 0.05 ft/sec at the design flowrate. The scaling laws can thus be used to generate a set of efficiency curves describing the predicted performance of the swirl concentrator design.

To illustrate how the efficiency curves can be used to predict the concentrator performance for a particular sewage–storm-water mix, a sample computation has been performed. A typical source mixture in which particle sizes and specific gravity are distributed as indicated in Figure 33, Cumulative Distribution of Settling Velocities for Prototype Storm Water Particles, was assumed. The settling velocities in Figure 31 were computed by entering the settling velocity curve shown in Figure 30 with each of the specific gravities and particle diameters comprising the waste water composition. The 100 cfs prototype curve in Figure 32 was then utilized to determine the removal efficiency for each settling velocity. This assumes that the scale factor of 12:1 applies for this example since the settling velocities and flowrates shown in Figure 32 have been adjusted using the prototype scale factor. The fifth column in Table 5, Sample Calculation of Concentrator Performance for a Specified Particle Size Distribution, represents an efficiency obtained from Figure 32, for the settling velocity indicated in column 4. The efficiencies can then be adjusted by the weight fraction of particles exhibiting that settling velocity and summed to determine the overall removal efficiency. Thus, the overall removal efficiency of the particles with a specific gravity of 1.2 will be 85 percent. In a similar manner, removal efficiency of 90 percent for the 1.5 specific gravity and 97 percent for the 2.65 specific gravity were obtained. The scaling laws therefore make it possible to predict the performance of any chamber design for a waste water mixture.

CONCLUSIONS

Many important conclusions can be drawn from the results obtained with the mathematical model of the swirl concentrator. In this section, the most significant findings and their importance are summarized.

TABLE 5

Sample Calculation of Concentrator Performance for a Specified Particle Size Distribution

D-Particle Size (mm)	Specific Gravity	Percent Particle of Size D	Settling Velocity from Figure 30 (ft/sec)	Percent Recovery for Particle Size D from Figure 32	Percent of Total Particles Removed (3) X (5)
3.0	1.2	40	0.385	100	40.0
2.5	1.2	25	0.33	99	24.7
1.0	1.2	15	0.145	84	12.6
0.5	1.2	10	0.058	57	5.7
0.2	1.2	10	0.0108	22	2.2

(Total recovery for mixture of particle sizes of specific gravity 1.2 is 85.2 percent)

a) For flowrates up to 165 cfs, the mathematical model provides a reasonably accurate description of the liquid flowfield, within the limitations of the axisymmetric assumption, as demonstrated by comparisons with laboratory data. Above 250 cfs, significant non-axisymmetric effects arise due to the jet-like behavior of the inlet flow. These effects cannot be accounted for in the axisymmetric mathematical model.

b) The mathematical model correctly predicts trends in concentrator efficiency due to variations in flowrate, size, settling velocity, geometric changes, and underflow rate. None of the geometric alterations calculated gave better results than the baseline design.

c) The predicted separation efficiencies are very close to those measured for very slow and very fast settling particles. The mathematical model over-predicts the performance at intermediate settling rates, probably because of non-axisymmetric flow effects in the physical model. The agreement between mathematical model and physical model is very good at 50 cfs, and becomes somewhat poorer at 100 and 162 cfs, as a result of non-axisymmetric flow effects. At still higher flows, the mathematical model will markedly over-predict the concentrator performance since the jet-like behavior of the inlet flow has not been modeled.

d) The mathematical model demonstrates that the performance of the prototype scale device can be accurately predicted from the laboratory scale tests. This is especially important because the particle flow cannot be completely simulated in the laboratory. The mathematical model confirms that the most important effects are properly simulated and the laboratory results are representative of the prototype performance.

e) The equations developed for the mathematical model have been used to derive scaling relationships for the liquid and particle flows. The accuracy of these scaling laws has also been verified by detailed computer calculations, the scaling laws permit either the laboratory results, or the mathematical model results to be extended to flowrates, chamber sizes, particle sizes and particle specific gravities other than those for which laboratory results or calculations are available. The mathematical model or laboratory test results can be scaled to any reasonable chamber size, using Froude number scaling to relate the flowrate to the size ($Q \sim s^{5/2}$). The results can also be scaled approximately to other flowrates, within the accuracy of the axisymmetric approximation (up to 162 cfs with a 36-ft. diameter chamber.) The usefulness of the laboratory and mathematical model results are thereby greatly increased.

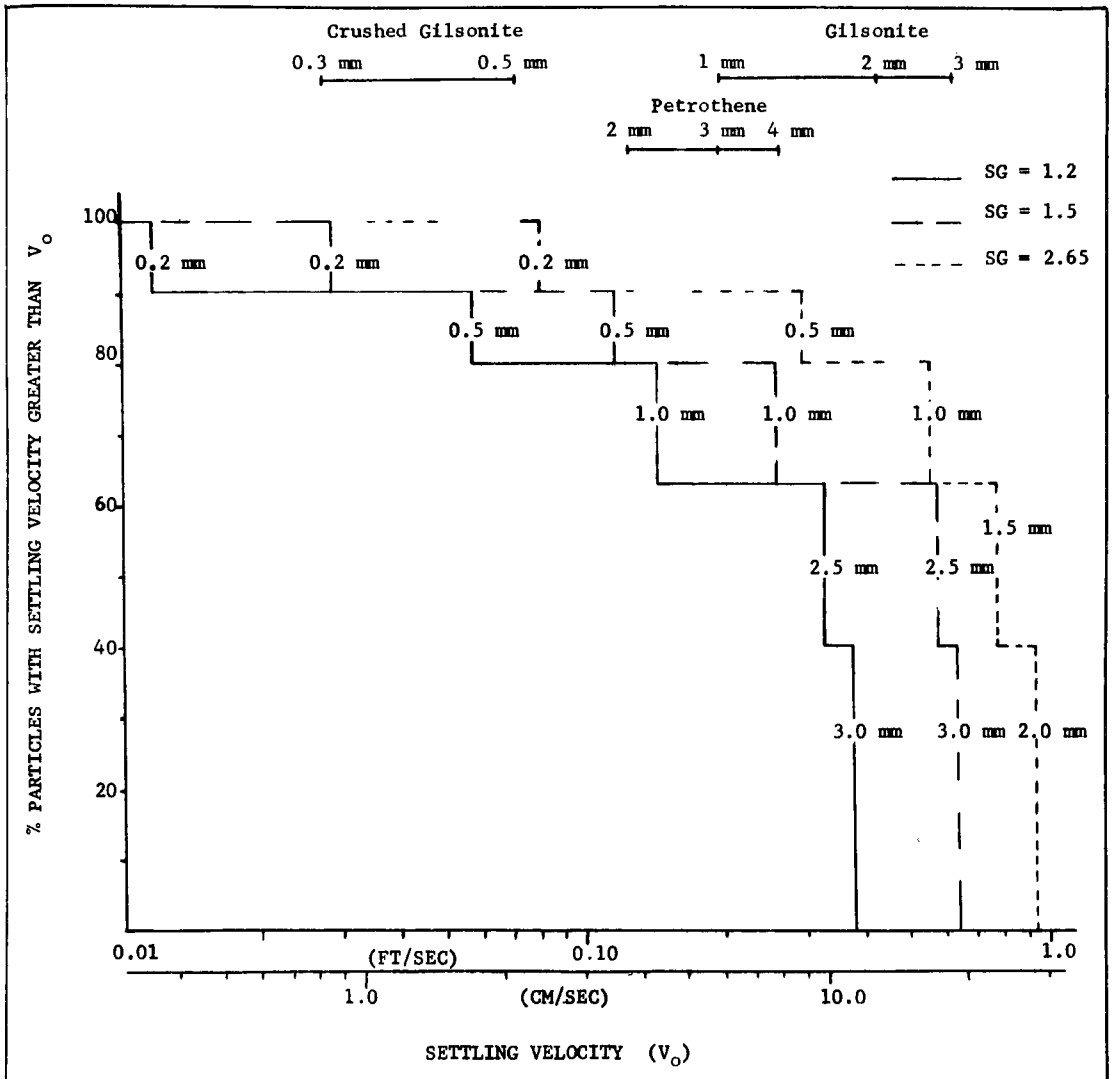

FIGURE 33
CUMULATIVE DISTRIBUTION OF SETTLING VELOCITIES FOR PROTOTYPE STORMWATER PARTICLES

f) The operating principles of the swirl concentrator are clearly demonstrated by the mathematical model. The details of the liquid and particle flow streamlines and velocities are shown in computer-generated plots. The separation mechanism is shown to be gravitational, with the liquid secondary flow serving to sweep the particles on the bottom into the center where they can be drawn off. The effect of turbulence is clearly demonstrated. Without turbulence, the particles would settle directly to the bottom. The effect of turbulence is to scatter particles from regions of high concentration near the bottom, into

regions of lower concentration at the top, where they can be drawn into the overflow.

g) Finally, and most importantly, the mathematical model results confirm that the swirl concnetrator as presently designed, is capable of achieving useful improvements in the quality of combined sewer overflows. This improvement is possible with reasonable size units (36 ft in dia x 9 ft deep) for overflow rates up to 162 cfs.

RECOMMENDATIONS

Based on the successful results from this study, the following recommendations are made for future work in the area of storm water overflows.

First, it would be desirable to predict the transient performance of the swirl concentrator for a typical storm sewer hydrograph. The present results, of course, apply only to steady state operation at a given flowrate and inlet concentration. In order to predict the total waste matter discharged, consideration should be given to time varying inlet concentration (due to the *first flush* effect), and to the accumulation of particles within the concentrator as it is charged and emptied. It should be possible to construct from the present results, a method for simulating the dynamic operation under varying inlet flowrates and concentrations. Using this simulation, studies could be carried out to determine the optimum concentrator size relative to typical hydrographs for a given area, and to predict the reduction in discharged waste matter for a typical year's operation.

The second area which deserves further study is the application of swirl concentrators to typical design requirements. For example, it is not clear whether better efficiencies can be achieved with two half-size concentrators or one full-size unit. With two units one chamber could be used for all flows less than 100 cfs and the second chamber would be needed only if the storm flow exceeded this preset value. This might provide better separation at both higher and lower flows because the unit can be tailored to a smaller range of flowrates. This example corresponds to operating two units in parallel, and the concept can readily be extended to an arbitrary number of units. The possibility of operating units in series to improve the overall separation efficiency should also be examined. Other questions which could be answered in such an application study include optimum inlet pipe configurations to avoid settling during low flow conditions; methods for controlling the foul sewer flowrate; means of predicting head losses; use as a flow regulator as well as particle separator; design recommendations for areas where head loss is critical; and design charts for preliminary size selection as a function of sewer hydrograph data.

NOMENCLATURE

A	Area
C_D	Drag coefficient
C_f	Skin friction coefficient
d_p	Particle diameter
E	Efficiency
$\vec{e}_g$	Unit vector in direction of gravitational force
$\vec{e}_r, \vec{e}_z$	Unit vectors in radial and axial directions, respectively
f	Non-dimensional stream function defined in Equation (17e)
g	Gravitational acceleration
g^{jk}	Metric tensor
G	Non-dimensional tangential velocity function defined in Equation (17c)
ℓ	Mixing length
N	Concentration (number density)
n	Fluctuation in number density
p	Pressure
p_2	Pressure less the hydrostatic term
Q	Volume flowrate
Q_p	Particle flowrate—number of particles per second
Re	Reynolds number
r	Radial coordinate
S	Scaling factor
S_{ij}	Deformation tensor defined by Equation (11)
S_g	Specific gravity
s	Reference length
T_{ij}	Reynolds stress tensor defined by Equation (7)
t	Time
U	Liquid velocity
u	Fluctuation in liquid velocity, or radial velocity component
V	Particle velocity
V_s	Settling velocity
v	Fluctuation in particle velocity, or tangential velocity component
v_p	Particle volume
w	Vertical velocity component
x^i	General coordinate direction component
z	Axial coordinate
$\aleph$	Mixing length constant
α	Ratio of rms velocity fluctuations in liquid to those of particle
ϵ	Eddy viscosity
ζ	Non-dimensional axial coordinate
η	Virtual mass coefficient
θ	Constant used in design calculations
μ	Molecular viscosity
ν	Kinematic viscosity
ξ	Non-dimensional radial coordinate
ρ	Density
τ	Shear stress
Φ	Dissipation function defined by Equation (10)
ϕ	Constant used in design calculations
ψ	Stream function defined by Equation (16), or constant used in design calculation
ω	Reference frequency (taken as $Q/r_o A_{in}$)
Ω	Non-dimensional vorticity function defined by Equation (17d)

SUBSCRIPTS

b	Boundary value, or bottom
b+1	Value at point adjacent to boundary
i	Inner standpipe
in	Inlet
L	Liquid
m	Model scale
o	Overflow outer boundary
p	Prototype scale, or particle
w	Water

SUPERSCRIPTS

$\wedge$	Denotes non-dimensional quantity
$-$	Denotes mean value
$\rightharpoonup$	Vector quantity
	Denotes fluctuating quantity, or differentiation with respect to argument

TENSOR NOTATION

U_i	Co-variant form of the vector, $\vec{U}$
U^i	Contra-variant form of the vector, $\vec{U}$
$U_{i,j}$	Denotes co-variant differentiation of the vector; the result is tensor of order two, and is equivalent to writing $\nabla \vec{U}$
$U^i{}_{,i}$	Repeated index appearing once as superscript and once as subscript denotes summation. Thus this form is equivalent in Cartesian coordinates, to

$$U^i{}_{,j} = \nabla \cdot \vec{U} = \frac{\partial u}{\partial x} + \frac{\partial v}{\partial y} + \frac{\partial w}{\partial z}$$

REFERENCES

1. Smisson, B., *Design, Construction, and Performance of Vortex Overflow,* Symposium on Storm Sewage Overflows; Institution of Civil Engineers, 1967, (pp. 99).
2. Ackers, P., Harrison, A.J.M., and Brewer, A.J., *Laboratory Studies of Storm Overflows with Unsteady Flow,* Symposium on Storm Sewage Overflows, Institution of Civil Engineers, 1967 (p. 37).
3. Anonymous, *Final Report–Technical Committee on Storm Overflows and The Disposal of Storm Sewage,* London: Her Majesty's Stationery Office, 1970.
4. Zielinski, P.B., *The Vortex Chamber as a Grit Removal Device for Water Treatment,* Project No. A-019 sc, supported by U.S. Department of the Interior, Office of Water Resources, at Clemson University, Clemson, South Carolina.
5. Donaldson, O duP., *Calculation of Turbulent Shear Flows for Atmospheric and Vortex Motions,* AIAA J., Vol. 10, No. 1, January, 1972.
6. Dorfman, L.A. and Romanenko, Yu.B., *Flow of a Viscous Fluid in a Cylindrical Vessel with a Rotating Cover,* Izv. An SSR, Mekhanika Zhidkosti i Gaza, Vol. 1, No. 5, pp. 63-69, 1966.
7. Camp, T. R., *Sedimentation and the Design of Settling Tanks,* ASCE Proc. April, 1945, pp. 895-959.
8. Hinze, Vo., *Turbulence,* McGraw Hill Book Co., Inc., New York, 1959. (esp Chapter 5, "Transport Processes in Turbulent Flows").
9. Torobin, L.B. and Gauvin, W.H., *Fundamental Aspects of Solids–Gas Flow Part IV: The Effects of Particle Rotation, Roughness and Shape,* The Canadian Journal of Chemical Engineering, October 1960, pp. 142-153. Other parts of this survey appear in Aug., Oct., and Dec. 1959, and Dec. 1960.
10. Viets, H. and Lee, D.A., *Motion of Freely Falling Spheres at Moderate Reynolds Numbers,* AIAA J., Vol. 9, No. 10, pp. 2038-2042.
11. Viek, H., *Accelerating Sphere-Wake Interaction,* AIAA J., Vol. 9, No. 10, Oct., 1971, pp. 2087-2089.
12. Maccoll, J.W., *Aerodynamics of a Spinning Sphere,* Royal Aeronautical Society Journal, Vol. 32, No. 213, pp. 777-798, September 1928.
13. Lumley, J.L., *Some Problems Connected with the Motion of Small Particles in Turbulent Fluid,* Ph.D. Dissertation John Hopkins University, Baltimore, Md., 1957.
14. Fair, G.M. and Geyer, J.C., *Water Supply and Waste-Water Disposal,* (John Wiley and Sons, Inc., New York, 1954).

*U.S. GOVERNMENT PRINTING OFFICE:1972 514-148/63 1-3

1 Accession Number	2 Subject Field & Group	SELECTED WATER RESOURCES ABSTRACTS INPUT TRANSACTION FORM
W		

5 Organization

American Public Works Association

6 Title

The Swirl Concentrator as a Combined Sewer Overflow Regulator Facility

10 Author(s)

American Public Works Association

16 Project Designation

Demo Project 11023GSC, APWA 70-7

21 Note

22 Citation

Environmental Protection Agency report number EPA-R2-72-008, September 1972.

23 Descriptors (Starred First)

*Regulation, *Overflow, design

25 Identifiers (Starred First)

*Combined sewers, solid separation, quantity of overflow, quality of overflow

27 Abstract

A study was conducted by the American Public Works Association to determine the applicability of a combined sewer overflow regulator which by induced hydraulic conditions separates settleable and floatable solids from the overflow. The study used a hydraulic model to determine swirl concentrator configurations flow patterns and settleable solid removal efficiency. A mathematical model was also prepared to determine a basis for design.

Excellent correlation was found between the two studies. It was found that at flows which simulate American experience a vortex flow pattern was not effective. However, when flows were restricted, a swirl action occurred and settleable solids were concentrated in the outflow to the interceptor in a flow of two to three percent as compared to the quantity of overflow through a central weir and down shaft.

The swirl concentrator appears to offer a combined sewer overflow regulator that effectively regulates the flow and improves the quality of the overflow, with few moving parts.

The complete hydraulic laboratory and mathematical reports are included as appendices.

This report was submitted in fulfillment of the agreement between the City of Lancaster, Pennsylvania, and the American Public Works Association under the partial sponsorship of the Office of Research and Monitoring, Environmental Protection Agency, in conjunction with Research and Demonstration Project 11023GSC.

Abstractor Richard H. Sullivan | Institution American Public Works Association

WR:102 (REV JULY 1969) WRSIC

SEND, WITH COPY OF DOCUMENT, TO: WATER RESOURCES SCIENTIFIC INFORMATION CENTER U.S. DEPARTMENT OF THE INTERIOR WASHINGTON, D. C. 20240